FINAL REPORT

NASA PROJECT NRA-03-OES-02:

EARTH SYSTEM SCIENCE RESEARCH USING DATA AND PRODUCTS FROM TERRA, AQUA, AND ACRIM SATELLITES

Project Long Title: Toward the Development of Advanced Data Products from EOS Terra and Aqua Direct Broadcasts for Air Quality Management in the State of Texas

(Short Title: Advanced EOS products for Air Quality Management)

To
Dr. Doreen O. Neil
Atmospheric Sciences
NASA Langley Research Center
Hampton, VA 23681

Prepared By
Dr. Keith D. Hutchison,
Senior Research Scientist and Principal Investigator
Center for Space Research
The University of Texas at Austin

December 21, 2007

Table of Contents

List of Tables

List of Figures

1. PROJECT DESCRIPTION

This report documents the research conducted at the Center for Space Research (CSR) under NASA Project Number NNL04AA70G, which has a long title of "*Toward the Development of Advanced Data Products from EOS Terra and Aqua Direct Broadcasts for Air Quality Management in the State of Texas*" and a short title: "*Advanced EOS products for Air Quality Management*."

The report describes the research conducted at CSR to extend MODIS data and products to the applications required by users in the State of Texas. This research presented in this report was completed during the timeframe of August 2004 - December 31, 2007. However, since annual reports were filed in December 2005 and 2006, results obtained during calendar year 2007 are emphasized in the report. All research was conducted under the direction and supervision of Dr. Keith D. Hutchison, Senior Research Scientist and Principal Investigator (PI) at CSR. We believe the results from our research bring great value to the local, state, and international air quality communities. Bold-type publications were completed under this grant, those in italics come from other projects.

1. **Hutchison, K. D., 2003:** "Applications of MODIS Satellite Data and Products for monitoring Air Quality in the State of Texas," Atmospheric Environment, **37**, 2403-2412. (Appendix 8.1.1)
2. *Hutchison*, K. D. and J. M. Jackson, 2003: "Cloud detection over desert regions using the 412 nanometer MODIS channel, Geophysical Research Letters, **30**, 2187-2191.
3. **Hutchison, K. D., Smith, S. and S. Faruqui, 2004:** "The Use of MODIS Data and Aerosol Products for Air Quality Prediction, Atmospheric Environment **38**, 5057-5070. (Appendix 8.1.2)
4. Knebl, M. R. (doctoral thesis), Yang, Z-L. *Hutchison*, K. D. and D. R. Maidment, 2005: "Towards developing a regional scale flood forecast product using precipitation forecasts, GIS, and hydrological modeling," Journal of Environmental Management, **75**, 325-336.
5. **Hutchison, K. D., Smith, S. and S. Faraqui, 2005:** Correlating MODIS Aerosol Optical Thickness Data with Ground-Based $PM_{2.5}$ Observations Across Texas for Use in a Real-time Air Quality Prediction System, Atmospheric Environment. **39**, 7190-7203. (Appendix 8.1.3)
6. Ou, S. C., Liou, K. N., Takano, Y. , Wong, E., *Hutchison*, K., and T. Samec, 2005: "Comparison of the UCLA-LBLE Radiative Transfer Model and MODTRAN for Accuracy Assessment of the NPOESS-VIIRS Cloud Optical Property Algorithms," Applied Optics, **44,** 6274-6284.
7. *Hutchison*, K. D. and A. P. Cracknell, 2005: "VIIRS – A New Operational Cloud Imager," CRC Press of Taylor and Francis Ltd, London, pp 218.
8. *Hutchison*, K.D., Roskovensky, J.K., Jackson, J.M., Heidinger, A.K., Kopp, T. J., Pavolonis, M.J, and R. Frey, 2005: "Automated Cloud Detection and Typing of Data Collected by the Visible Infrared Imager Radiometer Suite (VIIRS)," Int'l Journal of Remote Sensing, **20**, 4681 - 4706.
9. *Hutchison*, K. D., Wong, E. and S. C. Ou, 2006: "Cloud Base Heights Retrieved During Nighttime Conditions with MODIS Data," International Journal of Remote Sensing, **27**, 2847-2862.
10. **Hutchison, K. D., Pekker, T., and S. Smith, 2006**: Improved Retrievals of Cloud Boundaries with MODIS Data for Use in Air Quality Modeling, Atmospheric Environment, **40**, 5798-5806. (Appendix 8.1.4)
11. Wong, E. *Hutchison*, K. D., Ou, S. C. and K. N. Liou, 2007: Cloud Top Temperatures of Cirrus Clouds Retrieved from Radiances in the MODIS 8.55-μm and 12.0-μm Bandpasses, Applied Optics, **46**, 1316-1325.
12. **Hutchison, K. D., Faraqui, S. and S. Smith, 2007:** Improving Correlations between MODIS Aerosol Optical Thickness and Ground-Based $PM_{2.5}$ Observations through 3D Spatial Analyses, Atmospheric Environment, (in press). (Appendix 8.1.5)
13. *Hutchison*, K.D., Iisager, B., Kopp, T., and J. M. Jackson, (manuscript accepted for publication): "Discriminating between Clouds and Aerosols in the VIIRS Cloud Mask Algorithms," J. Atmospheric & Oceanic Technology.
14. **Hutchison, K. D., Pekker, T., and S. Smith,** (manuscript in preparation): Examining the Impact of Errors in Liquid Water Path on the Accuracy 3-Dimensional Cloud Fields Generated from Remote Sensed Data and Numerical Models , Int'l Journal of Remote Sensing.

1.1 Background

NASA launched the first major Earth Observing System (EOS) satellite [also known as (aka) both Terra and EOS-AM] on December 19, 1999 into a sun-synchronous orbit 705-km above the Earth. Terra has a 10:30 AM descending node and carries five instruments including the MODerate Resolution Imaging Spectroradiometer (MODIS) sensor. Two and a half years later, the second major EOS satellite (aka Aqua and EOS-PM) was launched on May 6, 2002 into a similar type of orbit but with a 13:30 ascending node. Together, these satellites provided late-morning (EOS-AM), early afternoon (EOS-PM) and nighttime coverage of the globe in up to 36 spectral bands.

Shortly after the launch of MODIS Terra, CSR began to explore the use of EOS data to support the environmental and resource management needs of Texas under a NASA-funded projected known as "The Synergy Program" (Kalluri et al., 2003). CSR initially obtained MODIS data products through the NASA EOS Data Gateway (EDG), then known as the EOS Data and Information System (EOSDIS), to create a regional archive of readily available data for users across the State. Tools were built to extract, reformat, analyze and distribute these sensor data and products through a CSR data distribution system. This site can still be viewed at: http://synergyx.tacc.utexas.edu/ or accessed from the "Texas Synergy" spotlight on the CSR homepage: http://www.csr.utexas.edu

During the second year of the Synergy Program, staff from the Monitoring Operations Division of the Texas Commission on Environmental Quality (TCEQ), known then as the Texas Natural Resources Conservation Commission (TNRCC), requested CSR assistance in assessing the value of MODIS data for monitoring continental haze. This particular air pollution event originates in the industrialized mid-west portion of the US and migrates across state boundaries into Texas. TCEQ cited the inadequacies in monitoring continental haze with their existing ground and space-based data sources, including hourly direct broadcasts from two U.S. GOES weather satellites, i.e. GOES-East with a sub-point at 75^{o} W longitude and GOES-West, located over 130^{o} W longitude.

In September 2002, Texas experienced a severe continental haze event and this event was subsequently analyzed in detail at CSR. The results published in the literature (Hutchison, 2003). During the analysis of this event, MODIS imagery and aerosol optical thickness (AOT) products were used to identify the sources of the pollution and monitor its transport into and across Texas. A more detailed analysis of this event demonstrated that the MODIS AOT product qualitatively correlated with increases and decreases in ozone reported at ground-based monitoring facilities located across Texas, which are operated by TCEQ (Hutchison et al., 2004). CSR then postulated that these MODIS AOT products could be coupled with a trajectory forecast model to predict trends in air quality, e.g. to determine if existing air quality would become better or worse during the next 24-hours.

Also in 2004, CSR acquired an X-band direct broadcast receiving station (DBRS) to provide the Texas user community with real-time access to MODIS data. While NASA had steadily improved the distribution of MODIS data available over the EDG, from months in 2000 to hours today, a DBRS was needed to support the operational air quality management requirements of TCEQ, since regional analyses and forecasts are issued within hours of MODIS overflight of Texas. In addition, CSR hosted numerous algorithms to retrieve air quality products, e.g. AOT and active fire, within minutes of

data acquisition at the DBRS. Thus, in early 2004, CSR began providing MODIS imagery and AOT products to TCEQ for use in their air quality forecast decision support system. With the award of this grant by NASA to PI Hutchison in 2005, CSR was fully prepared to begin examining quantitatively the correlations between MODIS AOT product and ground-based air quality measurements available through TCEQ.

In addition, CSR has long been aware of the need to retrieve more accurate cloud boundary information from MODIS data for use in full-physics air quality prediction models. Cloud fields impact air quality models in various and profound ways, including aqueous chemistry pathways, cloud-aerosol interactions, surface energy and radiation balance, radiative flux for photochemistry (photolysis rates), and wet deposition. Historically most chemistry models, such as the Comprehensive Air quality Model with Extensions (CAMx), have assumed cloud-free conditions to generate the actinic fluxes that regulate photochemical reactions. More recently, the air quality modeling community has aggressively sought to remedy this situation and developed more modular systems that facilitate the incorporation of improved input data fields, such as aerosol and cloud data fields. Still, analysis of cloud fields for air quality simulations are considered a significant modeling challenge even for the more advanced models, such as the CMAQ modeling system (Byun and Ching, 1999), which use cloud field derived from the MM5/WRF regional forecast models. These problems in specifying cloud data are exacerbated by the more stringent requirement of models used in air quality management to accurately obtain 3-dimensional (3D) cloud fields and only increases in the generation of cloud forecasts (Byun, personal communication).

2. PROJECT OBJECTIVES AND GOALS

In our original proposal, CSR outlined a robust program, spanning four NASA budget periods and covering 36 consecutive months, to address *Science Data Analysis and Modeling Research* under NASA NRA-03-OES-02, "Earth System Science Research Using Data and Products from TERRA, AQUA, and ACRIM Satellites." Our program advocated the need for basic research to extend the application of existing EOS Level 1b data and Level 2 products into new, Level 3 data products that are needed to better understand complex environmental parameters and processes, as outlined in NASA's Earth Science Enterprise (ESE) Research Strategy. CSR stated that this new research would result in improved data products to enhance air quality management in the State of Texas and would ultimately enhance decision-support systems for Federal, state, and tribunal groups across the nation and around the world. Section 3 validates that these major goals have been successfully met during the execution of this research program.

More specifically, the stated goals of the project were to complete the fundamental research needed to create two types of new, Level 3 products for the air quality community in Texas from data collected by NASA's EOS Terra and Aqua missions. Pursuant to the generation of these data products, CSR identified the following activities that were required, including:

- Research to extend the utility of the dimensionless MODIS AOT products into quantitative measures of pollution concentration, e.g. $\mu g/m^3$ for particulate matter, parts per billion (ppb) for ozone, and miles for surface visibilities. *CSR has published five papers on this topic, as shown in Appendix 8.1.1 – 8.1.5.*

- Research to extend numerous MODIS Level 2 cloud data products, including cloud cover or mask, cloud top phase, cloud top pressure, cloud optical thickness and cloud effective particle size into 3-dimensional cloud analyses for use in full-physics air quality models. *CSR has published one key paper on this subject (shown in 8.1.4) that (1) quantified the inaccuracies of existing MODIS cloud data products for use in air quality modeling, (2) identified errors in the current MODIS algorithms, (3) demonstrated an approach to improve the NASA Level 2* cloud data product (MOD06_L2 aka *MOD06) cloud data products, and (4) demonstrated procedures to significantly improve cloud boundaries for use in air quality modeling.*

Thus, objectives established to meet the project goals are shown in Table 1 along with the relevance of each objective and success criteria developed to measure performance. The contents of this table were taken from our original proposal. A brief discussion of the project objectives follows in this section while the current status of investigations at CSR to address each objective is presented in the next section.

Table 1. Objectives, relevance and success criteria for data products under this proposal.

PROJECT OBJECTIVES	RELEVANCE and SUCCESS CRITERIA
1. Conduct research to create new (Level 3) air quality data products from MODIS and MISR products and TCEQ surface-based pollution data.	Provide cost-effective approach to more accurately monitor internal and external pollution sources that affect Texas air quality across all of Texas and entire US. Success declared if remotely-sensed data are consistently within 20% of ground-based measurements.
2. Assess methods to extend air quality analyses into regional, short-term air quality forecasts.	Provides approach to issuing 24-hour air quality forecasts. Success declared if 24-hour forecast within 25-35% of surface-based (truth) observations.
3. Conduct research needed to generate MODIS cloud base height and cloud top height products and establish performance accuracies.	Cloud top heights are used in cloud base height retrieval algorithm but MODIS provides only cloud top pressure and temperature. Success is declared if actual retrieved accuracies are as predicted by sensitivity analyses for VIIRS program, i.e. 500-1000 m
4. Evaluate approaches to integrate conventional weather observations into MODIS cloud base analyses.	Apply conventional observations to reduce errors in MODIS cloud base heights. Success is declared if improvement is one-half order of magnitude or better.
5. Investigate methods to incorporate microwave data into MODIS cloud base height algorithm and assess improvements in performance for optically thick cloud systems.	Microwave moisture data are needed to extend range of optical depths that can be retrieved with MODIS cloud base height algorithm. Success is declared if MODIS cloud base height accuracy degrades by less than 25% as cloud optical depths are doubled.

2.1. Heritage and Approach

CSR had agreed, during discussion with TCEQ, to provide them with near real-time EOS data and products, collected at its EOS DBRS along with advanced air quality management products as research on these products in completed under this project. The approaches and heritages for these new products to be created at CSR are shown in Table 2. The approach to the retrieval of aerosol products was to be based upon existing technology developed by NASA for the EOS program (King et al., 1999). Retrieval of 3D cloud data products would follow the heritage algorithms developed by the CSR

principal investigator (Hutchison, 2002; Wilheit and Hutchison, 2000) for the National Polar-orbiting Operational Satellite System (NPOESS) as modified for air quality applications. Data delivery was proposed to be via the high-speed, web-based Texas InfoMart system, created under the NASA Synergy Program for the distribution of EOS data and products to Federal, State, local, and tribal user communities (Hutchison and Smith, 2002; Tapley et al., 2001). With the installation of a new EOS DBRS, CSR acquired the capability to support the real-time delivery of EOS data and products to the Texas air quality user community.

Table 2. Approach and heritage for each solution proposed to meet all project objectives.

OBJECTIVE	APPROACH	HERITAGE
1. Conduct research to create new (Level 3) air quality data products from MODIS and MISR products and TCEQ surface-based pollution data.	• Develop statistical-based relationships between satellite and surface observations, • Constrain solution by aerosol source, type and meteorological condition.	• Extend MODIS aerosol products that were described by P/I in peer-reviewed literature (Hutchison, in press – accepted by Atm. Environ.). • Assess the potential improvement of using MISR versus MODIS products for air quality applications.
2. Assess methods to extend air quality analyses into regional, short-term air quality forecasts.	• Convert aerosol product to gridded field, forecast via trajectory scheme, • Allow gravity and vertical wind velocities to reduce aerosol concentrations.	• Conduct original research to create external knowledge on aerosol vertical profiles used in trajectory-based scheme, • Use backward trajectory scheme created from NCEP data to move entire aerosol field forward in time.
3. Conduct research needed to generate MODIS cloud base height and cloud top height products and establish performance accuracies.	• Use NCEP data to obtain cloud top heights, • Retrieve cloud base heights using MODIS cloud products, e.g. cloud optical depths, effective particle size, etc.	• Apply technology developed by P/I (Hutchison, 2000), • Demonstrate with more extensive MODIS data sets than used in peer-reviewed journal. Include optically thicker clouds to test limits of solutions.
4. Evaluate approaches to Integrate conventional weather observations into MODIS cloud base analyses.	• Assess methods to apply conventional weather observations to a range of satellite observations.	• Use concept developed for cloud forecast modeling by US Air Force (Kiess and Cox, 1988), • Conduct new research to apply variable versus static spreading of surface observations.
5. Investigate methods to extend MODIS cloud base height algorithm with microwave data and quantify value with optically thick cloud patterns.	• Assess use of cloud liquid water and cloud ice path from AMSR-E, • Develop test cases for a variety of cloud types and scenarios.	• Use cloud products available from microwave sensors, e.g. AMSR-E, • Use truth information collected at instrumented observation sites, e.g. Southern Great Plains (SGP) Cloud and Radiation Testbed (CART), during Aqua overflights.

2.2 Overview of Tasks

The proposed research necessary to extend the application of existing EOS Level 1b data and Level 2 products into new, Level 3 products are briefly highlighted. Research was proposed to develop two types of advanced (Level 3) data products that were deemed critical to the successful exploitation of remotely-sensed satellite data for air quality

management. The first level of research supports the development of advanced aerosol products that extend aerosol optical thickness (AOT) products, which are dimensionless, into a quantitative measure of pollution concentration, e.g. $\mu g/m^3$ for particulate matter (PM) or parts per billion (ppb) for ozone. The second is to conduct the necessary research needed to retrieve 3-dimensional cloud fields for use in full-physics air quality models, e.g. Models-3 Community Multi-scale Air Quality (CMAQ) or Comprehensive Air quality Model with Extensions (CAMx).

2.2.1 Conduct Research Needed to Generate New (Level 3) MODIS Air Quality Products

We proposed research necessary to enhance regional air quality monitoring by extending MODIS Level 2 (MOD04) aerosol optical thickness products into Level 3 data products to supplement the relatively small number of surface-based air quality observation sites operated by TCEQ. These products would also become the input parameter for the trajectory-based air quality forecast model discussed below.

2.2.1.1 Investigate Relationships Between MODIS AOT and Surface-Based $PM_{2.5}$ Observations

The fundamental task, in effectively using MODIS AOT observations for air quality management applications, is to establish relationships that correlate satellite observations with key air quality measurements reported by TCEQ ground-based instruments, i.e. $PM_{2.5}$ observations. [TCEQ MOD personnel collect data from a variety of sources including the US National Weather Service, central and mobile laboratories based in Austin and Houston, a network of over 200 Continuous Air Monitoring Stations (CAMS) sites, including 52 PM measurement sites.] The research conducted under this task sought to establish relationships between remotely-sensed satellite observations and CAMS observations in order to assess air quality not only within Texas but in adjacent regions that ultimately affect Texas air quality. Initially, we propose to evaluate purely statistical relationships that are a function of aerosol sources, i.e. continental haze, smoke for the Yucatan Peninsula, and Saharan sand. These statistical relationships are expected to stratify solutions according to aerosol characteristics (e.g. total concentration, size distribution, vertical distribution) which affect sedimentation rate and aerosol terminal velocities (Byers, 1965). If necessary, additional atmospheric parameters (e.g. humidity, vertical wind fields, atmospheric stability) will be included in the analyses.

2.2.1.2 Assess Methods to Generate Real-time Air Quality Forecast Products

A backward trajectory approach was proposed to move the MODIS AOT analysis products forward in time as a gridded forecast field. It was planned to use a purely Lagrangian advection scheme. The proposed trajectories would be based upon the forecast u-, v-, and ω–wind fields, available from the National Center of Environmental Prediction (NCEP). The proposed backward trajectories would be generated for the entire Texas forecast region, which is a rectangular area approximately 2000 x 1500 km, prior to MODIS overflight of the CSR DB ground station which makes this approach a real-time, operational forecast capability.

2.2.2 Proposed Research To Create New (Level 3) MODIS Cloud Data Products

The proposed methodology to generate the 3D cloud fields was based on two different approaches developed to retrieve cloud base heights from EOS data: one relies

exclusively upon MODIS data (Hutchison, 1998; 2002) while the other requires cloud top heights from MODIS to exploit a cloud base signature in the microwave moisture sounder data (Wilheit and Hutchison, 2000). The EOS Aqua satellite was the first spacecraft that collected data in all spectral bands needed to generate 3D cloud fields from passive radiometry. The plan called for using, as much as possible, cloud data products created by NASA and distributed under the MOD06 product listing. Unfortunately, these MODIS cloud products do not include either the cloud top height or cloud base height data products, so CSR proposed to create both of these. Thus, cloud top heights could be retrieved at CSR from the MOD06 cloud top temperatures or cloud top pressure data products after further investigations to confirm the accuracy of them.

2.2.2.1 Evaluate Cloud Top Height Products

Since error analyses showed that the specification of cloud top height is the largest error source in NPOESS cloud base height algorithms (Hutchison, 2000), i.e. being on order of 500-1000 m for typical water clouds, CSR proposed to investigate approaches to retrieve cloud top heights suitable for use in air quality applications. In one approach, CSR would couple NCEP gridded fields of temperature, pressure, and heights with MODIS cloud top parameters to convert the MOD06 cloud top parameters into cloud top heights. In the case of water clouds, MODIS cloud top temperatures would be correlated with NCEP temperature and moisture profiles to define cloud top heights. In the case of ice clouds, the MOD06 cloud top pressures would correlate directly with NCEP pressure fields to determine cloud top heights. In an alternate approach, we would use cloud top pressures for both ice and water clouds along with surface pressure and elevation information to determine cloud top height with the Hypsometric Equation, shown in Equation 1. In both cases, verification is against cloud data collected by the highly instrumented sites, e.g. Atmospheric Radiation Measurement (ARM) Southern Great Plains (SGP) Cloud and Radiation Testbed (CART) site.

$$P_2 = P_1 \exp[- g (Z_2 - Z_1) / (RT)] \quad (1)$$

where:

P_2, Z_2 = pressure and geopotential height of surface 2, where $P_1 > P_2$
P_1, Z_1 = pressure and geopotential height of surface 1 where $Z_2 > Z_1$
g = gravitational constant
R = gas constant from dry air
T = virtual temperature for the layer

2.2.2.2 Assess Cloud Boundaries derived from MODIS Data

For water clouds, cloud thickness (ΔZ) would be based upon the relationship between liquid water path (LWP), in gm m^{-2}, and liquid water content (LWC) in gm m^{-3}, as shown in Equation 2 (Hutchison, 1998; 2000). LWP is related to cloud optical depth or cloud optical thickness (τ) and cloud effective particle size (r_e) as shown in Equation 3 (Liou, 1992).

$$Z_{cb} = Z_{ct} - (\Delta Z) = Z_{ct} - [LWP/LWC] \quad (2)$$

where:

$$LWP = \text{Liquid water path} = [2 \tau r_e] / 3 \quad (3)$$

τ = cloud optical depth

r_e = cloud droplet effective particle size

The MOD06 product (King et al., 1997) contains all information needed to test the MODIS cloud base height algorithms, except for cloud top height as noted above. The MOD06 product provides a 1-km resolution cloud mask along with cloud optical thickness and cloud effective particle radius. Other cloud parameters are available at 5-km resolution including cloud top phase, cloud top pressure, and cloud top temperature. Cloud optical thickness and particle size are available only for sunlit regions of the Earth; therefore, cloud base height retrievals are currently restricted to daytime MODIS data although procedures have been developed for NPOESS to retrieve these products under nighttime conditions (Hutchison et al., 2006).

2.2.2.3 Integrate Surface-Based Observations into Cloud Boundaries

Surface observations represent the most accurate source of cloud base height data that are routinely available. Therefore, it was considered highly desirable to integrate surface-based observations of cloud heights with those retrieved from satellite data into a Level_3 product. However, difficulties are experienced in using these observations since the ground-based observations are not available on a global basis. Thus, in this proposal, differences between surface and satellite observations would be evaluated to create an optimal mixing of these observations to improve the cloud base height data product. The combined cloud base height algorithm is expected to produce accuracies useful for air quality and climate modeling applications.

2.2.3 Study use of Microwave Products in Cloud Boundaries

The retrieval of cloud thickness with the MODIS algorithm was limited to cloud optical thickness values of about 60 (Hutchison, 2002). Therefore, data collected by microwave instruments had potential value to extend the MODIS-only cloud base height algorithm to more optically thick water clouds (Hutchison, 2002; Hutchison, 2000) using LWP retrieved from microwave imagery. In addition, a spectral signature of the cloud base height for water clouds has been detected in microwave moisture sounder data collected in the 183 GHz region (Wilheit and Hutchison, 2000). However, an algorithm had not been developed to exploit this signature. In this task, research would be conducted to determine the feasibility of extending the MODIS cloud base height algorithms to more thick clouds and, if possible, evaluate cloud thickness values and cloud base heights retrieved from this synergist approach using data collected by the Aqua satellite.

3. CURRENT PROJECT STATUS

Research has now been completed to satisfy Project Objectives 1-5, listed in Table 1, and the results have been either published in the refereed literature or they are pending publication. Table 3 is color-coded to reflect relationships between the approach proposed to satisfy each objective and these publications. The progress towards meeting each of the Objectives 1-5 is now provided in detail. (Note: Progress on Objective 6 in the original proposal has been eliminated from this report. When inaccuracies in the MODIS cloud optical properties product (COP), shown in Section 3.3 became evident during the second year of our investigations, CSR proposed methods to resolve these inaccuracies under ROSES 2006 because the theoretical basis for these inaccuracies was

outside the scope of our original proposal. Our proposal was not selected for funding; thus, as a consequence, CSR refocused efforts associated with Objective 6 to quantify the impact of these inaccuracies on the cloud base height. In addition, we examined a new approach to reduce the impact of these inaccuracies through the selective use of NWP data, which is reported in a manuscript currently under review.)

Table 3. Objectives, approaches, and status of research related to project objectives.

Project Objective	Approach	Project status
1. Conduct research to create new (Level 3) air quality data products from MODIS and MISR products and TCEQ surface-based pollution data.	Develop statistical-based relationships between satellite and surface observations, Constrain solution by aerosol source, type and meteorological condition.	- Hutchison et al., 2004: "The Use of MODIS Data and Aerosol Products for Air Quality Prediction, Atmospheric Environment **38**, 5057-5070. - Hutchison et al., 2005: Correlating MODIS Aerosol Optical Thickness Data with Ground-Based $PM_{2.5}$ Observations Across Texas for Use in a Real-time Air Quality Prediction System, Atm Env **39**, 7190-7203. - Hutchison, et al., 2007: Improving Correlations between MODIS Aerosol Optical Thickness and Ground-Based $PM_{2.5}$ Observations through 3D Spatial Analyses, Atm Env, (in press).
2. Assess methods to extend air quality analyses into regional, short-term air quality forecasts.	Convert aerosol product to a gridded-field, forecast via a trajectory scheme. Allow gravity and vertical wind velocities to effect aerosol concentrations.	- Access the latest forecast at website http://synergyx.tacc.utexas.edu/Magic/shared/Products/modis_aot_trajectory/20061119/traj_fx_20061119.gif - Hutchison, et al., 2007: Improving Correlations between MODIS Aerosol Optical Thickness and Ground-Based $PM_{2.5}$ Observations through 3D Spatial Analyses, Atm Env, (in press).
3. Conduct research needed to generate MODIS cloud base height and cloud top height products and establish performance accuracies.	Retrieve cloud base heights using NCEP data along with MODIS cloud products, e.g. cloud optical depths, effective particle size	- Hutchison, et al., 2006: Improved Retrievals of Cloud Boundaries with MODIS Data for Use in Air Quality Modeling, Atm Env, **40**, 5798-5806. - Hutchison et al., (in press): Examining the Impact of Errors in Liquid Water Path on the Accuracy 3-Dimensional Cloud Fields Generated from Remote Sensed Data and Numerical Models, Int'l J. Remote Sensing.
4. Evaluate approaches to integrate conventional weather observations into improved cloud (base) analyses.	Assess methods to apply conventional weather observations to a range of satellite observations.	- Hutchison, et al., 2006: Improved Retrievals of Cloud Boundaries with MODIS Data for Use in Air Quality Modeling, 40, 5798-5806, Atm Env. - Hutchison et al., (in press): Examining the Impact of Errors in Liquid Water Path on the Accuracy of 3-Dimensional Cloud Fields Generated from Remote Sensed Data and Numerical Models, Int'l J. Remote Sensing.
5. Investigate methods to extend MODIS cloud base height algorithm for optically thick cloud patterns.	- Demonstrate with test cases for a variety of cloud types and scenarios. - Assess use of cloud liquid water and cloud ice path from AMSR-E,	- Hutchison et al., (in press): Examining the Impact of Errors in Liquid Water Path on the Accuracy 3-Dimensional Cloud Fields Generated from Remote Sensed Data and Numerical Models, Int'l J. Remote Sensing. - Ability to exploit AMSR-E over land was not adequately address by microwave community.

3.1 Objective 1: Extend MODIS AOT Products for Air Quality Applications

Completed research resulted in significant improvement in correlations between MODIS aerosol optical thickness (AOT) values and ground-based pollution measurements made at CAMS locations operated by the TCEQ. The following highlights are taken from Hutchison et al., (2004, 2005, 2007).

- Initial results at CSR showed correlations in the 0.4-0.5 range.
- CSR demonstrated improvement in correlations was achieved through 3D spatial analyses, with the aid of airborne lidar data.
    - 2D spatial analyses showed that correlations were improved substantially, falling in the range 0.7 - 0.8, when a minimum number of valid AOT observations were required for a grid cell to be valid, i.e. 16 for a 5x5 gridded AOT cell and 6 for a 3x3 AOT grid cell. In effect, the requirement for a minimum number of valid AOT 10-km pixels within the 50- and 30-km^2 grid cells achieves the following:
        - reduces the probability of unscreened clouds or shadows contaminating the AOT product,
        - reduces the probability of ephemeral water impacting AOT product quality, and
        - emphasizes larger scale (transient) pollution events over localized events.
    - 3D spatial analyses showed that correlations could improve to > 0.9 with information about the aerosol profile concentration available.
        - Airborne lidar data showed that the vertical component of the trajectory could be used in some cases to provide insights into aerosol profile information.
        - Stratifying results based upon aerosol concentration resulted in improvements from 0.4-0.5 to > 0.9
        - Results suggest different linear coefficients are needed to translate between MODIS AOT and $PM_{2.5}$ concentrations as aerosol profile concentrations vary with pollution class and meteorological conditions governing transport processes
    - CSR has been working to develop a larger database to further investigate the application of 3D spatial analyses on MODIS AOT-PM2.5 correlations. CSR is expanding the multi-year database historically used at CSR to include additional years that include observations from MODIS Aqua collected after the launch of the CloudSat Mission, since Calipso data are needed to further study these concepts. However, aerosol profiles from Calipso have not yet been made available over the EDG and remain a limitation to these studies.

Significant differences exist between MODIS AOT and CAMS $PM_{2.5}$ observations and these differences must be considered before satellite-based observations can be effectively utilized in a real-time decision support system. For example, MODIS collects

data at 250-m, 500-m, and 1-km at nadir across a 2330-km data swath from satellites in near-Earth sun-synchronous polar-orbit from a nominal altitude of 705-km (Salomonson et al., 1989; Barnes et al., 1998). The MODIS AOT product covers the total atmospheric column from the satellite to the Earth's surface and has a horizontal spatial resolution of 10-km. The MODIS AOT product is dimensionless and is generated only during daytime conditions. On the other hand, ground-based pollution measurements made at TCEQ CAMS locations are generated every five minutes and reported as averages at hourly and 24-hour intervals. Typically, 12 observations are averaged in each hourly report. Although TCEQ may occasionally employ portable equipment, most observations are made at fixed ground sites. Thus, CAMS observations represent time averaged measurements PM, e.g. $PM_{2.5}$ ($\mu g/m^3$), and ozone [parts-per-billion (ppb)].

Thus, some statistical relationship is needed to compare MODIS AOT observations with ground-based $PM_{2.5}$ measurements, both in the MODIS AOT analysis and the trajectory-based AOT forecasts. Most commonly this relationship is based upon the Pearson linear correlation coefficient. Linear correlation tests calculate a Pearson *product-moment* correlation coefficient for each site sample consisting of all valid MODIS AOT retrievals with corresponding $PM_{2.5}$ ground measurements. The sign and magnitude of the coefficient indicate respectively the direction and strength of the linear relationship between AOT and $PM_{2.5}$ observations: Ranging from 0 to -1 for a negative relationship and 0 to +1 for a positive relationship, coefficients closer to zero indicate a weak or indeterminate relationship that increases in strength toward -1 or +1 limits. The strength of the coefficient is independent of its direction. The Pearson correlation coefficient (r) is calculated as follows:

$$r = \Sigma xy / NS_xS_y = \frac{\Sigma xy}{N * (\Sigma x^2/n_x-1)^{1/2} * (\Sigma y^2/n_y-1)^{1/2}} \quad (4)$$

where (xy) is the cross-product of the variation in each observation pair from the respective means of the variable distributions equal to the summation of $[(x_i-X)(y_i-Y)]$ where X and Y are the overall means of each sample distribution and x and y are positive or negative deviations from the means, (N) is the number of observation pairs in each sample, (S_x) and (S_y) are the overall standard deviations of each sample distribution, (n_x) the total number of x-variable sample independent observations, (n_y) the total number of y-variable sample independent observations.

In the following sections we first discuss the evolution of the MODIS AOT algorithms hosted at the CSR EOS DBRS. Next, we examine techniques and procedures developed at CSR to improve correlations between MODIS AOT and ground-based PM2.5 observations. We conclude this section with the current status of our work on this objective.

3.1.1 Evolution of the MODIS AOT Retrieval Algorithms

There is a lengthy heritage in using satellite data to monitor atmospheric aerosols, such as dust and sand particles (Carlson and Prospero, 1972; Shenk and Curran, 1974). While early research was directed toward the detection of these aerosols over ocean surfaces, major improvements in global aerosol monitoring were achieved when additional spectral

data became available with the first launch of the MODIS sensor on the EOS Terra satellite in December 1999. Today, EOS satellites are used to monitor aerosols on a global scale and to understand the impact of aerosols on cloud and climate feedback mechanisms (Kaufman et al, 1997a; Kaufman et al., 2002a).

The MODIS aerosol module contains two independent algorithms that were developed before the EOS Terra spacecraft launched in 1999. The algorithm used to retrieve aerosols over land was first described by Kaufman, et al. (1997b) while the algorithm used over the ocean was described in a separate publication by Tanré, et al. (1997). NASA advises that the central approach used in these MODIS aerosol algorithms has remained relatively unchanged through versions 3.0 - 5.1; however, there have been minor modifications (Remer et al., 2005; Remer et al., 2006). Basically, the core algorithm exploits atmospheric reflectance ratios, corrected for Rayleigh scattering, between 0.47-μm and 2.1-μm along with 0.65-μm and 2.1-μm to retrieve AOT under the assumption that these relationships are applicable under global conditions, e.g. differences in bi-directional reflectance functions in these bandpasses across the Earth's surface are negligible (Kaufman et al., 1997c; Kaufman et al., 2002b). [Changes in this assumption are reported to have been made in the version 5.2 land algorithms. These updated algorithms represent a major modification in the retrieval approach used to generate the MODIS AOT (Remer et al., 2006). The Version 5.2 algorithms have now been hosted at CSR but no discussion on their performance is possible at this time.] In essence, the minor modifications in the pre-5.2 versions of the AOT algorithms alter the logic that determines which pixels in a 10-km region are used to generate AOT values. Historically, these updates have been implemented through a process known as a "collection" which consists of products that were generated by similar, but not necessarily the same, versions of the algorithms (Remer et al., 2006). The MODIS algorithm theoretical basis document, dated 1996, described the pre-launch aerosol algorithms while the Collection 3 (i.e. version 3.0) algorithms were used to produce the first globally validated products over ocean backgrounds (Remer et al., 2002) and over land surfaces (Chu et al., 2002). The Collection 3 MODIS AOT algorithms were acquired by CSR through the purchase of a MODIS DBRS in 2003. The next major update to the aerosol products came with the release of the MODIS Collection 4 algorithms. CSR hosted the Collection 4.2.2 algorithms at the DBRS in March 2004. Recently, the NASA Aerosol Team created two additional versions: the Collection 5.1 algorithms which CSR hosted in March 2005 and the Collection 5.2 algorithms which recently became the operational algorithms used at the NASA Earth Science Data Information System (ESDIS). As this research is reported, the ESDIS distributes AOT products only from the Collection 4 algorithms. Results presented herein are based upon retrievals made at CSR with the MODIS Collection 4.2.2 and Collection 5.1 algorithms. A history of changes to the MODIS AOT algorithms can be found in algorithm theoretical basis documents (Kaufman et al., 1996; Remer et al., 2006), various publications (Kaufman et al., 1997a; Remer et al., 2005; Chu et al., 2003) and at the NASA Aerosol Team's website, i.e. http://modis-atmos.gsfc.nasa.gov/MOD04_L2/history.

Table 4 summarizes some of the minor modifications to the MODIS aerosol retrieval algorithms that affect the quality of the aerosol products and impact attempts to correlate these products with ground-based air quality measurements. First, it is seen that there are nominally 400 pixels used to retrieve aerosol optical thickness for a 10-km^2 area with all

versions of the algorithm. Initially cloud screening was based upon the MODIS 1-km cloud mask (Ackerman et al., 1998) as noted by Chu et al., (2003). However, dissatisfaction with the performance of the MODIS cloud mask (Brennan et al., 2005) resulted first in the use of supplemental cloud tests with version 4 algorithms (Martins et al., 2003; Remer et al., 2005). Finally the MODIS cloud mask was replaced with a completely internally-generated cloud masks based upon the spatial tests with the 0.47-μm bands to detect water clouds and threshold tests with the 1.38-μm band to exclude ice clouds from AOT analyses (Remer et al., 2006). To further reduce the possibility of clouds being included in the pixels used to retrieve AOT, a correction is applied that is referred to as a bright pixel correction in Table 4. After removing all cloudy pixels along with those found to contain snow or ice from the 400 pixel group, the remaining pixels are prioritized by descending reflectances in the 0.65-μm channel ($\rho_{0.65\text{-}\mu m}$). Between 40-50% of the pixels, depending upon which version of the algorithm is used, with the highest reflectance in this band are discarded to reduce cloud effects.

In addition to clouds, two other phenomena can degrade the quality of AOT retrievals with MODIS data. These include unscreened inland water features (Hutchison et al., 2005) and cloud shadows. Different approaches have been used to effectively detect and eliminate most problems associated with ephemeral inland water. However, at this time, there seems to be no suitable logic to identify cloud shadows and failure to detect these shadows can result in depressed aerosol retrievals. The MODIS aerosol retrieval approach attempts to eliminate cloud shadows and inland water surfaces using, what is referred to here, as a dark pixel correction. First, pixels with an NDVI < 0.1 are assumed to contain inland water (Chu et al., 2003). In addition, between 10-20% of the pixels, depending upon which version of the algorithm is used, with the lowest reflectance in the 0.65-μm band are discarded to further reduce cloud shadow and inland water effects. Finally, the MODIS AOT algorithms have varied the range of reflectance in the 2.1-μm ($\rho_{2.1\text{-}\mu m}$) band that is allowed to be part of the AOT retrieval. All versions of the MODIS AOT algorithms reviewed at CSR require 12 “good” pixels to remain after applying the aforementioned screening procedures to the 400 pixels that make up a nominal 10-km AOT analysis area. Those pixels remaining for analysis are examined in the 2.1-μm band to consider if 12 pixels are found in the range of 0.01-0.05. If 12 valid pixels are not found after the upper limit is increased to 0.15, in the earlier versions of the algorithm, no AOT retrieval was attempted. Initially, this upper limit was set at 0.15 (Chu et al., 2003) for high quality products but was increased to 0.25 in the collection 4 algorithms. Over bright surfaces, aerosol retrievals are made up to reflectances of 0.40 in the 2.13-μm band but the results are flagged as lower quality.

These minor modifications to the AOT algorithmic logic can have a direct impact on correlations with ground-based air quality measurements. As a result, CSR has maintained a multi-year database which is used to retrieve AOT values with each release of the NASA algorithms. Through the analysis of this dataset, techniques and procedures have been developed to assess the impact of AOT retrievals on air quality prediction. Some of those techniques are now presented in detail.

Table 4. Comparisons between versions of the MODIS algorithms used to retrieve high quality aerosol optical thickness over land surfaces (From Hutchison et al., 2007).

Algorithm Version	Total pixels in 10-km Product	Cloud Screening Approach	Bright Pixels Correction	Dark Pixel Correction	Other comments
3.1	400 @ 500m resolution	Uses only MODIS cloud mask product	Eliminate highest 40% $\rho_{0.65\text{-}\mu m}$	Lowest 10% $\rho_{0.65\text{-}\mu m}$	Requires 12 pixels with $\rho_{2.1\text{-}\mu m} < 0.15$
4.2.2	400 @ 500m resolution	Uses MODIS cloud mask & internal cloud tests	Eliminate highest 50% $\rho_{0.65\text{-}\mu m}$	NDVI < 0.1 & Lowest 20% $\rho_{0.65\text{-}\mu m}$	Requires 12 pixels with $\rho_{2.1\text{-}\mu m} < 0.25$
5.1	400 @ 500m resolution	Uses only internal cloud tests	Eliminate highest 50% $\rho_{0.65\text{-}\mu m}$	NDVI < 0.1 & Lowest 20% $\rho_{0.65\text{-}\mu m}$	Requires 12 pixels with $\rho_{2.1\text{-}\mu m} < 0.25$

3.1.2 Techniques and Procedures to Assess AOT Quality

In earlier publications, CSR demonstrated a process to correlate MODIS AOT observations with ground-based $PM_{2.5}$ observations made at ground-based facilities operated by the TCEQ (Hutchison et al., 2005). This process is now used to evaluate differences between MODIS Collection 4 and 5 algorithms while simultaneously demonstrating a methodology to further improve correlations through a 2-dimensional spatial analysis.

Table 5 contains the results of AOT-$PM_{2.5}$ correlation tests conducted with data produced with the MODIS version 5.1 land aerosol algorithms, based on a full-year of data collected in 2004 at the CSR MODIS DBRS. These correlations were created for two AOT grid sizes and each is centered on the CAMS locations shown in columns 4 and 5. One grid covers a 3x3 AOT pixel group of approximately 30 km while the second covers a 5x5 AOT pixel group of about 50 km. This allows correlations to be generated for a single (~10-km) AOT center pixel, a 3x3 AOT pixel group (30-km grid) or a 5x5 AOT pixel group (50-km grid). For these two grid sizes, denoted as AOT3 and AOT5, correlations were observed using: (1) all valid MODIS AOT retrievals in the area (unrestricted), i.e. AOT3 U and AOT5 U, and (2) a restricted subset requiring a minimum number of valid MODIS AOT pixels for each grid, i.e. AOT3 R and AOT 5 R. The restricted dataset required at least 6 (of the 9 possible) AOT values for the 30-km grid and 15 (of the 25) for the 50-km grid, which sharply reduces sample size for all sites yet increases the probability that the ground site location and/or nearest-neighbor pixels will be represented in the grid statistics for any included retrieval. The tables are arranged by Texas geographic sector, metropolitan area, CAMS site designator, latitude, and longitude in columns 1-5 respectively. The number of unrestricted, 3x3 AOT-$PM_{2.5}$ data values is shown in column 6 with the corresponding correlation coefficient in column 7 followed by the number of restricted data points and correlations in column 8 and 9 respectively. Columns 10-13 have similar data for comparisons for the 5x5 AOT grid.

An inspection of Table 5 shows that significant differences exist between correlations developed from restricted and unrestricted datasets. The difference in the correlation

coefficients for the unrestricted and restricted tests depends on how the exclusion of sparse retrievals affects the size and degree of variability in each site sample. Comparisons between correlations shown in columns 7 and 9 or 11 and 13 show increases in the Pearson coefficient for most sites, exceeding +0.2 in a few cases. For example, CAMS #34 (Coastal, Galveston-Texas City) shows correlations of 0.39 and 0.67 for the unrestricted and restricted data respectively on the 30-km grid. On the 50-km grid, CAMS #70 (Northeast Sector, Forth Worth-Arlington) shows correlations of 0.60 and 0.75 for unrestricted and restricted data and CAMS #80 (Coastal, Brownsville-Harlingen-San Benito) increases from 0.21 to 0.57. In fact, correlations at several CAMS facilities exceed 0.70 at both grid scales for several CAMS facilities although any significant effect of grid size (30-km vs. 50-km) on the correlation to PM2.5 measured at the center pixel location and the averaging of AOT statistics over different spatial scales is as yet indeterminate, and likely varies based on the composition of each sample.

Next, comparisons are made between restricted and unrestricted correlations generated from datasets using the MODIS collection 4.2.2 and 5.1 AOT algorithms. [Note: AOT-$PM_{2.5}$ correlations developed from the MODIS version 4.2.2 algorithms were previously reported in Table 2 of Hutchison et al., (2005) for the 10-km and 50-km grids. Updates of these tables are shown in the appendices.] Rather than repeating those statistics here, Table 6 shows differences in correlations based upon each set of retrieval algorithms. In this case, negative values reflect smaller values obtained with the Collection 5.1 algorithms. For example, Table 6 shows far fewer AOT products were retrieved with the newer algorithms in some regions of Texas. For example, the 30-km grid surrounding CAMS #1014 had 45 fewer days where at least one value AOT retrieval was available and 64 fewer days where at least 6-AOT valid values were analyzed. In the 50-km grid surrounding CAMS #34, there were 15 and 55 fewer observations available for these corrections, respectively. On the other hand, at other CAMS locations there more valid AOT retrievals resulted from application of the Collection 5.1 algorithms, e.g. CAMS #64 sample increased by 25 and 12 observations for the unrestricted and restricted datasets on the 30-km grid and CAMS #642 sample increased by 28 and 12 observations for these same conditions on the 50-km grid.

In general, differences between correlations shown in Table 6 for most entries in columns 7, 9, 11, and 13 are positive, which suggests that the modifications in the Collection 5.1 algorithms generally reflect improved AOT-$PM_{2.5}$ correlations for the Texas region: The differences may be attributable to changes in sample distributions, including the reduction of elevated AOT values recorded in previous versions of the data due to aforementioned screening issues. The requirement for a minimum number of valid AOT observations in grid cells may: (1) reduce the probability of unscreened clouds or shadows contaminating the AOT product, (2) reduce the probability of ephemeral water impacting AOT product quality, and (3) emphasize larger scale (transient) pollution events over localized events.

While in most cases, AOT-$PM_{2.5}$ correlations improved with the conversion at CSR from the collection 4.2 to the collection 5.1 MODIS algorithms, some problems remain. In addition, CSR identified cases where these AOT analyses have much lower than expected values compared to $PM_{2.5}$ observations. These “cold spots” were observed during the September 29 - October 3, 2004 timeframe for CAMS #64, located in Beaumont-Port

Arthur regions. CAMS #64 reported $PM_{2.5}$ levels near 15-20 μg m^{-3} while the MODIS AOT value is only about 0.2. Without going into a detailed proof, we simply note that cold spots appear to be associated with cloud shadows.

Correlations approaching 0.8, as shown in Table 5, are highly encouraging but further improvement is needed to fully exploit AOT analyses in a real-time forecast decision support system. CSR has long maintained that additional improvement in correlations can be achieved through knowledge of the vertical structure of the aerosols (Hutchison et al., 2004; Hutchison et al., 2005). Dr. Hutchison became co-PI of a small project sponsored by the Texas Advanced Research Commission (TARC) which required the analysis of airborne lidar (LIght Detecting and Ranging) data to help evaluate a number of MODIS data products, e.g. aerosol optical depth and fire analyses. These lidar data allowed CSR to include data on aerosol vertical structure in AOT-$PM_{2.5}$ correlations.

3.1.3 Further Advance in MODIS AOT-$PM_{2.5}$ Correlations

The results presented in the initial publications of CSR (Hutchison, 2003 and Hutchison et al., 2004) received widespread recognition. Representatives of the Republic of China formally contacted the US Environmental Protection Agency in Washington citing these papers in a request for technical assistance in preparation for hosting the 2008 Olympic Games in Beijing. (Correspondence from the EPA, shown in Appendix 8.2 documents the request.). In addition, Dr. Hutchison became co-PI of a small project sponsored by the Texas Advanced Research Commission (TARC) through Dr. David Allen, Director of the Center for Energy and Environmental Resources (CEER) and Principal Investigator (PI) for this UT Project Number UTA-0057A, titled "*Characterizing regional transport of air pollutants in Texas using air quality models and satellite measurements*." CSR was tasked under the TARC project to evaluate a number of MODIS data products, e.g. aerosol optical depth and fire analyses, using airborne lidar data. This study examined the value of MODIS air quality products to estimate the extent of regional transport of air pollutants during historical episodes associated with the Texas Air Quality Study 2000 (TXAQS-I). The goal was to identify which real-time MODIS products would be useful to support TXAQS-II, which was conducted during August-September 2006. The products created by CSR under this study can be accessed at:

http://synergyx.tacc.utexas.edu/Magic/shared/Products/modis_fire/
http://synergyx.tacc.utexas.edu/Magic/shared/Products/modisdaac_pass/

Airborne lidar data were collected as part of a large, multi-agency study that targeted the Houston-Galveston area (HGA) of Texas as a particulate matter supersite. This study is known as the Texas Air Quality Study 2000 or TXAQS-I. (A second data collection, known as TXAQS-II was conducted during August – September 2006 period.) The TXAQS-I study was conducted to improve the scientific understanding of factors that controlled the formation and transport of air pollutants in the Texas state area and across the U.S. south-central region. Harnessing the expertise and participation of numerous researchers from state-based and national organizations, the TXAQS 2000 involved a six-week period of intensive pollution sampling in the Texas Gulf Coast area beginning in mid-August 2000. Observational and remotely-sensed data were collected to facilitate

Table 5. Correlation statistics between MODIS AOT from Version 5.1 and $PM_{2.5}$ measurements for 2004 for unrestricted and restricted AOT observations on a 30-km and 50-km resolution grid.

Sector	Metro_Area	CAMS	Lat	Lon	AOT3 Unrestr Obs	AOT3 U vs PM25	AOT3 ≥ 6 Obs	AOT3 R vs PM25	AOT5 Unrestr Obs	AOT5 U vs PM25	AOT5 ≥ 15 Obs	AOT5 R vs PM25
Panhandle	Amarillo	305	35.19	-101.84	75	0.29	30	0.38	90	0.19	28	0.26
Panhandle	Odessa-Midland	1014	31.88	-102.36	46	0.35	6	0.45	68	0.32	7	0.30
Northeast	Dallas	401	32.86	-96.90	108	0.64	50	0.72	132	0.63	66	0.77
Northeast	Dallas	56	33.17	-97.25	140	0.60	95	0.71	158	0.58	96	0.74
Northeast	Dallas	74	32.76	-96.55	127	0.70	92	0.69	134	0.70	90	0.73
Northeast	Fort Worth-Arlington	61	32.67	-97.15	135	0.58	82	0.68	154	0.55	81	0.73
Northeast	Fort Worth-Arlington	308	32.78	-97.38	131	0.63	75	0.80	154	0.62	79	0.82
Northeast	Fort Worth-Arlington	70	32.97	-97.02	118	0.63	69	0.77	142	0.60	80	0.75
Northeast	Fort Worth-Arlington	310	32.78	-97.38	140	0.61	79	0.71	163	0.60	83	0.73
Northeast	Longview-Marshall	85	32.67	-94.17	148	0.56	111	0.64	160	0.53	115	0.59
Central	Austin-San Marcos	38	30.48	-97.91	102	0.63	80	0.59	118	0.61	74	0.58
Central	Austin-San Marcos	601	29.96	-96.77	87	0.52	55	0.59	97	0.49	56	0.48
Central	San Antonio	678	29.39	-98.39	98	0.54	64	0.56	118	0.55	64	0.61
Central	San Antonio	301	29.59	-98.27	98	0.60	62	0.53	120	0.63	63	0.50
Southeast	Houston	15	29.81	-95.16	119	0.47	70	0.56	148	0.45	71	0.57
Southeast	Houston	403	29.71	-95.28	95	0.49	53	0.59	118	0.50	58	0.63
Southeast	Houston	78	30.32	-95.48	132	0.48	90	0.57	153	0.46	89	0.59
Southeast	Houston	8	29.92	-95.38	104	0.56	58	0.69	134	0.52	63	0.69
Southeast	Houston	35	29.71	-95.16	113	0.60	54	0.67	146	0.53	70	0.70
Southeast	Houston	1	29.81	-95.27	107	0.56	59	0.62	133	0.55	64	0.71
Southeast	Houston	309	30.01	-95.15	105	0.49	69	0.61	130	0.51	70	0.62
Southeast	Beaumont-Port Arthur	54	30.07	-94.10	128	0.48	86	0.59	154	0.47	87	0.60
Southeast	Beaumont-Port Arthur	64	29.88	-94.34	115	0.48	83	0.62	142	0.48	81	0.62
Southeast	Beaumont-Port Arthur	642	30.15	-93.87	146	0.48	97	0.59	158	0.50	99	0.59
Coastal	Brownsville-Harlingen-San Benito	80	25.87	-97.45	87	0.22	37	0.42	108	0.21	36	0.57
Coastal	Corpus Christi	314	27.47	-97.29	130	0.53	40	0.72	143	0.51	26	0.80
Coastal	Galveston-Texas City	34	29.30	-94.84	112	0.39	24	0.67	140	0.43	15	0.72
South	McAllen-Edinburg-Mission	43	26.19	-98.33	116	0.49	69	0.54	136	0.48	70	0.53

Table 6. Differences between MODIS Version 4.2.2 and Version 5.1 correlation statistics with $PM_{2.5}$ measurements for unrestricted and restricted AOT observations on a 30-km and 50-km resolution grid. (Positive values reflect higher values in the 5.1 results)

Sector	Metro_Area	CAMS	Lat	Lon	AOT3 Unrestr Obs	AOT3 U vs_PM25	AOT3 ≥ 6 Obs	AOT3 R vs_PM25	AOT5 Unrestr Obs	AOT5 U vs_PM25	AOT5 ≥ 15 Obs	AOT5 R vs_PM25
Panhandle	Amarillo	305	35.19	-101.84	-14	-0.18	-39	-0.12	-16	-0.22	-33	-0.29
Panhandle	Odessa-Midland	1014	31.88	-102.36	-45	-0.09	-64	0.00	-28	-0.10	-40	-0.46
Northeast	Dallas	401	32.86	-96.90	-13	0.00	-49	0.15	1	0.00	-32	0.14
Northeast	Dallas	74	32.76	-96.55	15	0.08	5	-0.06	12	0.07	2	0.04
Northeast	Dallas	56	33.17	-97.25	7	0.00	-7	0.01	12	-0.04	-7	0.06
Northeast	Fort Worth-Arlington	61	32.67	-97.15	14	0.03	-21	0.12	19	0.02	-17	0.18
Northeast	Fort Worth-Arlington	308	32.78	-97.38	-1	0.05	-29	0.16	13	0.02	-22	0.21
Northeast	Fort Worth-Arlington	70	32.97	-97.02	-13	0.02	-34	0.13	-1	-0.01	-25	0.10
Northeast	Fort Worth-Arlington	310	32.78	-97.38	10	0.05	-27	0.16	23	0.03	-18	0.17
Northeast	Longview-Marshall	85	32.67	-94.17	34	-0.07	19	-0.07	37	-0.03	26	-0.12
Central	Austin-San Marcos	38	30.48	-97.91	-1	-0.04	-2	-0.12	0	-0.03	-4	-0.13
Central	Austin-San Marcos	601	29.96	-96.77	28	-0.15	7	-0.21	28	-0.13	10	-0.33
Central	San Antonio	678	29.39	-98.39	2	0.00	-15	0.09	14	-0.05	-10	0.08
Central	San Antonio	301	29.59	-98.27	7	0.03	-7	-0.05	14	0.11	-9	-0.16
Southeast	Houston	15	29.81	-95.16	13	0.15	-8	0.16	24	0.05	-7	0.17
Southeast	Houston	403	29.71	-95.28	-5	0.15	-19	0.20	2	0.12	-12	0.25
Southeast	Houston	78	30.32	-95.48	18	0.11	4	0.10	28	0.06	6	0.18
Southeast	Houston	8	29.92	-95.38	-2	0.04	-20	0.14	15	-0.01	-15	0.12
Southeast	Houston	35	29.71	-95.16	8	0.05	-24	0.10	25	0.05	-3	0.10
Southeast	Houston	1	29.81	-95.27	1	0.13	-17	0.08	9	0.05	-9	0.15
Southeast	Houston	309	30.01	-95.15	4	0.02	-8	0.15	14	-0.02	-4	0.16
Southeast	Beaumont-Port Arthur	54	30.07	-94.10	24	-0.01	7	0.08	27	0.11	13	0.09
Southeast	Beaumont-Port Arthur	64	29.88	-94.34	25	0.06	12	0.23	25	0.14	10	-0.01
Southeast	Beaumont-Port Arthur	642	30.15	-93.87	34	0.02	10	0.05	28	0.03	12	0.05
Coastal	Brownsville-Harlingen-San Benito	80	25.87	-97.45	10	-0.08	-21	0.04	21	-0.10	-23	0.10
Coastal	Corpus Christi	314	27.47	-97.29	13	0.08	-24	0.16	-11	0.08	-37	0.22
Coastal	Galveston-Texas City	34	29.30	-94.84	-3	-0.03	-45	0.17	-15	0.10	-55	0.20
South	McAllen-Edinburg-Mission	43	26.19	-98.33	28	0.10	4	0.18	37	0.11	6	0.02

studies on the formation, composition, and day-night cycles of ozone and particulate matter, and the reaction of these pollutants with other atmospheric constituents due to changes in meteorology and ground-level activity.

A principal goal of the TXAQS-I was to better understand and detect patterns of fluctuation in the Gulf Coast area's unique and complex continental-atmospheric-oceanic interactions, as well as gain insights into how meteorological conditions and industrial production processes affect the distribution and long-range transport of pollution over populated areas. Research efforts aimed to support automated modeling of photochemical transformations in the atmosphere, risk assessment of potential human health hazard, and formulation of cost-effective policies to help local constituencies meet regulatory requirements for developing environmental SIPs (State Implementation Plans). The study advanced a regional approach to describing the speciative composition and behavior of criteria pollutants. Scientists attempt to track the vertical and horizontal movement of plumes and changes in pollutant concentrations to observe accumulation and dispersion, as well as the duration and persistence of pollution events over a wide geographic area. Additional information on TXAQS-I may be found at:
http://www.tceq.state.tx.us/assets/public/comm_exec/pubs/pd/020/00-08/texas2000.pdf

While the TXAQS-I mission lasted nearly six weeks, two weeks of intensive data collections that included additional data collection systems. Six research aircraft were used to observe and measure aerosol and ozone concentrations above ground level, including a DC-3 aircraft provided by the NOAA Environmental Technology Laboratory-ETL (now NOAA Earth System Research Library-ESRL). The DC-3 aircraft harbored an airborne ozone lidar instrument to continuously measure the AOT of the air column at various points along the aircraft's flight track and at various multiple atmospheric levels of the air column. Lidar measurements were recorded in the Houston area during the August 25 - September 12 timeframe. A different flight path was covered by the flight team on each of eleven days of active measurements within the area of interest, centered on the Houston metropolitan area in Harris County.

During the August-September 2000 timeframe, 21 of 28 Texas CAMS sites equipped to measure $PM_{2.5}$ concentrations actively recorded local ground-level concentrations during this period, and nine of these stations lay within reasonable proximity of the lidar ground track. Figure 1 shows the location of CAMS sites in the Houston-Galveston area that were operated by TCEQ and provided some of these routine air quality measurements. Each CAMS location has been precisely mapped in this image along with 30x30-km and 50X50-km areas which were used in later analyses of the MODIS AOT products. Color-coding is used to show the variation in pollution intensity among sites in the Houston-Beaumont-Galveston Area and between the center pixel measurement recorded above the ground monitor and the 30-sq-km and 50-sq-km grids.

The lidar instrument flown by NOAA during the TXAQS 2000 study was a single-channel device that operated at a wavelength of 359-nm or 0.359-μm. The NOAA ESRL aircraft was flown at maximum height of approximately 3500-4000 meters above Mean Sea Level (MSL), and the majority of backscatter profiles were retrieved from about 2700-3200 m-MSL to the ground surface. Measurements closest to ground were recorded about 3000-meters (up to 3900-meters) from the plane's flight altitude, resulting in significantly fewer backscatter retrievals within the lowest 100-meters of the troposphere.

According to NOAA-ERSL, the "accuracy of the lidar aerosol backscatter data (collected for TXAQS 2000) was difficult to assess because the airborne lidar aerosol channel was not calibrated and independent aerosol backscatter measurements were not available. As such, CSR recognized that evaluation of the data retrieved provides insight into *relative* horizontal and vertical distributions of aerosol within an air parcel rather than a quantitative assessment of total aerosol loading or impact of pollution in a certain area on ground-zero conditions; therefore, we sought approaches to use these uncalibrated lidar data in a qualitative manner, e.g. by analyzing the structure of the aerosol profiles.

Figure 1. Locations of CAMS facilities, that provided useful air quality measurements during TXAQS 2000 along with 30x30-km and 50x50-km surrounding regions.

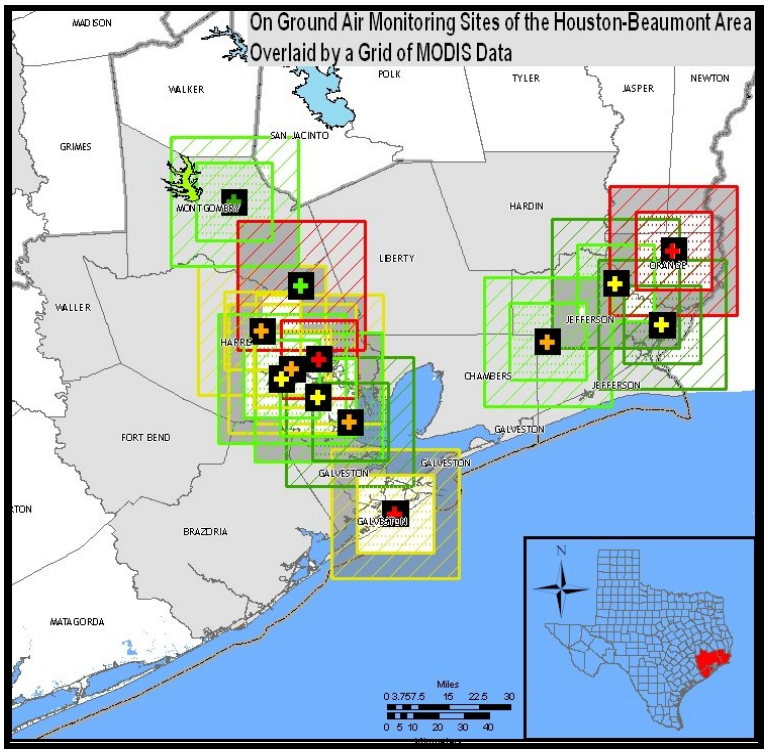

The lidar flight durations during TXAQS-I ranged between 2.34 - 6.9 hours, with flights starting between 15.41 UTC (10:25 AM CDT) and 18.63 UTC and ending in the interval between 20.97 UTC and 24.46 UTC. Over 60 total hours of lidar observation are represented by the collected set of 17,599 records, each record corresponding to a lidar transmission. The lidar transmissions generally occurred at 10-second intervals with some time gaps, indicating a 600-meter horizontal resolution with a plane speed of 60 meters per second. The numbers of measurements recorded by the lidar during each daily flight session, as well as the general geographic area covered and range of light backscatter values measured, are indicated in Table 7 below. For a given location indicated by latitude-longitude coordinates, backscatter values are retrieved in units of (m^{-1} sr^{-1}) within 15-meter vertical 'range gate' intervals from the aircraft to near-ground, and total columnar AOT is calculated by the integration of the sum of the range gate backscatter values. The conversion from lidar extinction-to-backscatter at 359-nm to optical thickness at 0.55-μm is completed by multiplying first by 30 sr and then by 0.81

to convert measurements at a 359-nm wavelength to the MODIS 550-nm wavelength for fine particulate matter. The reported columnar AOT does not include absorption values as ideally desired, yet is assumed to be proportional to an AOT that includes both backscatter and absorption values (Dr. Christoph Senff, ERSL, personal communication). A typical plot of backscatter profiles for a portion of the flight that occurred on 9/06/2000 is shown in Figure 2. Each block shows the total backscatter value in 100-m layers and these values are color coded according to the legend shown in the upper left corner of the figure, where gray is lowest and purple is the highest total backscatter in the layer. (It should be noted that the lowest 100-m, near the Earth's surface contains fewer range gate intervals than the other layers.) Similar plots were made for each lidar flight but only a small portion of the data is shown due to the size of these files.

Table 7: Test period daily summary of lidar flight paths and durations.

Date	LIDAR Column Obs	Total Obs (%)	Focus Counties	Flight Duration	Per Column Lidar Value Mean/Max
8/25	1173	6.67 %	Harris, Galveston, Montgomery (Central)	5.11 hrs	.0105/.027
8/26	632	3.59 %	Harris, Brazoria, Chambers, Grimes (N/S)	2.34	.0103 / .015
8/28	1941	11.03 %	Harris, Grimes, Polk, San Jacinto (N)	6.00	.0136 / .096
8/29	2222	12.63 %	Harris, Liberty, Chambers, Jefferson, Hardin (E)	6.69	.0109 / .015
8/30	1766	10.03 %	Harris, Galveston, Chambers (SE)	6.00	.0117 / .014
8/31	1313	7.46 %	Harris, Brazoria, Chambers, Galveston (S)	6.75	.0133 / .016
9/01	2066	11.74 %	Harris, Liberty, Chambers, Jefferson, Galveston (SE)	6.32	.0127 / .016
9/03	1701	9.67 %	Harris, Liberty, Chambers, Jefferson, Galveston, Brazoria (S)	5.18	.0146 / .043
9/06	1976	11.23 %	Harris, Galveston, Brazoria, Fort Bend, Matagorda, Jackson, (SW)	6.90	.0189 / .052
9/07	1383	7.86 %	Harris, Galveston, Brazoria, Fort Bend, Matagorda, Jackson, (SW)	4.53	.0131 / .022
9/12	1426	8.10 %	Harris, Galveston, Montgomery, Chambers, Fort Bend (Central)	6.12	.0121 / .035
Total	17599	100%		61.94	.0129 / .096

The vast majority of backscatter values in all the 15-meter vertical 'range gates' fell within a narrow measurement range for this time period. Ninety-five percent of the observations fell between 0 and 0.02 while 70% of backscatter values fell between 0.011 and 0.015 (total column). Following transformation of the backscatter values to the corresponding MODIS satellite-measured AOT at 550-nm, the total lidar columnar AOT showed a broader distribution with 95% of observations between 0.21 and 0.6, and 60% of adjusted values between 0.251 and 0.35 Our preliminary analysis includes lidar-detected air columns with a minimum of 168 measurements per column, covering a vertical distance of at least 2520 meters.

Figures similar to that shown in Figure 3 (for September 6, 2000) were created using the GIS software package ArcIMS to show composites of Terra MODIS data and the flight-paths of the NOAA aircraft used to collect lidar data for several days during TXAQS 2000. For three days (August 26, September 3, and September 12) valid MODIS AOT

Figure 2. Vertical structures of aerosol profiles are evident in the graphical presentation of airborne lidar backscatter profiles shown for a portion of the flight that occurred on 9/6/2000.

Date	06 September 2000																			
LiDAR	16.75 - 17.25 UTC			Terra Satellite Overpass: 1720 UTC																
Backscatter m^{-1} sr^{-1}	CDT Hour Time																			
Vertical Bin 100m	12:00 PM		1:00 PM																	
Time UTC -->	16.763	16.765	17.177	17.179	17.182	17.185	17.193	17.196	17.199	17.202	17.204	17.207	17.210	17.213	17.215	17.218	17.221	17.224	17.227	17.257
Latitude	29.801	29.806	29.454	29.448	29.441	29.435	29.416	29.410	29.404	29.398	29.391	29.385	29.379	29.373	29.366	29.360	29.354	29.347	29.341	29.272
2601_2700			171	183	188	193	162	172	170	159	153	172	152	156	153	158				117
2501_2600	205	211	179	188	192	202	173	177	176	163	158	174	161	161	160	167	153	159	153	121
2401_2500	214	215	184	195	204	208	180	183	182	171	167	182	171	172	170	177	161	167	158	120
2301_2400	213	219	189	202	209	212	185	192	186	176	168	185	174	176	171	181	169	168	164	127
2201_2300	221	223	195	201	217	223	188	187	194	182	175	195	177	177	179	184	167	168	165	128
2101_2200	218	225	194	211	218	232	189	192	204	184	181	197	186	185	186	193	180	179	176	141
2001_2100	236	239	218	237	235	247	212	213	221	201	194	213	200	209	206	215	196	196	190	145
1901_2000	324	298	333	329	336	310	314	316	312	297	295	320	303	310	315	311	263	260	246	149
1801_1900	696	600	451	466	469	477	430	443	430	415	398	416	380	368	361	374	369	380	362	276
1701_1800	879	860	505	522	514	547	463	467	459	428	410	451	425	407	417	411	372	365	359	318
1601_1700	905	901	561	661	681	778	575	543	547	455	425	431	402	388	390	408	455	487	465	375
1501_1600	903	923	732	835	898	1064	836	857	809	618	492	482	429	421	498	715	790	825	820	654
1401_1500	960	1002	978	1109	1149	1193	935	921	938	843	762	822	718	712	808	981	937	925	936	735
1301_1400	1065	1127	1084	1112	1153	1207	960	951	998	936	925	1102	1041	986	1041	1078	1005	962	981	711
1201_1300	1070	1099	1075	1108	1138	1170	1001	1014	1034	1014	981	1110	1065	1042	1003	1021	921	908	888	638
1101_1200	1009	1040	1025	1091	1100	1126	1021	1015	1047	976	954	1023	964	972	946	950	872	858	843	608
1001_1100	954	987	971	1026	1063	1086	941	967	980	928	911	970	916	911	922	912	832	821	798	571
901_1000	906	932	912	1023	1006	1074	890	932	953	889	865	953	938	914	928	880	795	763	793	579
801_900	880	1085	1051	1479	1168	1504	942	1018	1075	935	852	994	974	961	973	949	793	769	716	549
701_800	983	1409	1490	1918	2191	2860	2380	2500	2674	1619	1629	1824	1457	1316	1294	1041	855	871	738	468
601_700	1159	1327	1460	1654	2358	2716	2470	2365	2511	2177	2169	2255	1752	1643	1557	1318	1268	1684	1189	805
501_600	1187	1217	1391	1411	1752	1865	1802	1685	1656	1679	1660	1712	1525	1452	1415	1287	1440	1800	1497	1292
401_500	1144	1137	1170	1238	1251	1270	1321	1350	1274	1239	1216	1181	1204	1173	1172	1177	1235	1241	1239	1279
301_400	1074	1068	1076	992	1006	1006	880	854	974	985	1008	1044	1035	1036	1041	1048	980	977	996	963
201_300	927	950	797	693	785	548	502	661	791	719	740	900	782	848	962	1092	708	763	806	608
101_200	837	901	682	482	625	517	276	429	552	448	517	706	628	663	772	755	583	421	697	393
0_100	877	943	0	0	0	0	0	0	0	0	0	0	0	0	0	700	480	262	533	322

retrievals were not available due to extensive cloud cover or other issue. True color images of the MODIS data are in the left panels of each figure along with gray-scale MODIS aerosol optical thickness values in the right panels, where brighter gray-shades indicate higher retrieved AOT values. In both panels, CSR has added demographic features along with CAMS locations, denote by red boxes, especially in the Houston-Galveston area. (We did not include the separate MODIS AOT products for ocean backgrounds, since all aircraft observations were made over land.) Trajectories are also shown in each of the figures while the impact of cloud cover on AOT retrievals can be seen in the last two datasets. Finally, the growth in MODIS AOT analysis area, between the nominal 10-km value at nadir and the edge of swath, can be seen in comparing the 9/06 and 9/07/2000 analyses. (Maps for additional days of TXAQS-I are shown in the 2006 Annual Report on this project.)

Figure 3. Maps of MODIS AOT, CAMS locations, and airborne lidar flight path for 9/06/2000.

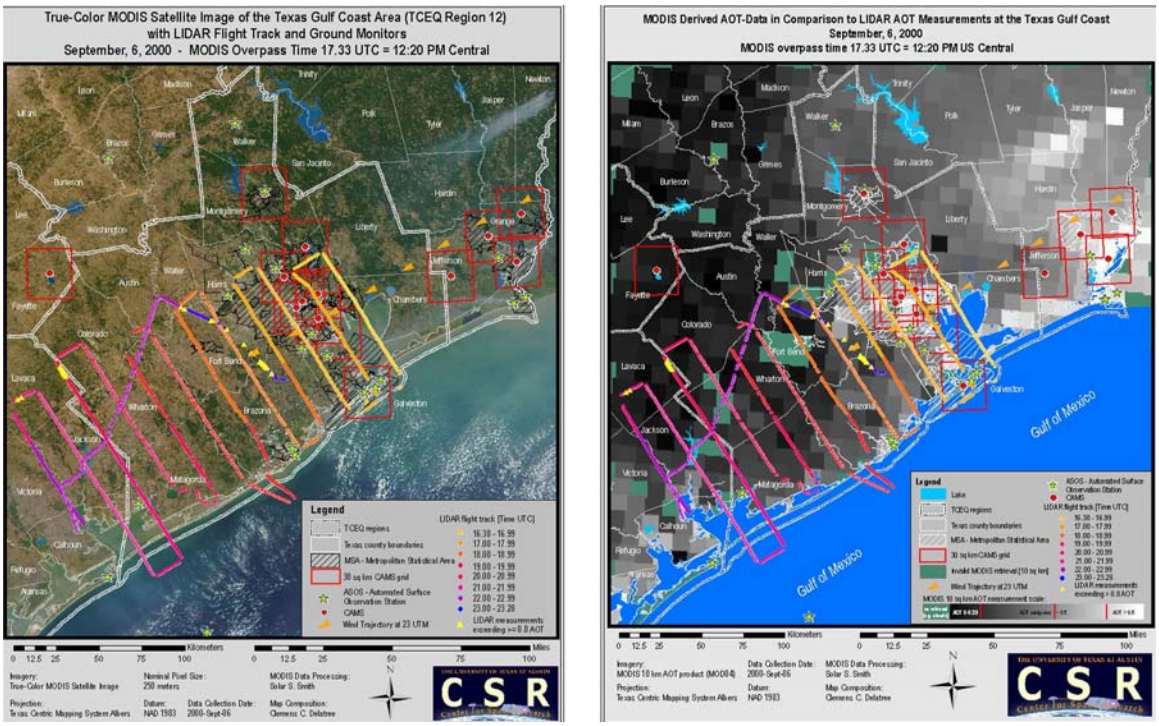

During the August-September 2000 time period, nine CAMS stations were within reasonable proximity of the lidar flight path. For each lidar measurement the three nearest stations and their time-coincident hourly $PM_{2.5}$ average values were identified. Since the number of CAMS actively measuring $PM_{2.5}$ concentrations was relatively small in 2000 and some stations were not regularly reporting measurements at that time, most of the ground-based $PM_{2.5}$ measurements were not within reasonable proximity of the lidar observations. In addition, several stations recorded measurements sporadically, so that (although a 1-hour $PM_{2.5}$ average may have been reported at certain times of day) a sufficient number of hourly averages were not present for a 24-hour daily average $PM_{2.5}$ reading to be recorded. Of 17,599 lidar total column observations, only 21 measurements occurred within one kilometer of an active $PM_{2.5}$ CAMS station, 70 observations were

within two kilometers of a CAMS, 421 within 5 kilometers, and 1371 observations (7.8%) within 10-km of a CAMS site.

The lidar measurements were matched to ground-based $PM_{2.5}$ measurements by rounding the time of the former to the nearest hour and retrieving the closest corresponding $PM_{2.5}$ hourly average from among the three CAMS sites nearest to the lidar flight location. Measurements of $PM_{2.5}$ at five-minute intervals, if these were made available by TCEQ, could be used to reduce the temporal gap between the compared readings.

The results of correlation tests between lidar readings of the 8/26-9/12/2000 period and the closest $PM_{2.5}$ readings at various spatial distances is shown by Figures 4-5. These figures show that the relationship between the lidar measurement and corresponding ground-based $PM_{2.5}$ hourly average weakens as the radial distance and number of observations increases. The strongest Pearson correlation coefficient is 0.81 for comparisons within one kilometer, 0.71 at two kilometers, 0.52 at 5-km. and 0.5 at 10-km radius. These analyses show the impact that horizontal variations in aerosol concentration have on AOT-$PM_{2.5}$ correlations and suggest that satellite-derived AOT observations are best used to monitor larger-scale pollution events rather than smaller scale, highly non-homogenous events.

Figure 4. Correlation between lidar AOT and $PM_{2..5}$ measured within 1-km (left) and 2-km (right) of the NOAA aircraft flight path.

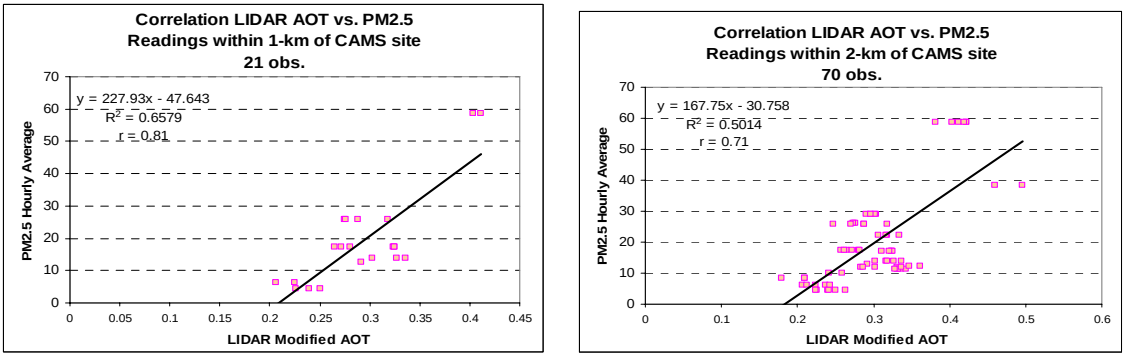

Figure 5. Correlation between lidar AOT and $PM_{2..5}$ measured within 5-km (left) and 10-km (right) of the NOAA aircraft flight path.

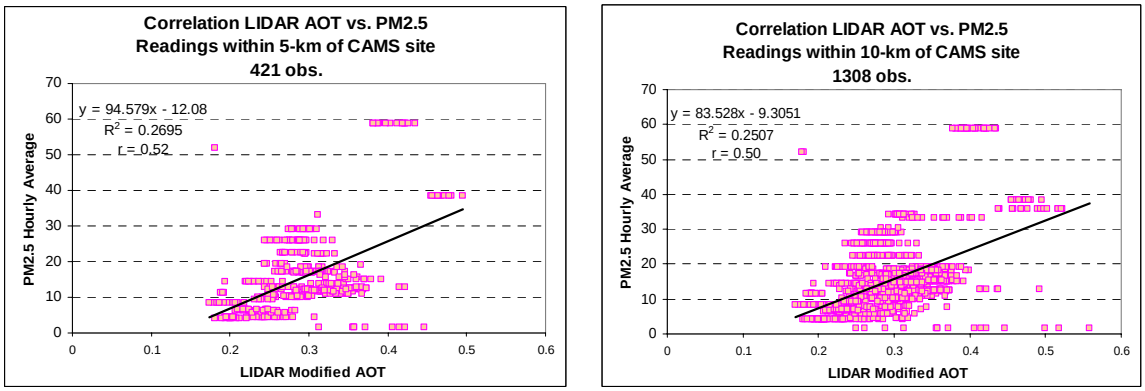

The airborne lidar observations collected during TXAQS 2000 were also used to assess the value of aerosol profile information for improving correlations between MODIS AOT and CAMS $PM_{2.5}$ data. In particular, this part of the study sought to (1) determine if the vertical motions in the trajectory forecast could be used to gain insights into the location of the maximum aerosol concentration in the profiles and (2) assess the value of information about the aerosol profile for further improving AOT-$PM_{2.5}$ correlations. To complete this study, it was first necessary that the airborne lidar data be referenced from the Earth's surface rather than from the aircraft. Each value within an aerosol profile, as shown in Figure 2, was converted from a measurement by distance from the plane (as the plane ascends and proceeds along a flight track) to an indication of the distance from ground level at the time the observations were collected. This conversion allowed the backscatter and optical depth values to be compared at similar altitudes. To evaluate total backscatter in an air column, values are integrated over the (variable) column height by adding backscatter values retrieved across range gates, multiplying each value times its range gate height. For a given spatial area that has numerous backscatter retrievals in an atmospheric layer, these values are averaged over the horizontal spatial grid, multiplying by range gate height, and sum the results for multiple vertical range gates. Each measurement was then classified into range gate 'bins' of 10, 15, 25, 50, 100, 250, 500 and 1000 meters in height, as well as horizontal spatial grids of one-tenth, one-quarter, and one-half degrees. The exact time of each measurement was classified by centering the time on the closest-hour and half-hour [15 minutes before and after 1730 UTC (1716 – 1745) classified as 1730], and converted to local central daylight savings time (12:30 PM). Within these classifications, measurements are aggregated to identify distinct variations in aerosol accumulation in the vertical atmospheric profile over an area covered by the flight path.

Shown in Table 9 are the aerosol profiles generated on August 28 (left) and September 6 (right). Missing observations are accounted for by averaging all available observations and using this value to determine the backscatter for a layer. This process introduces some unavoidable error. These results also show that the estimated lidar-derived AOT values along the flight path ranged between 1.545–2.930 on 29 August 2000 and 1.342-1.977 on 6 September 2000. In both cases, the majority of the backscatter values come from the lowest 100-m of the profile and are considered to be suspect, perhaps due to increased calibration errors for layers near the Earth's surface.

Trajectories were generated for key portions of the flight path on each day with a terminus near the location of heavy pollution reported by the aircraft, as shown in Figure 6 for September 6, 2000. The starting location of the air parcels that ended at about 100-m, 500-m. and 1-km above the ground at this terminus are shown in red, blue and green respectively. The trajectories show that the vertical component of the trajectory (shown in the bottom insert) in the lowest part of the atmosphere has been descending during the 1200-1800 UTC timeframe when MODIS Terra flew over the region. This atmospheric subsidence helps keep the maximum aerosol concentrations near the Earth's surface in agreement with the airborne lidar observations shown in Table 9 on this date. Thus we recognize that aerosol vertical profile information can be inferred from the vertical motion vectors in the trajectory forecast fields.

Table 9. Aerosol profiles generated from airborne lidar observations on August 28 (left) near CAMS #78 and September 6, 2000 (right) over Colorado-Lavaca counties (north of Victoria).

	Date 8/28/00				Date 9/06/00	Backscatter (BSV) * 10^{-6}, units m^{-1} sr^{-1}			
Time UTC	22.384	22.389	22.392	22.395	Time UTC	20.804	20.807	20.810	20.813
Latitude	30.690	30.691	30.693	30.696	Latitude	29.443	29.437	29.431	29.425
Longitude	-95.435	-95.422	-95.415	-95.408	Longitude	-96.682	-96.678	-96.674	-96.670
2601_2700	597	460	462	556	2601_2700	126	98	103	104
2501_2600	662	499	520	612	2501_2600	148	127	131	128
2401_2500	669	545	584	630	2401_2500	172	151	156	151
2301_2400	695	552	589	626	2301_2400	183	161	170	167
2201_2300	647	556	565	585	2201_2300	276	184	193	185
2101_2200	579	543	538	557	2101_2200	441	278	203	230
2001_2100	558	533	513	536	2001_2100	575	434	298	302
1901_2000	551	505	498	506	1901_2000	672	665	493	361
1801_1900	519	478	486	486	1801_1900	748	743	691	546
1701_1800	505	487	494	482	1701_1800	789	755	761	751
1601_1700	481	459	439	477	1601_1700	830	788	813	800
1501_1600	463	461	472	470	1501_1600	841	790	811	827
1401_1500	462	460	477	446	1401_1500	843	820	834	857
1301_1400	455	468	461	484	1301_1400	853	827	855	882
1201_1300	459	487	486	466	1201_1300	885	812	842	877
1101_1200	489	445	489	461	1101_1200	896	807	855	920
1001_1100	476	447	466	481	1001_1100	899	847	866	920
901_1000	416	481	516	456	901_1000	920	872	943	954
801_900	478	454	467	439	801_900	844	848	880	998
701_800	523	455	492	479	701_800	962	956	1011	976
601_700	486	427	533	462	601_700	1004	929	967	1002
501_600	466	438	511	515	501_600	967	932	982	980
401_500	511	490	489	515	401_500	1102	1083	1089	1062
301_400	527	532	538	514	301_400	1087	1117	1138	1141
201_300	554	549	655	569	201_300	1109	1118	1117	1219
101_200	10,199	11,272	5119	6541	101_200	1224	1327	1318	1258
0_100	85,280	66,858	45,795	101,358	0_100	62,057	59,464	48,826	36,699
Sum Column Loading	108,705	90,371	63,652	120,708	Sum Column Loading	81,454	77,932	67,346	55,294
Est. AOT @ 550nm	2.638	2.193	1.545	2.93	Est. AOT @ 550nm	1.977	1.891	1.634	1.342

Figure 6. Trajectory for air parcels terminating near Houston Conroe CAMS site on 8/28/2000 at 2300 UTC.

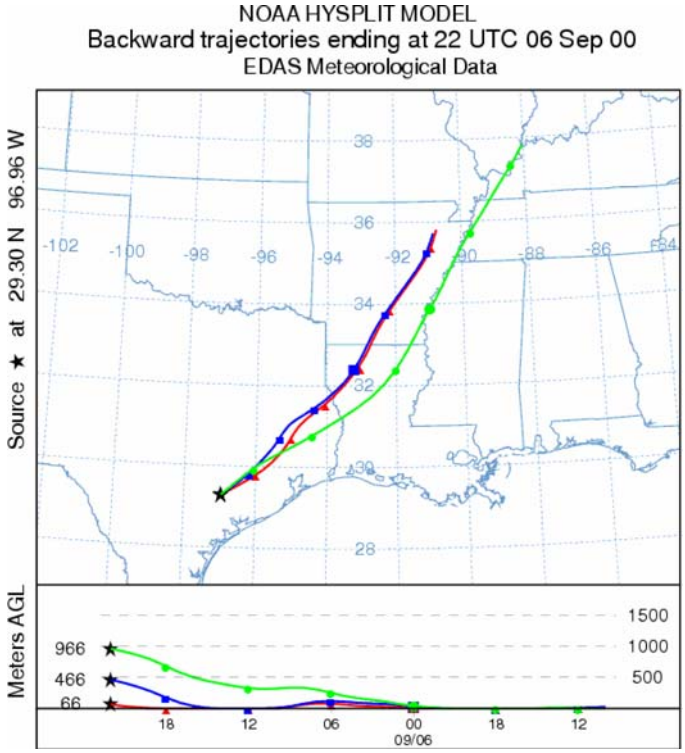

Finally, comparisons are made between MODIS AOT and CAMS $PM_{2.5}$ observations for all match-up occurring during the TXAQS-I data collection and for only those days where the vertical motion vectors reveal prolonged subsidence. These results are shown in Panels (a) and (b) respectively in Figure 7. These results show that satellite-based AOT retrievals and ground-based $PM_{2.5}$ observations are more highly correlated when the aerosols are concentrated near the Earth's surface. In addition, the trajectory data in Figure 6 suggest that the vertical motion in the IDEA trajectories could provide useful information to predict when the aerosols are concentrated in the lower levels of the atmosphere.

Figure 7. MODIS AOT-$PM_{2.5}$ correlations for all matchups during TXAQQ-I (left) versus days when subsiding air near the Earth's surface is implied by trajectory forecasts (right).

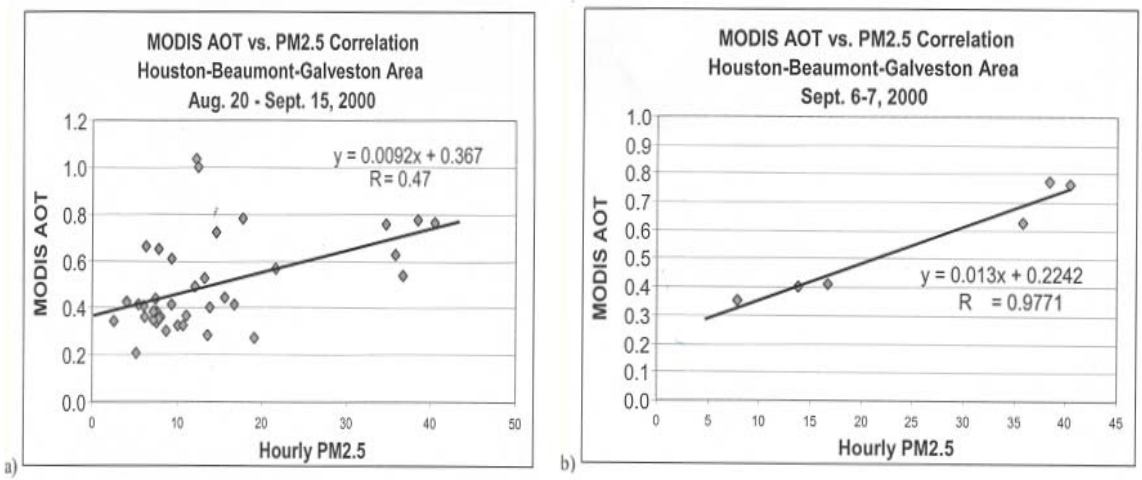

The synergy from results obtained during the analysis of airborne lidar data collected during the TXAQS-I project accelerated CSR progress under this NASA research project. In previous articles, CSR has postulated that AOT-$PM_{2.5}$ correlations could be improved through the classification of pollution types which are characterized by the meteorology the govern transport process. In effect different correlations were expected to exist for events of continental haze, Saharan dust, smoke from biomass burning across Central American, and West Texas dust events. Through the analysis of the vertical component of trajectories generated with the NOAA Hysplit Model, CSR has now obtained the first confirmation, using airborne lidar data collected during TXAQS-I, that insights can be obtained into the vertical concentrations of the aerosol profiles using the vertical motion vectors of the trajectory model (Hutchison et al., 2007).

CSR is extending its currently multi-year MODIS imagery and AOT datasets to include both MODIS Aqua and Terra data for additional years. In addition, we are attempting to gain access to aerosol profile information from Calipso to serve as truth measurements for the aerosol profile data; however, to date only figures of aerosol profiles are available via the EDIS, not the profile data needed for our analyses.

3.2 Objective 2: Integrate MODIS AOT Products into Regional, Short-term Air Quality Forecasts

In our original proposal, CSR proposed to develop a backward trajectory forecast model to generate short-term air quality trend forecasts from MODIS AOT observations (Hutchison et al., 2004). However, shortly after this project was awarded to CSR, we learned that NASA has already developed such a backward trajectory model and used NCEP forecast fields as input data. Thus CSR obtained the IDEA (Infusing Satellite Data into Environmental Applications) trajectory forecast model (Al-Saadi et al., 2005) from NASA, which expedited the implementation of air quality forecasts for TCEQ.

The NASA trajectory-based forecast model is known as IDEA (Infusing satellite Data into Environmental Applications) and had a forecast domain that covered much of the continental US. However, the TCEQ forecast domain extended further south into Central America so the software was modified at CSR to cover this larger domain. In addition, CSR provide a capability for TCEQ analysts, at their request, to modify AOT analyses, e.g. by manually adding pollution observations into the satellite analysis field.

CSR has provided issuing daily, real-time AOT forecast guidance for use at TCEQ in 2006. In addition, CSR provided training sessions to TCEQ on interpretation of data products and the proposed utilization of these data in a trend forecast, while CSR continued to study ways to improve MODIS AOT-$PM_{2.5}$ correlations that were needed to make more quantitative air quality forecasts for these products. Thus, in addition to the MODIS data available at the CSR website noted in Section 1.1, CSR also provides MODIS full-resolution images in sectors as required by TCEQ along with trajectory-based MODIS AOT forecasts based upon NASA's IDEA software package. TCEQ and their customers can access the MODIS imagery and air quality forecast guidance at the following websites:
http://www.tceq.state.tx.us/compliance/monitoring/air/monops/modis.html
http://www.tceq.state.tx.us/compliance/monitoring/air/monops/modis_cuts.html

While CSR has provided many useful products to TCEQ, the inability to retrieve AOT values from MODIS under cloudy conditions has proven to be a severe limitation to the trajectory-based forecast approach. The large amount of cloud cover that typically exists over the Southwestern US and Gulf of Mexico regions was found to be the major limitation for this trajectory-based air quality forecast tool. Cloud cover frequently impacts much of the TCEQ forecast region by limiting the number of AOT retrievals available for a given MODIS datasets. In addition, clouds further impact the number of "good" pixels available for use in the AOT–$PM_{2.5}$ correlations. The CSR 2D spatial requirement that 16 (or 6) valid AOT pixels be present in a 50x50-km^2 (or 30x30-km^2) analysis region, as discussed earlier, was seldom satisfied.

In addition, as real-time air quality products from CSR have become increasingly useful, the requirements identified by air quality managers in Texas continue to evolve and expand. TCEQ personnel are increasingly required to generate more accurate and extensive air quality forecasts for Texas, including forecasts of 4-day $PM_{2.5}$ predictions along with PM_{10}, and O_3. TCEQ has also identified new interests in air quality that include CO, SO_2, NO_X, all of which are needed to for accurate AQI (Air Quality Index) analyses and forecasts but cannot be generated from the trajectory-based AOT forecast

model. Thus, TCEQ currently lacks a single integrated tool that incorporates meteorological, air quality, and photo-chemical observations and models into their DSS.

As a result, early in 2007, CSR began to examine the feasibility of generating air quality forecasts from a full-physics model. The goal was to evaluate a model that would incorporate the cloud fields generated from MODIS data at CSR along with the ground-based $PM_{2.5}$ observations into the forecast logic. Working in conjunction with Dr. Yang from the UT Department of Geosciences, CSR settled on the Weather Research and Forecasting model with CHEMistry components (WRF-CHEM) as a proposed forecast tool to overcome deficiencies in the trajectory-based forecast model.

Discussion between CSR and TCEQ were held and it was agreed that WRF-CHEM offered the best option for generating a deterministic air quality forecast. TCEQ was particularly interested in the added capabilities of this model to predict additional key pollutants, which are becoming increasingly important at TCEQ, including O_3 and $PM_{2.5}$ along with CO, SO_2, and NO_X. A proposal was submitted under ROSES 2007. It was learned in mid-December that our proposal was rejected.

In that proposal, CSR offers to quantitatively evaluate the output of the WRF-CHEM as a more robust DSS tool for air quality managers in Texas. On the positive side, the WRF-CHEM model (1) incorporates both satellite and ground based observations into the forecast scheme (2) is not adversely affected by clouds, (3) includes aerosol-cloud feedback mechanisms that regulate actinic fluxes which regulate pollution formation and destruction mechanisms through the full-physics WRF-CHEM modeling system. On the negative side, the WRF/MM5 meteorological models are not recognized to accurately specify cloud fields in analyses and predictions only become worse in time (Byun, personal communication). Thus, CSR has proposed to develop and quantitatively demonstrate the capability of the full-physics WRF-CHEM model in order to create a deterministic forecast of key pollutants monitored by TCEQ including O_3 and $PM_{2.5}$ along with CO, SO_2, and NO_X. The value of the enhanced model would be quantified through comparisons with the existing model using data collected by EOS A-Train (afternoon train) satellites, including MODIS, CloudSat, and Calipso (Cloud-Aerosol Lidar and Infrared Pathfinder Satellite). Improvements in the TCEQ air quality DSS would be demonstrated through comparisons with their current capability which continues to rely heavily upon ground-based observations collected at CAMS facilities.

3.3 Objective 3: Generate MODIS Cloud Boundaries and Establish Performance Accuracies

As previously noted, cloud fields impact air quality models in various and profound ways, including aqueous chemistry pathways, cloud-aerosol interactions, surface energy and radiation balances, and radiative fluxes for photochemistry (photolysis rates). Historically most chemistry models, such as the Comprehensive Air quality Model with Extensions (CAMx – See http://www.camx.com) have assumed cloud-free conditions to generate the actinic fluxes that regulate photochemical reactions. More recently, the air quality modeling community has aggressively sought to remedy this situation by developing a modular system that facilitates the incorporation of improved input data fields, such as aerosol and cloud data fields. Still, the accurate specification of cloud boundaries remains a significant challenge even for the most advanced models, such as the Models-3 Community Multiscale Air Quality (CMAQ) modeling system (Byun and

Ching, 1999). The problem is exacerbated by the difficulty in obtaining accurate 3-dimensional cloud analyses using existing technology (D. Byun, personal communication).

CSR initiated this task to create cloud boundaries, i.e. cloud top heights and cloud base heights, from MODIS data with accuracies suitable for use in air quality modeling. While efforts are ongoing to fully characterize the performance of MODIS cloud top parameters, which are contained in the MOD06 product, recent publications suggest that MOD06 cloud top heights can differ from truth measurements by as much as 1.5 km for low clouds and 2.5 km for high clouds when compared to lidar observations (Naud, et al., 2004). In addition, others have found that the MOD06 cloud top temperatures of high clouds can be in error by 20-K when compared to millimeter wave cloud radar (MMCR) observations which serve as truth (Mace et al., 2005). [Note: there is no cloud top height in the MOD06 product. For higher-level clouds, the algorithm first solves for cloud top pressure using the CO2 slicing algorithm (Menzel et al., 2005) which can be converted directly into cloud to height. For lower-level clouds, the algorithm first retrieves cloud top temperature values that must then be related to cloud top pressures and then cloud top height.] Air quality models require cloud boundaries within an accuracy of ± 50-m (Mark Z. Jacobson, personal communication). In addition, MODIS generates no cloud base height product; therefore, algorithms developed by PI Hutchison for the National Polar-orbiting Operational Environmental Satellite System (NPOESS) were proposed for this research.

The approach developed to retrieve cloud base heights for NPOESS is illustrated in Figure 8 and now briefly summarized. The retrieval of cloud base height solely from MODIS or VIIRS data converts cloud optical thickness into geometric thickness using the cloud optical properties data product, i.e. effective particle size and optical depth in the MOD06 product. Then, cloud base height is found by subtracting cloud thickness from cloud top height, as presented in Section 2.2.2.2 (Hutchison 1998, 2002). There are two algorithms that differ slightly according to cloud top phase; however, only the algorithm for water clouds is presented in this text.. This approach to retrieving cloud base heights has been successfully demonstrated with data collected during the daytime by NASA's MODIS sensor and provides a complete description of the algorithms used when ice clouds are present (Hutchison, 2002).

More recently, the approach was shown to provide accurate retrievals of cloud thickness and cloud base height with nighttime MODIS data with the new VIIRS COP algorithms (Hutchison et al., 2006) as shown in Figure 9 and 10. In Figure 9 are shown cloud boundaries recorded by the millimeter wave cloud radar (MMCR) located at Southern Great Plains (SGP) Atmospheric Radiation Measurement (ARM) Site in Oklahoma (left) which served as truth for these comparisons. In the right panel, cloud base heights retrieved from COP values generated with the VIIRS algorithms are shown for this nighttime MODIS dataset. Blue dashed lines in the right panel show the accuracy requirement for cloud base height in the NPOESS program, which is ± 2-km. The final cloud base height, shown as green in the right panel, shows the product just within the NPOESS accuracy requirement.

Figure 10 shows the cloud thickness retrieved with Equation 2 in Section 2.2.2.2 to be nearly identical to the cloud thickness recorded by the MMCR. These results confirmed

Figure 8. Architecture for retrieval of 3-dimenisional cloud fields (From Hutchison, 2002).

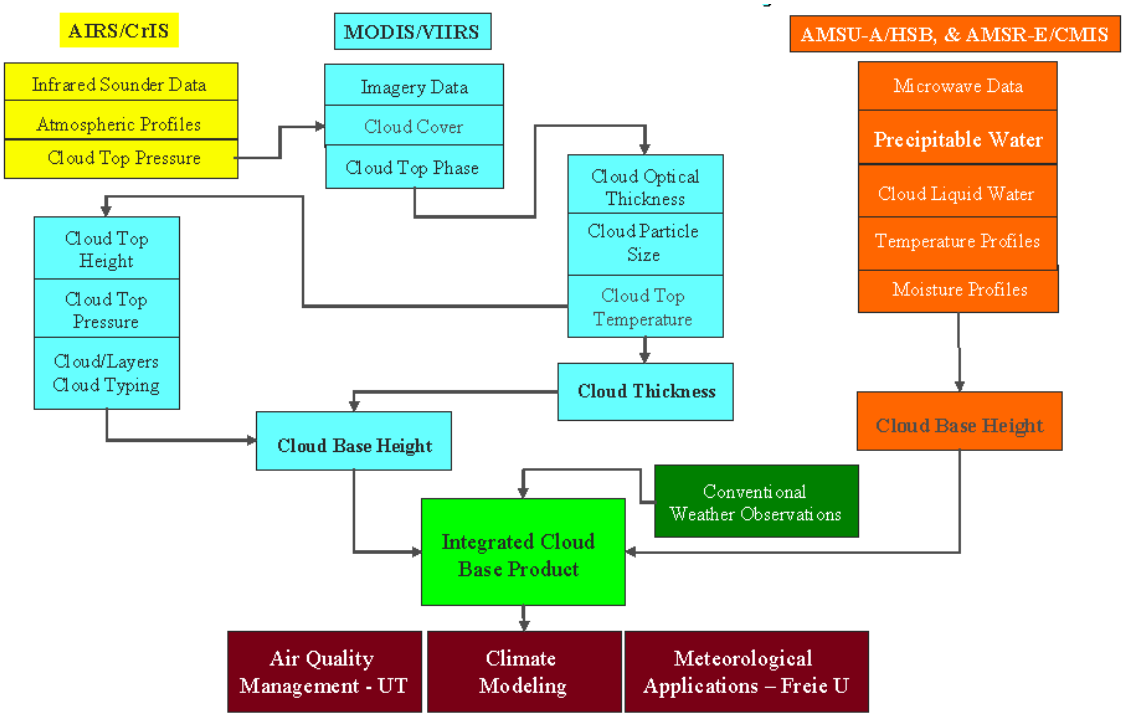

the error analysis conducted for NPOESS (Hutchison, 1998) that predicted the major source of error in the retrieval of cloud base height would result from the inaccuracies in the specification of cloud top height, not the retrieval of cloud thickness from the cloud optical properties. However, there are additional error sources in the retrieval of cloud base height from satellite data. Measurements show the value of LWC varies between about 0.20 g m^{-3} and 0.45 g m^{-3}, as a function of cloud type. It is difficult to accurately predict cloud type with automated cloud algorithms. In addition, this approach to retrieving cloud base height assumes liquid water content (LWC) is constant throughout the vertical extent of the cloud, which is not correct (Slingo1982; Martin et al.1994). This assumption becomes increasingly less reliable as clouds become thicker. However, these same error budgets predicted that inaccuracies in cloud top heights represented the largest source of uncertainty in the retrieval of cloud base heights (Hutchison, 1998). In these error budgets, it was assumed that the accuracy of cloud top height retrievals would vary between 1-2 km with cloud phase and cloud optical thickness. Larger errors would be associated with optical thin, ice clouds (NPOESS VIIRS SRD, 2000). These NPOESS errors budgets, coupled with verification of the MODIS cloud top heights by Naud et al. (2004) implied that cloud boundaries would lack the accuracy required for use in air quality applications (Hutchison et al., 2006).

CSR further examined errors in cloud boundaries derived from the MOD06 product using the VIIRS cloud base height algorithm in a study that utilized match-ups between MODIS and SGP ARM site datasets. The study was undertaken to analyze data for a

Figure 9. Cloud base height from MMCR observations at SGP ARM Site Oklahoma (left) and comparisons of truth with retrieved cloud thickness from nighttime MODIS data (right) [From Hutchison et al., 2006].

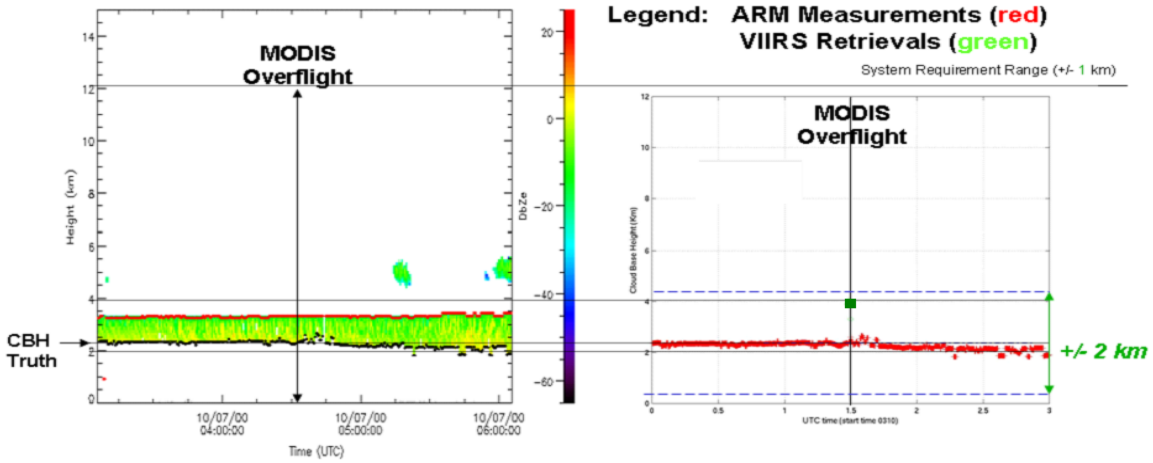

Figure 10. Time series of cloud thickness from MMCR observations at SGP ARM Site Oklahoma and cloud thickness retrieved using MODIS nighttime optical properties [From Hutchison et al., 2006]

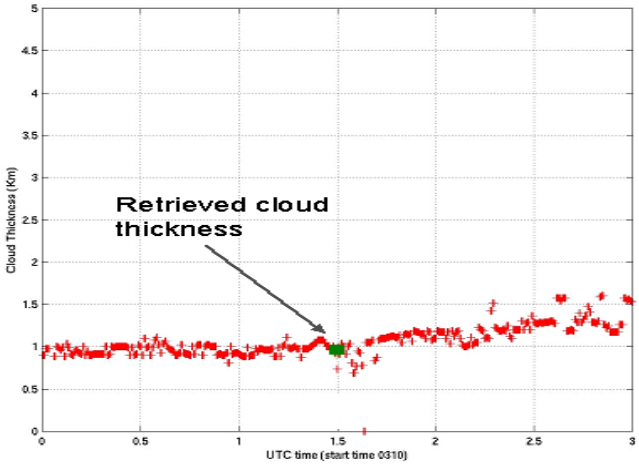

variety of cloud systems that had cloud base heights below the maximum height reported by FAA automated surface observing system sites, i.e. 12,000 ft or 3.66 km. Several years of MODIS were previewed in an attempt to identify suitable cloud patterns that remained in stratiform layers by the time MODIS/Terra overflew the SGP ARM facility. Unfortunately, only a few cases were found suitable for use in this study after examining MODIS, ground-based, and in-situ observations. These cases occurred primarily in spring and fall months when single-layered, stratiform clouds can persist until MODIS overflight of the ARM site. (During the summer months, more intense solar heating results in a higher occurrence of convective clouds while the winter brings multi-layered cloud patterns which were not suitable for the study.) On the other hand, this very limited dataset contains a good range in cloud thickness values, between about 50 - 1700 m, with

distinct cloud boundaries in the truth data, which are shown in Table 10. Cloud base heights were derived from ceilometer data collected at MODIS overflight of the ARM site. Two separate measures of truth data were available for cloud top heights: MMCR data and radiosonde. MMCR data are especially useful when cloud top heights are not near the Earth's surface and as noted previously, the cloud top in the radiosonde data was distinct. (The radiosondes are released at SGP ARM site one-hour prior to MODIS overflight of the area.)

Table 10. Truth data for cloud boundaries derived for MODIS data sets used in study [From Hutchison et al., 2006b].

MODIS Granule ID			Cloud Top Temperature (K)	Cloud Base Height (m)		Cloud Top Height (m)	
Case No.	Date (dd/mm/yy)	Time (UTC)	Radiosonde	MMCR	Ceilometer	MMCR	Radiosonde
1	12/02/2000	1725	264.4	1100	1137	1300	1233
2	04/02/2002	1635	274.3	1450	1507	2250	2372
3	04/08/2002	1735	278.8	400	387	1400	1312
4	04/26/2002	1725	278.3	350	284	2200	2469
5	04/08/2003	1705	262.4	1000	1312	1700	1523
6	11/08/2003	1805	272.7	200	149	2400	2219

The cloud top height for each MOD06 product was calculated at CSR from the cloud top pressure (P_{CT}) and the observed surface pressure (P_{Sfc}) at the SGP ARM site using Equation 5. In this equation, Z_{Sfc} represents the height of the surface, Z_{CT} is the height of the cloud top, g is the gravitational constant (9.8065 m sec^{-2}), R is the gas constant for dry air (286.8 j kg^{-1} K^{-1}) and T_v is the virtual temperature (K) of the layer. In each case T_v is taken as the mean temperature between the surface and the cloud top in the truth data. Cloud top heights calculated from the MOD06 data are shown in column 6 in Table 11 while columns 7 and 8 show differences between the MOD06 cloud top height and the truth measurements.

$$Z_{CT} = Z_{Sfc} + R*T_{v(mean)}/g * Ln(P_{Sfc}/P_{CT}) \quad (5)$$

Inaccuracies in the calculation of cloud top height with Eq. 5 can result from variations in humidity profiles and cloud liquid water content. Therefore, each MOD06 cloud top pressure shown in Table 11 was converted into a corresponding cloud top height using only the NCEP operational analysis fields for 1800 UTC on the day of each MODIS overflight. The relative error in cloud top heights calculated from the MOD06 cloud top pressures using these two approaches was less than one percent.

Results shown in Table 11 are in good agreement with those in publications by others (Naud et al., 2004; Welch et al., in press). Errors in MODIS cloud top heights are generally between 500-1.9 km for water clouds. On rare instances, e.g. Case 1, smaller errors were observed in the MOD06 product.

The reason for these large errors in MODIS cloud top heights was also identified during this study. First, it is necessary to understand better the MOD06 cloud top parameter retrieval algorithms. There are two approaches used in the MODIS algorithms to retrieve the representative cloud top (temperature and pressure) parameters for each 5x5 MODIS pixel-group that is reported in the MOD06 product: The primary algorithm relies upon the CO_2 slicing method. [See Menzel et al., (2002) for a more complete discussion of the MOD06 product.] The CO_2 slicing method retrieves cloud top pressure directly which can be converted readily to cloud top height. This method is used as long as the cloud signal in the MODIS 13-μm bands remains sufficiently strong, i.e. cloud top heights are above about 3 km (Naud et al., 2003) or lower than about 700-mb (Platnick et al., 2003). The alternative approach is used when the cloud signature in the MODIS 13-μm bands become weaker. With this approach cloud top temperature is retrieved first using the 11-μm brightness temperature data, i.e. the T_{B11} method. This method assumes each cloud has an emissivity of unity and retrieves cloud top.

Table 11. MODIS cloud boundaries derived from MOD06 product alone [Update to table from Hutchison et al., 2006b].

Case No.	Cloud Top Temperature (5-km) reported in MODIS Product (K)	Cloud Top Pressure (5-km) reported in MODIS Product (mb)	Cloud Optical Thickness (Center Pixel over ARM Site) reported in MODIS Product (n/a)	Cloud Effective Particle Size (Center Pixel over ARM Site) reported in MODIS Product (μm)	Cloud Top Height using Equation 1 and MODIS Cloud Top Pressure (m)	Difference between MODIS Cloud Top Height and Radiosonde Truth (m) (%)	Difference between MODIS Cloud Top Height and MMCR Truth (m) (%)
1	267.3	850	5.4	5.3	1280	47 (4%)	20 (1%)
2	273.0	850	49.1	8.3	1140	1233 (52%)	1111 (49%)
3	276.6	780	86.9	12.6	1805	493 (78%)	405 (29%)
4	278.1	920	70.4	8.7	544	1926 (78%)	1657 (75%)
5	260.6	645	30.8	8.4	3385	1870 (122%)	1693 (99%)
6	271.0	670	77.8	12.8	3162	942 (42%)	761 (32%)

In the retrieval of the cloud top parameters with these two MODIS algorithms, NCEP global, 1x1 degree latitude/longitude, 6-hourly analysis fields are vertically interpolated to 101 pressure levels of temperature and water vapor mixing ratio. Next, transmittance profiles are computed for each MODIS band used to retrieve cloud top pressure, i.e. MODIS bands 31 and 33-36. No horizontal interpolation is used except for surface temperature and pressure. Clear-sky radiances are then calculated along with CO_2-slicing computations. First, a "window channel" value is obtained, i.e. $T_{B11,}$ then the CO_2-slicing solution. If a CO_2 solution is not available, the window channel result will be reported as the cloud top pressure, which will be one of the 101 pressure levels, rounded to the nearest 5-mb increment (MODIS Cloud Team Member, personal communication).

During the course of our investigations, it was necessary to map the 1-km MODIS cloud optical properties (thickness and particle radius) fields into the MODIS 5-km resolution cloud top parameters (temperatures and pressures) fields that are contained in the MOD06 product. While great care was taken to ensure only stratiform clouds were included in the cases developed for this study, (through analysis of MODIS imagery and signatures, millimeter wave cloud radar (MMCR) and ceilometer observations at the ARM site), it was discovered that large variations occurred in the 25, 1-km resolution MODIS cloud optical thickness values found within a single 5-km resolution MODIS cloud top parameter field, as shown by the statistics in Table 12.

Table 12. Sample variations in MODIS 1-km cloud optical properties products found in the 5-km cloud top products for stratiform clouds observed over the SGP ARM site in Oklahoma.

Case	MODIS Product	Center Pixel	Mean	Median	Min	Max	Std.Dev.
1	Cloud Top Pres (mb)	850					
	Cloud Top Temp. (K)	267.30					
	Cloud Part Rad (μm)	6.27	5.35	5.27	4.49	6.82	0.61
	Cloud Optical Thick.	4.17	5.26	5.42	3.35	7.05	1.18
2	Cloud Top Pres (mb)	850					
	Cloud Top Temp. (K)	273.00					
	Cloud Part Rad (μm)	7.97	8.31	7.97	6.90	9.98	1.19
	Cloud Optical Thick.	47.77	49.14	47.77	31.49	70.64	10.86
3	Cloud Top Pres (mb)	780					
	Cloud Top Temp. (K)	276.55					
	Cloud Part Rad (μm)	12.53	12.60	12.69	11.44	13.22	0.51
	Cloud Optical Thick.	89.06	86.88	88.00	67.63	99.00	9.97
4	Cloud Top Pres (mb)	920					
	Cloud Top Temp. (K)	278.09					
	Cloud Part Rad (μm)	9.56	8.65	8.53	7.54	9.63	0.61
	Cloud Optical Thick.	70.39	70.40	68.39	52.38	93.87	13.43
5	Cloud Top Pres (mb)	645					
	Cloud Top Temp. (K)	260.57					
	Cloud Part Rad (μm)	8.39	8.40	8.23	7.86	9.57	0.55
	Cloud Optical Thick.	17.80	30.77	27.27	17.80	59.76	11.57
6	Cloud Top Pres (mb)	670					
	Cloud Top Temp. (K)	271.02					
	Cloud Part Rad (μm)	12.99	12.77	12.73	11.60	13.90	0.57
	Cloud Optical Thick.	74.29	77.79	75.59	61.53	99.00	11.85

A close inspection of the MODIS imagery revealed that these variations were not due to physical variations in the cloud but resulted from the sensitivity between the 0.664-μm reflectance function and the retrieved cloud optical thickness. The sensitivity in this retrieval is evident by inspection of Figure 11 (King et al., 1997). Thus, it is clear that cloud base heights with the MODIS approach become questionable when cloud optical thickness values exceed about 40 or less, depending upon scattering geometry.

Figure 11. Reflectance functions used in the retrieval of cloud optical thickness and water drop effective particle size (radius) with MODIS bands (from King et al., 1997).

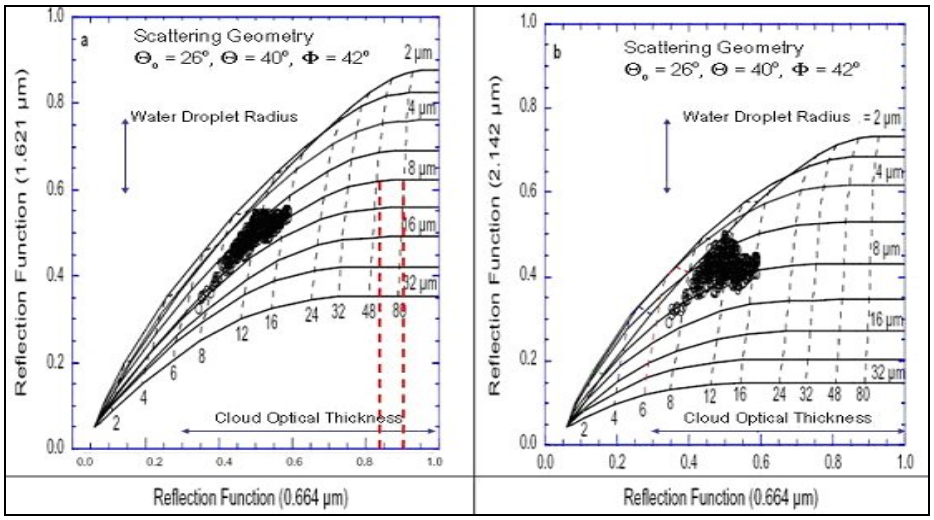

3.4 Objective 4. Using Conventional Weather Data to Improved Cloud Boundaries

The large errors in cloud top heights found in the MOD06 product served as motivation to examine new approaches to more accurately retrieve cloud top heights (and thus cloud base heights) for regional air quality applications.

The approach initially developed for use combines cloud base height observations made at ground-based weather observing facilities with satellite-derived cloud thickness values retrieved from MODIS to determine cloud top height. The improvement in the specification of cloud boundaries is achieved by reducing the relatively large observational errors in the MODIS cloud top height products with much smaller errors in the surface-based measurements of cloud base height, which are considered to be routinely available from aerodromes in most urban regions that experience anthropogenic air pollution (Hutchison et la., 2006). Figure 12 demonstrates the change in the original 3D cloud retrieval concept, which was shown in Figure 8. The results from this approach proved to be greatly improved by those contained in the MOD06 product so no further attempts were made to improve upon the new procedures.

The improved accuracy of cloud boundaries created with the new approach developed under this project and shown in Figure 11 has been demonstrated through the analyses of the dataset shown in Table 10, where truth is based upon ground-based observations collected at the United States Department of Energy's (DOE) Southern Great Plains (SGP) Atmospheric Radiation Measurement (ARM) site in Oklahoma. Results obtained with the new approach are shown in Table 13.

Cloud thickness values calculated with Equations 2 and 3 using MODIS observations contained in Table 12, are found in column 2 of Table 13. Surface observations, taken from ceilometer measurements at the ARM site, are combined with these cloud thickness values so errors are due to the conversion of cloud optical thickness into geometric thickness using Equations 2 and 3. These data are next used to calculate a new cloud top height as shown in column 4. Comparisons between these new cloud top heights and the

two sources of cloud top height truth data, i.e. MMCR and radiosondes shown in Table 11, are found in columns 4-5 of Table 13.

Figure 12. Modified architecture to retrieve 3-dimenisional clouds for air quality applications based upon availability of conventional weather reports (From Hutchison, 2006)

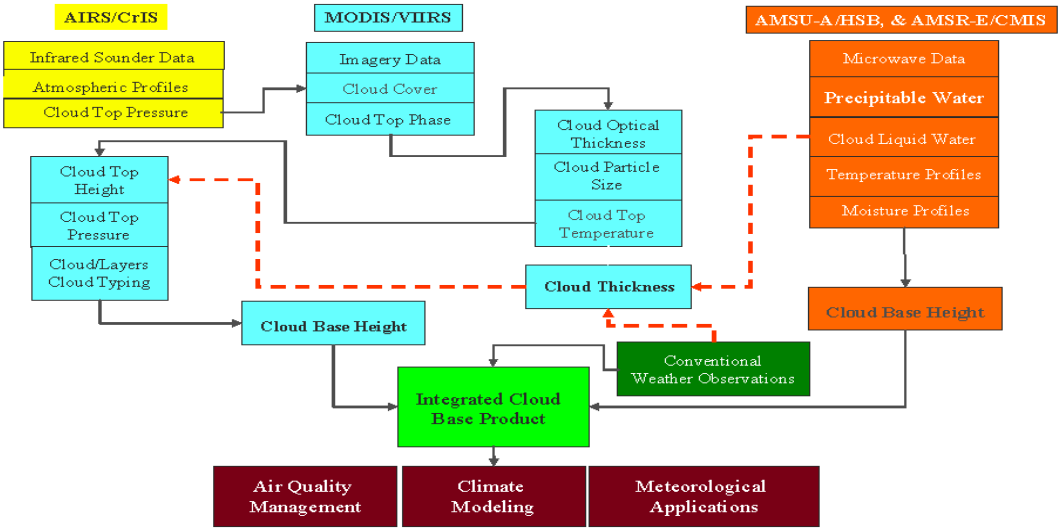

Comparisons between columns 4-5 in Table 13 and columns 7-8 of Table 11 show errors in cloud top heights from this new approach are significantly smaller than those obtained directly from the MOD06 cloud top pressure product. These differences ranged between 0-654 m while the average difference for all cases was slightly less than 223-m. In contrast the average difference between truth cloud top heights and those retrieved from the MOD06 cloud top pressures was 1013-km. Thus, it is concluded that the approach of using surface observations with retrieved cloud thickness values inferred from the MOD06 cloud optical properties can result in greatly improved specification of cloud boundaries for air quality applications over cloud top heights in the MOD06 products.

Table 13. Cloud boundaries derived from new approach developed for air quality modeling [Update to table from Hutchison et al., 2006b]

Case No.	Cloud Thickness Retrieve with Equation 3 (m)	Cloud Top Height from Equation 2 and Ceilometer Observation at ARM Site (m)	Difference between Cloud Top Height with new approach and Radiosonde Truth (m) (%)	Difference between Cloud Top Height with new approach and MMCR Truth (m) (%)
1	59	1196	33 (3%)	104 (8%)
2	865	2372	0 (0%)	122 (5%)
3	1483	1870	558 (42%)	470 (33%)
4	1531	1815	654 (26%)	385 (17%)
5	340	1651	128 (8%)	49 (3%)
6	2195	2344	125 (3%)	56 (2%)

One surprising result seen in Table 13 is the accuracy of cloud thickness values retrieved for cloud systems with large cloud optical thickness values shown in Table 12. While an error in cloud thickness of 558-m appears large, these results were associated with a cloud optical depth of 77.8, i.e. case 3. It was originally assumed that cloud optical depths of 64 would represent an upper limit in retrieving useful cloud base heights with the approach outlined in Equation 2 and Equation 3. This predicted limitation was based on the assumption that liquid water content is constant with height in the cloud base height retrieval formulation (Hutchison, 2002; Hutchison, 1998). The fact that useful cloud thickness values, compared to the NPOESS cloud base height performance requirement of 2-km (NPOESS VIIRS SRD, 2000), are retrieved for cloud optical depths in this range suggests that our initial assumption may not be a major limitation. In fact, one recent study examined cloud thickness estimates obtained with this approach using constant liquid water content values, an empirical relationship between cloud thickness and cloud optical properties, and an adiabatic model. The authors found that assuming a constant cloud liquid water content provided the most reliable retrieval of cloud thickness and concluded that it may be possible to monitor cloud base height globally in cloud mist forest regions with the approach outlined in Equation 2 and Equation 3 (Zeng et al., 2006).

Another surprising result from this study is that relatively small errors in MOD06 cloud top temperatures were routinely associated with much larger errors in cloud top pressures and additional analyses were under-taken to understand why this occurs. Case 6 is presented in detail to understand the difficulties that can arise when converting from cloud top temperature to cloud top pressure in the MOD06 product using NCEP analysis fields. Panel (a) of Figure 13 (left panel) shows a plot of temperature and dewpoint profiles on a skew-T, log P diagram constructed from data collect by the radiosonde launched from the SGP ARM site at 1730 UTC on 8 November 2003 (case 6). From this data, the cloud top pressure is accurately located at 760-mb and the corresponding cloud top temperature is 272.7-K as shown in column 4 of Table 10. Panel (b) contains a report of the MMCR observations (right panel) collected during the approximate period of 1630-1930 UTC at the same location. The cloud top temperature from the MOD06 product is reported to be 271.0 K, as seen in column 2 of Table 11, which is a difference of only 1.7-K from the truth. Based upon a standard lapse rate, it might be expected that the cloud top height would differ from the truth observation by about 250-m. However, Table 11 shows the actual difference between the cloud top height derived from Equation 4 and the truth measurement is nearly 4-times larger.

The magnification in errors in the conversion between cloud top temperature and cloud top pressure in the MOD06 product results from the procedures used in the algorithm. While it was discussed previously, it is worth repeating due to the importance of this error. In the retrieval of the cloud top parameters with these two MODIS algorithms, NCEP global, 1x1 degree latitude/longitude, 6-hourly analysis fields are vertically interpolated to 101 pressure levels of temperature and water vapor mixing ratio. Next, transmittance profiles are computed for each MODIS band used to retrieve cloud top pressure, i.e. MODIS bands 31 and 33-36. No horizontal interpolation is used except for surface temperature and pressure. Clear-sky radiances are then calculated along with CO_2-slicing computations. First, a "window channel" value is obtained, i.e. $T_{B11,}$ then the

CO_2-slicing solution. If a CO_2 solution is not available, the window channel result will be reported as the cloud top pressure, which will be one of the 101 pressure levels, rounded to the nearest 5-mb increment (MODIS Cloud Team Member, personal communication). The error in this conversion becomes evident by examining more closely the data shown in Figure 13.

It is evident by the sharp drop in dewpoint that coincides with a similar rise in temperature in the thermodynamic diagram in Panel (a) of Figure 13 that the cloud top height for case 6 is between 700-mb and 800-mb as shown on the ordinate of this chart. Therefore, a CO_2 slicing solution is likely not available and cloud top temperature is based upon the T_{B11} brightness temperature under the assumption that the cloud is a black body (Platnick et al., 2005). Thus, the cloud top temperature shown in column 3 or Table 11 is converted into cloud top pressure using one of the 101-levels generated from the 26-levels of NCEP data. In this case, the cloud top pressure was found to be 670-mb, which is about 100-mb lower than the actual cloud top pressure in the radiosonde. The error in cloud top pressure is understandable by looking at the temperature profile shown in the Skew-T, Log P diagram. The retrieved cloud top temperature occurs at many locations in the diagram because cloud top temperature does not uniquely identify cloud top heights. Both temperature and moisture profiles must be examined to determine accurately the cloud top pressure or cloud top height.

Figure 13. Radiosonde observation for Case 3 (left) and MMCR observation during MODIS overflight of SGP ARM Site Oklahoma (right)

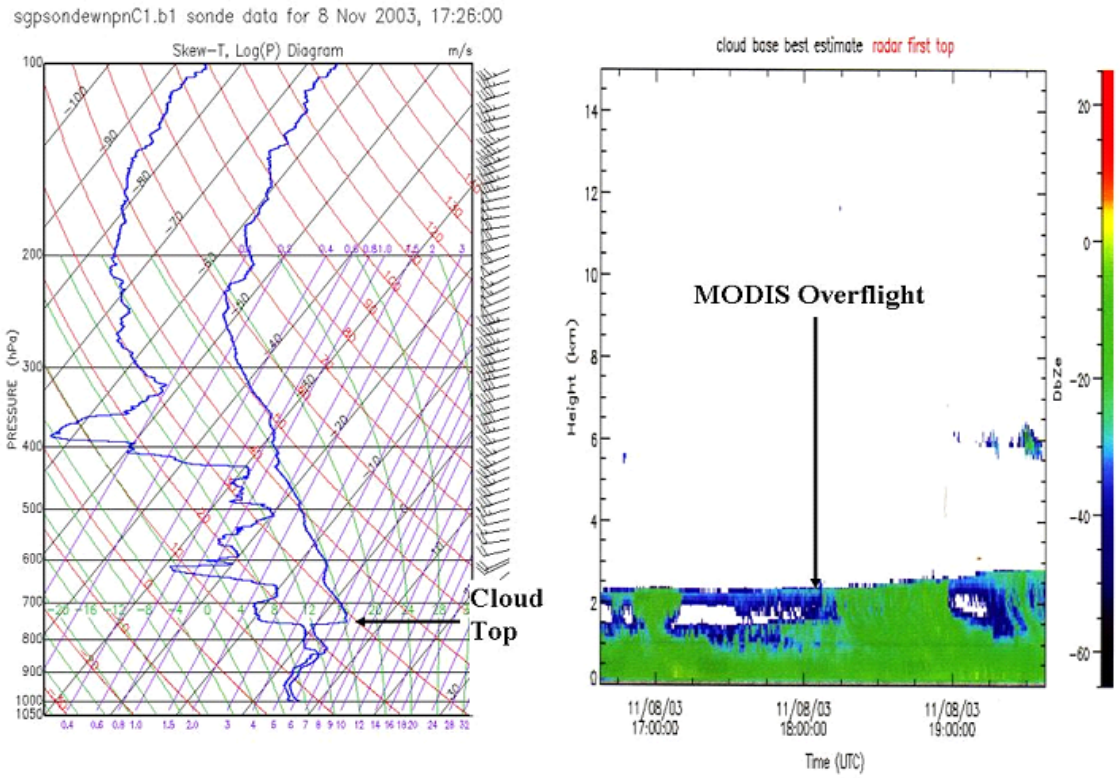

As a result, CSR obtained the NCEP reanalysis fields, used in the generation of the MOD06 product, to further evaluate this conversion between cloud top temperature and cloud top pressure when there is no cloud signature in the CO_2 slicing algorithm. Table 14 shows the NCEP analysis fields for the SGP ARM site at 1800 UTC on 8 November 2003. In this case the data shown are based upon the average of the four, 1-degree data points that surround the SGP ARM site, since the site lies between these gridded values. Column 2 shows the NCEP temperature profile, Column 3 contains the NCEP pressure profile, and Column 4 the NCEP humidity profile. Column 5 of Table 14 shows the location in the NCEP profiles of the cloud top pressure reported in the MOD06 product. It lies in a humidity range of 54-43 percent. Thus, the conversion of the MOD06 cloud top temperature into a cloud top pressure of 670-mb is inconsistent with the moisture profile in the NCEP analysis fields. So, it is apparent that using temperature profiles alone is an inadequate approach to convert between these cloud top parameters using thermodynamic charts like the Skew-T, Log-P diagram or the NCEP fields.

Therefore, CSR developed and tested an alternative approach to convert between MODIS cloud top temperature and cloud top pressure that includes humidity information contained in the NCEP profiles. This new conversion procedure assumes that cloud top temperatures are not perfect but that quantifiable errors exist in this MOD06 cloud top product. [For example, in the NPOESS program, cloud top temperature is assumed to have an accuracy of 2 K and 3 K for optically thicker clouds, i.e. optical depth of unity or more, during daytime and nighttime conditions respectively (NPOESS VIIRS SRD, 2000). For more optically thin clouds, the expected error increases to 6 K.] Then, NCEP moisture fields are examined over this range of possible temperatures to find the most desirable location to assign the cloud top pressure.

Using this new conversion logic developed at CSR, the moisture profile in Table 14 is examined over the temperature range that includes the MOD06 cloud top temperature plus its expected error range, *as denoted by the shaded area in the NCEP temperature profile*. Next, the NCEP humidity profile is examined to identify locations where a cloud might exist, e.g. 87% greater (Wang et al., 1999; 2000). If such a region is found, the cloud top is placed in the lowest pressure in this range and the retrieval is given a high quality signifying there is sufficient moisture present in the NCEP data to support the formation of a cloud. If no region is found where sufficient moisture is present to form and sustain a cloud, the cloud top pressure is place at the level of maximum humidity within this temperature range but the retrieval is flagged as degraded quality.

Again, column 6 of Table 14 shows the cloud top pressure, using the new CSR conversion logic, to be at 750-mb for case 6. (Note that no attempt has been made to interpolate the NCEP data to 101 pressure levels at this time; however, even better accuracy might be achieved with this conversion.) After converting these data to cloud top heights using Equation 4, it is found that the new approach locates the cloud top height at 2252-m, compared to 3162-m shown in Table 11, while the truth data for this case shows the cloud top height at 2219-m as shown in Table 10 (radiosonde). Thus, the error in cloud top height, generated using cloud top temperature data in the MOD06 product, is reduced from 942-m to 33-m. There is a fundamental error in the interpolation scheme in the NASA MOD06 cloud top parameters algorithms that converts cloud top temperature to cloud top pressure when the CO2 slicing algorithm finds no cloud

signature. This conversion error is probably the cause for large errors reported by other investigators (Naud et al., 2004). This discovery by CSR as described by Hutchison et al., (2006) was more recently verified independently by another research team (Welch et al., in press).

Table 14. Conversion of cloud top temperature into cloud top pressure using MOD06 algorithm and new logic developed at CSR to include moisture as an independent variable [From Hutchison et al., 2006b]

NCEP Level	Temperature (K)	Pressure (mb)	Relative Humidity (%)	MODO6 Cloud Top Location	Proposed Cloud Top Location
1	281.2	1000	78		
2	279.5	975	80		
3	277.6	950	86		
4	276.3	925	89		
5	276.0	900	92		
6	276.1	850	97		
7	276.4	800	97		
8	274.2 (Radisonde CTT = 272.7K	750	92	Radiosonde CTP = 760 mb	New Method CTP = 750 mb
9	274.3	700	54		
10	271.0 MOD06 CTT	650	43	MOD06 CTP = 670 mb	
11	269.5	600	45		
12	261.3	550	50		
13	256.7	500	72		

The results of investigations into the retrieval of 3D clouds at CSR have identified two problems that require further analyses.

- First, there exists an error in the algorithm used by NASA to convert between cloud top temperature and cloud top pressure when no cloud signature is evident in the CO_2 slicing algorithm. The problem has been reported by CSR to the NASA Cloud Team.
- Secondly, the MOD06 algorithms used to retrieve cloud optical thickness and effective particle size are highly sensitive to noise, e.g. small changes in the reflectance function shown in Figure 11 can produce large variations in cloud optical thickness. These variations can be caused by phenomena not related to clouds, e.g. some atmospheric aerosols at levels above the cloud top, especially for those extending across a range of scan angles. Since our proposal to address this problem was not funded by NASA, CSR has been investigating the use of multiple data sources to retrieve 3D cloud fields, including the use of NWP models of cloud liquid water in addition to remote-sensing methods discuss herein. Those studies were initiated in cooperation with Dr. Eberhard Reimer of Freie University under the MOU contained in Appendix 8.3. While CSR made valiant efforts to foster this collaboration, distances between Austin and Berlin were difficult to overcome. As a result, CSR completed the study independently and will provide our findings to Dr. Eberhard for possible use in his work there.

As noted above, initial research was completed that significantly reduces the errors in cloud boundaries (cloud top height and cloud base height) using conventional weather observations along with MODIS cloud optical properties (Hutchison et al., 2006). The original concepts proposed for this task followed heritage cloud algorithms used by the US Air Force and procedures shown in Figure 8 for the retrieval of 3D cloud fields. However, the new procedures developed by CSR, as shown in Figure 12, significantly reduced the errors in cloud boundaries derived with the aid of conventional weather observations and the erroneous logic in the MOD06 cloud top parameters has been identified and solutions demonstrated. Thus, we believe this objective has been satisfied. In addition, we have moved forward with new research to determine the value of the improvements in cloud boundary for full-physics atmospheric chemistry models. The research was proposed under ROSES 2007 to quantitatively assess the accuracy of cloud boundaries in WRF-CHEM. In addition, we proposed to enhance the cloud boundaries in the MM5 model that drives WRF-CHEM and assess the value of 3D clouds on air quality forecasts, ozone, PM, and other products that impact AQI, including CO, SO_2, and NO_X. A doctoral candidate from the Jackson School of Geosciences at UT Austin has made this task her doctoral thesis and she has passed her qualifying exams. PI Hutchison had previously agreed to supervise her research as a member of her doctoral committee; however, since funding under the ROSES 2007 was rejected, these task will not be pursued by PI Hutchison.

3.5 Objective 5: Assess Use of Microwave Data in Cloud Boundaries.

Originally, CSR had planned to integrate LWP retrieved directly from microwave imagery into estimates of cloud thickness to retrieve cloud base height. These data from microwave radiometry would be used when MODIS cloud optical depth values, reported in the MOD06 product, become large, e.g. exceeding values of about 100.

However, progress in the retrieval of LWP from microwave radiometry has been much slower than expected. In fact, the only progress reported in the literature on the use of microwave imagery for the retrieval of clouds parameters over land during the last 5-years was made by a researcher at NCAR (Deeter et al., 2006).

CSR has discussed this slow progress in the maturation of microwave techniques for cloud property retrievals with some leading international scientists in this field, including Prof. Juergen Fischer of Freie University of Berline and Prof. Rolf Bennatz of the University of Wisconsin. As a result, CSR teamed with Dr. Deeter of NCAR to further advance this science in our response to the ROSES 2006 solicitation when it became clear that significant research is needed to evaluate the accuracy of LWP retrievals over land from the AMSR-E (Advanced Microwave Scanning Radiometer for EOS). Again, NASA chose not to fund this CSR proposal so further progress has been impeded. Our discussion did help establish truth observations for these studies (Ulrich and Crewell; 2005; Crewell and Ulrich, 2005) which are now being used in ongoing analyses at CSR to establish the accuracy of LWP from modeling and MODIS data (Hutchison et al., in press).

4. REFERENCES AND CITATIONS

Ackerman S.A., Strabala K.I., Menzel W.P., Frey R.A., Moeller C.C., and L.E. Gumley, 1998: Discriminating clear sky from clouds with MODIS, J. Geophys. Res., **103 (D24)**: 32141-32157.

Ackerman, Strabala, Menzel, Frey, Moeller, Gumley, Baum, Schaaf, & Riggs, 2002: Discriminating Clear-Sky from Cloud with MODIS - Algorithm Theoretical Basis Document . *Products: MOD35. ATBD Reference Number: ATBD-MOD-06*

Al-Saadi, J. A., Szykman, J., Pierce, R. B., Kittaka, C., Neil, D., Chu, D. A., Remer, L., Gumley, L., Prins, E., Weinstock, L. MacDonald, C., Wayland, R., Dimmick, F., and J. Fishman, 2005: Improving national air quality forecasts with satellite aerosol observations, Bulletin of the American Meteorological Society (BAMS), **86**,1249-1261.

Barnes, W.L., T.S. Pagano, and V. Salomonson, 1998: Prelaunch characteristics of the Moderate Resolution Imaging Spectroradiometer (MODIS) on EOS AM-1. IEEE Trans. Geosci. Remote Sens., **36**, 1088-1100.

Carlson, T. M., and J. M. Prospero, 1972: The large-scale movement of Saharan air outbreaks over the northern equatorial Atlantic, Journal of Applied Meteorology, **11**, 283-297.

Chu, D. A., Kaufman, Y. J., Ichoku, C., Remer, L. A. Tanre', D., and B. N. Holben: 2002: Validation of the MODIS aerosol optical depth retrieval over land, Geo. Res. Lett., **29**, doi: 10.1029/2001GL013205.

Chu, D. A., Kaufman, Y. J., Ichoku, Zibordi, G., Chern, J. D., Mao, J. Li, C. and B. N. Holben, Remer, and Tanre', 2003: Global monitoring of air pollution over land from the Earth Observing System-Terra Moderate Resolution Imaging Spectroradiometer (MODIS), J. Geophy. Res., **108**, doi:10:1029/2002JD003179.

Crewell, S. and U. Loehnert, 2003: Accuracy of cloud liquid water path from ground-based microwave radiometry, 2. Sensor accuracy and synergy, Radio Science, **38**, doi:10.1029/2002RS002634.

Hutchison, K, 2006: Annual report on NASA project NRA-03-OES-02: Earth System Science Research Using Data and Products from TERRA, AQUA, and ACRIM Satellite, CSR Report dated 21 Dec 06, pp. 100.

Hutchison, K, 2005: Annual report on NASA project NRA-03-OES-02: Earth System Science Research Using Data and Products from TERRA, AQUA, and ACRIM Satellite, CSR Report dated 21 Dec 05, pp. 80.

Hutchison, K. D. 2000: Cloud Base Height, Visible *Infrared Imager Radiometer Suite (VIIRS) Algorithm Theoretical Basis Document*, Version 3, Raytheon Santa Barbara Remote Sensing, pp 40.

Hutchison, K. D. and A. P. Cracknell, 2005: "VIIRS - A New Operational Cloud Imager," CRC Press of Taylor and Francis Ltd, London, pp 218.

Hutchison, K. D., 1998: Cloud base height, VIIRS algorithm theoretical basis document, version 1.0, Raytheon Information Technology and Scientific Services, Lanham, MD, pp. 35. (See: http://www.ipo.noaa.gov/library_NPOESS.html)

Hutchison, K. D., 2002: "The Retrieval of Cloud Base Heights from MODIS and 3-Dimensional Cloud Fields from NASA's EOS Aqua Mission," Int. J. Rem. Sens., **23**, 5249-5265.

Hutchison, K. D., 2003: "Applications of MODIS satellite data and products for monitoring air quality in the state of Texas," Atmospheric Environment, **37**, 2403-2412.

Hutchison, K. D., Pekker, T., and S. Smith, (manuscript in preparation): Examining the Impact of Errors in Liquid Water Path on the Accuracy 3-Dimensional Cloud Fields Generated from Remote Sensed Data and Numerical Models , International Journal of Remote Sensing.

Hutchison, K. D., Pekker, T., and S. Smith, 2006: Improved Retrievals of Cloud Boundaries with MODIS Data for Use in Air Quality Modeling, Atmospheric Environment, **40**, 5798-5806.

Hutchison, K. D., Smith, S. and S. Faruqui, 2004: The use of MODIS data and aerosol products for air quality prediction, Atmospheric Environment **38**, 5057-5070.

Hutchison, K. D., Smith, S. and S. Faruqui, 2005: Correlating MODIS aerosol optical thickness data with ground-based PM2.5 observations across Texas for use in a real-time air quality prediction system, Atmospheric Environment **39**, 7190-7203.

Hutchison, K. D., Wong, E. and S. C. Ou, 2006: "Cloud Base Heights Retrieved During Nighttime Conditions with MODIS Data," International Journal of Remote Sensing, **27**, 2847-2862.

Hutchison, K.D., Faruqui, S., and S. Smith, 2007: Improving Correlations between MODIS Aerosol Optical Thickness and Ground-Based $PM_{2.5}$ Observations through 3D Spatial Analyses, Atmospheric Environment, (in press).

Kalluri, S., Gilruth, P., and R. Bergman, 2003: The potential of remote sensing data for decisions makers at the state, local and tribal level: experiences from NASAS's Synergy Program, Environmental Science and Policy, 6, 487-500

Kaufman, Y. A., Tanre', D., and O. Boucher, 2002a: A satellite view of aerosols in the climate system, Nature, **419**, 215-223.

Kaufman, Y. J., Gobron, N., Pinty, B., Widlowski, J.L., and M. M. Verstraete, 2002b: Relationship between surface reflectance in the visible and mid-IR used in MODIS aerosol algorithm – theory, Geophysical Research Letters, **29**, (23), 2116, doi:10.1029/2001GL014492

Kaufman, Y. J., Tanre, D., Remer, L. A., Vermote, E. F., Chu, A. and B. N. Holben, 1997b: "Operational remote sensing of tropospheric aerosol over land from EOS moderate resolution imaging sprectroradiometer, Journal of Geophysical Research, **102** (D14), 17051-17067.

Kaufman, Y. J., Wald, A. E., Remer, L. A., Gao, B.-C., Liand, R.-R. and L. Flynn, 1997c: The MODIS 2.1 μm Channel - Correlation with visible reflectance for use in remote sensing of aerosol. IEEE Trans. Geo, **35**, 1286-1298.

Kaufman, Y.J. and D. Tanre, 1996; Strategy for direct and indirect methods for correcting the aerosol effect on remote sensing: From AVHRR to EOS-MODIS, Rem. Sens. Envir., **55**, 65-79.

Kaufman, Y.J., D. Tanré, H.R. Gordon, T. Nakajima, J. Lenoble, R. Frouin, H. Grassl, B.M. Herman, M.D. King and P.M. Teillet, 1997a: Passive remote sensing of tropospheric aerosol and atmospheric correction for the aerosol effect. J. Geophys. Res., **102**, 16815-16830.

King, M. D., Tsay, S-C., Platnick, S. E., Wang, M., and K-N. Liou, , 1997: Cloud Retrieval Algorithms for MODIS: Optical Thickness, Effective Particle Radius, and Thermodynamic Phase, *MODIS Algorithm Theoretical Basis Document*, No. ATBD-MOD-05, Version 5, pp. 83.

Liou, K-N., 1992: Radiation and Cloud Processes in the Atmosphere, Oxford press, 487 pp.

Liu, Y., Sarnat, J. A., Kilaru, V., Jacob, D. J., and P. Koutrakis, 2005: Estimating ground-level PM2.5 in the Eastern United States using satellite remote sensing, Envir. Sci. Technol., **39**, 3269-3278.

Loehnert, U. and S. Crewell, 2003: Accuracy of cloud liquid water path from ground-based microwave radiometry, 1. Depedency on cloud model statistics, Radio Science, **38**, doi:10.1029/2002RS002654.

Mace, G. G., Y. Zhang, S. Platnick, M. D. King, P. Minnis, and P. Yang, 2005: Evaluation of cirrus cloud properties derived from MODIS data using cloud properties derived from ground-based observations collected at the ARM SGP site. *J. Appl. Meteor*. **44**, 221-240.

Martins, J.V., D. Tanré, L.A. Remer, Y.J. Kaufman, S. Mattoo and R. Levy, 2002: MODIS Cloud screening for remote sensing of aerosol over oceans using spatial variability. Geophys. Res. Lett., **29**, 10.1029/2001GL013252.

McClain, E.P., Pichel, W.G., and C. C. Walton, 1985: Comparative performance of AVHRR-based multichannel sea-surface temperatures, J. GEOPHYS. RES., 90, 1587-1601.

Nakajima T. and M. D. King, 1990: Determination of the optical-thickness and effective particle radius of clouds from reflected solar-radiation measurements. 1. Theory, J. Atmos. Sci. **47**, 1878-1893.

National Polar-Orbiting Operational Environmental Satellite System (*NPOESS) VIIRS Sensor Requirements Document (SRD)*, Ver. 3, June, 2000, pp 91. (See: http://www.ipo.noaa.gov/library_NPOESS.html)

Naud, C. Muller, J. P., Haeffelin, M., Morille, Y. and A. Delaval, 2004: Assessment of MISR and MODIS cloud top heights through intercomparison with a back-scattering lidar at SIRTA, Geophysical Research Letters, **31**, L041134, doi:10.1029/2003GL018976.

Naud, C. Muller, J. P. and E. E. Clothiaux, 2003: Comparison between active sensor and radiosonde cloud boundaries over the ARM Southern Great Plains site, Journal of Geophysical Research - Atmospheres, **108**(D4), AAC 3-1 – 3-12.

Neil, D., Szykman, J., Fishman, J., Pierce, R. B., Saddi, J. A., and C. Kittaka, 2004: A good IDEA (Infusing Data into Environmental Applications), Amer. Meteor. Soc., Proceeding of the 13th Conference on Satellite Meteorology, Norfolk, VA.

Ou, S. C., Liou, K. N., Takano, Y. , Wong, E., Hutchison, K., and T. Samec, 2005: "Comparison of the UCLA-LBLE Radiative Transfer Model and MODTRAN for

Accuracy Assessment of the NPOESS-VIIRS Cloud Optical Property Algorithms," Applied Optics, **44,** 6274-6284.

Remer, L.A., Tanré, D., and Y. Kaufman, 2006**:** Algorithm for Remote Sensing of Tropospheric Aeosol from MODIS: Collection 5, MODIS Algorithm Theoretical Basis Document, pp 87. See http://modis-atmos.gsfc.nasa.gov/MOD04_L2/atbd.html

Remer, L.A., Kaufman, Y.J., Tanré, D., Mattoo, S., Chu, D.A., Martins, J.V. Li, R-R., Ichoku, C., Levy, R. C. , Kleidman, R.G., Eck, T.F., Vermote, E. and B.N. Holben: 2005**:** The MODIS Aerosol Algorithm, Products and Validation, Journal of the Atmospheric Sciences, **62**, 947-973.

Remer, L.A., Tanre, D., Kaufman, Y.J., Ichoku, C., Mattoo, S., Levy, R., Chu, D.A., Holben, B., Dubovik, O., Smirnov, A., Martins, J.V., Li, R.R., and Z. Ahmad, 2002 : Validation of MODIS aerosol retrieval over ocean, Geophysical Research Letters, 29, doi:10.1029/2001GL013204.

Salomonson, V. V., Barnes, W. L., Maymon, P.W. Montgomery, H. E., and H. Ostrow, 1989: MODIS : Advanced Facility Instrument for Studies of the Earth as a System, IEEE Transactions in Geoscience and Remote Sensing, 27, 145-153

Shenk, W., and R. Curran, 1974: The detection of dust storms over land and water with satellite visible and infrared measurements, Monthly Weather Review, **102**, 830-837.

Tanre D., Kaufman Y.J., Herman, M., S. Mattoo, 1997: Remote sensing of aerosol properties over oceans using the MODIS/EOS spectral radiances, J. GEOPHYS. RES., **102** (D14), 16971-16988.

Tucker, C.J., Gatlin, J.A. and S. R. Schneider, 1984: Monitoring vegetation in the Nile Delta with NOAA-6 and NOAA-7 AVHRR imagery, Photogram. Eng. Rem. Sens., **50**, 53-61.

Tuinder, O.N.E., de Winter-Sorkina, R. and P.H.J. Builtjes, 2002: Impact of satellite derived cloud fraction on calculated actinic flux, photodissociation rates, and OH production, J. Geophy. Res., **107**, N19, doi:10:1029/2001JD001491.

Vaughan, M., Young, S., Winker, D., Powell, K., Omar, A., Liu, Z., Hu, Y., and C. Hostetler, 2004: Fully automated analysis of space-based lidar data: an overview of CALIPSO retrieval algorithms and data products. *Proc. SPIE*, **5575**, pp. 16-30.

Wang and Christopher, 2003: Intercomparison between satellite-derived aerosol optical thickness and PM-$_{2.5}$ mass: Implications for air quality studies, Geophysical Research Letters, **30**, doi:10.1029/2003GLO181174.

Welch, R., Zeng, J., Nair, U.S., Han, Q., Asefi, S., Lawton, R. O., Ray, D.K., and V. S. Manoharan, 2007, Biogeography of Tropical Montane Cloud Forests, 1: Remote Sensing of Cloud Base Heights, J. Climate (in press).

Wong, E. Hutchison, K. D., Ou, S. C. and K. N. Liou, 2006: "Cloud Top Temperatures of Cirrus Clouds Retrieved from Radiances in the MODIS 8.55-μm and 12.0-μm Bandpasses," Applied Optics, **46**, 1316-1325.

Zeng, J., Han, Q., Asefi, S., Welch, R. M., Lawton, R. O., Nair, U. S., and D. K. Ray, 2006: Observations of orographic Cloud Base Heights from satellite and in-situ measurements at the Monteverde Cloud Mist Forest Reserve, Costa Rica, Poster 3.17, 14th *Conference on Satellite Meteorology and Oceanography*, American Meteorological Society, Atlanta, GA, USA

5. SUMMARY OF PERSONNEL AND WORK EFFORTS

Table 15 shows the support provided to CSR staff under this project during the FY 2007 timeframe, rounded to the nearest percentile. These results are based upon certification of the through the UT accounting system, which is completed at 6-month intervals.

Table 15. Roles and responsibilities of key CSR team members supporting this project

TEAM MEMBER	RESPONSIBILITIES	LEVEL OF SUPPORT
PI Dr. Keith D. Hutchison - Center for Space Research (CSR), The University of Texas at Austin	• Led the project, oversees utilization of resources, • Developed the technical approaches used in the study, • Reviewed results and provided direction for further investigations, and • Summarized results and prepared reports and manuscripts for publication.	< 20%
Ms. Shazia Faruqui – Research Associate and Data Analyst (Statistician) Center for Space Research (CSR), The University of Texas at Austin	• Conducted detailed studies to quantify correlations between MODIS aerosol optical thickness data and ground-based pollution observations made at TCEQ's CAMS locations, • Completed all data pre-processing of airborne lidar observations, and vertical motions from IDEA trajectories, • Conducted analyses of temporal and spatial characteristics of pollution types using MODIS, airborne lidar, and CAMS data, and	100%
Mr. Solar Smith – Research Associate, Systems Analyst, and Algorithm Developer Center for Space Research (CSR), The University of Texas at Austin	• Implemented and maintained all algorithms used to retrieval aerosol products from the CSR MODIS direct broadcast ground station, • Hosted all MODIS algorithms used to generated fire products for use during TXAQS II operations, • Hosted NASA's IDEA software at CSR MODIS ground station and issuance of air quality forecasts during TXAQS II, and	75%
Ms. Tatyana Pekker – Research Associate, Center for Space Research (CSR), The University of Texas at Austin	• Analyze 3-dimensional cloud fields, • Conduct sensitivity studies of cloud boundaries on CMAQ and CAMX chemistry models • Acquire, manage and assess global NCEP and ECMWF databases used in algorithm verification studies.	< 69%
Other CSR staff	• Assisted with financial management of the project, • Generated GIS-graphics of results, and • Computer support	<7%

6. CSR FACILITIES AND EQUIPMENT

The University of Texas at Austin, Center for Space Research (CSR) was established in 1981 under the direction of Dr. Byron D. Tapley as a component of the Bureau of Engineering Research in the College of Engineering. The Center currently manages ~ $15 Million annually in grants and contracts for a variety of customers in federal and state government agencies and private industry. It currently employs 10 faculty members and 58 full-time staff members with an impressive variety of technical capabilities and accomplishments. The addition of 51 graduate students and 24 undergraduate students brings the total strength of CSR to near 150 people. CSR occupies approximately 25,000 sq ft of office, laboratory and operations space in facilities located at 3925 W. Braker Lane, near the Pickle Research Center (PRC).

MISSION

The mission of CSR is to coordinate, execute, and enhance academic and research programs associated with studies of the Earth and the solar system by providing an organizational structure for interdisciplinary research.

CAPABILITIES

• Internationally recognized center of excellence in the area of space geodesy and a leader in the development and application of precision orbit determination methodology.
• Leading research center associated with manned and unmanned exploration of the solar system. Research includes the lunar and Mars exploration programs, and planetary gravity field modeling.
• Operates NASA EOS (MODIS) and NOAA direct broadcast ground stations. Maintains the University of Texas Orbit Prediction, Integration, and Statistical Analysis (UTOPIA) program. UTOPIA has been employed to perform precision orbit determination tasks under contract to NASA/JPL. Analysts use UTOPIA, with the CSR developed 70x70-geopotential model (JGM-3), to provide weekly updates of the TOPEX/POSEIDON satellite position with a radial accuracy of 2-3 cm. In addition, the Lageos satellite location is determined to the sub-cm level, and other low-earth orbiting satellite positions are determined to a few cm accuracy. This system has been further enhanced to support the satellite formation flying of the two GRACE satellites now on-orbit.

COMPUTATIONAL CAPABILITY

CSR owns a 16 processor Cray SV1-1A vector-parallel supercomputer that is operated under a cooperative agreement with the Texas Advanced Computing Center (TACC) located at the PRC. High-speed access through fiber optics and HIPPI connection is available directly from CSR to this supercomputer.

The University provides operational support for the SV1-1A as well as a file system and data migration facility with approximately 800 GB of on-line storage and 60 TB of tape archive. This storage system also supports the Texas InfoMart which is an element of the NASA Synergy Program. The TACC also maintains a 272-node T3E and a new IBM Regatta-class computer. These resources have supported the ongoing gravity model development (such as the recent TEG-4 model) as well as the computationally demanding

GRACE simulations. UT is a partner in the NSF National Partnership for Advanced Computational Infrastructure (NPACI).

CSR maintains a variety of computers and other scientific equipment, including Origin 200 & 3400 servers managing archival storage for the Texas InfoMart. CSR currently operates a Sun E450 Server (4 440 MHz processors, 4 GB), a Sun E250 Server (2 440 MHz processors, 2 GB), 3 Sun Ultra 10 Workstations (440 MHz, 1GB), 2 HP 735 Workstations (99 MHz, 384 Mb, 60-Gb of data storage), HP L1000 (2 550 Mhz processors), and 2 HP C110 Workstations (125 MHz, 512 Mb, 60-Gb of data storage).

AREAS OF RESEARCH INTEREST

- Precision orbit determination
- High-resolution geopotential modeling from gravity gradient data
- Earth gravity field modeling and precision satellite ephemerides
- Ocean tide modeling
- Ocean circulation
- Satellite altimetry
- Remote sensing from space
- Ocean and Gulf of Mexico modeling
- Tectonic plate & polar motion and earth rotation
- Global geodesy and geodynamics
- Ecological studies on impact of fires
- Multi-sensor topographic/geomorphological analyses
- Multi-resolution image analysis for environmental mapping applications
- Remote-sensing of meteorological products for air quality modeling

RECENT AND CURRENT PROJECTS

- The Gravity Recovery and Climate Experiment (GRACE), a mission to measure time variable gravity to a much higher precision than previously possible, as well as to probe the atmosphere with GPS signals
- NASA Synergy Project to distribute EOS data and product to Federal, State, and local user groups via the Internet and assist in development of new applications for these non-research communities
- IceSat, a mission to measure the ice sheet heights using a laser altimeter
- Precision orbit determination (POD) for the TOPEX/POSEIDON mission and supporting POD efforts for the follow-on mission, Jason-1
- Development of improved Earth gravity field models and techniques to provide and verify precise satellite ephemerides
- Development of ocean tide models and estimation of mean sea surface levels using TOPEX altimeter data,
- Development of mesoscale variability maps and large-scale dynamic topography solutions and the determination of general ocean circulation,
- Development of high resolution geoid and mean sea surface models using satellite altimetry,
- Collection and analysis of satellite imagery data for global ocean and Gulf of Mexico modeling, and land cover change studies of Texas and Australia.

7. BIOGRAPHICAL SKETCHES

Principal Investigator, Dr. Keith D. Hutchison

TITLE: Senior Research Scientist
DEPARTMENT: Center for Space Research (CSR), The University of Texas at Austin
EDUCATION:

University of Utah	Meteorology	PhD	1982

PROFESSIONAL EXPERIENCE:
Senior Research Scientist, Center for Space Research, The University of Texas at Austin, 2000 - present.
Senior Staff Scientist, Advanced Technology Center (ATC) Lockheed Martin, Palo Alto, CA, 1996 – 2000 and Lockheed Martin Austin Division, Austin, TX, 1990 - 1995.
Member of the Technical Staff, The Analytic Science Corp. (TASC), Reading, MA, 1988 - 1989.
Senior Meteorologist, US Air Force - 1988.

MEMBERSHIPS IN PROFESSIONAL AND HONORARY SOCIETIES:
Phi Kappa Phi
Member, American Meteorological Society

PROJECT MANAGEMENT EXPERIENCE AND PROGRAM HIGHLIGHTS:
2004 – Current: Co-Principal Investigator for the Texas Air Research Center (TARC) project to study effects of regional air pollution on local air quality. Total project value $180,000.
2003 – Current: Principal Investigator for HQ NASA NRA-03- OES-02, Earth System Science Research using Data and Products from TERRA, AQUA and ACRIM Satellites. Total project value $867,384.
2003 – Current: Principal Investigator (P/I) for Northrop Grumman Space Technology as VIIRS Algorithm Lead on NPOESS program. Total project value $608,000.
2000 – 2004: Program Manager for the EOSDIS and State of Texas Data Synergy Project, under contract to Raytheon Systems Company. Total project value $3,261,877.

RELEVANT JOURNAL PUBLICATIONS:

1. Hutchison, K. D., Faruqui, S. and S. Smith, (accepted for publication): "Improving Correlations between MODIS Aerosol Optical Thickness and Ground-Based $PM_{2.5}$ Observations through 3D Spatial Analyses," Atmospheric Environment.
2. Hutchison, K.D., Iisager, B. D., and J. M. Jackson, (accepted for publication): "Discriminating between clouds and aerosols in VIIRS cloud mask algorithm," J. Atmospheric & Oceanic Technology.
3. Wong, E. Hutchison, K. D., Ou, S. C. and K. N. Liou, 2006: "Cloud Top Temperatures of Cirrus Clouds Retrieved from Radiances in the MODIS 8.55-μm and 12.0-μm Bandpasses," Applied Optics, 46, 1316-1325.
4. Hutchison, K. D., Pekker, T., and S. Smith, 2006: Improved Retrievals of Cloud Boundaries with MODIS Data for Use in Air Quality Modeling, Atmospheric Environment, 40, 5798-5806.
5. Hutchison, K. D., Wong, E. and S. C. Ou, 2006: "Cloud Base Heights Retrieved During Nighttime Conditions with MODIS Data," International Journal of Remote Sensing, 27, 2847-2862.
6. Hutchison, K.D., Roskovensky, J.K., Jackson, J.M., Heidinger, A.K., Kopp, T. J., Pavolonis, M.J, and R. Frey, 2005: "Automated Cloud Detection and Typing of Data Collected by the Visible Infrared Imager Radiometer Suite (VIIRS)," International Journal of Remote Sensing, 20, 4681 - 4706.
7. Ou, S. C., Liou, K. N., Takano, Y. , Wong, E., Hutchison, K., and T. Samec, 2005: "Comparison of the UCLA-LBLE Radiative Transfer Model and MODTRAN for Accuracy Assessment of the NPOESS-VIIRS Cloud Optical Property Algorithms," Applied Optics, 44, 6274-6284.

8. Hutchison, K. D. and A. P. Cracknell, 2005: "VIIRS - A New Operational Cloud Imager," CRC Press of Taylor and Francis Ltd, London, pp 218.
9. Hutchison, K. D., Smith, S. and S. Faruqui, 2005: Correlating MODIS Aerosol Optical Thickness Data with Ground-Based $PM_{2.5}$ Observations Across Texas for Use in a Real-time Air Quality Prediction System, Atmospheric Environment. 39, 7190-7203.
10. Knebl, M. R., Yang, Z-L. Hutchison, K. D. and D. R. Maidment, 2005: "Towards developing a regional scale flood forecast product using precipitation forecasts, GIS, and hydrological modeling," Journal of Environmental Management, 75, 325-336.
11. Hutchison, K. D., Smith, S. and S. Faruqui, 2004: "The Use of MODIS Data and Aerosol Products for Air Quality Prediction, Atmospheric Environment 38, 5057-5070.
12. Hutchison, K. D. and J. M. Jackson, 2003: "Cloud detection over desert regions using the 412 nanometer MODIS channel, Geophysical Research Letters, 30, 2187-2191.
13. Hutchison, K. D., 2003: "Applications of MODIS Satellite Data and Products for monitoring Air Quality in the State of Texas," Atmospheric Environment, 37, 2403-2412.
14. Hutchison, K. D., 2002: "The Retrieval of Cloud Base Heights from MODIS and 3-Dimensional Cloud Fields from NASA's EOS Aqua Mission," International Journal of Remote Sensing. 23, 5247-5263.
15. Wilheit, T. T. and K. D. Hutchison, 2002: "Retrieval of Cloud Base Heights from Passive Microwave and Cloud Top Temperature Data," IEEE Transactions on Geoscience and Remote Sensing, 38, 1253-1259.
16. Hutchison, K. D., Wilheit, T. T. and P. C. Topping, 2000 (patent awarded to Lockheed Martin) "3DCLOUDS - Cloud Base Height and Weather Characterization, Visualization and Prediction Based on Satellite Meteorological Observations."
17. Hutchison, K. D., 1999: "Application of AVHRR/3 Imagery from NOAA-K for Improved Detection of Thin Cirrus Clouds and Specification of Cloud Top Phase," Journal of Atmospheric and Oceanic Technology, 16, 1885-1899.
18. Hutchison, K. D., Marusa, S., Henderson, J. R., Kenley, R. C., Topping, P. C., Uplinger, W. and J. Twomey, 1999: "System Design Considerations for the Retrieval of Sea Surface Temperatures during the NPOESS Era," Journal of Atmospheric and Oceanic Technology, 1, 107-116.
19. Hutchison, K. D., Etherton, B. J., and P. C. Topping, 1997: "Validation of Automated Cloud Top Phase Algorithms: Distinguishing Between Cirrus Clouds and Snow in A-priori Analyses of AVHRR Imagery," Optical Engineering, 36, 1727-1737.
20. Hutchison, K. D., Etherton, B. J., Topping, P. C., and A. H. L. Huang, 1997: "Cloud Top Phase Determination from the Fusion of Signatures in Daytime AVHRR Imagery and HIRS Data," International Journal of Remote Sensing, 18, 3245-3262.
21. Wilheit, T. T. and K. D. Hutchison, 1997: "Water Vapor Profile Retrievals using Passive Microwave Data Constrained by Infrared-Based Cloud Information," International Journal of Remote Sensing, 18, 3263-3278.
22. Hutchison, K. D. and J. K. Locke, 1997: "Snow Identification through Cirrus Cloudy Atmospheres using AVHRR Daytime Imagery," Geophysical Research Letters, 24, 1791-1794.
23. Rosenkranz, P. W., Hutchison, K. D., Hardy, K. R. and M. S. Davis, 1997: "An Assessment of the Impact of Satellite Microwave Sounder Incidence Angle and Scan Geometry on the Accuracy of Atmospheric Temperature Profile Retrievals," Journal of Atmospheric and Oceanic Technology, 14, 488-494.
24. Hutchison, K. D. and N. J. Choe, 1996: "Application of 1.38 Micron Imagery for Thin Cirrus Detection in Daytime Imagery Collected Over Land Surfaces," International Journal of Remote Sensing, 17, 3325-3342.
25. Hutchison, K. D. and K. R. Hardy, 1995: "Threshold Functions for Automated Cloud Analysis of Global Meteorological Satellite Imagery," International Journal of Remote Sensing, 16, 3665-3680.
26. Hutchison, K. D., Hardy, K. R. and G. C. Gao, 1995: "Improved Detection of Optically-Thin Cirrus Clouds in Nighttime Multispectral Meteorological Satellite Imagery using Total Integrated Water Vapor Information," Journal of Applied Meteorology, 34, 1161-1168.

Mr. Solar Smith

TITLE: Research Associate IV

DEPARTMENT: Center for Space Research (CSR), The University of Texas at Austin

EDUCATION: University of Texas at Austin – BS, MS Aerospace Engineering

PROFESSIONAL EXPERIENCE:

May 1995 - present	Research Associate III University of Texas at Austin Center for Space Research
May 1991 - May 1995	Graduate Student Assistant University of Texas at Austin Center for Space Research
Feb 1989 – May 1991	Undergraduate Assistant University of Texas at Austin Center for Space Research
Sep 1988 – May 1990	Cooperative Education Employee Davis Aerospace Company, Canyon Lake, Texas

PROJECT PARTICIPATION:

Mr. Smith is involved with the development of the software and procedures to maximize the automation in the application of satellite remote sensing data for improved monitoring and understanding of environmental processes. He has worked to develop and implement algorithms involving a variety of airborne and spaceborne remote sensing data. He has integrated internally developed data processing methods with commercial image processing software. He supported the publication of numerous articles in research journals, conferences, project reports and web-based media. He also developed the computer hardware and software requirements to support research conducted at CSR. Mr. Smith integrated hardware and software elements to support research goals and contractual requirements and led field campaigns to collect information to support the development and verification of processing algorithms.

RELEVANT JOURNAL PUBLICATIONS:

1. Hutchison, K. D., Faruqui, S. and S. Smith, (accepted for publication): "Improving Correlations between MODIS Aerosol Optical Thickness and Ground-Based $PM_{2.5}$ Observations through 3D Spatial Analyses," Atmospheric Environment.
2. Hutchison, K. D., Pekker, T., and S. Smith, 2006: Improved Retrievals of Cloud Boundaries with MODIS Data for Use in Air Quality Modeling, Atmospheric Environment, 40, 5798-5806.
3. Hutchison, K. D., Smith, S. and S. Faruqui, 2005: Correlating MODIS Aerosol Optical Thickness Data with Ground-Based $PM_{2.5}$ Observations Across Texas for Use in a Real-time Air Quality Prediction System, Atmospheric Environment. 39, 7190-7203.
4. Hutchison, K. D., Smith, S. and S. Faruqui, 2004: "The Use of MODIS Data and Aerosol Products for Air Quality Prediction, Atmospheric Environment 38, 5057-5070.

Ms. Shazia Faruqui

TITLE: Research Associate III

DEPARTMENT: Center for Space Research (CSR), The University of Texas at Austin

EDUCATION: University of Texas at Austin – BBA, BS, MPA

PROFESSIONAL EXPERIENCE:
Center for Space Research, The University of Texas at Austin, 2001 - present.
Apple Computer Corp., 2001
Dell Computer Corp., 1998 - 2000.
Emerson Process Management (formerly Fisher-Rosemount Systems), 1995-1998

PROJECT PARTICIPATION:
2005 – 2006: Supported a project funded by the Texas Air Research Center (TARC) to study effects of regional air pollution on local air quality

2001 – 2004: Participated EOSDIS and State of Texas Data Synergy Project – Cost-benefit analysis for the application of MODIS data to invasive species management in Texas.

RELEVANT JOURNAL PUBLICATIONS:
1. Hutchison, K. D., Faruqui, S. and S. Smith, (accepted for publication): "Improving Correlations between MODIS Aerosol Optical Thickness and Ground-Based $PM_{2.5}$ Observations through 3D Spatial Analyses," Atmospheric Environment.
2. Hutchison, K. D., Smith, S. and S. Faruqui, 2005: Correlating MODIS Aerosol Optical Thickness Data with Ground-Based $PM_{2.5}$ Observations Across Texas for Use in a Real-time Air Quality Prediction System, Atmospheric Environment. 39, 7190-7203.
3. Hutchison, K. D., Smith, S. and S. Faruqui, 2004: "The Use of MODIS Data and Aerosol Products for Air Quality Prediction, Atmospheric Environment 38, 5057-5070.

Ms. Tatyana Pekker

TITLE: Research Associate III

DEPARTMENT: Center for Space Research (CSR), The University of Texas at Austin

EDUCATION: St. Petersburg Hydrometeorological Institute, St. Petersburg Russia

PROFESSIONAL EXPERIENCE:

1993 – present Center for Space Research, The University of Texas at Austin
Extensive experience in predictions of processes and phenomena of the atmosphere based on real data; construction of models for short range scientific and practical purposes

1992 - 1993 Instructor in Meteorology, Saint Cloud University, MN

1978 - 1991 Novosibirsk Hydrometeorological Institute, Russia
Hydrodynamic and statistical local weather forecasts, Boundary layer parameterizations in numerical models, Synoptic map's analysis, comparisons of numerical and synoptic forecasts, statistical forecast of low clouds based on synoptic archive

PROJECT PARTICIPATION:

Ms. Pekker's research has focused on retrieval of 3-dimensional cloud fields and conducting error analyses of these results against MODIS cloud products. In addition, she leads the investigations into the value of more accurate cloud boundaries for applications that include full-physics air quality model, including CAMX. She is also supported by the GRACE project and has performed many studies for that program that involved exploitation of atmospheric data.

RELEVANT JOURNAL PUBLICATIONS:

1. Hutchison, K. D., Pekker, T., and S. Smith, 2006: Improved Retrievals of Cloud Boundaries with MODIS Data for Use in Air Quality Modeling, Atmospheric Environment, 40, 5798-5806.
2. Tapley B, Ries J, Bettadpur S, Chambers D, Cheng M, Condi F, Gunter B, Kang Z, Nagel P, Pastor R, Pekker T, Poole S, and F Wang, 2005: GGM02 - An improved Earth gravity field model from GRACE, J. Geodesy, 79 (8): 467-478.
3. Chen JL, Wilson CR, Tapley BD, and T Pekker, 2002: Contributions of hydrological processes to sea level change, Physics and Chemistry of the Earth, 27 (32-34): 1439-1443
4. Chen JL, Wilson CR, Tapley BD, Chambers DP, and T Pekker, 2001: Hydrological impacts on seasonal sea level change, Global and Planetary Change 32 (1): 25-32.
5. Urban TJ, Pekker T, Tapley BD, Kruizinga GL, and CK Shum, 2001: A multiyear intercomparison of wet troposphere corrections from TOPEX/Poseidon, ERS-1, and ERS-2 Microwave Radiometers and the European Centre for Medium-Range Weather Forecasts model, J. of Geophysical Research-Oceans 106 (C9): 19657-19669

8. APPENDICES

8.1 Reprints and Preprints Published Under this Grant

Preprint of article published in Atmospheric Environment, 2003, 37, pp. 2403-2412.

Applications of MODIS Satellite Data and Products for Monitoring Air Quality in the State of Texas

Keith D. Hutchison
The University of Texas at Austin
Center for Space Research
3925 W. Braker Lane, Suite 200
Austin, Texas 78759-5321

ABSTRACT

The Center for Space Research (CSR), in conjunction with the Monitoring Operations Division (MOD) of the Texas Commission on Environmental Quality (TCEQ), is evaluating the use of remotely-sensed satellite data to assist in monitoring and predicting air quality in Texas. The challenges of meeting air quality standards established by the U.S. Environmental Protection Agency (USEPA) are impacted by the transport of pollution into Texas that originates from outside our borders and are cumulative with those generated by local sources. In an attempt to quantify the concentrations of all pollution sources, MOD has installed ground-based monitoring stations in rural regions along the Texas geographic boundaries including the Gulf coast, as well as urban regions that are the predominant sources of domestic pollution. However, analysis of time-lapse GOES satellite imagery at MOD, clearly demonstrates the shortcomings of using only ground-based observations for monitoring air quality across Texas. These shortcomings include the vastness of State borders, that can only be monitored with a large number of ground-based sensors, and gradients in pollution concentration that depend upon the location of the point source, the meteorology governing its transport to Texas, and its diffusion across the region. With the launch of NASA's MODerate resolution Imaging Spectroradiometer (MODIS), the transport of aerosol-borne pollutants can now be monitored over land and ocean surfaces. Thus, CSR and MOD personnel have applied MODIS data to several classes of pollution that routinely impact Texas air quality. Results demonstrate MODIS data and products can detect and track the migration of pollutants. This paper presents one case study in which continental haze from the northeast moved into the region and subsequently required health advisories to be issued for 150 counties in Texas. It is concluded that MODIS provides the basis for developing advanced data products that will, when used in conjunction with ground-based observations, create a cost-effective and accurate pollution monitoring system for the entire state of Texas.

KEY WORDS: Remote Sensing, MODIS, Pollution, Air Quality, Continental Haze

Corresponding Author: Dr. Keith D. Hutchison, Center for Space Research, Tele: 512-471-7295, Fax: x-3570, e-mail: keithh@csr.utexas.edu

1. INTRODUCTION

The Texas Commission on Environmental Quality (TCEQ) is the regulatory agency in Texas responsible for air and water quality. Its stated mission is to "Strive to protect our state's human and natural resources consistent with sustainable economic development with a goal of clean air, clean water, and the safe management of waste." To accomplish its mission, TCEQ:

- ensures that regulations are necessary, effective, and current;
- applies regulations clearly and consistently;
- ensures consistent, just, and timely enforcement when environmental laws are violated;
- ensures meaningful public participation in the decision-making process;
- promotes and fosters voluntary compliance with environmental laws and provides flexibility in achieving environmental goals; and
- hires, develops, and retains a high-quality, diverse workforce.

Three full-time commissioners are appointed by the Governor to establish agency direction and policy, and to make final determinations on contested permitting and enforcement matters. Each is appointed for a six-year term with the advice and consent of the State Senate. The governor names the commission chairman. An organizational chart of TCEQ can be found at: http://163.234.20.106/AC/about/organization/index.html.

The executive director, who is hired by the commissioners, is responsible for managing the day-to-day operations of TCEQ and its members in Austin. Major responsibilities of the executive director include implementation of commission policies, making recommendations to the commissioners about contested permitting and enforcement matters, and approving uncontested permit applications and registrations.

The Office of Compliance and Enforcement (OCE) oversees agency enforcement, emergency response, dam safety, monitoring activities, and operation of regional offices across the state. The Field Operations Division, within OCE, consists of 16 field offices and two special project offices located throughout the state, and a central office located in Austin.

The Monitoring Operations Division (MOD), also within OCE, is responsible for monitoring air and water quality within the State of Texas and for reporting information to the public and the USEPA. MOD personnel examine and interpret the causes, nature, and behavior of air and water pollution in Texas. MOD personnel also provide analytical services for air, water, and waste samples, issue forecasts of ground-level ozone concentrations in Texas cities, and produce the water quality inventory as an overview of the quality of the state's

surface waters. Thus, the MOD staff has requirements for “real-time” data needed for forecast purposes and archived data for less time critical analyses.

MOD personnel collect data from a variety of sources including the US National Weather Service, central and mobile laboratories based in Austin and Houston, a network of over 200 continuous air monitoring stations (CAMS), and 52 particulate matter (PM) measurement sites. In addition, MOD collects weather observations for all Texas stations that report to the Federal Aviation Administration’s Automated Surface Observation System (ASOS) program. MOD staff also operates a gas chromatography laboratory to analyze samples collected by its field monitoring sites. Information on CAMS and PM sites can be viewed at the following websites:
http://www.tnrcc.state.tx.us/cgi-bin/monops/site_info
http://www.tnrcc.state.tx.us/air/monops/finepm/finepm.html#1

In 1995, MOD installed two GOES satellite direct-broadcast (DB) ground stations to create time-series images for monitoring pollution. Time series images from GOES data have proven highly valuable for monitoring the migration of dense smoke from fires and other pollutants, such as Saharan dust, across the relatively dark ocean surface. However, GOES data are less effective for monitoring some pollution events over land. In addition, the GOES data lack the spectral content to retrieve aerosol products that could be used to infer the severity of pollution events.

MODIS data have been proposed to significantly increase the knowledge of global, tropospheric aerosols (King et al., 1999) and the techniques have been developed to retrieve aerosol data over land as well as ocean surfaces (Kaufman and Tanre, 1998). (See Table 1 for comparisons of MODIS and GOES imaging sensors.) In 2001, TCEQ requested CSR assess the value of MODIS data to improve air quality monitoring capabilities across Texas. As a member of the NASA Synergy project, administered by Raytheon Systems Company, CSR was assessing the value of EOS data and products to federal, state, local, and tribunal groups outside the climate change program and distributing these data via the Texas InfoMart, a high-speed, web-based system (Tapley et al., 2001; Hutchison and Smith, 2002). Thus, the request from TCEQ fell within the charter of the Texas InfoMart and the NASA Synergy Program.

Table 1 here.

The results discussed below are based upon EOS data obtained from the EOS Distributed Information System (EOSDIS). Currently, data from the EOSDIS do not become available until days, weeks, or months after satellite overpass of Texas, depending upon the product requested. However, the full value of EOS data for air quality management requires user access to real-time data. Therefore, CSR has recently purchased an EOS DB ground station to collect,

process, and distribute EOS data and products in near real-time, via the Texas InfoMart.

2. ASSESSING THE VALUE OF MODIS FOR AIR QUALITY MONITORING

First, TCEQ staff identified three classes of pollution that represent current challenges to Texas meeting attainment requirements established by the US EPA. These classes include continental haze that arrives in Texas from the industrial middle US, fine sand particles from west Texas or the Saharan Desert, and smoke from seasonal fires that burn on the Yucatan Peninsula and across Central America.

Next, success criteria were established to assess the value of MODIS data for enhancing current TCEQ monitoring capabilities. These criteria are:

1) The manual detection of pollution is more readily accomplished with EOS data and products than possible with existing data routinely available to MOD.
2) The use of EOS data or products improves the capability to exploit existing data routinely used by MOD personnel.
3) The use of EOS data or products extends the period in which an air pollution event, or residuals of an event, can be monitored by MOD personnel, whether the origin of the event is internal or external to the State of Texas.
4) The use of EOS data or products provides increased knowledge into the severity (based upon an assessment of concentration) or the extent (based upon aerial coverage) of a pollution event over that otherwise known by TCEQ using existing data sources.
5) The use of remotely-sensed EOS data or products allows improved estimates of surface conditions in regions where MOD observing systems are not available.

The potential impact of the pollution sources identified by TCEQ on Texas air quality is demonstrated by two examples. In 1998, dense smoke from fires burning over Central America resulted in the first and only state-wide health alert issued by the State. TCEQ measured 140 parts per billion (ppb) of ozone in a plume over the Gulf of Mexico near Brownsville, Texas using an airplane operated by Baylor University that was equipped for aerial sampling. At a TCEQ monitoring site located 10 miles inland, particulate matter of 10 microns (PM_{10}) or less were measured in excess of 540 micrograms per cubic meter ($\mu g/m^3$) with an 8-hour ozone average of 89 ppb. This external ozone event exceeded the EPA attainment standard of 80 ppb. As a result, TCEQ appealed for a coherent and flexible environmental policy at the national level that deals with such episodic, large-scale events which are beyond the control of air quality agencies in Texas. In response, the USEPA issued new guidance that addresses possible impacts on peak daily ozone levels reported downwind of such fires and

described methods for justifying the exclusion of concentration levels that exceed standards in subsequent compliance calculations. The EPA guidance states that, "For purposes of determining attainment of air quality standards, the burden of proof for justifying data exclusion belongs to the State."

Strong winds can blow sand, from sparsely vegetated regions, high into the atmosphere where it migrates great distances before falling to the Earth. As an example, winds in excess of 50 miles per hour, associated with an approaching weather front, blew sand particles high into the troposphere and reduced surface visibilities at El Paso International Airport to near zero on March 24, 2002. Particulate matter of 2.5 microns ($PM_{2.5}$) or less and PM_{10} measurements were 128.31 and 1413.53 $\mu g/m^3$ respectively at the El Paso CAMS site in the early afternoon. The sand was advected eastward and ($PM_{2.5}$) measurements in Odessa/Midland reached 73.18 $\mu g/m^3$ near midnight, before returning to single-digit values the next day.

Unfortunately, sand pollution events from West Texas are frequently associated with extensive areas of cloud cover and MODIS aerosol products are only created for cloud-free regions. Thus, the value of MODIS for monitoring airborne sand pollution over Texas is better demonstrated with Saharan sand, which is readily monitored in cloud-free regions as it transits the Gulf of Mexico. While time-lapse GOES imagery allows these sand pollution events to be monitored over the ocean, details on their severity cannot be inferred. However, CSR results with MODIS show that aerosol optical thickness values associated with airborne Saharan sand can increase dramatically, e.g. optical thickness values increased by nearly an order of magnitude in some instances. In addition, the Saharan sand pollution event can be monitored in the MODIS aerosol product over land, after the pollutant crosses Texas and moves toward the eastern US (Hutchison et al., 2003).

3. CONTINENTAL HAZE CASE STUDY

Next, test cases were identified for each of the three pollution classes identified by TCEQ. Archived datasets were reviewed at both CSR and MOD in an attempt to locate suitable test data sets. Using the search engine to preview EOS data contained on the Texas InfoMart website (http://synergy1.csr.utexas.edu), data were located for each scene shown in Table 2. CSR then submitted requests to the EOSDIS for the MODIS imagery (MOD02_L2 or MOD02 product) and aerosol data (MOD04_L2 or MOD04) products needed to complete the study.

Table 2 here.

Data from the MODIS Terra mission, which has a descending nodal time of 1030 local, are highly susceptible to sun glint over the Gulf of Mexico and the MODIS Aerosol Science Team does not generate aerosol products in these regions. On the other hand, data collected from the MODIS Aqua mission, with an ascending

nodal time of 1330 local, are less susceptible to sun glint over the Gulf of Mexico. As a result, MODIS Aqua data are preferred for the analyses of Case 2 and Case 3 in Table 2. However, normal check-out procedures for the newly launched Aqua spacecraft meant that no MODIS data were useful from this sensor prior to October, 2002. Therefore, the remainder of this paper focuses on the analyses of continental haze. This approach seems justified since the ability to detect blowing sand and smoke in MODIS imagery is widely recognized from MODIS examples shown on the NASA Visible Earth website (e.g. see http://visibleearth.nasa.gov/Sensors/Terra/MODIS.html.) and the sample CAMS reports, shown in Table 4, will demonstrate the continental haze event to be the most severe. In addition, no paper appears in the literature on assessing the value of satellite data for monitoring continental haze over land surfaces.

During the September 11-15, 2002 timeframe, a significant continental haze pollution event brought ozone-laden aerosols from the industrial midwest into Texas. The news release in Table 3 was issued on September 13th by TCEQ as a health alert to residences in 150 Texas counties. Subsequently, CSR collected data on this event which is reported in the next section.

Before examining this event, some background information on EPA attainment standards is provided. Attainment standards are based upon time-averaged observations. There is a 1-hour standard of 0.12 ppm and an 8-hour standard of 0.08 ppm. Since surface observations are made in ppb, there is an “exceedance” of the standard if the reported value is 125 ppb or greater for any 1-hour period or 85 ppb or greater for any 8-hour period. It is understood that the one-hour average is taken from 9-10, 10-11, 11-12, etc. using observations collected at 5 minute intervals. The 8-hour average is obtained using 8-consecutive one-hour averages as described above. If a surface-based observation exceeds the 1-hour or 8-hour averaged exceedance values, the site fails to attain standard and is declared to be in “nonattainment.”

A post-analysis of this continental haze event began at CSR with the arrival of MODIS Terra imagery, i.e. MOD02 product, from the EOSDIS which are seen in the sequence of color composites shown in Figure 1. MODIS aerosol products became available over the EOSDIS within the next 60 days. Geographic boundaries and features in these figures will become more evident after examining them in detail, along with corresponding GOES data collected by TCEQ, in the panels of Figure2.

Table 3 here.
Figure 1 here.

4. RESULTS

As shown in Table 1, the spatial resolution of the MODIS imagery (MOD02) product is 250, 500, and 1000 m while the MODIS aerosol product (MOD04) has

a resolution of 10 km. In addition, separate aerosol products are created over land and ocean surfaces, since different algorithms are used to retrieve these two products. Thus, initial tests were made by CSR to evaluate the acceptability of co-registering these datasets into mosaic analyses using simple pixel replication techniques. Color-composite images of the MOD02 imagery and MOD04 aerosol optical thickness product showed sufficient agreement (but not shown in the manuscript) between features, e.g. coastlines were well aligned in the composite and MOD02 imagery product. Thus, the simple pixel replication technique was used to co-register subsequent data sets.

Figure 2a shows GOES and MODIS data for September 10th as the continental haze event heads toward Texas. The GOES data are positioned to facilitate reader orientation of the MODIS products. For example, the large mass of thunderstorms seen over northern Mexico and extending east over the Gulf of Mexico in the GOES imagery, shown in Panel 2a(1), are evident in the lower, middle part of the MODIS color composite image, shown in Panel 2a(2). This color composite was created by mapping the MODIS bands centered at 0.645, 0.555, and 0.469 microns to the red, green, and blue guns, respectively, of a color monitor. While features in the MODIS aerosol product, shown in Panel 2a(3), are not as evident as those in the color composite, both MODIS data products represent identical geographic areas and projections. Thus, the GOES data can be used to provide orientation of the MODIS data.

The most important feature in Figure 2a is the relatively cloud-free area over northeastern Texas, eastern Oklahoma, and Arkansas. Only small scale, cumulus clouds are discernable in the GOES data. However, in the upper right corner of the MODIS imagery, a bluish hue suggests the presence of some feature and it is confirmed as aerosol in the MOD04 product shown in Panel 2a(3). This particular aerosol product is the aerosol optical thickness at 0.55 microns for both ocean (best) and land (corrected) as described on the MODIS product website, i.e. http://modis-atmos.gsfc.nasa.gov/MOD04_L2/format.html. (Note that clouds appear black in the MOD04 product.) The brighter shades of gray in Panel 2a(3) represent regions with higher aerosol optical thickness values than the darker shades. Maximum optical depth values exceed 1.0 for this case. Again, note that no indication of this pollution is seen in the GOES imagery.

A weakness of using polar-orbiting data for air quality monitoring is seen in Figure 2b which contains GOES and MODIS data for September 11, 2002. Multiple MODIS passes must be integrated into a mosaic in order to cover the same geographic area shown in Figure 2a. Upon inspection, the western edge of the thunderstorm mass contained in the MODIS imagery is seen on the far-right, lower edge of the GOES data. By carefully examining the MODIS imagery in Panel 2b(2), the Gulf Coast, from the Florida panhandle to the Houston area, can be identified while the Yucatan Peninsula is seen near the lower-left corner.

In the MODIS products, the continental haze again appears blue in the color composite shown in Panel 2b(2) while the aerosol product, in Panel 2b(3), shows this feature to be aerosol. The largest aerosol optical thickness values (brightest features) are now over Louisiana and eastern Texas, not Arkansas. Clearly the continental haze is moving from the northeast toward the southwest in the clockwise circulation of a high pressure center over the central US. The detail in the aerosol product is noteworthy as it appears almost as a frontal boundary with a long, narrow maximum that diffuses (becomes darker) at the edges.

Figure 2c shows only MODIS data for September 12, 2002 due to a problem with the GOES data archive at TCEQ. MODIS Band 12, centered at 0.565 microns, is shown in Panel 2c(1) since it lies in the spectral range of the GOES visible band shown in Figures 2a(1) and 2b(1). In these data, the Gulf coast and the Great Lakes are clearly visible to provide orientation. Along the Gulf coast region, features readily identified include Galveston Bay and the extensive Louisiana coastline. Cumuliform clouds are shown over portions of Texas.

In Panel 2c(2), the continental haze continues to have a bluish hue and extends across the entire Gulf coast from the Florida panhandle into Texas. In the MOD04 product, the greatest concentration of pollution occurs along the Gulf Coast with maximum optical depth values near New Orleans and central Texas. Again, lower optical thickness values (darker features) occur toward the edges of the extensive “aerosol cloud.”

During the next 24-hours, the pollution continued to advance towards Texas and required TCEQ to issue a health advisory for much of Texas on September 13, 2002. Unfortunately, Texas was on the edge of scan for the MODIS data on September 13th making the product not suitable for presentation in this paper. (These data can be viewed by accessing the Texas InfoMart website.) Furthermore, no MODIS aerosol product was available from the EOSDIS for September 14th, a day in which Texas was centered in the MODIS imagery, as seen in Figure 1(d), and experienced cloud-free conditions. GOES data on September 14th, shown in Figure 3, reveal the presence of the pollution after it moves over the Gulf of Mexico, as seen by the light bluish hue over cloud-free regions near the Texas Gulf Coast.

5. DISCUSSION

While MODIS data presented in the last section shows the advancement of continental haze from the middle US into Texas, surface-based observations are currently needed to assess its impact upon Texas air quality. Table 4 shows ozone levels reported at TCEQ surface-based CAMS sites located across the eastern half of Texas. Values shown are daily maximums for all hours during the eight day period, before, during, and after the pollution event. The data were taken directly from the TCEQ website. For this study, reporting stations outside the center of metropolitan areas and windward of the pollution event were sought

in an attempt to isolate the effect of the continental haze upon air quality, rather than its cumulative effect upon attainment at any given site. Therefore, these data qualitatively demonstrate the impact of this external pollution source upon Texas air quality.

Table 4 here.

Table 4 shows that ozone levels begin relatively low early in the week for every city and peak as the continental haze moves from northeast Texas toward the Gulf Coast. Maximum values at the Houston site exceeded 160 ppb which is nearly 5-8 times the values reported each Monday, before and after the event. A similar trend exists in all other ground-based observation sites. The effects of commuter traffic can be ruled out since the maximum values in the week are: a) greatest in Dallas on Wednesday, then decrease, b) greatest in Houston on Friday and subsequently decrease, and c) greatest in Austin on Friday, which is typically a low traffic day, but remains high on Saturday before decreasing. Clearly excellent agreement exists between manual interpretation of the pollution "cloud" in the MODIS aerosol data product and "truth" observations reported by TCEQ ground-based observation sites.

From inspection of Figure 2a(1) and Figure 3, it is evident that the continental haze does not become discernible in GOES imagery until after the pollution reaches a water surface, i.e. continental haze cannot be detected in GOES imagery while over the land even though TCEQ has tried many enhancements to these data (private communication).

CSR believes the use of MODIS imagery and aerosol data products satisfies success criteria (1) through (4) listed in Section 2. Clearly the results of this case study demonstrate that the use of EOS data or products:

- improves dramatically the manual detection of pollution compared to use of existing GOES data routinely available at TCEQ,
- enhances the ability to exploit existing (surface-based) data routinely available at TCEQ,
- extends the period in which an air pollution event or residuals of an event can be monitored by TCEQ personnel, and
- provides increased knowledge into the severity (based upon optical thickness values which qualitatively reflect variations in pollution concentration) and the extent (based upon aerial coverage) of a pollution event.

Currently, the use of EOS data does not support improved estimates of surface conditions in regions where TCEQ observing systems are not available. To satisfy this requirement, CSR must correlate aerosol optical thickness values in the MODIS Level 2 aerosol (MOD04) product with TCEQ surface based observations collected at CAMS sites to create a new (Level 3) data product.

Research is currently underway to create this Level 3 data product and will be the subject of a future publication.

Finally, results from this case study encourage CSR to believe that operational forecast tools can be created to accurately predict air quality for this class of pollution using a simplistic gridded-field of trajectories. (Hutchison and Janota, 1988). The forecast scheme envisioned would use backward trajectories to advect aerosol "clouds" forward in time while reducing aerosol concentrations through sedimentation.

6. CONCLUSIONS

The primary purpose of this research was to evaluate the potential value of EOS data and products for enhanced air quality monitoring in the State of Texas. The approach used MODIS data products created by NASA scientists and distributed to potential users over the EOSDIS. Results presented in this paper clearly demonstrate the significant value of MODIS imagery for manually monitoring continental haze and the MODIS aerosol data product for qualitatively assessing concentration levels, based upon optical thickness values.

In addition, the use of MODIS data with TCEQ ground-based observations establishes a defendable cause and effect relationship between poor Texas air quality and external sources of pollution. Since current USEPA guidance states that "For purposes of determining attainment of air quality standards, the burden of proof for justifying data exclusion belongs to the State" the application of simplistic techniques used in this research do constitute scientific proof which needs to be documented in the literature.

The goal at CSR is to support decision-makers responsible for air quality management who seek to safeguard the health and quality of life for all Texans. Therefore, CSR will soon install a MODIS direct broadcast ground station to generate real-time MODIS data and products for use at TCEQ and other locations across Texas. These data will be distributed over high-speed (gigabit) Internet2 via the Texas InfoMart. Additionally, we intend to provide TCEQ and other interested parties with short-range (24 hour) forecasts to predict the impact of external pollution sources on Texas air quality. Progress toward achieving these goals will be the subject of future publications.

7. REFERENCES

Hutchison, K. D., White, H. D., and Ruetner, C. A.: The potential for monitoring Texas air quality with an optimum mix of ground-based and remotely-sensed satellite data, Proceedings of the 96th Annual Conference on Air and Waste Management, June 23-27, San Diego, CA.

Hutchison, K. D. and S. Smith: Distribution of earth observing system data via the Texas InfoMart, Proceedings of the EUMETSAT User's Conference, 2-6 September 2002, Dublin, Ireland.

Hutchison, K. D. and P. J. Janota, 1988: Cloud models enhancement project, Analysis Phase Report, Technical Note 5773-1, The Analytic Sciences Corporation, pp. 65 available through US Air Force Combat Climatology Center - http://www.afccc.af.mil/.

Kaufman, Y. J. and D. Tanre, 1998: "Algorithm for remote sensing of tropospheric aerosol from MODIS," NASA MODIS Algorithm Theoretical Basis Document, Goddard Space Flight Center, pp 85.

King, M. D., Kaufman, Y. J., Tanere, D., and T. Nakajima,1999: "Remote sensing of tropospheric aerosols from space: past, present, and future, Bulletin of the American Meteorological Society, Vol. 80, No. 11, 2229-2259.

Tapley, B. D., Crawford, M. M., Howard, T., Hutchison, K. D., Smith, S., and G. L. Wells: A vision for creating advanced products from EOS core system data to support geospatial applications in the State of Texas, Proceedings from the IEEE International Geoscience and Remote Sensing Symposium, 9-13 July 2001, Sydney, Australia.

Table 1. Comparisons between imaging sensors on EOS and GOES spacecraft.

Characteristic	GOES-I Imager	EOS Terra MODIS	EOS Aqua MODIS
Orbit type @ Altitude	Geostationary @ 35,800 km	Polar-orbiting and sun-synchronous @ 705 km	Polar-orbiting and sun-synchronous @ 705 km
Nodal Time	Not applicable	1030 local	1330 local
Spectral Bands	5 (1-solar, 4-IR)	36 (19-solar, 17-IR)	36 (19-solar, 17-IR)
Resolution	1km, 8km, & 4 km	250m, 500m, & 1km	250m, 500m, & 1km
Coverage (km)	Full-disk	2330 km	2330 km
Refresh Rate	< 26 minutes	Twice daily	Twice daily

Table2. Dates that significant pollution was observed by ground-base sensors in Texas.

Pollution Class	Date	Comments	Satellite Data Available	Sample CAMS reports on pollution levels
Case 1. Continental Haze transported from central US into Texas	September 10-16, 2002	Haze reported in Texas on September 11th with worst conditions on 13th. See TCEQ news release below.	GOES, MODIS Terra, MODIS Aqua	Ozone 161 ppb, $PM_{2.5}$ 68.11 $\mu g/m^3$
Case 2. Small dust particles transported from Saharan Desert into Texas	July 27 - 31, 2002	Dust moved into eastern Caribbean on July 27th and into Texas on July 30th.	GOES, MODIS Terra	$PM_{2.5}$ 39.88 $\mu g/m^3$
Case 3. Dense smoke in Texas from fires on Yucatan Peninsula	May 2 - 6, 2002	Heavy smoke evident in imagery on May 2nd. Other days impacted by extensive cloud cover.	GOES, MODIS Terra	Ozone 95 ppb, $PM_{2.5}$ 49.27 $\mu g/m^3$

Table3. TCEQ news release for Friday September 13, 2002 on Continental Haze pollution event.

For Immediate Release Friday September 13, 2002

Continental Haze Blankets More Than 150 Texas Counties.

Stagnant air containing industrial pollutants - known to meteorologists as Continental haze - covers all Texas counties east of a line from the Oklahoma border south to Abilene, then south to Mission. The air contains very small particles, known as particulate matter, which can irritate the throat and lungs of sensitive groups, including children, the elderly, and persons with a history of respiratory or heart ailments. Individuals in these categories should consider avoiding outdoor activity. The haze has reduced visibility and increased ground-level ozone readings. Houston-Galveston, Dallas-Fort Worth, Longview-Tyler, and Corpus Christi are metropolitan areas which have been most affected. Meteorologists from the Texas Commission on Environmental Quality (TCEQ) predict the haze will linger over much of the state and spread to West Texas by Sunday. A cold front is expected to clear Texas air by Monday. The hazy pollutants gathered in the mid-western United States, over the Mississippi and Ohio Rivers, earlier this week before moving to Texas. The TCEQ will continue to monitor the situation.

Table4. Maximum ozone levels report by several TCEQ continuous air monitoring station (CAMS) during the September 2002 continental haze pollution event.

Location		Maximum	Ozone Levels	Reported in	Parts Per Billion	(ppb)		
(CAMS Sites)	Monday	Tuesday	Wednesday	Thursday	Friday	Saturday	Sunday	Monday
	9-Sep-02	10-Sep-02	11-Sep-02	12-Sep-02	13-Sep-02	14-Sep-02	15-Sep-02	16-Sep-02
Dallas Hinton St. C401/C60/C161	56	78	109	102	95	101	69	62
Longview C19/C127	49	62	89	81	87	92	107	47
Beaumont C2/C112	36	67	79	95	81	98	69	24
Austin Northwest C3	39	56	80	100	103	103	53	33
Houston Deer Park 2 C35/139/1001	36	75	93	145	161	102	74	22
San Antonio Northwest C23	38	63	79	130	99	101	52	40
Corpus Christi West C4	46	39	76	107	104	82	42	48
Brownsville C80/C180	47	33	29	48	88	55	25	32

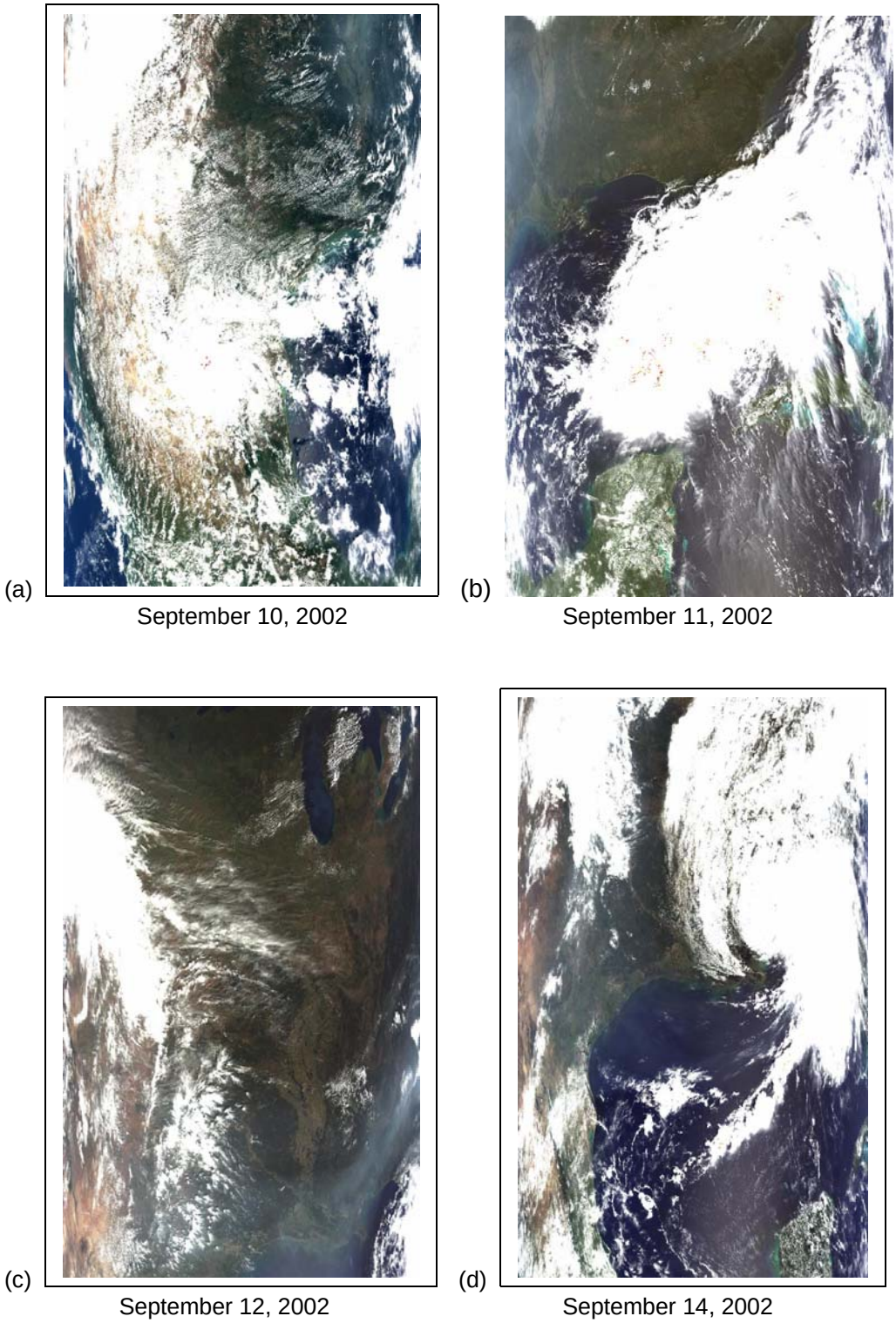

Figure 1. MODIS imagery sequence shows continental haze originates in the central US and enters Texas precipitating a health alert in over 150 counties on September 13, 2002. Geographic boundaries of these data are more evident in panels shown in Figures 2(a) – (c).

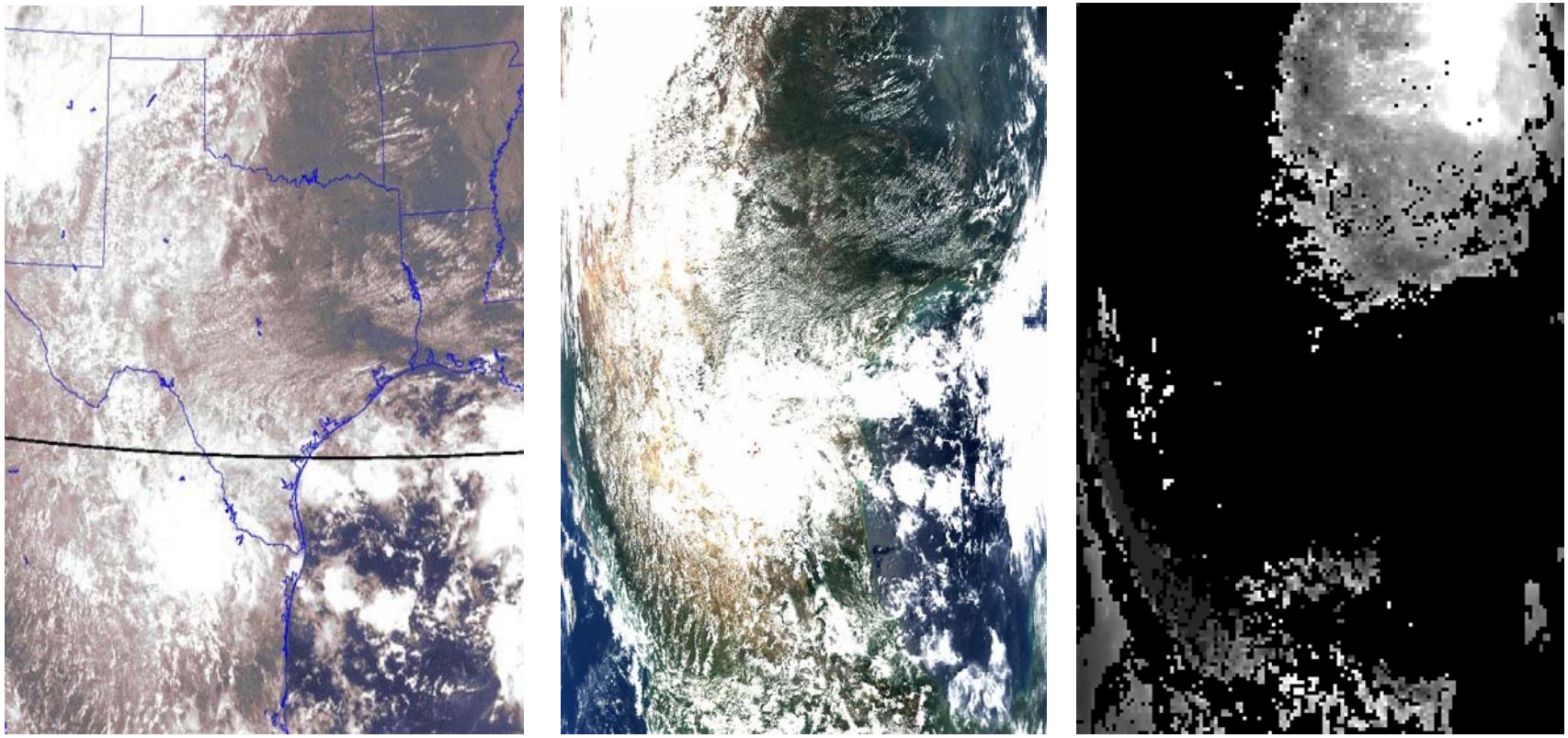

(1) GOES Channel 1 from TCEQ (2) MODIS Color Composite (3) Aerosol Analysis from NASA

Figure 2a. GOES Channel 1 in Panel (1) shows no indication of mid-continental haze at 1700 UTC on September 10, 2002. However, a color composite of MODIS bands at 1720UTC (red = 0.645, green = 0.555, and blue = 0.469 microns) in Panel (2) reveals this pollution as a “blue” cloud over Arkansas (top right corner of scene). The MODIS MOD04 aerosol product in Panel (3) accurately detects this pollution, i.e. lighter gray-shades denote higher aerosol optical thickness values.

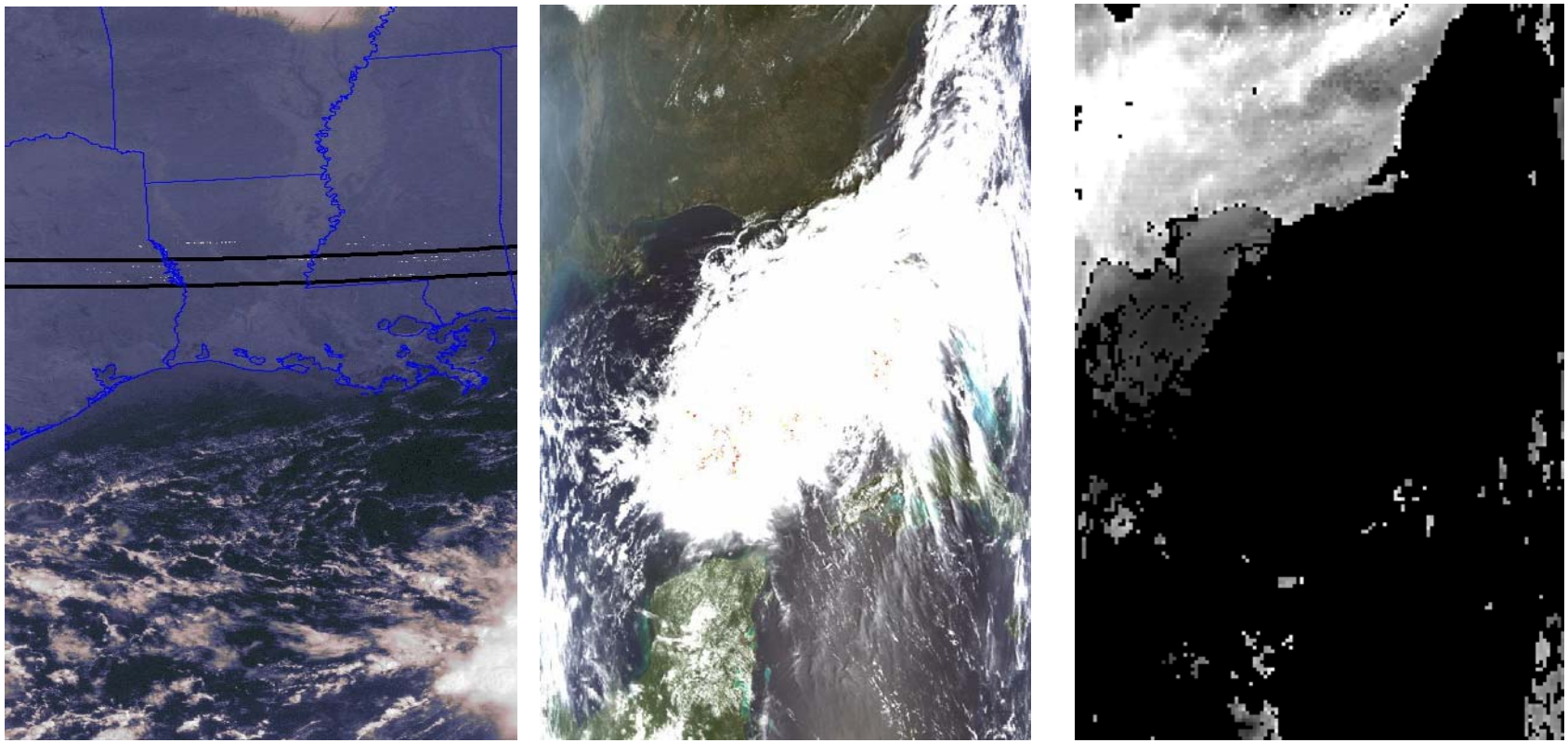

(1) GOES Channel 1 (2) MODIS Color Composite (3) Aerosol Analysis from NASA

Figure 2b. MODIS Band 12 (centered at 0.565 microns) in Panel (1) is representative of visible data collected by GOES satellites and shows no indication of mid-continental haze on September 11, 2002. However, a color composite of MODIS bands at 1625 UTC in Panel (2) reveals this pollution as a “blue” cloud. The MODIS MOD04 aerosol product (best reports for land and ocean) in Panel (3) shows the horizontal extend of the pollution and the relative concentration, with optical depths exceeding unity. Again, lighter gray-shades denote higher aerosol optical thickness values.

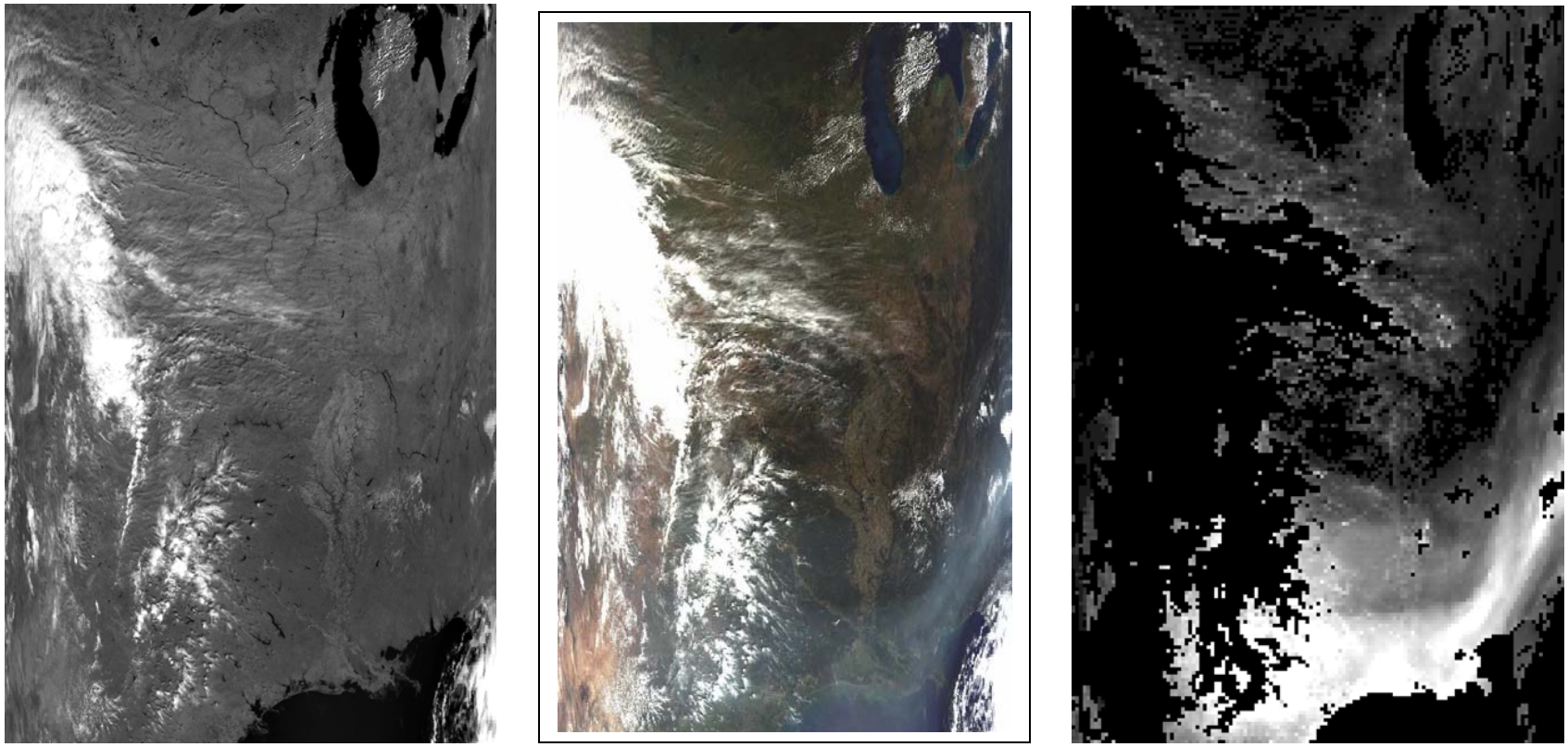

(1) MODIS Channel 12 (2) MODIS Color Composite (3) Aerosol Analysis from NASA

Figure 2c. Since GOES was not available from TCEQ, MODIS Band 12 is in Panel (1), MODIS color composite for 1705 UTC in Panel (2), and MODIS aerosol analysis from NASA in Panel (3). The MODIS MOD04 aerosol product shows the continental haze continues to be advected by strong northeasterly winds into Texas, since gray-shades denote higher aerosol optical thickness values. TCEQ issues a health alert for 150 counties in Texas on September 12, 2002.

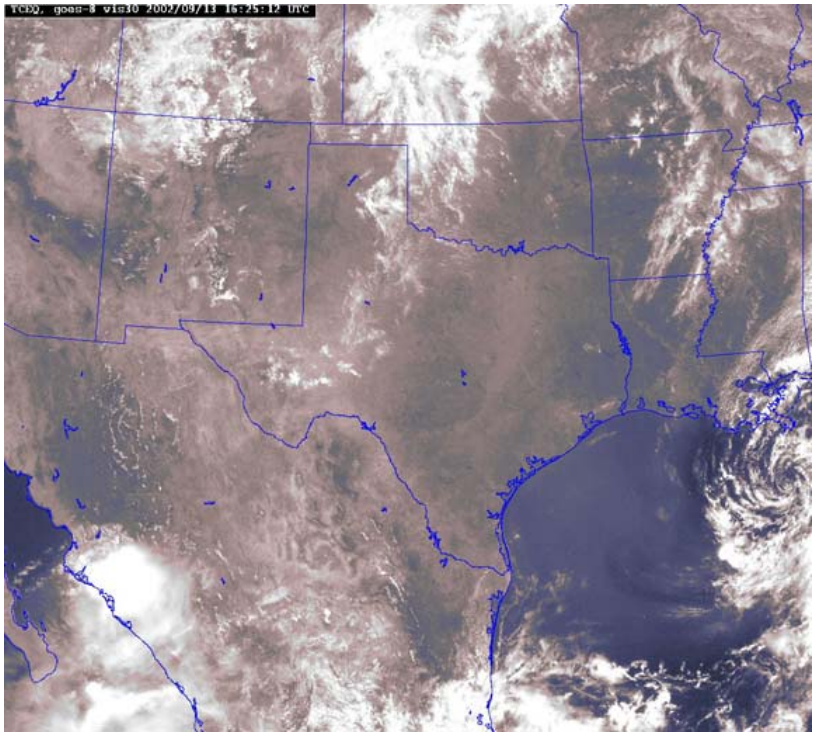

Figure 3. The aerosol “cloud” is evident by a bluish hue in cloud-free regions off the Texas coast of the GOES imagery received by TCEQ on September 14, 2002 but no indication is evident of pollution over land.

Preprint of article published in Atmospheric Environment 2004, vol. 38, pp. 5057-5070

The Use of MODIS Data and Aerosol Products for Air Quality Prediction

Keith D. Hutchison,* Solar Smith, and Shazia Faruqui
The University of Texas at Austin
Center for Space Research
3925 W. Braker Lane, Suite 200
Austin, Texas 78759-5321

ABSTRACT

The Center for Space Research (CSR) is exploring new approaches to integrate data collected by the MODerate resolution Imaging Spectroradiometer (MODIS) sensor, flown on NASA's Earth Observing System (EOS) satellites, into a real-time prediction methodology to support operational air quality forecasts issued by the Monitoring Operations Division (MOD) of the Texas Commission on Environmental Quality (TCEQ). Air pollution is a widespread problem in the United States, with over 130 million individuals exposed to levels of air pollution that exceed one or more health-based standards. Texas air quality is under assault by a variety of anthropogenic sources associated with a rapidly growing population along with increases in emissions from the diesel engines that drive international trade between the US and Central America. The challenges of meeting air quality standards established by the Environmental Protection Agency are further impacted by the transport of pollution into Texas that originates from outside its borders and are cumulative with those generated by local sources. In an earlier study, CSR demonstrated the value of MODIS imagery and aerosol products for monitoring ozone-laden pollution that originated in the central US before migrating into Texas and causing TCEQ to issue a health alert for 150 counties. Now, data from this same event are re-analyzed in an attempt to predict air quality from MODIS aerosol optical thickness (AOT) observations. The results demonstrate a method to forecast air quality from remotely-sensed satellite observations when the transient pollution can be isolated from local sources. These pollution sources can be separated using TCEQ's network of ground-based Continuous Air quality Monitoring (CAM) stations.

KEY WORDS: Remote Sensing, MODIS, Pollution, Air Quality, Forecasting, Continental Haze

Corresponding Author: Dr. Keith D. Hutchison, Center for Space Research, Tele: 512-471-7295, Fax: x-3570, e-mail: keithh@csr.utexas.edu

1. INTRODUCTION

Air pollution is a widespread problem in the United States (US) and, according to the Environmental Protection Agency (EPA), it is estimated that over 100 million individuals are routinely exposed to levels of air pollution that exceed one or more of their health-based standards (EPA, 2003). Texas air quality is under assault by a variety of anthropogenic sources, especially those associated with a rapidly growing population along with increases in emissions from the diesel engines that drive international trade between the US and Central America. The challenges of meeting air quality standards established by the EPA are further impacted by the transport of pollution into Texas that originates from outside its borders and are cumulative with those generated by local sources.

In 2001, staff from the Monitoring Operations Division (MOD) of the Texas Commission on Environmental Quality (TCEQ) requested CSR assess the value of remotely-sensed data from NASA's Earth Observing System research satellites to improve air quality management across Texas with emphasis on the detection of air pollution that originates outside its borders. TCEQ collects air quality data from a variety of sources including a network of ground-based Continuous Air quality Monitoring (CAM) sites, mobile laboratories, the Federal Aviation Administration's Automated Surface Observation System, forecasts from the US National Weather Service, and imagery from the US Geostationary Operational Environmental Satellites. However, these sources of operational data are not fully effective for detecting or quantifying the severity of pollution that originates over land while outside the borders of Texas (Hutchison, 2003).

Initially, staff from TCEQ MOD requested that CSR focus on assessing the value of data collected by the MODerate resolution Imaging Spectroradiometer (MODIS) sensor for monitoring pollution referred to as "continental haze." Two reasons were given:

- Continental haze originates over the middle-US and was deemed most difficult to detect and monitor with existing TCEQ data resources. MODIS data had been proposed to significantly increase the knowledge of global, tropospheric aerosols (King et al., 1999) and techniques were developed to retrieve aerosol data over land as well as ocean surfaces (Kaufman and Tanre, 1998). Two key aerosol products are generated from MODIS data: aerosol optical thickness (AOT) and an effective size parameter. The former is a function of the aerosol mass concentration, mass extinction efficiency, and relative humidity of the atmosphere through its hygroscopic growth factor (Kaufman and Fraser, 1983). In general, higher AOT values are associated with increased loading of tropospheric aerosols. Aerosol products are retrieved only during daytime and cloud-free conditions.
- Continental haze consists of high levels of ozone mixed with fine particulate materials, defined as those of diameter 2.5 microns or smaller ($PM_{2.5}$) which are generally composed of sulfate, nitrate (NO_x), organic and elemental carbon,

chloride and ammonium compounds. In regions of high NOx concentrations, e.g. industrial regions, a photochemical sequence initiated by the reaction of carbon monoxide (CO) with the hydroxyl radical (OH) leads to ozone production (Penner et al., 1991; Crutzen, 1979). These pollutants have been linked to a range of serious respiratory and cardiovascular health problems (Krewshi et al., 2000) and can remain in the atmosphere for days to weeks while being transported through the atmosphere across state boundaries.

During the September 11-15, 2002 timeframe, a significant continental haze pollution event brought ozone-laden aerosols from the industrial mid-west US into Texas and resulted in TCEQ issuing a health alert to residences in 150 Texas counties. Subsequently, CSR collected data on this event and demonstrated that this type of pollution is readily detected and monitored in both MODIS imagery and AOT data products (Hutchison, 2003). In the analysis of this case study, it was postulated that MODIS data products might also be used with trajectory-based forecasts to predict air quality associated with continental haze events. Thus, another study was undertaken to assess the potential for using MODIS data with trajectory-based forecasts to predict future air quality in Texas and the results are reported below.

2. METHODOLOGY

An approach for using MODIS imagery and AOT data products in a real-time, operational, trajectory-based forecast scheme was briefly overviewed in an earlier publication (Hutchison, 2003) and is now discussed at length. The methodology assumes that MODIS AOT values can be used to assess air quality. Then, trajectories are used to predict the quality of air being advected into the region during the forecast period. This change in forecast air quality is coupled with existing air quality measurements, based upon ground-base observations at CAM sites, to predict whether air quality is expected to improve, deteriorate or remain unchanged during the forecast period. The approach also assumes locally generated pollution remains constant. Thus, this “trend” forecast follows these steps:

1. Assess the air quality reported at a CAM facility on the first day,
2. Determine the MODIS AOT value at the site on this first day,
3. Forecast the expected AOT values to arrive at the CAM facility at six-hour intervals during the forecast period,
4. Identify the expected changes in forecast air quality, and
5. Predict the expected air quality.

At this time, a trend forecast approach is preferred to incorporate satellite-based observations into a real-time prediction scheme since ground-based pollution measurements cannot yet be specified from satellite-based AOT observations. For example, MODIS AOT values are dimensionless while CAM sites record ozone in parts-per-billion (ppb) and $PM_{2.5}$ in micrograms-per-cubic meter ($\mu g/m^3$). In addition, CAM sites represent point measurements while MODIS AOT values are reported for 10x10 km areas.

It is also important to consider whether the MODIS aerosol models used to retrieve AOT values adequately describe the constituents found in a particle type of pollution. Briefly, the algorithms used to retrieve MODIS AOT values, which differ for ocean and land backgrounds, assume that "aerosol models" adequately represent the different types of aerosols present in the atmosphere (Kaufman and Tanre, 1998). Typically, these models are used to make complex calculations of the expected energy arriving at the MODIS sensor in key bandpasses for a wide range of sun-Earth-satellite viewing geometries using sophisticated radiative transfer models. Comparisons between the MODIS observations and theoretical calculations are used to determine AOT as well as other aerosol parameters. Retrievals over land are based upon (1) continental, (2) biomass burning, (3) industrial/urban, or (4) dust aerosol models. Each model contains different data, e.g. aerosol size distribution and total particle concentration. The MODIS AOT product is reported to have an accuracy of +/- 0.05 +/- 0.2 over land (Chu et al., 2002) and +/- 0.02 with no offset over oceans (Remer et al., 2002) for aerosol optical depths across the range of 0-2.

While the accuracies of MODIS algorithms used to retrieve AOT values have been validated, it is less certain whether the aerosol models that form the basis for these retrievals adequately characterize the aerosols found in the continental haze observed over Texas. Thus, it remains a challenge to correlate MODIS AOT values with ground-based ozone and $PM_{2.5}$ pollution measurements made at CAM sites. Recent studies to correlate MODIS AOT values to ground-based pollution observations have been completed and the results are encouraging (Wang and Christopher, 2003). In addition, CSR plans additional studies using pollution measurements made with airborne lidar that will be collected coincident with MODIS data during the upcoming Texas Air Quality II Study (TCEQ, 2004). Meanwhile, MODIS AOT values can be used in a trend forecast approach to compensate for uncertainty between MODIS AOT values and ground-based pollution measurements. This approach is demonstrated in Section 4.

In this study, the transport of pollution considers only the horizontal component of the trajectories, i.e. aerosol sources and depletion processes are left as topics for future investigations. Backward trajectories were generated for selected TCEQ CAM sites using the HYSPLIT model developed by NOAA's Air Resource's Laboratory. (More information on the model is available at the following NOAA website: http://www.arl.noaa.gov/ready/hysplit4.html). Backward trajectories of 24-hour duration and valid at nominal MODIS overflight times of 1700 UTC each day were generated to terminate at the coordinates of TCEQ CAM sites used in the study. For example, TCEQ sites in the Dallas-Ft. Worth and Houston-Galveston areas are shown in Figure 1. Sites selected for this study include CAM sites 71 and 52 near Dallas and site 78 near Houston, which are highlighted by dashed-boxes. These sites were selected in an attempt to minimize the influence of locally generated pollution on study results by considering the location of the external pollution source, the position of the CAM sites in the metropolitan region, and the direction of the prevailing wind that carried the transient pollution into and across Texas.

Since the vertical distribution of the pollution was not precisely known, trajectories were generated to terminate at three different altitudes over each CAM site: 100m, 500m, and 3000m. Sample trajectories for three days (September 10, 14, and 15) at CAM site 71 near Dallas are shown in Figure 2, which will be referred to later in the text. Horizontal movement of the air parcels is shown in the top center of the figure with red depicting the trajectory terminating at 100m above ground level, blue at 500m, and green at 3000m. The vertical movement of the trajectory is shown in the bottom third of the figure. For example, in Panel (c), the air parcels that arrived at 500m originated at an altitude slightly higher than 2000 m.

Figure 1 here.

Again, the forecast approach assumes that trends in air quality can be predicted by examining changes in the quality of air transported into a given region, i.e. locally generated pollution remains constant. For example, assuming a gridded field of MODIS AOT values is available for 1700 UTC on 10 September 2002, the trajectories shown in Figure 2 are used to translate air parcels from their current location in the MODIS imagery to their predicted location some time in the future. In this case, trajectories were generated at six-hour intervals, e.g. 2300, 0500, 1100, and 1700 UTC.

Figure 2 here.

Thus, it is postulated that coupling the predicted air parcel movement, using backward trajectories, with the MODIS AOT analyses and existing ground-based observations would provide useful information on future air quality. When AOT values are predicted to continuously decrease or increase across the forecast timeframe, the trend forecast is straightforward, i.e. the forecast is for air quality to improve or deteriorate over that currently observed at the CAM facility. However, in cases where the forecast AOT first increases (decreases) and then decreases (increases) during a 24-hour timeframe, additional analyses are required to make the trend forecast. For example, a small deterioration (improvement) in air quality for a few hours, followed by improvement (deterioration) in air quality for a more extended period would result in a trend forecast for improved (degraded) air quality.

3. CONTINENTAL HAZE EVENT CASE STUDY

A brief overview is provided on compliance with EPA attainment standards, which is based upon time-averaged observations using a network of CAM sites similar to those shown in Figure 1. There is a 1-hour standard of 0.12 ppm and an 8-hour standard of 0.08 ppm. Since surface observations are made in ppb, there is an “exceedance” of the standard if the reported value is 125 ppb or greater for any 1-hour period or 85 ppb or greater for any 8-hour period. It is understood that the one-hour average is taken from 9-10, 10-11, 11-12, etc. using observations at CAM sites collected at 5 minute intervals.

The 8-hour average is obtained using 8-consecutive one-hour averages as described above. If a surface-based observation exceeds the 1-hour or 8-hour averaged exceedance values, the site fails to attain standard and is declared to be in "nonattainment." Daily maximums and minimums reported at CAM sites correspond to 0000-2359 local time each day.

TCEQ has demonstrated that ozone and $PM_{2.5}$ are strongly correlated in continental haze pollution events, as seen in Figure 3. Panels (a) and (b) document the 8-hour maximum and minimum observations of both ozone and $PM_{2.5}$ for the period June 1 – September 30, 2002 at TCEQ's CAM sites, shown in Figure 1, for the Dallas-Ft. Worth and Houston-Galveston areas, respectively. Units for ozone are in ppb (gold) with the scale of 0 – 160 found along the left ordinate while units for $PM_{2.5}$ (blue) are in $\mu g/m^3$ with the scale shown along the right ordinate. It is evident that the concentrations of ozone and $PM_{2.5}$ are strongly correlated in this type of pollution. Additionally the figure shows that continental haze events are common in Texas with nearly a dozen separate events observed between June 1, 2002 and September 30, 2002. The ozone component of continental haze remains the current focus at CSR since it appears instrumental in creating the unique signature in MODIS color imagery used to monitor this type of pollution, e.g. blowing sand from west Texas, which contains $PM_{2.5}$ particles without ozone, appears grayish in similar false color composites shown in Figure 2 by Hutchison (2003).

The September 10-16 continental haze event has been studied due to its severity. (Hutchison, 2003; Wang and Christopher, 2003). AOT values of at least 1.65 were observed in the MODIS data products for this pollution event. In addition, the prolonged cloud-free conditions accompanying the event allowed high quality MODIS AOT products to be created on a near-daily basis for the duration of the event.

Figure 3 here.

The 9-16 September 2002 continental haze event brought ozone-laden aerosols from the industrial mid-west into Texas and resulted in TCEQ issuing a health alert for 150 Texas counties on 13 September 2002 (Hutchison, 2003). The source of the pollution is clearly seen in the 9 September 2002 MODIS data, shown in Panel (a) of Figure 4, as the mid-west where high AOT values are observed from Illinois through Michigan. (Note: brighter shades of gray in the aerosol product represent regions of higher AOT values while the darker shades depict lower values. Also, note that aerosol products are not created for cloudy areas or for cloud-free water surfaces that contain sun-glint. Therefore, pixels not included in the aerosol analysis appear as black in these gray scale images.)

It is believed that this pollution event originated from anthropogenic sources, e.g. possibly coal-fired power plants or similar industrial activities. The daily migration of the pollution, shown in Panels (a) – (h) of Figure 4, is readily monitored in the MODIS AOT analyses from 10-16 September respectively. The pollution enters Texas during the 10 -

11 September timeframe, with the major pollution levels found along a line from the Louisiana-Arkansas border due west into northern Texas. From earlier results (Hutchison, 2003) it was found that CAM facilities in the Dallas-Ft. Worth area were the first to show exceedances of ozone standards. The pollution then moves in a more southerly direction in the 12 September image [Panel (d)] with highest aerosol levels extending from central Texas toward the southern part of Louisiana then eastward. On 13 September, shown in Panel (e), the pollution appears to be most heavily concentrated in central Texas but has also moved into Oklahoma and Kansas showing a change in the wind direction at the level of transport, which is confirmed by the trajectories shown in Figure 2. On September 14, there is little apparent change in the location of the pollution, although there appears to be a decrease in the pollution concentration, due to sedimentation, as shown by reduced AOT values. Cloud cover obscures most of Texas on 15-16 September. Thus, the analysis of a trend forecast from these MODIS data is limited to the period 10-15 September.

The original post-event analysis of this continental haze event began at CSR with the arrival of MODIS imagery from the EOSDIS. At the time of the earlier report, MODIS aerosol products did not become available at CSR in a manner sufficiently timely to support the operational data requirements at TCEQ (Hutchison, 2003). Subsequently, CSR purchased a MODIS ground station that now provides real-time MODIS imagery and aerosol products for use at TCEQ. Using the software in the CSR ground station, all MODIS data shown in Figure 4 were re-processed. In addition, the ground station software provides the capability to interrogate pixel-level data to determine precisely the AOT values along the paths shown by trajectories similar to those in Figure 2.

4. RESULTS

Table 1 shows the observed AOT values and those predicted to arrive by the 500 m trajectories over the next 24 hours at each CAM facility. (Data were collected for 12 different CAM sites but cloud cover or missing data reduced this number to seven. If only a small number of AOT values were missing, “no value (nv)” was entered rather than eliminate the station from the study.) Below each MODIS observation is the predicted values at each site for the following 6, 12, 18, and 24 hours. These forecast values appear in the table under “trajectory 2300”, “trajectory 0500”, “trajectory 1100”, and “trajectory 1700” respectively. (Similar tables were created for trajectories that terminate at 100m and 3000m.)

Table 1 here.

Next, the MODIS observations and trajectory forecasts were combined to make trend forecasts at each CAM facility. As previously noted, in cases where AOT values were predicted to continuously decrease or increase across the 24-hour period, the trend forecast in air quality was to improve or deteriorate, respectively, over that currently observed at the CAM facility. For example, as shown in Table 1, the MODIS AOT value for CAM 71 site near Dallas (32.56N/96.32W) on 10 September 2002 was 0.28. The

trajectory forecasts show increasingly polluted air would arrive at each of the 6-hour intervals over the next 24 hours, as indicated by AOT values of 0.29, 0.42, 0.43, and 0.50 at 1700 UTC on 11 September 2002. Thus the trend forecast for 11 September 2002 for CAM 71 site is 0.38 which is “worse” than the 0.28 value at the beginning of the forecast interval. Thus, deteriorating air quality is predicted for this CAM facility over that observed on 10 September 2002.

In cases where smaller deteriorations (improvements) were predicted to be followed by larger improvements (deteriorations) in air quality for a more extended time period, the trend forecasts shown in Table 1 consists of a “+” (“-“) based upon the weighted average of all prediction AOT values over the 24-hour timeframe. For example, the MODIS observation at the same CAM site on 11 September was 0.77. The trajectory forecast for each of the following 6-hour intervals was 0.91, 0.82, 0.63, and 0.57 and the 24-hour weighted average value was 0.76 or slightly lower in value than the MODIS observation on 11 September. Thus, the 24-hour trend forecast calls for a slight improvement on 12 September over conditions observed in the CAM reports on 11 September. This trend forecast is reflected by the “+” in Table 1.

Table 2 contains the observed 24-hour changes in ground-based pollution measurements at each of the TCEQ CAM locations. These observations serve as truth for the verification of the satellite and trajectory-based air quality trend forecasts shown in Table 1. The surface-based observations were taken from the 8-hour maximum ozone levels collected between 0000-2359 local time on consecutive days. This method of reporting air quality means the verification window (unavoidably) covers a larger timeframe than the trend forecast. To demonstrate the process used to verify trend forecasts, attention turns again to the CAM 71 site discussed in the proceeding paragraph. From Table 2, it is seen that the 8-hour maximum ozone concentration measured on 11 September was 75 ppb while the worst report on 12 September was 68 ppb. Thus, the trend in the CAM measurements showed improved air quality during this period, which agrees with the trend forecast made from the MODIS data using HYSPLIT trajectories.

Table 2 here.

Table 3 contains the comparisons between trend forecasts, based upon the transport of MODIS AOT data with trajectories that terminate at 500m (shown in Table 1) and changes in ground-based observations at CAM sites that serve as verification data sets (shown in Table 2) for this study.

Table 3 here.

5. DISCUSSION

Since Texas was mostly cloud covered on 9 September, as indicated by the absence of AOT observations in Panel (a) of Figure 4, trend forecasts could not be generated for 10

September as shown in Table 1. In addition, cloud cover prevented forecasts from being issued from the 15 September data, as well as several instances at individual CAM locations during the continental haze event, e.g. in the MODIS AOT analysis for Dallas Kaufman CAM 52 facility on 13 September 2002.

It was possible to issue and verify 32 forecasts for the 7-CAM facilities over the 5-day period of the study shown in Table 3. The success rate of these forecasts was (25/32) 78% for this single case study. Thus, the vast majority of trend forecasts agreed with the changes reported in the CAM observations. Seven forecasts were in error with three only slightly in error, e.g. by 1-2 ppb, while another three were more grossly in error, e.g. by more than 10 ppb. Those grossly in error include: (a) Mauriceville CAM 642 site (13-14 September) was predicted to have improved air quality but the CAM observations showed increased ozone levels of 12 ppb, (b) Mauriceville CAM 642 site (14-15 September) was forecast to experience poorer air quality but the CAM observations showed improvement of 19 ppb, and (c) Austin CAM 38 site (14-15 September) was forecast to have more polluted air but reports showed significant improvement by 36 ppb in ozone.

Forecasts were poorest for the 13-14 September timeframe when eastern Texas was located at the edge of scan of the two MODIS passes that comprise the image shown in Panel (e) of Figure 4. Typically, retrieved AOT values are less accurate at edge of the MODIS scan than nearer the center position. Forecasts were worst for the Houston Conroe CAM 78 site than any other CAM facility. A review of the MODIS data for 11-12 and 12-13 September periods suggested the forecasts should have been accurate; but, the trend in CAM reports disagreed with the forecast trends. The reason could be due to differences between validation times and will be further examined in the future after a more fully automated system has been implemented so larger data sets can be studied.

From the results shown in Table 3, there are reasons to incorporate a satellite-based, trend forecast approach at this time into an operational, air quality decision support system. First, this type of forecast system effectively predicts the deterioration in air quality associated with a continental haze event as shown by the successes across all stations during the 10-11 September timeframe in Table 3. The capability to predict the arrival of transient pollution into a metropolitan area could be most valuable for those communities with mitigation plans to help avoid exceedances of air quality standards. Secondly, the trend forecast approach appears to predict the culmination of the pollution event, which is needed to minimize the financial penalty to communities that provide subsidies to residents, e.g. no-cost mass transit, as incentives to reduce local pollution during periods when air quality is expected to deteriorate. Most notably, the trajectory-based approach accurately predicted improved air quality for the Dallas-Ft. Worth metropolitan area on September 15th behind an advancing cold front.

The trend forecasts along with trajectories shown in Panels (a) – (c) of Figure 2 provide greater insight into CAM observations recorded during the continental haze event. Initially, the CAM reports in the Dallas-Ft. Worth area show increased levels of pollution

on 9-11 September as the ozone-laden pollution moves into Texas as predicted by the trajectories for 10 September in Panel (a). Air quality in the region then begins to improve between 12-13 September as the maximum levels of pollution move south, toward central Texas and the Gulf Coast. Then, higher ozone levels return on 14 September as the circulation pattern reverses on 13 September, as seen in Panel (b) of Figure 2, from a northerly to a southerly direction, which pushes the polluted air a second time into the Dallas-Ft. Worth region. Ozone levels then remain high until less polluted air arrives behind a frontal system on 15 September as predicted in Panel (c). The insights obtained using the MODIS AOT product with trajectories clearly show that a primary contributor to the poor air quality observed at these CAM locations, in the Dallas-Ft. Worth region, originated from external sources.

The MODIS AOT values and trajectory forecasts also provide information on sources of pollution. In this study, it was clearly shown that the source of the continental haze event was the mid-western states. The trajectories also show that air from Arkansas would bring pollution from this source to Austin by 1700 UTC on 10 September 2002. It was also noted, but not shown due to space limitations, that a second source of pollution, from central Louisiana where biomass burning appears to be in progress, would combine with the continental haze to bring much poorer air quality to San Antonio on the same date. This second source of pollution impacted the quality of air at locations east of San Antonio, including the Conroe (Houston) and Mauriceville (Beaumont) regions. Thus, two separate sources of pollution combined over south-central Texas to make the air in San Antonio highly polluted during this timeframe.

To more closely examine cases where the AOT values did not consistently increase or decrease during a 24-hour forecast period, the one-hour maximum CAM observations were examined for Austin CAM 3 and Austin CAM 38 sites. Results are shown in Table 4. Changes in CAM reports used to verify the MODIS-based trend forecasts are shown in bold type for the period 10-12 September for Austin CAM 3 facility. The legend for this table is as follows:

- W = air quality is forecast to become Worse (higher ozone levels)
- B = air quality is forecast to become Better (lower ozone levels)
- Blue = CAM reports and MODIS-based trend forecasts are in agreement
- Red = CAM reports and MODIS-based trend forecasts are not in agreement

For example, the trend forecasts for this site between 11AM and 5 PM on 11 September was an increase in ozone reflected by AOT values increasing from 0.53 to 0.57 respectively indicating a deterioration in air quality. The actual CAM 3 observations during this period increased from 73 to 82 and then back to 78 ppb. By comparison, the CAM observations for the previous day started at 53 and gradually increased to 56. So, the trend in ozone levels reported at each hour during this period was worse on 11 September than the corresponding hour on 10 September. Thus, the “Ws” are all shown in blue font for this timeframe.

The results for these two Austin sites are summarized in Table 5 to show the accuracy of MODIS AOT and trajectory-based trend forecasts as a function of oscillations in the AOT forecast values. In addition, the table demonstrates the need to segregate locally generated pollution from transient pollution in order to predict air quality from MODIS AOT values. This is apparent since the data for CAM 38 facility, which is located in the northwest Austin suburb of Cedar Park, shows that trend forecasts are most reliable when AOT values increase through the period. When trends in AOT values change only once, e.g. increase then decrease, forecast skill drops but the predictions remain useful. When trends in AOT values change more frequently, e.g. increase then decrease and increase again, the accuracy of the trend forecasts further degrades. However, similar inferences cannot be made from the CAM 3 site data which is placed at the intersection of two heavily congested Austin thoroughfares, i.e. Highway 183 and Loop 1. (The same type of analysis was done for two CAM facilities located in the Dallas-Ft. Worth area and similar results were obtained.) Thus, the ability to predict air quality from MODIS AOT values using a trajectory-based system requires the capability to isolate locally generated pollution from transient sources. If this capability does not exist, it becomes most difficult to understand the impact of externally generated pollution upon local communities.

6. CONCLUSIONS

This study has demonstrated that MODIS AOT analyses used with trajectories in a trend forecast methodology should become an increasingly important part of a more comprehensive air quality decision support system, especially when used along with ground-based air quality observations. First, this type of forecast system can be used to predict the onset and impact of transient pollution on regional air quality, which could be valuable for those communities with mitigation plans to help protect the health of its residents and avoid exceedances of air quality standards. Secondly, such a system can also be used to predict the return to normal air quality that had deteriorated due to transient pollution, which could minimize the financial penalty to communities that provide subsidies to reduce locally generated pollution during periods of poor air quality. Finally, use of a satellite-based trend forecast methodology provides greater insight into data collected by ground-based air quality observations and could result in a reduced number of CAM sites, which are expensive to install and maintain, that are needed for air quality management.

CSR continues to explore new approaches to integrate EOS data into the operational environment of the Texas user community (Tapley et al., 2001). In 2003, a MODIS direct broadcast ground station was purchased to provide real-time imagery and aerosol data products to TCEQ and others in the Texas user community. Furthermore, results from this study demonstrate the need for a real-time, automated system to predict air quality in an operational forecast environment. The ultimate goal of such a forecast approach is to translate the entire 10x10 km^2 AOT gridded-fields, shown in Figure 4, forward in time using another gridded-field of trajectories. With a sufficiently short time-step, e.g. between 1-3 hours, it is envisioned that the final product would appear similar

to a time-series of clouds in geostationary meteorological satellite data, as frequently seen on television weather broadcasts. This system would allow air quality managers to visualize the migration of pollution across regional boundaries and into metropolitan centers.

However, before a fully automated system can be created, additional research is needed to address several inter-related topics. First, additional research is required to develop a more robust approach to differentiate between locally generated and transient pollution sources without added reliance upon ground-based observations. Secondly, satellite observations must be correlated with ground-based pollution monitoring systems for a variety of pollution classes. Research is also needed to incorporate pollution sources and sinks, i.e. through analyses of gravitational and wind forces using the vertical component of the trajectory. Finally, it is necessary to characterize the vertical profiles of particle size and total number distributions of pollution classes possibly with data from more advanced systems flown on future satellites, e.g. from the Aerosol Polarimeter Sensor scheduled to fly soon on the National Polar-orbiting Operational Environmental Satellite System.

It is becoming increasingly clear that the migration of pollution across regional boundaries can impact air quality across Texas and the quality of life of its residents. The ability to predict the onset and impact of transient pollution on metropolitan regions is of paramount importance to developing an effective air pollution management program. While it is still too early to quantify the value of data products derived from satellite-based observation for air quality management, the initial results of this study provide encouragement to implement an automated, trend forecast methodology in the CSR MODIS direct broadcast ground station and then continue assessing the value of these data for air quality management in Texas.

7. REFERENCES

Chu, D. A., Kaufman, Y. J., Ichoku, C., Remer, L. A., Tanre, D. and B. N. Holben, 2002: Validation of MODIS aerosol optical depth retrieval over land, Geophys. Res. Ltrs., 29, 10.1029/2001GLO13205.

Crutzen, P. J., 1979: The role of NO and NO2 in the chemistry of the troposphere and stratosphere, Ann. Rev. Earth Planet. Sci., **7**, 443-472.

Hutchison, K. D. and S. Smith: Distribution of earth observing system data via the Texas InfoMart, Proceedings of the EUMETSAT User's Conference, 2-6 September 2002, Dublin, Ireland.

Hutchison, K. D., 2003: Application of MODIS satellite data and products for monitoring air quality in the state of Texas, Atmospheric Environment, **37**, 2403-2412.

Kaufman, Y. J. and D. Tanre, 1998: Algorithm for remote sensing of tropospheric aerosol from MODIS, NASA MODIS Algorithm Theoretical Basis Document, Goddard Space Flight Center, pp 85.

Kaufman, Y. J. and R. S. Fraser, 1983: Light extinction by aerosols during summer air pollution, Journal of Applied Meteorology, **22**, 1694-1706.

King, M. D., Kaufman, Y. J., Tanre, D., and T. Nakajima,1999: Remote sensing of tropospheric aerosols from space: past, present, and future, Bulletin of the American Meteorological Society, Vol. 80, No. 11, 2229-2259.

Penner, J. E., Atherton, C. S., Dignon, J., Ghan, S. J., and J. J. Walton, 1991: Tropospheric nitrogen: A three-dimensional study of sources, distributions, and deposition, J. Geophy. Res., 96, 959-990

Remer, L. A., Tanre, D., Kaufman, Y. J., Ichoku, C., Mattoo, S., Levy, R., Chu, D. A., Holben, B., Dubovik, O., Smirnov, A., Martins, J. V., Li, R.-R., and Z. Ahmad, 2002: Validation of MODIS aerosol retrieval over ocean, Geophys. Res. Ltrs., 29, 10.1029/2001GLO13204.

Tapley, B. D., Crawford, M. M., Howard, T., Hutchison, K. D., Smith, S., and G. L. Wells: A vision for creating advanced products from EOS core system data to support geospatial applications in the State of Texas, Proceedings from the IEEE International Geoscience and Remote Sensing Symposium, 9-13 July 2001, Sydney, Australia.

Texas Commission on Environmental Quality Draft Science Plan for The Texas Air Quality Study II, 29 January 2004. (http://www.tnrcc.state.tx.us/air/aqp/airquality_techcom.html#topic2b3)

United State Environmental Protection Agency, The Ozone Report, Measuring Progress through 2003, (See: http://www.epa.gov/airtrends/ozone.html)

Wang J. and S. A. Christopher, 2003: Intercomparison between satellite-derived aerosol optical thickness and $PM_{2.5}$ mass: Implications for air quality studies, Geophysical Research Letters, **30**, doi: 10.1029/2003GLO18174.

Figure Captions:

Figure 1. TCEQ Continuous Air quality Monitoring (CAM) sites in the greater Dallas-Ft. Worth and Houston areas. CAM 71 site, CAM 52 site in Panel (a) and CAM 78 site in Panel (b) were used in this study and shown in green-dashed boxes. These sites were chosen due to their proximity to the metropolitan regions and the migration of the continental haze.

Figure 2. Graphical representation in Panels (a), (b), and (c) show 24-hour backward trajectories from NOAA's HYSPLIT model, at 6-hour intervals, for air parcels terminating at the Kaufman (CAM 71 site) southeast of Dallas, TX at 1700 UTC on September 10, 14, and 15 respectively for altitudes of 100m (red), 500m (blue), and 300m (green).

Figure 3. Graphical representation of daily maximum and minimum of ozone and PM2.5 for a series of continental haze events impacting the Dallas-Ft. Worth area, in Panel (a), and Houston-Galveston, in Panel (b) between 1 June and 30 September 2002. (Courtesy of TCEQ MOD)

Figure 4. Panels (a) – (h) show daily aerosol optical thickness analyses from MODIS Terra of the continental haze pollution event during September 9-16, 2002. (Composite analyses were made from consecutive MODIS passes from the Terra spacecraft.)

Table Captions

Table 1. Aerosol optical thickness values from MODIS analyses and trend forecasts based upon 24-hour HYSPLIT trajectories that terminate at an altitude of 500m above ground level for each CAM facility.

Table 2. Trends in maximum 8-hour ozone concentrations, reported in part-per-billion, observed at TCEQ ground-based CAM locations serve as truth for the forecasts predicted in Table 1.

Table 3. Comparisons between trajectory-based forecasts of aerosol optical thickness values and truth observations from TCEQ ground-based pollution measurements.

Table 4. Comparisons of trend forecasts from MODIS AOT values using trajectories and 1-hour maximum ozone levels observed at locations in the Austin area. (CAM 3 site is an inner city Austin site at intersection of Highway 183 and Loop 1 and CAM 38 site is in residential NW Austin) Results show locally generated pollution masks externally generated pollution. (W = worse air quality, B = better air quality, Red = missed forecast, Blue = correct forecast)

Table 5. Accuracy of MODIS AOT value and trajectory-based trend forecasts, compared to 1-hour maximum ozone observations at continuous air quality monitoring sites, as a function of oscillations in forecast AOT values and proximity of CAM locations to sources of locally generated pollution.

List of Figures

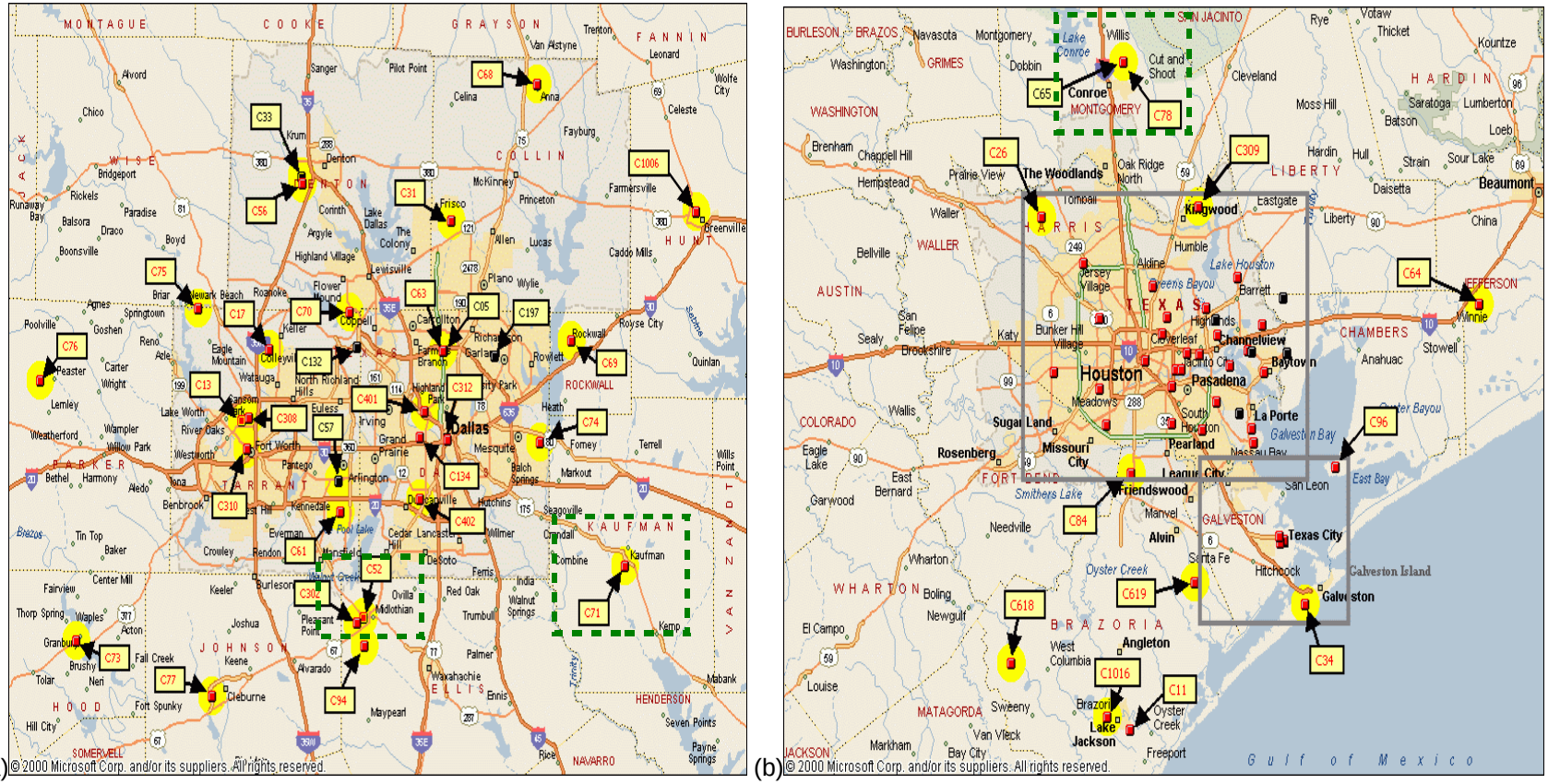

Figure 1.

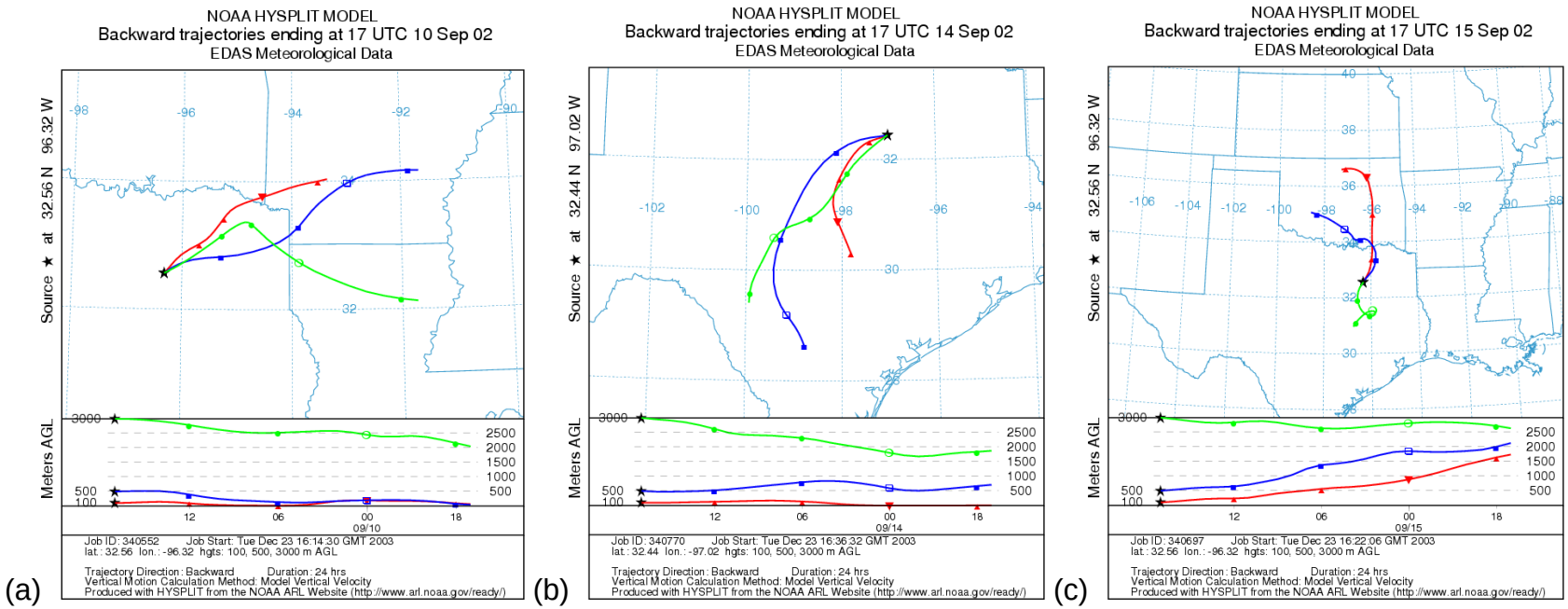
NOAA HYSPLIT MODEL
Backward trajectories ending at 17 UTC 10 Sep 02
EDAS Meteorological Data
Source ★ at 32.56 N 96.32 W
Meters AGL
Job ID: 340552 Job Start: Tue Dec 23 16:14:30 GMT 2003
lat: 32.56 lon: -96.32 hgts: 100, 500, 3000 m AGL
Trajectory Direction: Backward Duration: 24 hrs
Vertical Motion Calculation Method: Model Vertical Velocity
Produced with HYSPLIT from the NOAA ARL Website (http://www.arl.noaa.gov/ready/)
NOAA HYSPLIT MODEL
Backward trajectories ending at 17 UTC 14 Sep 02
EDAS Meteorological Data
Source ★ at 32.44 N 97.02 W
Meters AGL
Job ID: 340770 Job Start: Tue Dec 23 16:36:32 GMT 2003
lat: 32.44 lon: -97.02 hgts: 100, 500, 3000 m AGL
Trajectory Direction: Backward Duration: 24 hrs
Vertical Motion Calculation Method: Model Vertical Velocity
Produced with HYSPLIT from the NOAA ARL Website (http://www.arl.noaa.gov/ready/)
NOAA HYSPLIT MODEL
Backward trajectories ending at 17 UTC 15 Sep 02
EDAS Meteorological Data
Source ★ at 32.56 N 96.32 W
Meters AGL
Job ID: 340697 Job Start: Tue Dec 23 16:22:06 GMT 2003
lat: 32.56 lon: -96.32 hgts: 100, 500, 3000 m AGL
Trajectory Direction: Backward Duration: 24 hrs
Vertical Motion Calculation Method: Model Vertical Velocity
Produced with HYSPLIT from the NOAA ARL Website (http://www.arl.noaa.gov/ready/)

(a) (b) (c)

Figure 2.

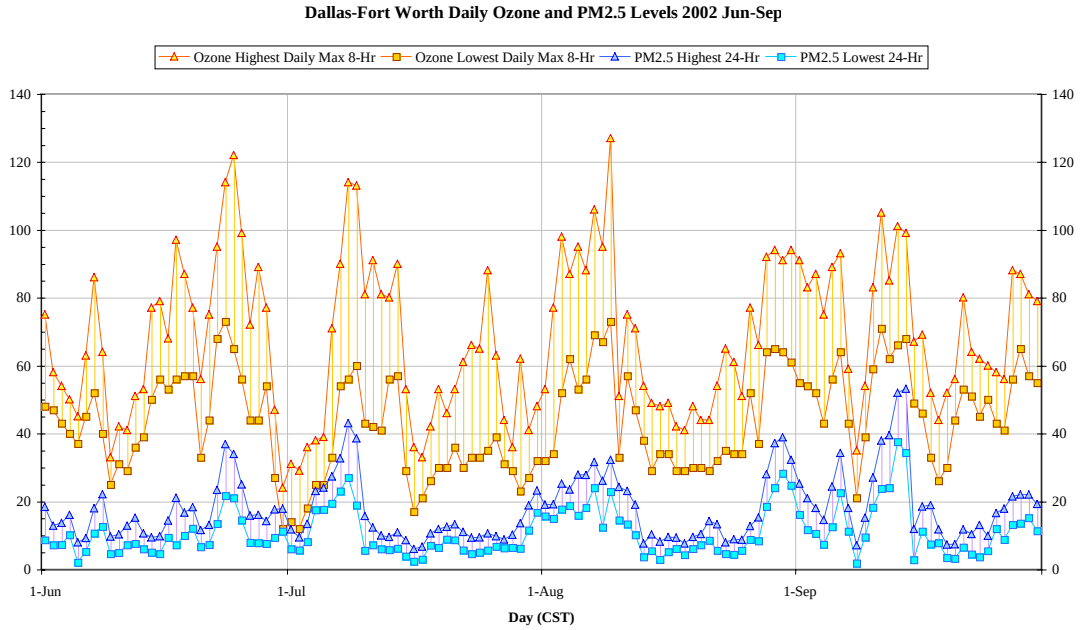
Dallas-Fort Worth Daily Ozone and PM2.5 Levels 2002 Jun-Sep
Ozone Highest Daily Max 8-Hr
Ozone Lowest Daily Max 8-Hr
PM2.5 Highest 24-Hr
PM2.5 Lowest 24-Hr
140
120
100
80
60
40
20
0
1-Jun
1-Jul
1-Aug
1-Sep
Day (CST)

(a)

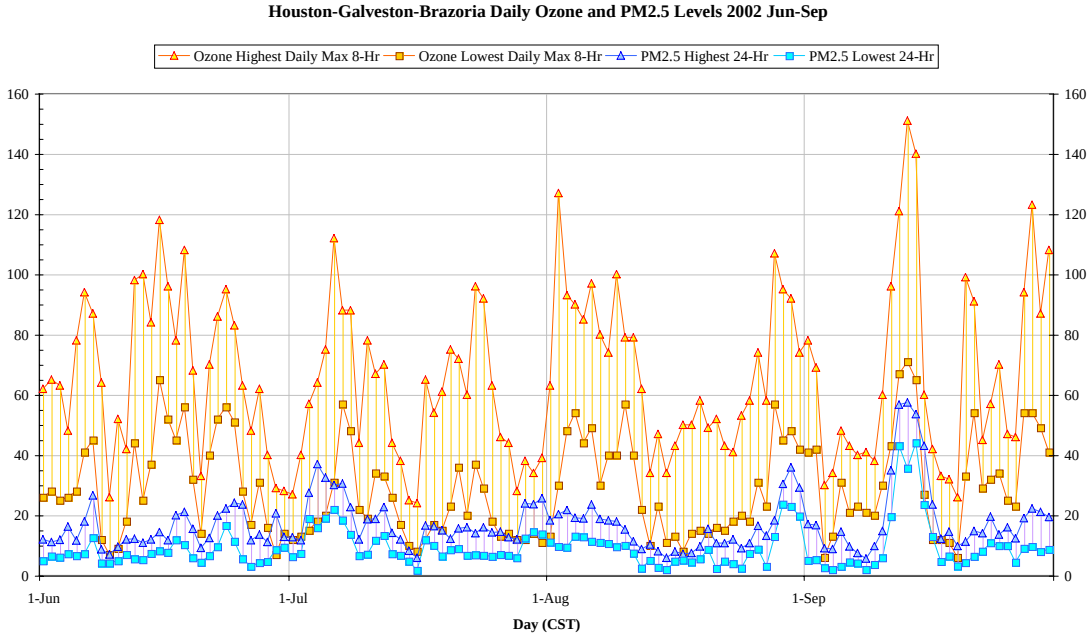
Houston-Galveston-Brazoria Daily Ozone and PM2.5 Levels 2002 Jun-Sep
Ozone Highest Daily Max 8-Hr
Ozone Lowest Daily Max 8-Hr
PM2.5 Highest 24-Hr
PM2.5 Lowest 24-Hr
160
140
120
100
80
60
40
20
0
1-Jun
1-Jul
1-Aug
1-Sep
Day (CST)

(b)

Figure 3.

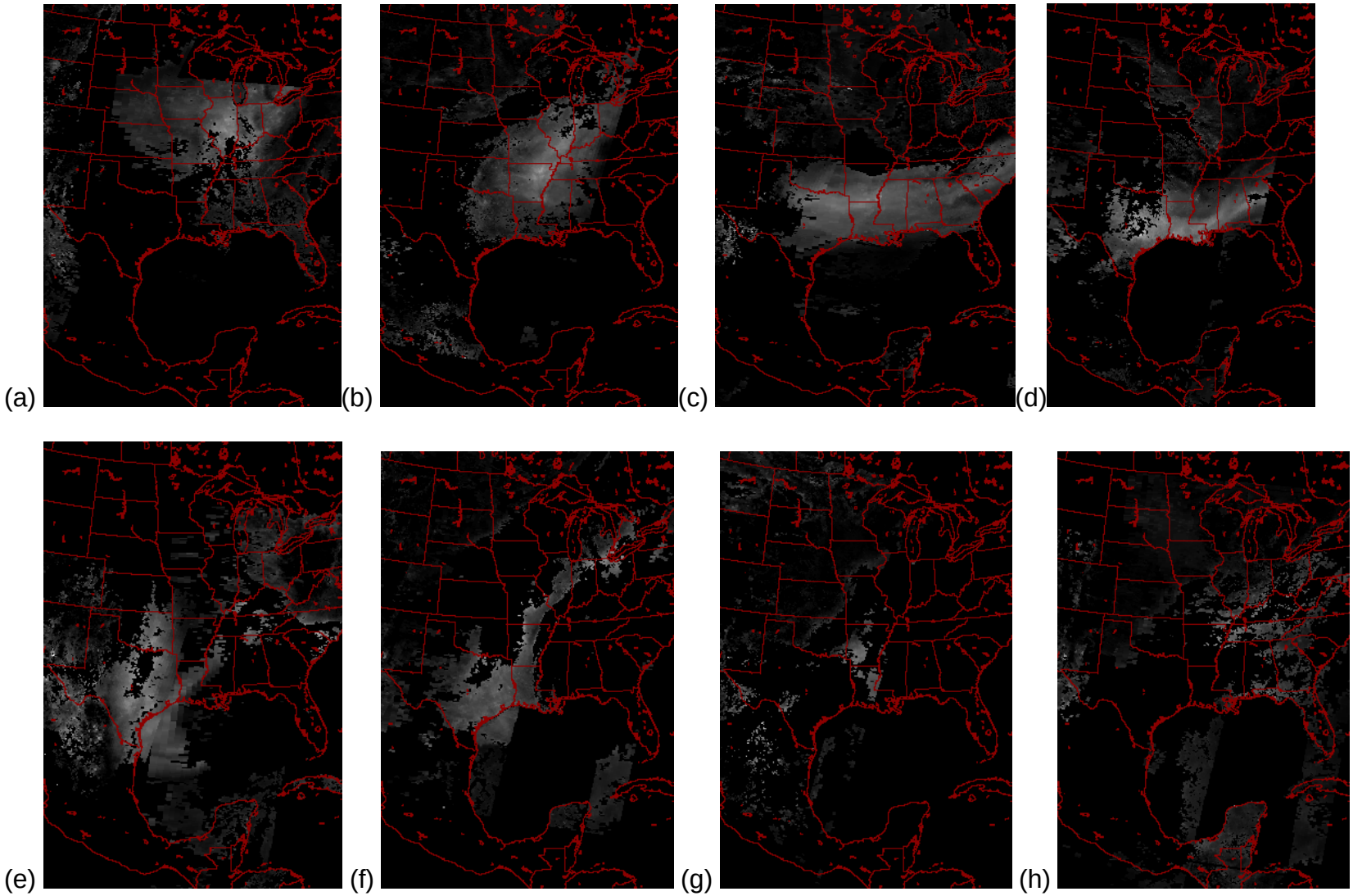

Figure 4.

List of Tables

Table 1.

Date	Valid Time	Dallas Kaufman (C71)	Beaumont Mauriceville (C642)	Austin Cedar Park (C38)	Corpus Christi (C4)	Dallas Midlothian (C52)	San Antonio Calveras Lake (C59)	Houston Conroe (C78)
(mm/dd/yy)	(UTC)	32.56/96.32	30.18/93.87	30.48/97.87	27.76/97.43	32.44/97.02	29.59/98.31	30.35/95.43
9/09/2002 MODIS	1700	No value (nv)	nv	nv	nv	nv	nv	nv
Trajectory	2300	nv	nv	nv	nv	nv	nv	nv
Trajectory	500	nv	0.53	nv	nv	nv	nv	nv
Trajectory	1100	nv	nv	0.37	nv	nv	nv	0.23
Trajectory	10/1700	0.50	nv	nv	Nv	1.16	0.52	0.38
24Hr Average		N/A	N/A	N/A	N/A	N/A	N/A	N/A
Trend Forecast	9/1700 -10/1700	N/A	N/A	N/A	N/A	N/A	N/A	N/A
9/10/2002 MODIS	1700	**0.28**	**0.24**	**0.29**	**nv**	**0.31**	**0.28**	**0.20**
Trajectory	2300	0.29	0.34	0.29	nv	0.40	0.28	0.34
Trajectory	500	0.42	0.35	0.40	nv	0.40	0.37	0.41
Trajectory	1100	0.43	0.36	0.40	nv	0.43	0.37	0.62
Trajectory	11/1700	0.50	0.39	0.49	0.25	0.44	0.40	0.69
24Hr Average		**0.38**	**0.34**	**0.37**	**N/A**	**0.40**	**0.34**	**0.45**
Trend Forecast	10/1700 -11/1700	worse	worse	worse	N/A	worse	worse	worse
9/11/2002 MODIS	1700	**0.77**	**0.53**	**0.53**	**0.24**	**0.72**	**0.35**	**0.52**
Trajectory	2300	0.91	0.47	0.57	0.19	0.71	0.39	0.54
Trajectory	500	0.82	0.52	0.63	0.23	0.81	0.54	0.59
Trajectory	1100	0.63	0.67	0.80	0.52	0.67	0.63	0.70
Trajectory	12/1700	0.57	0.70	0.85	0.56	0.42	0.66	0.91
24Hr Average		**0.76**	**0.57**	**0.67**	**0.35**	**0.69**	**0.52**	**0.64**
Trend Forecast	11/1700 -12/1700	+	-	worse	-	+	worse	worse
9/12/2002 MODIS	1700	**0.87**	**0.77**	**1.15**	**0.69**	**0.94**	**0.76**	**0.95**
Trajectory	2300	0.90	1.07	1.10	Nv	1.02	0.70	0.81
Trajectory	500	0.96	0.47	0.97	Nv	1.19	0.71	0.84
Trajectory	1100	0.71	0.50	1.10	nv	1.12	1.00	0.48
Trajectory	13/1700	0.80	0.35	1.00	0.81	1.24	1.65	0.45

24Hr Average		**0.85**	**0.65**	**1.06**	**0.81**	**1.11**	**0.90**	**0.71**
Trend Forecast	12/1700 -13/1700	+	better	+	N/A	-	-	+
9/13/2002 MODIS	1700	**0.99**	**0.65**	**1.05**	**0.69**	**nv**	**1.00**	**0.49**
Trajectory	2300	1.20	0.44	0.92	0.69	1.09	0.62	1.06
Trajectory	500	0.95	0.63	0.78	0.49	0.78	0.80	0.76
Trajectory	1100	1.01	0.81	0.76	0.55	0.77	0.77	0.76
Trajectory	14/1700	1.01	0.62	0.81	0.64	0.70	0.81	0.76
24Hr Average		**1.04**	**0.63**	**0.85**	**0.60**	**N/A**	**0.77**	**0.80**
Trend Forecast	13/1700 -14/1700	-	+	+	+	-	+	-
9/14/2002 MODIS	1700	**0.99**	**0.52**	**0.60**	**0.88**	**0.96**	**0.53**	0.59
Trajectory	2300	0.96	0.61	0.75	0.37	1.03	0.53	0.57
Trajectory	500	0.74	0.68	0.67	0.22	0.80	0.53	0.63
Trajectory	1100	0.52	0.71	0.77	0.22	0.42	0.4	0.5
Trajectory	15/1700	0.36	0.61	0.55	0.17	0.36	0.46	0.52
24Hr Average		**0.72**	**0.64**	**0.69**	**0.33**	**0.73**	**0.49**	**0.56**
Trend Forecast	14/1700 -15/1700	better	-	-	better	+	+	+

Table 2.

Date	Valid Time	Dallas Kaufman C71	Beaumont Mauriceville (C642)	Austin Cedar Park (C38)	Corpus Christi (C4)	Dallas Midlothian (C52)	San Antonio Calavaras Lake C59	Houston Conroe C78
(yy/mm/dd)	Local	32.56/ 96.32	30.18/ 93.87	30.48/ 97.87	27.76/ 97.43	32.44/ 97.02	29.59/ 98.31	30.35/ 95.43
20020909	0000-2359	43	21	32	40	45	40	36
20020910	0000-2359	60	39	47	35	70	51	43
24-hr trend		**-17**	**-18**	**-15**	**+5**	**-25**	**-11**	**-17**
20020910	0000-2359	60	39	47	35	70	51	43
20020911	0000-2359	75	60	71	69	94	67	77
24-hr trend		**-15**	**-21**	**-24**	**-34**	**-24**	**-16**	**-34**
20020911	0000-2359	75	60	71	69	94	67	77
20020912	0000-2359	68	65	80	100	74	86	75
24-hr trend		**+7**	**-5**	**-9**	**-31**	**+20**	**-19**	**+2**
20020912	0000-2359	68	65	80	100	74	86	75
20020913	0000-2359	66	57	80	96	86	90	82
24-hr trend		**+2**	**+8**	**0**	**+4**	**-12**	**-4**	**-7**
20020913	0000-2359	66	57	80	96	86	90	82
20020914	0000-2359	81	69	81	71	79	78	81
24-hr trend		**-15**	**-12**	**-1**	**+25**	**+7**	**+12**	**+1**
20020914	0000-2359	81	69	81	71	79	78	81
20020915	0000-2359	57	50	45	36	58	46	47
24-hr trend		**+24**	**+19**	**+37**	**+35**	**+21**	**+32**	**+34**
20020915	0000-2359	57	50	45	36	58	46	47
20020916	0000-2359	46	16	31	36	57	29	42
24-hr trend		**+11**	**+34**	**+14**	**0**	**+1**	**+17**	**+5**

Table 3.

Category	Date/ Time	Dallas Kaufman (C71)	Beaumont Mauriceville (C642)	Austin Cedar Park (C38)	Corpus Christi (C4)	Dallas Midlothian (C52)	San Antonio Calavaras Lake C59	Houston Conroe C78
	Local	32.56/ 96.32	30.18/ 93.87	30.48/ 97.87	27.76/ 97.43	32.44/ 97.02	29.59/ 98.31	30.35/ 95.43
24-hr fcst (500m)	9/1100 -10/1100	N/A	N/A	N/A	N/A	N/A	N/A	N/A
24-hr trend (Truth)	09/0000-10/23 59	-17	-18	-15	+5	-25	-11	-17
24-hr fcst (500m)	10/1100 -11/1100	worse	worse	worse	N/A	worse	worse	worse
24-hr trend (Truth)	10/0000-11/23 59	-15	-21	-24	-34	-24	-16	-34
24-hr fcst (500m)	11/1100 -12/1100	+ (better)	- (worse)	worse	- (worse)	+ (better)	worse	**worse**
24-hr trend (Truth)	11/0000-12/23 59	+7	-5	-9	-31	+20	-19	**+2**
24-hr fcst (500m)	12/1100 -13/1100	+ (better)	better	+	N/A	- (worse)	- (worse)	**+ (better)**
24-hr trend (Truth)	12/0000-13/23 59	+2	+8	0	(+4)	-12	-4	**-7**
24-hr fcst (500m)	13/1100 -14/1100	- (worse)	**+ (better)**	**+ better**	+ (better)	N/A	+ (better)	**- (worse)**
24-hr trend (Truth)	13/0000-14/23 59	-15	**-12**	**-1**	(+25)	+7	+12	**+1**
24-hr fcst (500m)	14/1100 -15/1100	better	**- (worse)**	**- (worse)**	better	+ (better)	+ (better)	+ (better)
24-hr trend (Truth)	14/0000-15/23 59	+24	**+19**	**+36**	(+35)	+21	+32	+34
24-hr fcst (500m)	15/1100 -16/1100	N/A	N/A	N/A	N/A	N/A	N/A	N/A
24-hr trend (Truth)	15/0000-16/23 59	+11	+34	+14	0	+1	+17	+5

Table 4.

Austin	CAM 3 Site	0AM	1AM	2AM	3AM	4AM	5AM	6AM	7AM	8AM	9AM	10AM	11AM	Noon	1PM	2PM	3PM	4PM	5PM	6PM	7PM	8PM	9PM	10PM	11PM
Location	183 & 1																								
Monday	9 Sep	21	21	21	18	16	13	10	10	15	18	23	28	35	33	32	35	**39**	37	39	37	32	26	26	25
Tuesday	10 Sep	25	21	16	18	14	11	7	10	24	38	49	51	**53**	**53**	**54**	**55**	**55**	**56**	**49**	**38**	**32**	**34**	**39**	**46**
Wed'y	11 Sep	**45**	**41**	**35**	**35**	**37**	**39**	**32**	**32**	**38**	**52**	**68**	**80**	**73**	**73**	**78**	**82**	**82**	**78**	**66**	**35**	**38**	**30**	**31**	**36**
Trend Fcst	**11-12 Sep**												**0.53**	W	W	W	W	W	**0.57**	W	W	W	W	W	**0.63**
		W	W	W	W	W	**0.80**	W	W	W	W	W	**0.85**												
Thursday	12 Sep-02	**41**	**36**	**32**	**35**	**37**	**31**	**23**	**23**	**46**	**44**	**71**	**85**	99		95	97	87	62	49	15	10	13	24	26
Trend Fcst	12 13 Sep												**1.15**	B	B	B	B	B	**1.10**	B	B	B	B	B	**0.97**
		W	W	W	W	W	**1.10**	B	B	B	B	B	**1.00**												
Friday	13 Sep-02	22	12	15	17	16	11	10	6	47	56	82	93			98			96	79	49	31	35	46	59
Trend Fcst	13 -14 Sep												**1.15**	B	B	B	B	B	**1.10**	B	B	B	B	B	**0.97**
		W	W	W	W	W	**1.10**	B	B	B	B	B	**1.00**												
Saturday	14 Sep	38	34	60	60	57	63	57	51	58	72	83	86	89			97	93	80	63	39	35	23	Missing	Missing
Sunday	15 Sep	46	47	47	48	42	40	38	38	41	40	39	37	37	43	**53**	50	49	46	33	31	27	18	13	6
Monday	16 Sep	12	15	18	24	27	27	16	13	10	8	14	25	29	**33**	28	24	18	18	20	18	15	11	22	18
Austin	**CAM 38 Site**	**0AM**	**1AM**	**2AM**	**3AM**	**4AM**	**5AM**	**6AM**	**7AM**	**8AM**	**9AM**	**10AM**	**11AM**	**Noon**	**1PM**	**2PM**	**3PM**	**4PM**	**5PM**	**6PM**	**7PM**	**8PM**	**9PM**	**10PM**	**11PM**
Location	Cedar	Park																							
Monday	9 Sep	19	18	16	16	16	15	14	15	17	19	22	25	29	35	34	32	31	33	**37**	27	24	18	16	14
Tuesday	10 Sep	12	14	14	12	12	11	10	14	24	37	46	45	45	45	47	49	**52**	52	44	42	41	39	40	45
Wed'y	11 Sep	46	45	43	38	36	32	32	34	36	48	69	74	71	69	71	74	**75**	67	53	50	58	52	52	52
Trend Fcst	11-12 Sep												**0.53**	W	W	W	W	W	**0.57**	W	W	W	W	W	**0.63**
		W	W	W	W	W	**0.80**	W	W	W	W	W	**0.85**												
Thursday	12 Sep	51	54	45	47	45	41	43	38	47	57	76	87	**91**	89	85	88	71	60	43	44	34	25	21	27
Trend Fcst	12-13 Sep												**1.15**	B	B	B	B	B	**1.10**	B	B	B	B	B	**0.97**
		W	W	W	W	W	**1.10**	B	B	B	B	B	**1.00**												
Friday	13 Sep	32	36	37	32	31	29	17	30	50	58	73	81	81	**84**	81	80	80	81	55	49	42	50	61	62
Trend Fcst	13-14 Sep												**1.05**	W	W	W	W	W	**1.07**	B	B	B	B	B	**0.98**
		B	B	B	B	B	**0.80**	W	W	W	W	W	**0.81**												
Saturday	14 Sep	53	44	38	45	49	39	36	43	54	66	73	78	78	78	78	87	**94**	82	53	49	38	41	Missing	Missing
Sunday	15 Sep	41	36	37	37	36	35	33	33	35	35	37	40	38	46	**53**	53	53	43	28	23	20	17	11	20
Monday	16 Sep	16	20	27	22	23	22	18	10	14	20	24	27	35	**42**	36	37	31	23	22	14	8	6	14	25

Table 5.

CAM Site Number	Forecast Date	Forecast Oscillations	Number of Correct Forecasts	Number of Incorrect Forecasts
CAM 38 Site – Residential area in NW Austin	11-12 September 2002	0 (24-hr worse)	24	0
	12-13 September 2002	2 (12-hr better, then 6-hr worse, 6-hr better)	12	12
	13-14 September 2002	2 (6-hr worse, 12-hr better, then 6-hr worse)	7	17
CAM 3 Site – intersection of Freeways 183 & 1 inside Austin		0 (24-hr worse)	11	13
		2 (12-hr better, then 6-hr worse, 6-hr better)	9	15
		2 (6-hr worse, 12-hr better, then 6-hr worse)	7	17

3B2v8.06a/w (Dec 5 2003).51c + model | AEA : 6133 | Prod.Type:FTP pp.1–14(col.fig.:2,3,4,5) | ED:AnilaM. PAGN:gopal SCAN:v4soft

ARTICLE IN PRESS

Available online at www.sciencedirect.com

SCIENCE DIRECT®

ELSEVIER

Atmospheric Environment ▮ (▮▮▮▮) ▮▮▮–▮▮▮

ATMOSPHERIC ENVIRONMENT

www.elsevier.com/locate/atmosenv

Correlating MODIS aerosol optical thickness data with ground-based $PM_{2.5}$ observations across Texas for use in a real-time air quality prediction system

Keith D. Hutchison*, Solar Smith, Shazia J. Faruqui

Center for Space Research, 3925 Braker Lane Ste 200, Austin, TX 78759, USA

Received 23 March 2005; received in revised form 26 July 2005; accepted 8 August 2005

Abstract

Investigations have been conducted at the Center for Space Research (CSR) into approaches to correlate MODIS aerosol optical thickness (AOT) values with ground-based, $PM_{2.5}$ observations made at continuous air monitoring station locations operated by the Texas Commission on Environmental Quality (TCEQ). These correlations are needed to more fully utilize real-time MODIS AOT analyses generated at CSR in operational air quality forecasts issued by TCEQ using a trajectory-based forecast model developed by NASA. Initial analyses of two data sets collected during 3 months in 2003 and all of 2004 showed linear correlations in the 0.4–0.5 range in the data collected over Texas. Stronger correlations (exceeding 0.9) were obtained by averaging these same data over longer timescales but this approach is considered unsuitable for use in issuing air quality forecasts. Peculiarities in the MODIS AOT analyses, referred to as hot spots, were recognized while attempting to improve these correlations. It is demonstrated that hot spots are possible when pixels that contain surface water are not detected and removed from the AOT retrieval algorithms. An approach to reduce the frequency of hot spots in AOT analyses over Texas is demonstrated by tuning thresholds used to detect inland water surfaces and remove pixels that contain them from the analysis. Finally, the potential impact of hot spots on MODIS AOT-$PM_{2.5}$ correlations is examined through the analysis of a third data set that contained sufficient levels of aerosols to mask inland water surfaces from the AOT algorithms. In this case, significantly stronger correlations, that exceed the 0.9 value considered suitable for use in a real-time air quality prediction system, were observed between the MODIS AOT observations and ground-based $PM_{2.5}$ measurements.

Keywords: ■; ■; ■

1. Introduction

A methodology for using MODIS imagery and aerosol optical thickness (AOT) data products in a real-time, operational, trajectory-based forecast scheme has been demonstrated (Hutchison et al., 2004). The methodology assumes that remotely sensed AOT values can be used to assess air quality at the time of MODIS overflight of Texas through correlations between satellite and ground-based air quality observations. Trajectories are then used to

*Corresponding author. Tel.: +1 512 471 7295; fax: +1 512 471 3570.

E-mail address: keithh@csr.utexas.edu (K.D. Hutchison).

1352-2310/$ - see front matter © 2005 Elsevier Ltd. All rights reserved.
doi:10.1016/j.atmosenv.2005.08.036

predict the quality of air that will be advected into any region of interest during the forecast period. The change in forecast air quality, i.e. change between the current and forecast AOT values, is coupled with air quality measurements made with ground-base observations at continuous air monitoring station (CAMS) locations operated by the Texas Commission on Environmental Quality (TCEQ), to predict whether air quality is expected to improve, deteriorate or remain unchanged at any given CAMS location during the forecast period.

This trend forecast approach was initially intended to demonstrate the viability of using MODIS AOT as a qualitative indicator of air quality fluctuations in the absence of an established quantitative relationship between the MODIS AOT and ground-based observations. Some recent studies that correlated MODIS AOT values to ground-based pollution observations provided encouraging results (Wang and Christopher, 2003; Chu et al., 2002); however, no similar capability had been demonstrated with a statistically significant data set collected across Texas. Thus, in our earlier paper (Hutchison et al., 2004) it was concluded that additional research was needed to address several inter-related issues before a fully automated, near real-time air quality prediction model could be implemented. First, additional research was required to develop a more robust approach to differentiate between locally generated and transient pollution sources in satellite data without added reliance upon ground-based observations. Secondly, strong correlations between satellite observations and ground-based pollution measurements across Texas needed to be established for a variety of pollution classes, e.g. continental haze, smoke from biomass burning in Central America, and airborne sand from the Sahara Desert. Third, research was also needed to include pollution sources and sinks, i.e. through the vertical component of the trajectory and gravitational forces acting on the particulate material. Finally, it would be necessary to characterize the pollution classes and particulate sizes, possibly using data from more advanced sensors that will be flown on future satellites, e.g. from the Aerosol Polarimeter Sensor which is scheduled to fly on the National Polar-orbiting Operational Environmental Satellite System.

In the meantime, the Center for Space Research (CSR) has continued to implement a real-time AOT-based air quality forecast model. The model uses trajectories generated by a NASA program called Infusing satellite Data into Environmental Applications (IDEA). However, the IDEA software has been tailored by CSR to include the TCEQ region of interest which extends from about 15–45° north latitude and 80–110° west longitude. The IDEA model has also been modified by CSR to increase its vertical and spatial resolutions. This prototype model is currently running at CSR and expected to become operational during the Fall of 2005. Preparation for validating the model output proceeds concurrently as CSR staff examine approaches for correlating MODIS AOT values with ground-based pollution measurements collected at the CAMS locations operated by TCEQ. The results obtained from these investigations are the topic of this paper.

2. Methodology

Initial analyses at CSR focused on correlating MODIS AOT observations with hourly, ground-based $PM_{2.5}$ measurements made at all active CAMS locations across Texas during the period 2000–2004. $PM_{2.5}$ monitoring stations were first installed during the 1997–1998 timeframe and by the year 2000 were considered sufficiently capable of providing reliable and regular measurements of local pollutant concentrations. Stations are located principally near urban metropolitan areas, as well as along the Gulf coast region, the southern border with Mexico, and proximal to significant sources of natural and industrial emissions. Currently, 51 stations monitor $PM_{2.5}$ in 16 areas statewide. Hourly $PM_{2.5}$ observations are derived from 5-min measurements averaged and reported in units of $\mu g\,m^{-3}$. There are a number of CAMS facilities that report these measurements but sites may be activated or deactivated without notice. More information on these CAMS facilities is available at the TCEQ website: http://www.tnrcc.state.tx.us/air/monops/index.html

MODIS observations were generated at the CSR direct broadcast ground station using version 3.1 of the algorithms developed by the NASA aerosol team (Kaufman et al., 1997a–c). NASA currently uses version 4.2 of these algorithms, so some aspects of the algorithms have continued to evolve, e.g. the 10–40 (in version 2 and 3) vs. 20–50 (in version 4) percentile of radiances are used in the retrieval (Chu et al., 2003) and the approach to cloud screening has changed (Martins et al., 2002). However, the theoretical approach used to retrieve AOT, with

observations in the 0.47-, 0.66-, and 2.13-μm bands, has remained essentially unchanged (Levy et al., 2005). Relevant aspects of the approach for this paper may be summarized by noting that MODIS AOT analyses are retrieved with one of two very different algorithms: one for ocean regions the other for land. Ideally, the land algorithm is applied only to a sub-set of those 500-m MODIS pixels that have no ocean or inland water within the field-of-view. In addition, analyses are not produced for pixels that are classified as cloud contaminated. Over ocean surfaces, analyses are not produced if the pixel falls within areas of possible sunglint. While detailed information on the MODIS AOT retrieval algorithms are provided in Section 3.2.1 below, other publications must be reviewed to obtain a more thorough understanding of these algorithms (Kaufman et al., 1997a; Tanre' et al., 1997; Remer et al., 2005; Levy et al., 2005).

Meaningful interpretation of AOT-$PM_{2.5}$ correlations can be complicated by differences between spatial and temporal scales of each data set (Ichoku et al., 2002). MODIS AOT analyses have a nominal horizontal spatial resolution of 10×10 km at nadir, i.e. based upon an analysis of 400, 500-m MODIS pixels. However, this analysis area increases to about 20×48 km for pixels collected at the edge of the 2330-km MODIS swath. $PM_{2.5}$ observations at CAMS sites represent point measurements taken at 5-min intervals and reported hourly. Any MODIS AOT analysis may include more than one ground-based CAMS site. CSR created statistics in a manner that follows others (Engel-Cox et al., 2004; Chu et al., 2003) from the analysis of 5×5 AOT pixel groups (covering an area of approximately 50×50 km at nadir), 3×3 AOT pixel groups (covering a 30×30 km area at nadir), and the center AOT pixel in these groups, which was set to correspond to the coordinates of the CAMS location. Thus, for each CAMS facility making $PM_{2.5}$ observations, statistics were generated from the MODIS AOT retrievals that reported the counts, minimum, maximum, mean and standard deviation of non-zero values in each pixel group. MODIS AOT pixel group statistics were then correlated with ground-based observations made at individual CAMS locations. The 5×5 and 3×3 AOT pixel group analyses were also correlated with statistics developed from $PM_{2.5}$ data collected at all CAMS locations within a metropolitan area.

3. Results

Results are presented in three stages that correspond to the process used during investigations at CSR to correlate MODIS AOT analyses with air quality observations. In Section 3.1, initial results are present that do not show strong linear correlations in the data collected over Texas. We do show that stronger correlations can be obtained by averaging CAMS data over longer timescales; however, this approach better supports climate modeling than a real-time air quality prediction system. In an attempt to better understand the reasons for the poorer than expected correlations, anomalies in the MODIS AOT retrievals were discovered and are discussed at length in Section 3.2. Additional studies were undertaken to better understand these anomalies in the MODIS AOT retrievals which led to the results shown in Section 3.3 that suggest significantly improved correlations are possible after compensating for AOT hot spots. The implication of these anomalies in MODIS AOT analyses upon a real-time air quality prediction system is discussed as part of the conclusions reached during these investigations.

3.1. Preliminary analyses

Initial attempts to develop useful AOT-$PM_{2.5}$ correlations relied upon two data sets that covered the periods August 12–November 25, 2003 and the entire 2004 calendar year. These data sets included AOT analyses and $PM_{2.5}$ observations from all CAMS facilities located in Texas. AOT analyses were generated in the Earth Observing System (EOS) direct broadcast ground station at CSR using version 3.1 of the algorithms and obtained from NASA's EOS Data Gateway (EDG) which currently uses version 4.2 of these algorithms.

Since the summer of 2003, CSR has been supplying TCEQ daily with AOT analyses that coincide with their $PM_{2.5}$ monitoring sites. Since these data were generated by CSR as part of an operational production process, as specified by TCEQ staff, not all statistics can be created from each data set. For example, only statistics for the 5×5 AOT pixel groups could be created from the 2003 data set while, in the 2004 data set, the center pixel data was also available along with data from the 5×5 pixel groups. Our analysis of these data suggested that the small statistical variations between pixel groups of different sizes did not warrant

regeneration of the 2003 data set. However, when additional data were processed to conduct further investigations, discussed in Section 3.3, data sets were generated for the 5×5 pixel groups, and 3×3 pixel groups and the center pixels.

Correlation statistics developed from the 2003 data set, created at CSR, are shown down in Table 1. For each Texas Metropolitan region (column 1) and CAMS facility (column 2), which is uniquely identified by the CAMS site reference number (column 3), the number of MODIS AOT and CAMS observation pairs (column 4) represents the sample size used for successive correlation tests. For each CAMS location the average AOT in the 5×5 pixel group was compared against the time-coincident, hourly $PM_{2.5}$ measurement of the CAMS facility and the minimum $PM_{2.5}$ measured at all CAMS facilities within the geographic metropolitan area, with coefficients reported in columns 6 and 7, respectively. Columns 8–11 contain statistics on the hourly $PM_{2.5}$ averages recorded at the time of the MODIS overflight by the CAMS site.

The '*p*-value' reported in Table 1, Column 4 indicates the probability that the same result would be obtained if the correlation between the data sets were zero. The '*p*-value' is directly related to the variability within a given data set and indirectly related to number of observations. A high probability indicates the result is random, i.e. could be arrived at by pure chance. Thus, it is desirable that values in this column be less than 0.1. In Table 1, it is noted that the lowest correlations are not relevant because the probabilities are high, indicating the specific CAMS site correlation test is statistically insignificant.

To summarize the results for the statistically significant tests shown in Table 1, correlation coefficients between MODIS average AOT in the 5×5 pixel group and hourly $PM_{2.5}$ measurements range between 0.31 and 0.43, for prominent sites in Amarillo (CAMS #305), Austin (CAMS #3), Dallas (CAMS #56, CAMS #71, CAMS #94, and CAMS #74), Longview (CAMS #85), and San Antonio (CAMS #301). When statistics for the MODIS AOT pixel group are compared with the minimum area $PM_{2.5}$ observations, the correlations for the Ft. Worth-Arlington CAMS #310 site also fall into this range. Lower correlations occur in data collected in the Galveston and Corpus Christi regions, while very low correlations of less than 0.1 are seen in the Houston and Beaumont-Port Arthur areas.

AOT-$PM_{2.5}$ linear correlations exhibit a wide spread (0.1–0.8) in MODIS AOT retrievals surrounding any given $PM_{2.5}$ bin. Examples of this scatter are shown in Fig. 1 for Dallas area CAMS #56 (Denton Airport) and Longview CAMS #85 (Karnack) facilities. The spread in these data are similar to that seen in comparisons between MODIS AOT values and aeronet data as shown in Fig. 4 of Levy et al. (2005).

Since many of the correlations listed in Table 1 were based upon a statistically insignificant data set, another analysis was performed on a full year's worth of data collected during 2004, which included center pixel data with each AOT analysis. Data generated from Julian Days 60-199 were obtained from the NASA EDG while the remaining data were created at CSR. Table 2 contains the results from the analysis of this expanded data set. The results were stratified by source of AOT analyses.

From Table 2, it is evident that all correlations are statistically significant since the probabilities associated with the null hypothesis are extremely small (<0.0001). In general, higher correlations exist between the hourly $PM_{2.5}$ data and the single, center pixel AOT data (0.32–0.60) than found with the 5×5 pixel group (0.26–0.49). However, comparisons between the observation counts (columns 3 and 4) show that valid values for the single pixels are available less frequently than the average of the 5×5 pixel group. This occurs for a variety of reasons, e.g. cloud contamination. The reasonably high correlations (0.80–0.92) that exist between the center pixel AOT values and those in the 5×5 AOT averages may mitigate concerns regarding use of 5×5 AOT averages for comparisons when the center pixel value is not available.

Next, it is seen that AOT-$PM_{2.5}$ correlation results in the 5×5 pixel group of this expanded 2004 data set are within the same range as those found in the more limited 2003 data set shown in Table 1. Stronger correlations were found in the 2004 data set at a few sites, such as CAMS #85 (Longview Karnack) and CAMS #78 (Houston Conroe Relocated). However, correlations found with this expanded data set do not approach the more desirable results described earlier in the literature (Wang and Christopher, 2003; Chu et al., 2003). There was no significant difference in correlation statistics when stratified by origin of the AOT analyses, i.e. CSR vs. the NASA EDG.

Therefore, an attempt was made to reproduce results in a manner similar to those published earlier

Table 1
Correlation statistics between MODIS AOT and $PM_{2.5}$ measurements for the period 12 August–25 November 2003

Texas metro area	CAMS facility	CAMS no.	No. of obs.	Pr. (T) Ho: $p = 0$	Avg_AOT5 vs. hourly $PM_{2.5}$	Avg_AOT5 vs. areamin $PM_{2.5}$	Mean $PM_{2.5}$	Max $PM_{2.5}$	Min $PM_{2.5}$	Std. dev. $PM_{2.5}$
Amarillo	Amarillo	305	98		0.3752	0.3752	8.928	23.250	0.900	4.157
Austin–San Marcos	Audubon	38	53		0.1675	0.2272	8.997	18.850	1.820	3.93
Austin–San Marcos	Austin_Northwest	3	104		0.4312	0.4102	7.185	18.200	0.290	4.263
Corpus Christi	Corpus_Christi_West	4	118		0.2236	0.2572	8.584	24.330	0.470	5.472
Corpus Christi	National_Seashore	314	129		0.1980	0.2027	7.523	25.410	0.410	4.811
Dallas	Dallas_Hinton_Street	401	108		0.1528	0.2416	11.942	28.450	−0.180	6.748
Dallas	Denton_Airport_South	56	114		0.3992	0.4296	10.092	35.640	−0.190	6.1598
Dallas	Kaufman	71	121		0.4024	0.4660	9.838	24.650	0.080	5.803
Dallas	Midlothian_Tower	94	117		0.3176	0.2928	8.596	23.250	0.720	4.795
Dallas	Midlothian_Wyatt_Road	302	113		0.1832	0.2816	9.911	24.220	0.180	5.761
Dallas	Sunnyvale_Long_Creek	74	113		0.3343	0.3822	9.68	26.370	0.020	5.783
Fort Worth–Arlington	Arlington_Municipal_Airport	61	119	$p > 0.2$	0.1139	0.1407	10.157	26.480	0.110	5.637
Fort Worth–Arlington	Diamond_Hill_Fort_Worth	308	114		0.1437	0.2623	10.7498	27.420	−0.200	6.161
Fort Worth–Arlington	Grapvine_Fairway	70	117		0.2449	0.2349	9.8282	26.930	−0.070	6.209
Fort Worth–Arlington	Haws_Athletic_Center	310	104	$p > 0.1$	0.1517	0.3370	10.735	27.930	−0.150	6.005
Galveston–Texas City	Galveston_Airport	34	126		0.2085	0.2085	9.742	33.180	0.530	6.03
Houston	Channelview	15	121	$p > 0.8$	0.0136	0.0398	13.405	40.340	0.890	8.283
Houston	Clinton	403	107	$p > 0.8$	−0.0307	0.0123	15.589	40.880	3.810	9.094
Houston	Conroe_Relocated	78	128	$p > 0.3$	0.1492	0.0820	10.433	28.070	0.600	5.903
Houston	Houston_Aldine		114	$p > 0.8$	0.0171	0.0646	12.214	36.760	0.200	7.443
Houston	Houston_Deer_Park	35	119	$p > 0.4$	0.0731	0.0980	12.461	53.320	0.810	9.377
Houston	Houston_East	1	117	$p > 0.9$	−0.0113	0.0085	13.291	45.540	1.710	7.963
Houston	Kingwood	309	128	$p > 0.9$	−0.0055	0.0407	11.02	44.120	0.020	7.567
Houston	Seabrook_Friendship_Park	45	99	$p > 0.3$	0.1015	0.0326	10.931	47.000	0.490	8.153
Longview–Marshall	Karnack	85	125		0.3308	0.3308	12.094	30.200	0.380	6.306
Lubbock	Lubbock	306	67	$p > 0.3$	0.1268	0.1268	6.442	19.470	0.210	4.121
San Antonio	CPS_Pecan_Valley		108	$p > 0.6$	0.0503	0.2703	9.891	32.810	−0.200	6.347
San Antonio	Calaveras_Lake	59	105	$p > 0.1$	0.1273	0.2917	8.817	33.240	0.030	5.844
San Antonio	Selma	301	102		0.3241	0.2919	8.169	22.770	−0.160	5.412

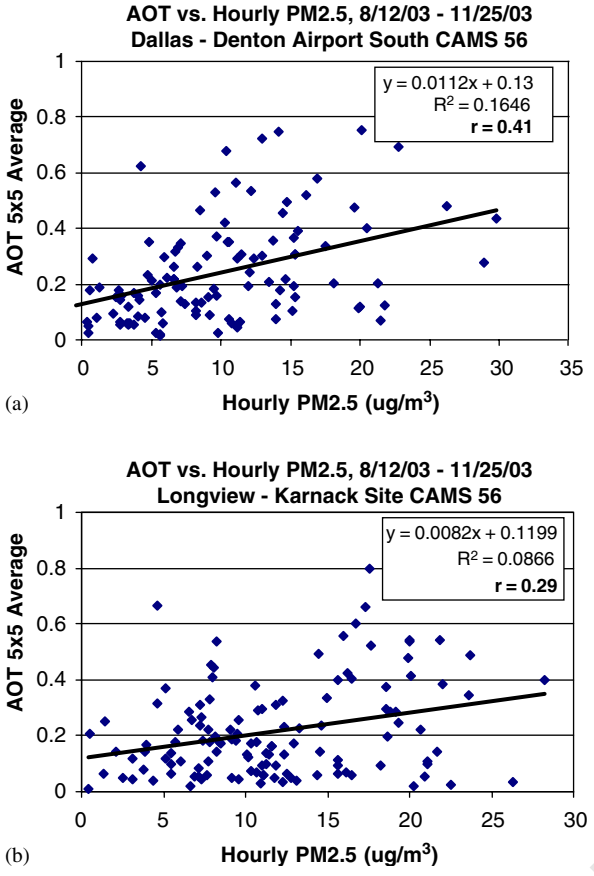

Fig. 1. Correlations between MODIS AOT averages in a 5×5 pixel group and CAMS #56 observations (left, $r = 0.41$) in Panel (a) and CAMS #85 observations (right, $r = 0.29$) in Panel (b) for the 12 August–25 November 2003 data set.

in the literature (Wang and Christopher, 2003). For this approach, daily MODIS AOT values in the 2004 data set were averaged along with 24-h mean $PM_{2.5}$ measurements using 5-$\mu g\,m^{-3}$ bins to produce AOT-$PM_{2.5}$ correlations. The average of all available data for observations made at 40 CAMS locations across Texas is shown in Fig. 2. For $PM_{2.5}$ values below 25-$\mu g\,m^{-3}$, found in Panel (a), the data closely followed a linear relationship with the MODIS AOT 5×5 pixel group averages, i.e. correlation coefficient of 0.98. However, the when higher values of $PM_{2.5}$ are considered, as shown in Panel (b), a non-linear relationship appears. For example, a linear correlation of 0.91 in Panel (b) improved to 0.99 by using a polynomial equation. Therefore, the procedure used by Wang and Christopher (2003) can be replicated with the entire 2004 data set collected over Texas.

The results of this bin-averaged comparison confirms that observed MODIS AOT analyses are likely to indicate the appropriate Air Quality Index category for the classification of ground-level pollution, e.g. as "Good" ($PM_{2.5}$ =0–15.4) "Moderate" ($PM_{2.5}$ = 15.5–40.4), "Unhealthy for sensitive groups" ($PM_{2.5}$ = 40.5–65.4), "Unhealthy" ($PM_{2.5}$ = 65.5–150.4), "Very Unhealthy" ($PM_{2.5}$ = 150.5–250.4), or "Hazardous" ($PM_{2.5}$ = 250.5+). However, this approach to establish AOT-$PM_{2.5}$ correlations requires a large set of historical observations and thus, lacks a predictive component since visibility into the variability in conditions necessary to distinguish events of importance is obscured by this analysis technique. Therefore, while useful for climatological studies, the bin-averaged approach to establish AOT-$PM_{2.5}$ correlations is considered less valuable for a real-time air quality prediction system.

3.2. Observed inaccuracies in the MODIS AOT retrievals

In an attempt to better understand correlations between MODIS AOT statistics and hourly $PM_{2.5}$ observations for use in a real-time air quality forecast system, retrieved values of MODIS AOT were examined to identify possible causes for the large spread in AOT analyses associated with any given $PM_{2.5}$ value, as seen in Fig. 1. A manual inspection of numerous MODIS AOT analyses revealed that unexplainable, large AOT values existed in the proximity of many inland bodies of water, especially across the south-eastern part of Texas. For simplicity, these regions are referred to as "AOT hot spots" in the remainder of this paper since they are characterized by elevated AOT values for a 10-km analysis area which is surrounded by lower AOT values for similar pixels found on each side.

Examples of some AOT hot spots are shown in Panel (d) of Fig. 3, which contains data for the MODIS granule collected at CSR on 16 January 2005 at 1700 UTC, i.e. MODIS A2005.016.1700. A color composite of the scene (using MODIS bands centered at 0.645, 0.555, and 0.469-μm in the red, green, and blue guns of the color monitor is shown in Panel (a). The box in the lower-right corner of the image highlights the region of interest. The box contains a 5×5 MODIS AOT pixel group that is located between Calcasicu Lake and Grand Lake in southern Louisiana, near the Texas border.

Table 2
Correlation statistics between MODIS AOT and $PM_{2.5}$ measurements for the 2004 calendar year

Texas metro area	CAMS facility	CAMS no.	No. of ctr obs	Avg no. of obs.	Pr (T) Ho: $p = 0$	Ctr_AOT vs. hrly $PM_{2.5}$	Avg_5 × 5_AOT vs. hrly $PM_{2.5}$	Avg_5 × 5_AOT vs. area_avg_$PM_{2.5}$
Amarillo	Amarillo	305	123	277	$p<0.0001$	0.3329	0.2757	0.3020
Austin–San Marcos	Audubon	38	102	192	$p<0.0001$	0.6019	0.4203	0.3835
Austin–San Marcos	Austin_Northwest	3	170	331	$p<0.0001$	0.4276	0.3670	0.3872
Corpus Christi	Corpus_Christi_West	4	104	352	$p = 0.038$	0.2036	0.2663	0.3134
Corpus Christi	National_Seashore	314	183	377	$p<0.0001$	0.4665	0.4868	0.4471
Dallas	Dallas_Hinton_Street	401	128	289	$p = 0.003$	0.2601	0.3756	0.4392
Dallas	Denton_Airport_South	56	175	319	$p<0.0001$	0.3197	0.3822	0.4059
Dallas	Kaufman	71	147	315	$p<0.0001$	0.3594	0.3466	0.4038
Dallas	Midlothian_Tower	94	134	294	$p<0.0001$	0.4073	0.4444	0.4429
Dallas	Midlothian_Wyatt_Road	302	149	302	$p<0.0001$	0.3491	0.4325	0.4530
Dallas	Sunnyvale_Long_Creek	74	134	263	$p<0.0001$	0.3700	0.4421	0.4377
El Paso	El_Paso_Sun_Metro	40	88	285	$p = 0.771$	0.0314	0.1670	0.1480
El Paso	El_Paso_UTEP	12	80	260	$p = 0.604$	0.0589	0.0492	0.0911
Fort Worth–Arlington	Arlington_Municipal_Airport	61	170	310	$p<0.0001$	0.4515	0.4246	0.3819
Fort Worth–Arlington	Diamond_Hill_Fort_Worth	308	151	310	$p = 0.0004$	0.3011	0.3730	0.3865
Fort Worth–Arlington	Grapvine_Fairway	70	155	305	$p<0.0001$	0.4576	0.3866	0.4094
Fort Worth–Arlington	Haws_Athletic_Center	310	163	326	$p<0.0001$	0.3719	0.3447	0.3658
Galveston–Texas City	Galveston_Airport	34	129	339	$p = 0.0007$	0.2940	0.1338	0.1351
Houston	Channelview	15	138	314	$p<0.0001$	0.3488	0.3745	0.4535
Houston	Clinton	403	109	273	$p = 0.0325$	0.2050	0.4001	0.4499
Houston	Conroe_Relocated	78	176	336	$p<0.0001$	0.3973	0.3328	0.3704
Houston	Houston_Aldine	8	134	305	$p<0.0001$	0.3839	0.3678	0.4544
Houston	Houston_Deer_Park	35	114	302	$p = 0.0003$	0.3348	0.4352	0.4604
Houston	Houston_East	1	117	311	$p = 0.0015$	0.2901	0.4258	0.4555
Houston	Kingwood	309	158	295	$p<0.0001$	0.4489	0.4437	0.4414
Houston	Seabrook_Friendship_Park	45	118	327	$p<0.0001$	0.4115	0.4078	0.4445
Longview–Marshall	Karnack	85	183	306	$p<0.0001$	0.5178	0.4548	0.4548
Lubbock	Lubbock	306	95	238	$p = 0.1194$	0.1609	0.1516	0.1696
San Antonio	CPS_Pecan_Valley	678	106	292	$p = 0.0001$	0.3647	0.2761	0.3196
San Antonio	Calaveras_Lake	59	127	300	$P<0.0001$	0.3802	0.3681	0.3472
San Antonio	Selma	301	104	300	$p = 0.0002$	0.3584	0.2413	0.2578

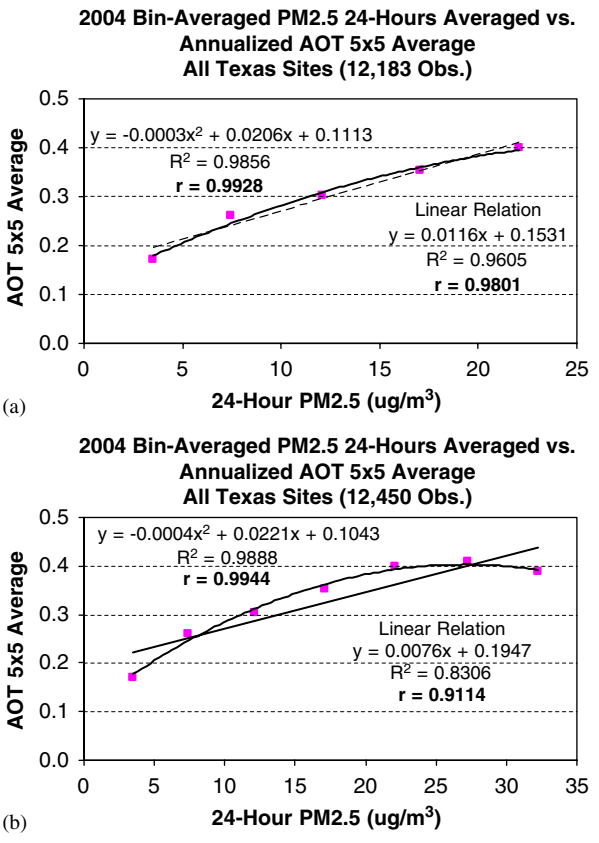

Fig. 2. Correlations between bin-averaged $PM_{2.5}$ observations from 10 to 25 $\mu g\,m^{-3}$ in Panel (a) and to 0 to 35 $\mu g\,m^{-3}$ at all Texas CAMS sites and MODIS AOT 5×5 pixel group averages for 2004 calendar year.

This MODIS granule was selected for presentation because of the extremely good air quality observed across Texas on this day. The passage of a weather front during the preceding 24-h brought pristine conditions to most of Texas, including cloud-free sky conditions. Low values of $PM_{2.5}$ were reported by CAMS facilities in east Texas at MODIS overflight time, including 2.3-$\mu g\,m^{-3}$ (Houston Clinton), 5.6-$\mu g\,m^{-3}$ at CAMS #642 (Mauriceville), 5.7-$\mu g\,m^{-3}$ at CAMS #38 (Austin Audubon), 5.8-$\mu g\,m^{-3}$ at CAMS #301 (San Antonio Selma), and 8.4-$\mu g\,m^{-3}$ at CAMS #85 (Longview Karnack). AQI was "good" for all sites across eastern Texas.

In Panel (b) of Fig. 3 is shown the MODIS ocean, coastal, and inland water masks (blue) used in the analysis and the retrieved values of AOT. The land and ocean AOT composite is shown, where brighter red indicates higher levels of AOT and darker red represents lower levels of AOT. (The actual value of each pixel is not critical to the discussion.)

Enlargements of the MODIS AOT 5×5 pixel group shown in Panels (a) and (b) are contained in Panels (c) and (d), respectively. In these enlargements, each of the single AOT 10-km pixels contained in the 5×5 pixel group are seen in Panel (d). Significantly larger AOT values are seen (evidenced by the bright red color) in three of the AOT pixels highlighted in Panel (d) than are present in surrounding AOT pixels. These higher AOT values are contained in white boxes so that the surface features present in the MODIS image can been seen more clearly in Panel (c). A visual inspection of the surface features in these AOT pixels, in Panel (c), reveals that each contains surface water but only one AOT pixel has these water bodies included in the inland water mask. That pixel is located in the bottom center of the image. A closer examination of the other two elevated AOT retrievals, in the mid-to-upper center of the 5×5 AOT pixel group, shows that elevated values in retrieved MODIS AOT are reported near lakes that appear relatively dark in true color image shown in Panel (c). Thus, a failure to completely eliminate surface water features from the MODIS land algorithm appears to produce hot spots in the AOT analysis.

3.2.1. Challenges for the MODIS AOT land algorithm

The MODIS land algorithm retrieves aerosol optical thickness using MODIS Channels 3, 1, and 7 (with bands centered at 0.47-, 0.66-, and 2.13-μm, respectively). The algorithm uses a 1-km resolution inland water mask, as shown in Panel (b) of Fig. 3. After eliminating pixels that are cloud contaminated, according to Levy et al. (2005) and Remer (2005), MODIS pixels that largely contain water, snow or ice are removed with a normalized difference vegetation index (NDVI) test using 250-m resolution data in the 0.66- and 0.86-μm bands. Land with healthy vegetation cover appears green in Panels (a) and (c) of Fig. 3 and has an NDVI value near the upper limit of unity. On the other hand, barren ground, snow, and water features have NDVI values toward the other extreme at near zero. Mixed pixels of land and water have values somewhere between these extremes, based upon the fractional composition of the mixture. Thus, screening for inland water employs both the static 1-km land/water mask and a dynamic NDVI test of the 250-m resolution data.

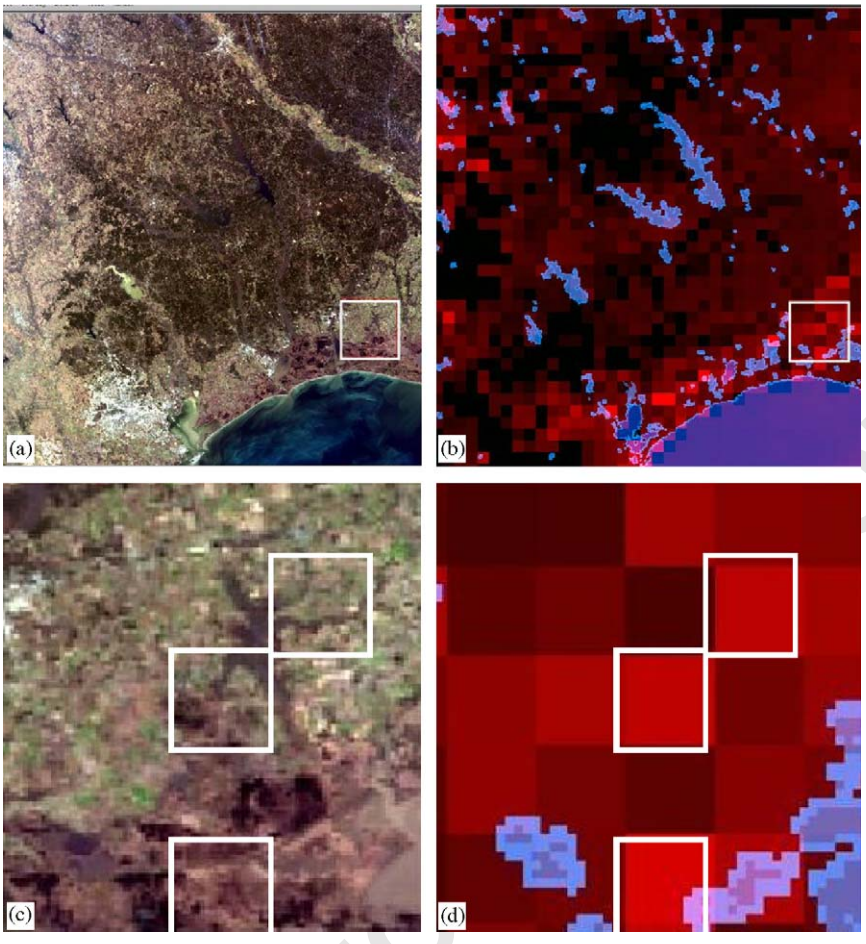

Fig. 3. Color composites of MODIS granule A2005.016.1700 shown in Panel (a) reveal no evidence of poor air quality during a day when "hot spots" seen in AOT analyses in Panel (b). Enlargements of highlighted areas in Panel (c) clearly shows un-masked surface water in 10-km AOT analysis pixels that have highest AOT values in Panel (d).

Not all of the 400, 500-m pixels in a 10-km AOT analysis cell are needed for the land AOT retrieval (Remer et al., 2005; Levy et al., 2005; Chu et al., 2003). An NDVI threshold is used to reject the MODIS pixels that are likely to be dominated by water while other tests eliminate pixels believed to contain snow and clouds. The AOT analysis is then performed on the remaining pixels. The algorithm identifies a set of dark surface pixels, based upon their reflectance in the 2.13-μm band. These dark pixels are then sorted by their reflectances in the 0.66-μm band. In this group, the darkest 20% and brightest 50% are further eliminated from the AOT analysis leaving pixels in the 20–50 percentile of MODIS measured radiances are used (Levy et al., 2005; Remer et al., 2005), which is a change from the 10–40 percentile used in an earlier version of the algorithm (Chu et al., 2003). The retrieval continues if at least 12 pixels remain.

For these remaining 500-m pixels in the AOT analysis, the core part of the algorithm calculates the mean reflectances for the three MODIS channels used in the retrieval. Then, using empirical relationships, the surface reflectances in the two shorter wavelengths are estimated from the reflectance in the 2.13-μm band, which is assumed to be minimally affected by the aerosol that scatter energy less in the larger wavelength than in either of the shorter wavelength bands. The difference between the surface reflectance and the Rayleigh path reflectance (based upon a standard atmosphere) is called the aerosol path reflectance. These aerosol path reflectances are compared to reflectances in a look-up table to determine the AOT for the 0.47- and 0.66-

μm band independently. The look-up table was generated using an assumption that the aerosol composition matches that of one of the aerosol models used in the algorithm (Levy et al., 2005; Remer et al., 2002).

Levy goes on to say that, in the MODIS aerosol algorithm, the land surface reflectance in the 0.47-μm band is assumed to be 25% of that found in the 2.13-μm band and the surface reflectance in the 0.66 μm band is assumed to be 50% of the 2.13-μm value (Kaufman et al., 1997c). While it has been demonstrated that these 0.47/2.13 (or blue/IR) and 0.66/2.13 (or red/IR) ratios of surface reflectances are valid under most global conditions, variations can occur on a regional scale, especially in the presence of highly heterogeneous surfaces, e.g. such as urban areas in proximity to forest, grassland, and agricultural fields. Most importantly, these ratios do not hold in the presence of water, since the 2.13-μm wavelength is much more strongly absorbed by water than the blue or red bands.

The MODIS land aerosol algorithm attempts to mask all small water bodies from the AOT analysis (Levy et al., 2005). However, some pixels that contain mixed land–water surfaces, e.g. swampy areas in and under forests, may exceed the NDVI threshold and thus be included in the aerosol retrievals, as clearly shown in Panel (c) of Fig. 3. In cases where the water surface is not adequately masked from the analysis, the retrieved AOT values could be too large since water has a nearly zero reflectance in the 2.13-μm band but somewhat higher reflectances in the red and blue bands. In such instances, the application of the standard ratios listed above results in an overestimation of the aerosol path radiance which in turn produces an AOT value that is too large. Comparisons between Panel (c) and Panel (d) in Fig. 3 supports this explanation as the cause for the excessively large MODIS AOT values are retrieved in east Texas on the 16 January 2005.

To further evaluate the possibility that unmasked water causes hot spots in the AOT analysis, a difference vegetation index (DVI) test was applied in addition to the NDVI threshold to better screen for inland water surfaces. The DVI test is the difference between the reflectances in the 250-m MODIS 0.86- and 0.66-μm bands and pixels with values of less than 0.10 were eliminated from the AOT analysis. In Panel (a) of Fig. 4, green dots identify the pixels found to contain water surfaces with the DVI test that were not identified by either the 1-km MODIS land/water mask or the NDVI test. It is clearly seen that the DVI test is more sensitive test than the NDVI test at detecting inland water features since rivers are now clearly seen extending south from the larger lakes in East Texas and marshy areas are evident along the Gulf Coast region.

Panel (b) of Fig. 4 shows the results obtained with version 3.1 of the aerosol land algorithm after pixels containing inland water, as shown in Panel (a), were removed from the analysis. The hot spots seen in Panel (d) of Fig. 3 are no longer present. Statistics

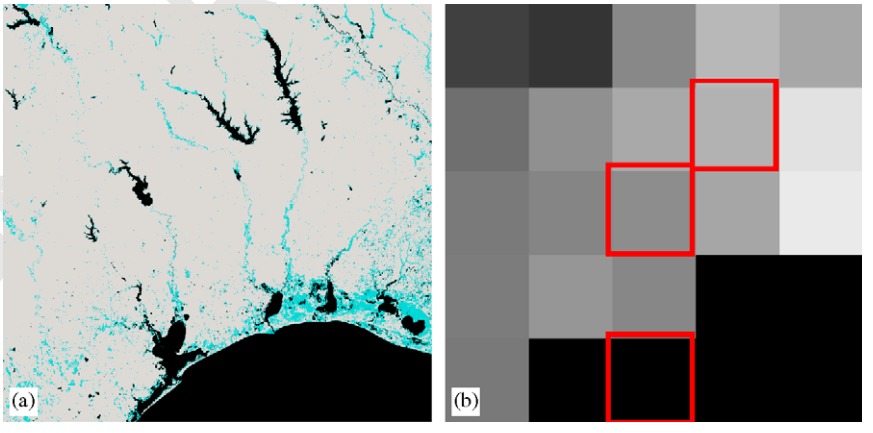

Fig. 4. Panel (a) shows the additional pixels found to contain water by using the DVI test with a threshold of 0.1 (in green) over those identified with the MODIS version 3.1 aerosol algorithms. Panel (b) shows the resulting analysis for the region contained in Fig. 3(d). The maximum AOT was about 25% lower than found in the original analysis but six areas (black) lack the number of pixels required to perform an AOT retrieval.

show a 25% reduction in the maximum AOT values through better masking of the inland water surfaces. However, AOT retrievals could not be created for six of the 10×10-km regions since the more stringent test to mask inland water surfaces left less than 12 pixels available to perform the AOT retrieval in these cases.

Due to the abundance of inland water surfaces in eastern Texas and the inadequacy of inland water screening in the AOT land algorithms, it was postulated that hot spots may be a significant contributor to the low correlations found between MODIS AOT analyses and ground-based $PM_{2.5}$ observations, as shown in Table 2.

3.2.2. Reducing the impact of AOT hot spots on correlations

If water contaminated pixels are a contributor to the poor correlations between the MODIS AOT algorithms and $PM_{2.5}$ measurements made at CAMS locations across Texas, two possible solutions exist to improve the correlations. First, improvements might be incorporated into the MODIS land algorithm. In fact, recent discussions with NASA staff led to their analysis of the MODIS granule shown in Fig. 3 with a newer version of the MODIS land aerosol algorithm. No hot spots were observed at CSR in the results provided by NASA. However, the algorithm continues to undergo internal testing and a release data has not been announced.

In the interim, a second possible approach to improve the AOT-$PM_{2.5}$ correlations with data collected over Texas is to modify the MODIS AOT algorithms for regional applications at CSR to eliminate AOT hot spots. While this approach sounds straight-forward, its implementation is non-trivial since the procedure requires modifying several thresholds and assessing the value of each change to the AOT-$PM_{2.5}$ correlations.

Therefore, it was first decided to assess the potential value of developing such a procedure on AOT-$PM_{2.5}$ correlations. This was done by analyzing a data set that has sufficient aerosol concentrations to mask water surfaces from the AOT land algorithm. A previously analyzed case study (Hutchison et al., 2004) was believed to contain sufficiently large aerosol concentrations to render the effects of unmasked inland water inconsequential on the AOT retrievals. The data set consists of all CAMS and MODIS AOT observations collected during the second week of September 2002, which has been the subject of several investigations (Hutchison et al., 2004; Christopher and Wang, 2003; Hutchison, 2003). If AOT-$PM_{2.5}$ correlations were significantly better in this data set, it would suggest that unmasked water surfaces had an adverse effect on correlations in the 2003 and 2004 data sets, especially during those conditions where smaller AOT values existed in the atmosphere.

3.3. Potential value of eliminating hot spots from $PM_{2.5}$ correlations

During the 9–16 September 2002 timeframe, a significant continental haze pollution event brought ozone-laden aerosols from the US industrial mid-west into Texas and resulted in TCEQ issuing a health alert to residences in 150 Texas counties. The pollution formed in the vicinity of Illinois and Indiana then was transported south toward the Gulf of Mexico and west toward Texas. It entered Texas along its eastern borders with Arkansas and Louisiana before its effects were observed in Dallas and Houston, then Austin and San Antonio and finally Corpus Christi. Subsequently, CSR collected data on this event and demonstrated that this type of pollution is readily detected and monitored in both MODIS imagery and AOT data products (Hutchison, 2003). It was later shown that MODIS AOT data products could also be used with trajectory-based forecasts to predict air quality associated with these continental haze events (Hutchison et al., 2004).

Table 3 contains statistics on AOT-$PM_{2.5}$ collections for the September 2002 data set, similar to those previously shown in Tables 1 and 2 for the 2003 and 2004 data sets. In this table correlations are also developed for 3×3 AOT pixel groups as well as the center pixel only and the 5×5 pixel groups. In addition, correlations are again tested against time-coincident, hourly $PM_{2.5}$ CAMS reports at the AOT center pixel and averages of all CAMS reports within each metropolitan area. In this table, the observations are restricted to cities in the eastern half of Texas, which were shown in previous tables, since only these stations were influenced by the continental haze pollution event.

It is clear from Column 4 of the table that the limited number of observations collected during this short timeframe casts uncertainty on the results in terms of their statistical significance. However, similar concerns were expressed with the results shown for the 2003 data set; however, no significant

Table 3
Correlation statistics between MODIS AOT and $PM_{2.5}$ measurements for the 9–16 September 2002 dataset

Texas metro_area	CAMS location	CAMS no.	No. of obs.	Ctr_AOT vs. hrly $PM_{2.5}$	Avg_AOT_3 × 3 vs. hrly $PM_{2.5}$	Avg_AOT_3 × 3 vs. avgarea_$PM_{2.5}$	Avg_AOT_5 × 5 vs. hrly $PM_{2.5}$	Avg_AOT_5 × 5 vs. avgarea $PM_{2.5}$
Austin–San Marcos	Audubon	38	5	0.7532	0.8820	0.9239	0.9048	0.9415
Austin–San Marcos	Austin_Northwest	3				0.8829		0.9288
Beamount–Port Arthur	Hamshire	64	4	0.7474	0.9501	0.8829	0.8812	0.7612
Beamount–Port Arthur	SETRPC_Mauriceville	642	4	0.9233	0.9009	0.9621	0.8528	0.9232
Beamount–Port Arthur	Thomas_Jefferson_School	303	4	0.8956	0.9255	0.9271	0.8562	0.8642
Brownsville–Harlingen	Brownsville	80	3				0.2294	0.2294
Corpus Christi	National_Seashore	314	3					0.9902
Dallas	Kaufman	71	5	0.7916	0.7836	0.9191	0.8713	0.9449
Dallas	Midlothian_Tower	94	4		0.9571	0.9770	0.9228	0.8259
Dallas	Midlothian_Wyatt_Road	302	3/4			0.9885	−0.0361	0.8411
Fort Worth–Arlington	Arlington_Municipal_Airport	61	5	0.9988	0.2400	0.5114	0.2701	0.4042
Fort Worth–Arlington	Diamond_Hill_Fort_Worth	308	6	0.9450	0.6266	0.6020	0.6473	0.6254
Fort Worth–Arlington	Grapvine_Fairway	70	5/6		0.7698	0.5681	0.8526	0.5372
Fort Worth–Arlington	Haws_Athletic_Center	310	6	0.9114	0.6859	0.6389	0.6133	0.6010
Galveston–Texas City	Galveston_Airport	34	3/4		0.9263	0.9263	0.8510	0.8510
Houston	Channelview	15	3/4		0.9920	0.9985	0.9934	0.9885
Houston	Clinton	403	4		0.9573	0.9738	0.9934	0.9839
Houston	Conroe_Relocated	78	4			0.9916		0.9810
Houston	Houston_Aldine	8	4	0.9737	0.9754	0.9950	0.9740	0.9922
Houston	Houston_Deer_Park	35	4	0.8776	0.9511	0.9874	0.9137	0.9613
Houston	Kingwood	309	4	0.9885	0.9703	0.9962	0.9706	0.9999
Houston	Seabrook_Friendship_Park	45	4		0.8319	0.9856	0.8192	0.9493
Longview–Marshall	Karnack	85	4	0.8293	0.8570	0.8570	0.8638	0.8638
San Antonio	CPS_Pecan_Valley	678	4/5	0.9194	0.9427	0.9667	0.7398	0.7589
San Antonio	Calaveras_Lake	59	5	0.9092	0.7009	0.6830	0.7114	0.6988

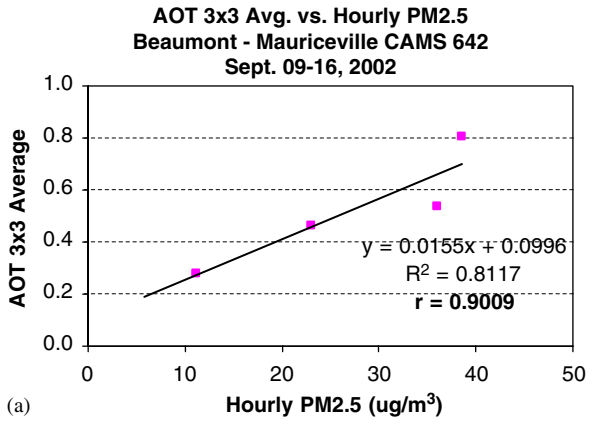

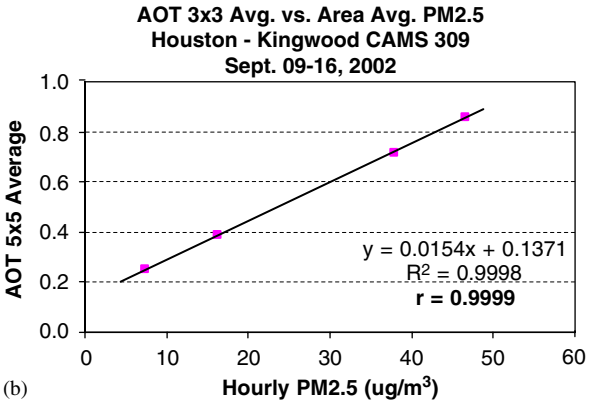

Fig. 5. Correlation plots for the September 2002 data set using hourly $PM_{2.5}$ observations at CAMS #642 (Panel a) and area averaged $PM_{2.5}$ observations at CAMS #309 (Panel b).

differences were found in correlations from the more extensive data set collected during calendar year 2004. Thus, with this precaution in mind, Table 3 is examined in more detail.

First, it is evident that the MODIS 5×5 AOT average values for the 2002 data set correlate much more strongly with hourly $PM_{2.5}$ measurements (column 8) than those shown for either the 2003 or 2004 data sets. In Table 3, with few exceptions, the correlations range between 0.61 and 0.99 with most of the values larger than 0.8. Panel (a) of Fig. 5 shows the AOT 3×3 averages versus the hourly $PM_{2.5}$ observations for Beaumont CAMS #642 while Panel (b) shows the AOT 5×5 averages vs. the area averaged $PM_{2.5}$ observations at Houston Kingwood CAMS# 309. These results demonstrate that the linear correlations with this data set are significantly better than those presented earlier in this paper.

4. Conclusions

The Center for Space Research (CSR) continues to implement the trajectory-based real-time forecast system for use at the Texas Center of Environmental Quality (TCEQ). The forecast approach is based upon MODIS AOT analyses which are translated in time using the IDEA software developed by NASA.

Forecasts from this system are expected to be available by the end of the summer 2005. In preparation for exploiting these data, CSR has been examining potential approaches to correlate MODIS AOT values with ground-based pollution measurements collected at the CAMS facilities operated by TCEQ. Initial results showed relatively low correlations between data collected during a 3-month period in 2003; however, the statistical significance of these results was questionable due to sample size. Therefore, a full year of data was analyzed for the 2004 timeframe and the results were comparable to those obtained with the 2003 data set.

In an attempt to understand why the correlations between MODIS AOT observations and $PM_{2.5}$ measurements were lower than expected based upon results in the published literature, CSR first applied the approach described by Wang and Christopher (2003) to the 2004 data set. The results of applying a bin-averaged approach for $PM_{2.5}$ measurements produced high correlations that were very similar to those reported in the literature. However, it was concluded that this approach relied upon smoothing of the data sets to produce these high correlations which eliminated the possibility of using this approach in a real-time forecast system.

Additional analyses were then undertaken to better understand the spread between $PM_{2.5}$ observations from CAMS facilities and MODIS AOT observations. This investigation led to the realization that "hot spots" occurred in the MODIS AOT analyses near inland lakes across Texas. Attempts to better understand this phenomenon led CSR staff to discussions with several NASA scientists working on the MODIS AOT products and a possible explanation for these hot spots. To confirm that unmasked inland water in the MODIS AOT land algorithm caused these hot spots, CSR modified the version 3.1 software to more thoroughly screen inland water surfaces in a small number of MODIS granules. The results showed a reduction in elevated AOT values. Next, another data set was analyzed

that contained aerosol concentrations sufficiently high to mask inland water surfaces from the AOT land algorithm. While the size of this 2002 data set affects the statistical significance of the test, very high correlations were found between $PM_{2.5}$ measurements and a variety of MODIS AOT pixel groups.

It is now concluded that inland water bodies, which are not adequately masked from the MODIS AOT land algorithm, will produce hot spots or erroneously high AOT values in MODIS data collected over Texas, especially when the aerosol concentration is not sufficiently high to mask them from the AOT algorithm. It is further concluded that hot spots can be reduced by more stringent screening of inland water surfaces using a difference vegetation index test with 250-m resolution MODIS bands. However, more detailed analyses are needed to establish the optimum threshold for this test in order to maximize the number of AOT observations generated at CSR and the quality of AOT-$PM_{2.5}$ correlations.

Acknowledgements

We are grateful for assistance received while conducting these investigations from members of the NASA Climate and Radiation Branch, at the Goddard Space Flight Center, in Greenbelt, MD. We extend our gratitude to Dr. L.A. Remer and special thanks to Dr. R.C. Levy and Dr. S. Mattoo. This work was supported by NASA Grant NNL04AA70G, Advanced EOS products for Air Quality Management.

References

Chu, D.A., Kaufman, Y.J., Ichoku, C., Remer, L.A., Tanre', D., Holben, B.N., 2002. Validation of the MODIS aerosol optical depth retrieval over land. Geophysical Research Letters 29.

Chu, D.A., Kaufman, Y.J., Ichoku, C., Zibordi, G., Chern, J.D., Mao, J., Li, C., Holben, B.N., Remer, L.A., Tanre', D., 2003. Global monitoring of air pollution over land from the Earth Observing System-Terra Moderate Resolution Imaging Spectroradiometer (MODIS). Journal of Geophysical Research 108.

Engel-Cox, J.A., Hollloman, C.H., Coutant, B.W., Hoff, R.M., 2004. Qualitative and quantitative evaluation of MODIS satellite sensor data for regional and urban scale air quality. Atmospheric Environment 38, 2495–2509.

Hutchison, K.D., 2003. Applications of MODIS satellite data and products for monitoring air quality in the state of Texas. Atmospheric Environment 37, 2403–2412.

Hutchison, K.D., Smith, S., Faruqui, S., 2004. The use of MODIS data and aerosol products for air quality prediction. Atmospheric Environment 38, 5057–5070.

Ichoku, C., Chu, D.A., Mattoo, S., Kaufman, Y.J., Remer, L.A., Tanre', D., Slutsker, I., Holben, B.N., 2002. A spatio-temporal approach for global validation and analysis of the MODIS aerosol products. Geophysical Research Letters 29, 100.

Kaufman, Y.J., Tanré, D., Gordon, H.R., Nakajima, T., Lenoble, J., Frouin, R., Grassl, H., Herman, B.M., King, M.D., Teillet, P.M., 1997a. Passive remote sensing of tropospheric aerosol and atmospheric correction for the aerosol effect. Journal of Geophysical Research 102, 16815–16830.

Kaufman, Y.J., Tanre, D., Remer, L.A., Vermote, E.F., Chu, A., Holben, B.N., 1997b. Operational remote sensing of tropospheric aerosol over land from EOS moderate resolution imaging sprectroradiometer. Journal of Geophysical Research 102 (D14), 17051–17067.

Kaufman, Y.J., Wald, A.E., Remer, L.A., Gao, B.-C., Liand, R.-R., Flynn, L., 1997c. The MODIS 2.1 μm Channel—Correlation with visible reflectance for use in remote sensing of aerosol. IEEE Trans. Geo. 35, 1286–1298.

Levy, R.C., Remer, L.A., Martins, J.V., Kaufman, Y.J., Plana-Fattori, A., Redemann, J., Wenny, B., 2005. Evaluation of the MODIS aerosol retrievals over ocean and land during CLAMS. Journal of Atmospheric Sciences 62, 974–992.

Martins, J.V., Tanré, D., Remer, L.A., Kaufman, Y.J., Mattoo, S., Levy, R., 2002. MODIS Cloud screening for remote sensing of aerosol over oceans using spatial variability. Geophysical Research Letters 29.

Remer, L.A., Kaufman, Y.J., Tanré, D., Mattoo, S., Chu, D.A., Martins, J.V., Li, R.-R., Ichoku, C., Levy, R.C., Kleidman, R.G., Eck, T.F., Vermote, E., Holben, B.N., 2005. The MODIS Aerosol Algorithm, products and validation. Journal of the Atmospheric Sciences 62, 947–973.

Wang, Christopher, 2003. Intercomparison between satellite-derived aerosol optical thickness and $PM_{-2.5}$ mass: implications for air quality studies. Geophysical Research Letters 30.

3B2v8.06a/w (Dec 5 2003).51c + model | AEA : 6719 | Prod.Type:FTP pp.1–9(col.fig.:1,2) | ED:TSripriya PAGN:mamatha SCAN:

ARTICLE IN PRESS

Available online at www.sciencedirect.com

SCIENCE DIRECT®

ELSEVIER

Atmospheric Environment ▮ (▮▮▮▮) ▮▮▮–▮▮▮

ATMOSPHERIC ENVIRONMENT

www.elsevier.com/locate/atmosenv

Improved retrievals of cloud boundaries from MODIS for use in air quality modeling

Keith D. Hutchison*, Tatyana Pekker, Solar Smith

The University of Texas at Austin, Center for Space Research (CSR), 3925 W. Braker Lane, Suite 200, Austin, TX 78759, USA

Received 6 February 2006; received in revised form 5 May 2006; accepted 9 May 2006

Abstract

A new approach has been developed at the Center for Space Research (CSR) to determine cloud boundaries from satellite data for use in air quality modeling. The approach combines remotely sensed cloud thickness, obtained from the MODIS cloud optical property products, with cloud base height measurements made at surface weather observing facilities to determine cloud top height. When compared to cloud truth estimates, compiled from measurements made at the Southern Great Plains Atmospheric Radiation Measurement Site in Oklahoma, errors in cloud top height from this new method were found to be significantly smaller than those in the MODIS (MOD06) cloud product. It was also found that relatively small errors in MOD06 cloud top temperatures can be magnified in MOD06 cloud top pressures because the interpolation scheme appears to not adequately consider humidity profiles in the NCEP data used to make these conversions.

Keywords: Cloud boundaries; Cloud top heights; Cloud base heights; MODIS

1. Introduction

Cloud fields impact air quality models in various and profound ways, including aqueous chemistry pathways, cloud–aerosol interactions, surface energy and radiation balances, and radiative fluxes for photochemistry (photolysis rates). Historically, most chemistry models, such as the Comprehensive Air quality Model with Extensions (CAMx—see http://www.camx.com) have assumed cloud-free conditions to generate the actinic fluxes that regulate photochemical reactions. More recently, the air quality modeling community has aggressively sought to remedy this situation by developing a modular system that facilitates the incorporation of improved input data fields, such as aerosol and cloud data fields. Still, the accurate specification of cloud boundaries remains a significant challenge even for the most advanced models, such as the Models-3 Community Multiscale Air Quality (CMAQ) modeling system (Byun and Ching, 1999). The problem is exacerbated by the difficulty in obtaining accurate three-dimensional cloud analyses using existing technology (D. Byun, pers. comm.).

An approach has been developed to retrieve cloud base heights for the National Polar-orbiting Operational Environmental Satellite System (Hutchison,

*Corresponding author. Tel.: +1 512 471 7295; fax: +1 512 471 7295x3570.
E-mail address: keithh@csr.utexas.edu (K.D. Hutchison).

1352-2310/$ - see front matter © 2006 Elsevier Ltd. All rights reserved.
doi:10.1016/j.atmosenv.2006.05.025

1998) using data that will be collected by the Visible Infrared Imager Radiometer Suite (VIIRS). The method has also been successfully demonstrated with data collected by NASA's MODerate-resolution Imaging Spectro-radiometer (Hutchison, 2002). The approach converts cloud optical properties, i.e. cloud optical depth and cloud effective particle size data available in the MODIS (MOD06) daytime cloud product, into cloud geometric thickness through a parameterization of cloud liquid path for water clouds and cloud ice path for cirrus clouds. Cloud base heights are then calculated to be the difference between cloud top height and cloud thickness. More recently, this approach was shown to provide accurate retrievals of cloud thickness and cloud base height with nighttime MODIS data using the new VIIRS algorithms, which confirmed for the first time that cloud optical properties and cloud thickness can also be retrieved accurately in nighttime data (Hutchison et al., accepted for publication).

Error budgets for the VIIRS cloud base height algorithm showed that inaccuracies in cloud top heights represented the largest source of uncertainty in the retrieval of cloud base heights (Hutchison, 1998). In these error budgets, it was assumed that the accuracy of cloud top height retrievals would vary between 1 and 2 km with cloud phase and cloud optical thickness. Larger errors would be associated with optical[illegible], ice clouds (NPOESS VIIRS SRD, 2000).

Efforts to fully characterize the performance of MODIS cloud top parameters, also contained in the MOD06 product, are ongoing. However, recent publications suggest that MOD06 cloud top heights can differ from truth measurements by as much as 1.5 km for low clouds and 2.5 km for high clouds when compared to lidar observations (Naud, et al., 2004), while MOD06 cloud top temperatures of high clouds can differ by 20 K when compared to millimeter wave cloud radar observations (Mace et al., 2005). These errors in cloud top height estimates are similar to those used in the original VIIRS error budgets for the cloud base height product.

Thus, expected errors in cloud boundaries, i.e. cloud top heights and resultant cloud base heights, obtained solely from MODIS data are considered too large for use in air quality modeling. Therefore, a new approach has been developed to more accurately retrieve cloud top heights for use in regional air quality applications. This approach combines cloud base height observations made at ground-based weather observing facilities with satellite-derived cloud thickness values retrieved from MODIS to determine cloud top height. The improvement in the specification of cloud boundaries is realized by reducing the relatively large observational errors in the MODIS cloud top heights with much smaller errors in the surface-based measurements of cloud base height, available from aerodromes in most urban regions that experience anthropogenic air pollution. This new approach is demonstrated through the analyses of a variety of data sets collected at the United States Department of Energy's Southern Great Plains (SGP) Atmospheric Radiation Measurement (ARM) site in Oklahoma.

2. Selection of case studies and cloud boundary truth data

An objective of this study was to analyze data for a variety of cloud systems that had cloud base heights below the maximum height reported by FAA automated surface observing system sites, i.e. 12,000 ft or 3.66 km. Also, to avoid using truth measurements of cloud base height made at the ARM site in the calculation of cloud top heights, surface weather observations were collected for several locations in the vicinity of the ARM site, e.g. Enid, Ponca City, and Altus Air Force Base. Therefore, it was important that the clouds extend across the region contained in Fig. 1 to include the SGP ARM central facility (36°37′N, 97°30′W, 320 m) at the time of the MODIS Terra overflight, which occurs typically between 1700 and 1800 UTC. After comparing surface observations made at the ARM site with those from the other locations, it was determined that cloud base height observations from Ponca City (KPNC, 36°44′N, 97°06′W, 308 m) best correlated with those reported at the SGP ARM site. Information on cloud types was taken from observations made at Altus Air Force Base. Finally, only daytime data were considered in this study since cloud optical properties are not available in the MOD06 nighttime products.

Several years of MODIS were previewed in an attempt to identify cloud situations that satisfied the conditions described above. These data were reviewed using the Texas Synergy–EOS Data Distribution system, a tool accessible from a spotlight on the homepage at the Center for Space Research (CSR), i.e. http://www.csr.utexas.edu. Unfortunately, only a few cases were found suitable for

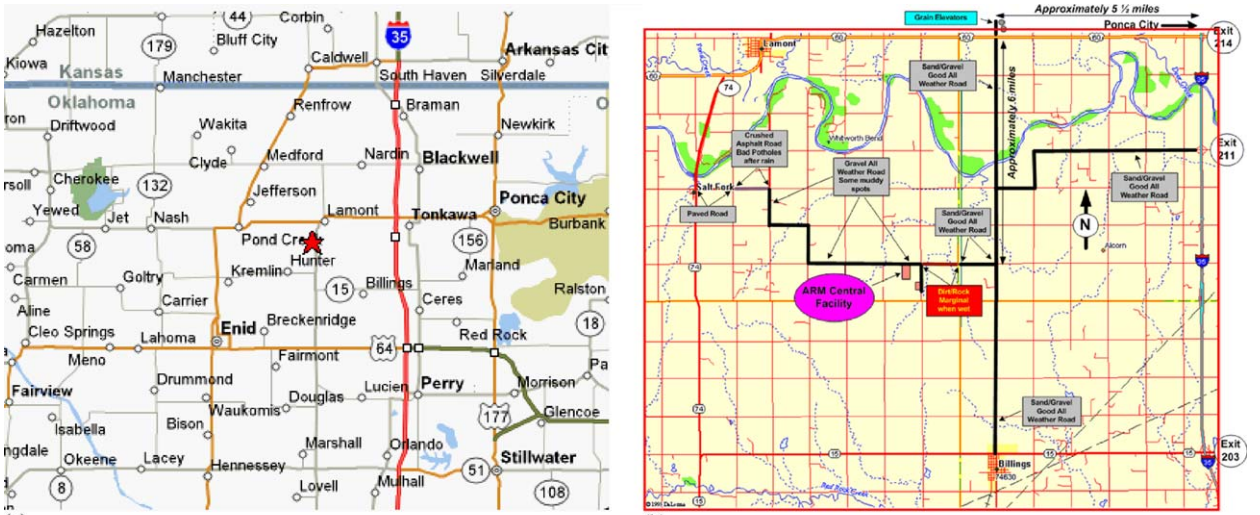

Fig. 1. The location of SGP ARM site (between Enid and Ponca City, OK) is shown in the left panel while an enlargement of this site is shown in the right panel. Cloud truth observations for this study were made at the ARM Central Facility.

Table 1
Measurements of cloud boundaries made from observations at the DOE SGP ARM site Oklahoma at the time of MODIS overflight

MODIS granule ID			Cloud top temperature (K)	Cloud base height (m)		Cloud top height (m)	
Case no.	Julian date (dd/mm/yy)	Time (UTC)	Radiosonde	MMCR	Ceilometer	MMCR	Radiosonde
1	337 (12/02/2000)	1725	264.4	1100	1137	1300	1233
2	98 (04/08/2003)	1705	262.4	1000	1312	1700	1523
3	312 (11/08/2003)	1805	272.7	200	149	2400	2219

use in this study after examining MODIS, ground-based, and in-situ observations. These cases occurred primarily in spring and fall months when single-layered, stratiform clouds can persist until MODIS overflight of the ARM site. (During the summer months, more intense solar heating results in a higher occurrence of convective clouds while the winter brings multi-layered cloud patterns which were not suitable for the study.) On the other hand, this very limited data set contains a good range in cloud thickness values, between about 50 and 1700 m, with distinct cloud boundaries in the truth data.

MODIS data identified for use in this study are shown in Table 1 along with the date and time of each data set in columns 2 and 3. (Each 5-min MODIS granule is uniquely identified by Julian day and universal time. Column 2 of Table 1 also shows the day of the year for each MODIS granule).

Cloud boundaries that serve as truth data for this analysis were collected from three sources located at the SGP ARM site central facility, including observations from a 35-GHz millimeter wave cloud radar (MMCR), a ceilometer, and radiosondes that are released daily at 1730 UTC to coincide with the nominal MODIS overflight of the facility. These observations are shown in columns 4–8 of Table 1.

There are errors associated with each of the observations that comprise the cloud truth measurements. For example, estimates of errors in cloud boundaries with MMCR are reported to be 50 m or larger, especially for lower clouds (Naud et al., 2003). In addition, there are numerous ways to determine cloud boundaries from radiosondes (Chernykh and Eskridge, 1996; Chernykh et al., 2001) and differences are reported between these methods, especially for multi-layered cloud situations. For this study, a manual analysis was performed using a skew-T, log-P thermodynamic diagram for each radiosonde observation and the cloud top height was assigned to the location where a rapid increase in temperature was accompanied by

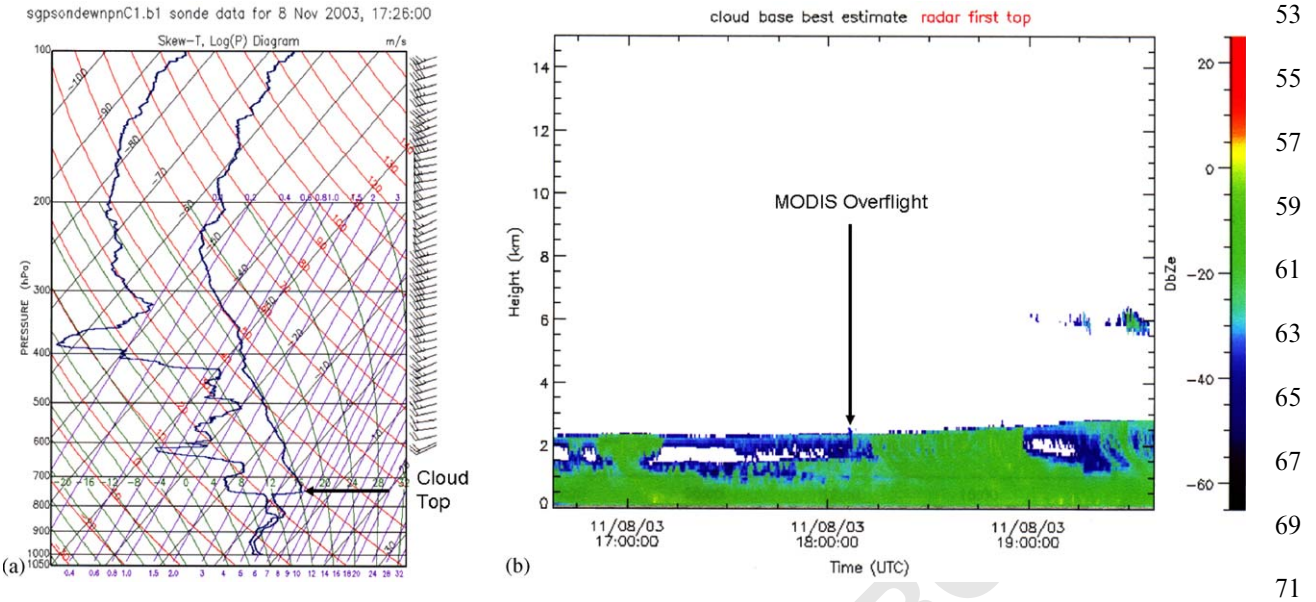

Fig. 2. A thermodynamic diagram of the radiosonde launched from the SGP ARM site at 1730 UTC on 8 November 2003 (case 3) is shown in panel (a) along with the millimeter wave cloud radar signatures in panel (b).

Table 2
MODIS cloud parameters and associated errors in cloud top heights when compared to cloud top height (radiosonde) truth measurements

Case no.	Cloud top temperature reported in MODIS product (K)	Cloud top pressure reported in MODIS product (mb)	Cloud optical thickness reported in MODIS product (n/a)	Cloud effective particle size reported in MODIS product (μm)	Cloud top height for MODIS using Eq. (1) and MODIS cloud top pressure (m)	Difference between MODIS cloud top height and radiosonde truth (m)	Difference between MODIS cloud top height and radiosonde truth (%)
1	267.3	850	5.3	5.4	1280	47	3.8
2	260.6	645	30.8	8.4	3393	1870	122.8
3	271.2	670	77.8	12.8	3161	942	42.4

a similar rapid decrease in dewpoint. (AWS TR, 1979–2006; Wang et al., 1999). The location of a rapid change in temperature and/or dewpoint constitutes a mandatory reporting level in a radiosonde observation. In general, the relative differences between the MMCR and radiosonde observations were very small compared to the estimated cloud top heights. Thus, the radiosonde cloud top heights were selected as truth since a distinct cloud top signature was present in each observation, as seen in Fig. 2. Ceilometer observations were selected as truth for the cloud base heights.

3. Analysis of case studies

Table 2 contains a listing of the MOD06 data products obtained from NASA's EOS Data Gateway for each of the cases shown in Table 1. Columns 2–5 contain data taken directly from the MOD06 products, including cloud top temperature, cloud top pressure, cloud optical thickness, and cloud effective particle size. The latter two (cloud optical properties) products are based upon the analysis of a single (1-km) MODIS pixel while the former two (cloud top parameter) products correspond to a 5×5 MODIS pixel group. Thus, the 1-km cloud products are aggregated to the 5-km resolution. Statistics on the cloud optical properties were developed for each corresponding 5-km pixel that contains the cloud top parameters product.

Large variations observed in some cloud optical thickness products, e.g. 50–100, further reduced the number of cases available for analysis.

The cloud top height for each MOD06 product was calculated at CSR from the cloud top pressure (P_{CT}) and the observed surface pressure (P_{Sfc}) at the SGP ARM site using Eq. (1). In this equation, Z_{sfc} represents the height of the surface, Z_{CT} is the height of the cloud top, g is the gravitational constant (9.8065 m s^{-2}), R is the gas constant for dry air (286.8 J kg^{-1} K^{-1}) and T_v is the virtual temperature (K) of the layer. In each case, T_v is taken as the mean temperature between the surface and the cloud top in the truth data. Cloud top heights calculated from the MOD06 data are shown in column 6 in Table 2, while columns 7 and 8 show differences between the MOD06 cloud top height and the truth measurements:

$$Z_{CT} = Z_{Sfc} + RT_{v(mean)}/g\mathrm{Ln}(P_{Sfc}/P_{CT}). \quad (1)$$

Inaccuracies in the calculation of cloud top height with Eq. (1) can result from variations in humidity profiles and cloud liquid water content (LWC). Therefore, each MOD06 cloud top pressure shown in Table 2 was converted into a corresponding cloud top height using only the NCEP operational analysis fields for 1800 UTC on the day of each MODIS overflight. The relative error in cloud top heights calculated from the MOD06 cloud top pressures using these two approaches was less than 1%.

Next, cloud top height was calculated using the new approach proposed for air quality modeling. In this approach, cloud thickness is first retrieved from the MOD06 cloud optical property products. For water clouds, cloud thickness (ΔZ) is based upon the relationship between liquid water path (LWP), in g m^{-2}, and LWC as shown in Eq. (2), where LWC is the integration of cloud size distribution over droplet size and has units of g m^{-3} (Hutchison, 2002). LWP has been related to cloud optical properties, i.e. cloud optical depth or cloud optical thickness (τ) and cloud effective cloud particle size (r_{eff}), as shown in Eq. (3) (Liou, 1992). A slightly different formulation is used for ice clouds (Hutchison, 2002):

$$Z_{cb} = Z_{ct} - (\Delta Z) = Z_{ct} - [\mathrm{LWP}/\mathrm{LWC}], \quad (2)$$

$$\mathrm{LWP} = \text{Liquid water path} = [2\tau r_{eff}]/3, \quad (3)$$

where LWC is the liquid water content based upon Table 4.2, Liou (1992), τ the cloud optical depth from the MOD06 product and r_{eff} the cloud droplet effective particle size from the MOD06 product

Cloud thickness values calculated with Eqs. (2) and (3), shown in column 2 of Table 3, are combined with surface observations from Ponca City, shown in column 3 of the table. Together, these data are used to calculate a cloud top height as shown in column 4. Comparisons between these new cloud top heights and the cloud truth data in Table 1 are shown in columns 5–6 in Table 3.

4. Discussion

Table 3 shows that differences between truth cloud top heights and those retrieved from this new approach are significantly smaller than those obtained directly from the MOD06 cloud top pressure product. These differences ranged between 4 and 425 m while the average difference for all cases was less than 200 m. In contrast, the average difference between truth cloud top heights and those retrieved from the MOD06 cloud top pressures were close to 1.0 km. Thus, it is concluded that the approach of using surface observations with retrieved cloud thickness values inferred from the MOD06 cloud optical properties can result in an improvement in the location of cloud boundaries

Table 3
Errors in cloud top heights for new approach when compared to cloud top height (radiosonde) truth measurements

Case no.	Cloud thickness retrieve with Eqs. (2) and (3) (m)	Cloud base height from Ponca City surface observation (m)	Cloud TOP Height from Eq. (2) and surface observations (m)	Difference between new approach to determine cloud top height and radiosonde truth (m)	Difference between new approach to determine cloud top height of and radiosonde truth (%)
1	47	1190	1237	4	0.3
2	430	960	1390	133	8.7
3	1659	135	1794	425	19.2

for use in air quality modeling over those obtained solely from MODIS cloud top pressure data.

One surprising result seen in Table 3 is the accuracy of cloud thickness values retrieved for cloud systems with large cloud optical thickness values shown in Table 2. While errors in cloud thickness of 425 m appear large, these results were associated with a cloud optical depth of 77.8, i.e. case 3. It was originally assumed that cloud optical depths of 64 would represent an upper limit in retrieving usefully cloud base heights with the approach outlined in Eqs. (2) and (3). This predicted limitation was based on the assumption that LWC is constant with height (Hutchison, 1998, 2002). The fact that useful cloud thickness values, compared to the NPOESS cloud base height performance requirement of 2 km (NPOESS VIIRS SRD, 2000), are retrieved for cloud optical depths in this range suggests that our initial assumption may not be a major limitation. In fact, one recent study examined cloud thickness estimates obtained with this approach using a constant LWC, an empirical relationship between cloud thickness and cloud optical properties, and an adiabatic model. The authors found that assuming a constant cloud LWC provided the most reliable retrieval of cloud thickness and concluded that it may be possible to monitor cloud base height globally in cloud mist forest regions with the approach outlined in Eqs. (2) and (3) (Zeng et al., 2006).

Another surprising result from this study is that relatively small errors in MOD06 cloud top temperatures were routinely associated with much larger errors in cloud top pressures. Additional analyses were needed to understand why this could occur. Thus, case 3 is presented in more detail to understand the difficulties that can arise when converting from cloud top temperature to cloud top pressure in the MOD06 product using NCEP analysis fields.

Panel (a) of Fig. 2 shows a plot of temperature and dewpoint profiles on a skew-T, log-P diagram constructed from data collected by the radiosonde launched from the SGP ARM site at 1730 UTC on 8 November 2003 (case 3). From these data, the cloud top pressure is accurately located at 760 mb and the corresponding cloud top temperature is 272.7 K, as shown in column 4 of Table 1. Panel (b) contains a report of the MMCR observations collected during the approximate period of 1630–1930 UTC at the same location. The cloud top temperature from the MOD06 product is reported to be 271.0 K, as seen in column 2 of Table 2, which is a difference of only 1.7 K from the truth. Based upon a standard lapse rate, it might be expected that the cloud top height would differ from the truth observation by about 250 m. However, Table 2 shows the actual difference between the cloud top height derived from Eq. (1) and the truth measurement is nearly 4 times larger. This magnification in error appears to result from the procedure used to convert between cloud top temperature and cloud top pressure in the MOD06 product.

There are two approaches used in the MODIS algorithms to retrieve the cloud top (temperature and pressure) parameters for a 5×5 MODIS pixel group that are reported in the MOD06 product: the primary algorithm relies upon the CO_2 slicing method while the alternative approach is based on the 11-μm brightness temperature (T_{B11}). The CO_2 slicing method is used as long as the cloud signal in the MODIS 13-μm bands remains sufficiently strong, i.e. cloud top heights are above about 3 km (Naud et al., 2003) or lower than about 700 mb (Platnick et al., 2003). The T_{B11} method assumes a cloud emissivity of unity. (See Menzel et al., (2002) for a more complete discussion of the MOD06 product.)

In the retrieval of cloud top parameters with these two MODIS algorithms, NCEP global, $1 \times 1^{\circ}$ latitude/longitude, 6-h analysis fields are vertically interpolated to 101 pressure levels of temperature and water vapor mixing ratio. Next, transmittance profiles are computed for each MODIS band used to retrieve cloud top pressure, i.e. MODIS bands 31 and 33–36. No horizontal interpolation is used except for surface temperature and pressure. Clear-sky radiances are then calculated along with CO_2-slicing computations. First, a "window channel" value is obtained, i.e. T_{B11}, then the CO_2 slicing solution. If a CO_2 solution is not available, the window channel result will be reported as the cloud top pressure, which will be one of the 101 pressure levels, rounded to the nearest 5 mb increment ~~(R.A. Frey, MODIS Cloud Team Member, pers. comm.)~~.

It is evident by the sharp drop in dewpoint that coincides with a similar rise in temperature in the thermodynamic diagram in panel (a) of Fig. 2 that the cloud top height for case 3 is below 700 mb. Therefore, a CO_2 slicing solution is likely not available and cloud top temperature is based upon the T_{B11} brightness temperature under the assumption that the cloud is a black body (Platnick et al., 2003). Finally, this cloud top temperature is

Table 4
Composite of NCEP atmospheric profiles for SGP ARM site at 1800 UTC on 8 November 2003 (case 3)

NCEP level	Temperature (K)	Pressure (mb)	Relative humidity (%)	MODO6 cloud top location (mb)	Cloud top location from CSR method (mb)
1	281.2	1000	78		
2	279.5	975	80		
3	277.6	950	86		
4	276.3	925	89		
5	276.0	900	92		
6	276.1	850	97		
7	276.4	800	97		
8	**274.2**	**750**	92		750
9	**274.3**	**700**	54		
10	**271.0**	**650**	43	670	
11	**269.5**	**600**	45		
12	261.3	550	50		
13	256.7	500	72		

converted into one of the 101 levels to obtain the cloud top pressure, which in this case is 670 mb as shown in column 3 of Table 2.

Table 4 shows the NCEP analysis fields for the SGP ARM site at 1800 UTC on 8 November 2003. In this case, the data shown are based upon the average of the four, 1° data points that surround the SGP ARM site, since the site lies between these gridded values. Column 2 shows the NCEP temperature profile, column 3 contains the NCEP pressure profile, and column 4 the NCEP humidity profile. Column 5 of Table 4 shows the location in the NCEP profiles of the cloud top pressure reported in the MOD06 product. It lies in a humidity range of 54–43%. Thus, the conversion of the MOD06 cloud top temperature into a cloud top pressure of 670 mb is inconsistent with the moisture profile in the NCEP analysis fields. So, it seems apparent that using temperature profiles alone is an inadequate approach to convert between these cloud top parameters.

Therefore, CSR developed and tested an alternative approach to convert between MODIS cloud top temperatures and cloud top pressures that directly applies humidity information contained in the NCEP profiles. In this new procedure proposed by CSR, it is first assumed that quantifiable errors exist in the MOD06 cloud top temperature data. Then, NCEP moisture fields are examined over this range of possible temperatures to find the most desirable location to assign the cloud top pressure. For example, in the NPOESS program, cloud top temperature is assumed to have an accuracy of 2 and 3 K for optically thicker clouds, i.e. optically depth of unity or more, during daytime and nighttime conditions, respectively (NPOESS VIIRS SRD, 2000). For more optically thin clouds, the expected error increases to 6 K. Thus, in the proposed CSR method, the moisture profile is examined over the temperature range that includes the MOD06 cloud top temperature plus its expected error range, as denoted by the shaded area in the NCEP temperature profile. Next, the NCEP humidity profile is examined to identify locations where a cloud might exist, e.g. 87% or greater (Wang et al., 1999, 2000). If such a region is found, the cloud top is placed in the lowest pressure in this range and the retrieval is given a high quality. If no region is found where sufficient moisture is present to form or sustain a cloud, the cloud top pressure is place at the level of maximum humidity within this temperature range but the retrieval is flagged as degraded quality.

Column 6 of Table 4 shows the cloud top pressure at 750 mb for case 3 using the CSR interpolation scheme. After converting these data to cloud top heights using Eq. (1), it is found that the new approach locates the cloud top height at 2252 m, compared to 3179 m shown in Table 2, while the truth data for this case shows the cloud top height at 2219 m as shown in Table 1. Thus, the error in cloud top height is reduced from 43.3% in the MOD06 product to 1.5% based upon the use of a different interpolation method to convert between the MOD06 cloud top temperature and cloud top pressure products.

5. Conclusions

Challenges in assimilating cloud data into air quality models arise in locations that lack a full compliment of ground measurements, e.g. as found at the SGP ARM site, due to inaccuracies in the retrieval of cloud top pressures (cloud top heights) and cloud base heights from MODIS data alone. Therefore, the primary objective of this research was to evaluate a new approach to improve upon the specification of cloud boundaries for air quality modeling. The approach combines surface-based cloud base heights, which are available in most urban regions that experience anthropogenic air pollution, with cloud thickness values retrieved from MODIS data. Our preliminary results demonstrate, as a proof-of-concept, that the use of more accurate surface-based observations with retrieved cloud thickness values can significantly reduce errors in cloud boundaries when compare to those obtained from MODIS data alone. Average errors in the limited but diverse data set developed for this study show that differences between retrieved cloud top heights, when compared to truth observations, were reduced from about 1.0 km to about 0.15 km.

During the course of these investigations, it was observed that a magnification in error occurs during the conversion between MOD06 cloud top temperatures and cloud top pressures for low-level clouds. In an attempt to understand the reason that relatively small errors in the former resulted in larger than expected errors in the latter, the MODIS cloud top parameters algorithm was examined in detail. It appears that the MODIS approach does not adequately consider errors in retrieved cloud top temperatures or effectively utilize available moisture data within the NCEP analysis fields. Thus, CSR developed an alternative procedure to convert MOD06 cloud top temperatures into cloud top pressures. In this procedure, it is first assumed that quantifiable errors exist in the MOD06 cloud top temperature. Then, the moisture profiles in the NCEP fields are examined over a range of possible cloud top temperatures to find the most desirable location to assign the cloud top pressure. It appears that this alternative approach successfully locates clouds within the moisture fields in the NCEP data and appears to reduce the errors in cloud top heights of lower-level clouds derived solely from the MOD06 cloud top temperature and cloud top pressure products.

With the recent launch of the NASA Calipso and CloudSat missions, our attention turns toward the collection of larger and more global data sets from the constellation of NASA satellites known as the A-Train to better understand the capabilities and limitation of this new approach for the retrieval of cloud boundaries (see http://csc.gallaudet.edu/soar-high/A-TrainExplain.html). In addition, we have already begun assessing the sensitivity of the CAMx and CMAQ photochemical models to inaccuracies in cloud boundaries based upon the results of this study.

6. Uncited reference

Wang and Rossow, 1995.

Acknowledgments

This work was supported by NASA Grant NNL04AA70G, Advanced EOS products for Air Quality Management.

References

AWS TR, 1979–2006. The use of the skew T, log P diagram in analysis and forecasting. AWS Technical Report 1979–2006, Air Force Weather Agency, Scott AFB, IL, 150pp. (Available through the Directorate of Weather, Deputy Chief of Staff for Air and Space Operations, Headquarters, United States Air Force.)

Byun, D.W., Ching, J.K.S. (Eds.), 1999. Science Algorithms of the EPA Models-3 Community Multi-scale Air Quality (CMAQ) Modeling System. EPA Report, EPA/600/R-99/030. NERL, Research Triangle Park, NC.

Chernykh, I.V., Eskridge, R.E., 1996. Determination of cloud amount and level from radiosonde soundings. Journal of Applied Meteorology 35, 1362–1369.

Chernykh, I.V., Alduchov, O.A., Eskridge, R.E., 2001. Trends in low and high cloud boundaries and errors in height determination of cloud boundaries. Bulletin of the American Meteorological Society 82, 1941–1947.

Hutchison, K.D., 1998. Cloud base height, VIIRS algorithm theoretical basis document, version 1.0. Raytheon Information Technology and Scientific Services, Lanham, MD, 35pp. (see http://www.ipo.noaa.gov/library_NPOESS.html).

Hutchison, K.D., 2002. The retrieval of cloud base heights from MODIS and 3-dimensional cloud fields from NASA's EOS Aqua mission. International Journal of Remote Sensing 23, 5247–5263.

Hutchison, K.D., Wong, E., Ou, S.C. Cloud base heights retrieved during nighttime conditions with MODIS data. International Journal of Remote Sensing, accepted for publication.

Liou, K.-N., 1992. Radiation and Cloud Processes in the Atmosphere. Oxford Press, 487pp.

Mace, G.G., Zhang, Y.Y., Platnick, S., King, M.D., Minnis, P., Yang, P., 2005. Evaluation of cirrus cloud properties derived from MODIS data using cloud properties derived from ground-based observations collected at the ARM SGP site. Journal of Applied Meteorology 44, 221–240.

Menzel, W.P., Baum, B.A., Stabala, K.I., Frey, R.A., 2002. Cloud top properties and cloud phase algorithm theoretical basis document, 66pp. (document is available via NASA's MODIS home page).

National Polar-Orbiting Operational Environmental Satellite System (NPOESS) Visible/Infrared Imager/Radiometer Suite (VIIRS) Sensor Requirements Document (SRD), 2000. Version 3, 91pp. (see http://www.ipo.noaa.gov/library_N-POESS.html).

Naud, C., Muller, J.P., Clothiaux, E.E., 2003. Comparison between active sensor and radiosonde cloud boundaries over the ARM Southern Great Plains site. Journal of Geophysical Research—Atmospheres 108 (D4), AAC 3-1–AAC 3-12.

Naud, C., Muller, J.P., Haeffelin, M., Morille, Y., Delaval, A., 2004. Assessment of MISR and MODIS cloud top heights through intercomparison with a back-scattering lidar at SIRTA. Geophysical Research Letters 31 (4), L041134.

Platnick, S., King, M.D., Ackerman, S.A., Menzel, W.P., Baum, B.A., Riedi, J.C., Frey, R.A., 2003. The MODIS cloud products: algorithms and examples from Terra. IEEE Transactions on Geoscience and Remote Sensing 41, 459–473.

Wang, J., Rossow, W.B., 1995. Determination of cloud vertical structure from upper-air observations. Journal of Applied Meteorology 34, 2243–2258.

Wang, J., Rossow, W.B., Uttal, T., Rozendaal, M., 1999. Variability of cloud vertical structure during ASTEX observed from a combination of rawinsonde, radar, ceilometer and satellite. Monthly Weather Review 127, 2484–2502.

Wang, J., Rossow, W.B., Zhang, Y., 2000. Cloud vertical structure and its variations from a 20 yr global rawinsonde dataset. Journal of Climate 13, 3041–3056.

Zeng, J., Han, Q., Asefi, S., Welch, R.M., Lawton, R.O., Nair, U.S., Ray, D.K., 2006. Observations of orographic cloud base heights from satellite and in-situ measurements at the Monteverde Cloud Mist Forest Reserve, Costa Rica, Poster 3.17. In: 14th Conference on Satellite Meteorology and Oceanography. American Meteorological Society, Atlanta, GA, USA.

Accepted for publication by Atmospheric Environment on September 2007

Improving Correlations between MODIS Aerosol Optical Thickness and Ground-Based $PM_{2.5}$ Observations through 3D Spatial Analyses

Keith D. Hutchison, Shazia J. Faruqui, and Solar Smith

ABSTRACT

The Center for Space Research (CSR) continues to focus on developing methods to improve correlations between satellite-based aerosol optical thickness (AOT) values and ground-based, air pollution observations made at continuous ambient monitoring sites (CAMS) operated by the Texas Commission on Environmental Quality (TCEQ). Strong correlations and improved understanding of the relationships between satellite and ground observations are needed to formulate reliable real-time predictions of air quality using data accessed from the Moderate Resolution Imaging Spectroradiometer (MODIS) at the CSR direct-broadcast ground station. In this paper, improvements in these correlations are demonstrated first as a result of the evolution in the MODIS retrieval algorithms. Further improvement is then shown using procedures that compensate for differences in horizontal spatial scales between the nominal 10-km MODIS AOT products and CAMS point measurements. Finally, airborne lidar observations, collected during the Texas Air Quality Study of 2000, are used to examine aerosol profile concentrations, which may vary greatly between aerosol classes as a result of the sources, chemical composition, and meteorological conditions that govern transport processes. Further improvement in correlations is demonstrated with this limited dataset using insights into aerosol profile information inferred from the vertical motion vectors in a trajectory-based forecast model. Analyses are ongoing to verify these procedures on a variety of aerosol classes using data collected by the Calipso (Cloud-Aerosol Lidar and Infrared Pathfinder Satellite) lidar.

Key Words: MODIS; air quality; particulate matter; aerosol optical thickness

Corresponding Author: Dr. Keith D. Hutchison, Center for Space Research, The University of Texas at Austin, 3925 W. Braker Lane, Austin, TX 78759, Tele: 512-471-7295, Fax: x-3570, e-mail: keithh@csr.utexas.edu

1. INTRODUCTION

Research at the Center for Space Research (CSR) continues to focus on methods to increase correlations between MODIS aerosol optical thickness (AOT) values and ground-based, $PM_{2.5}$ observations made at continuous ambient monitoring sites (CAMS) operated by the Texas Commission on Environmental Quality (TCEQ). In 2000, CSR began examining new applications for data collected by Earth Observing System (EOS) satellites with state, local, and tribal level agencies in the State of Texas community through a NASA-sponsored program known as Synergy (Kalluri et al., 2003). During this timeframe, TCEQ requested CSR assistance in detecting pollution events that eluded detection with their existing systems. MODIS data provided the capability to detect pollution never observed previously in operational weather satellite systems (Hutchison, 2003). In subsequent studies, CSR also demonstrated that MODIS aerosol products had value for air quality prediction as well as monitoring transient air pollution events (Hutchison et al., 2004) and TCEQ expressed a desire to incorporate these data into their operational forecast decision process. CSR now uses a trajectory-based forecast model, known as IDEA or Infusing Data into Environmental Applications (Al-Saadi et al., 2005), to generate real-time air quality forecasts from MODIS AOT analyses retrieved from data collected at the CSR X-band direct-broadcast ground station (DBGS) (Hutchison et al., 2004). These forecasts are available at: http://magic.tacc.utexas.edu/shared/Products/

A real-time air quality prediction system based upon MODIS AOT products must account for differences between satellite and ground-based observations. MODIS collects data at 250-m, 500-m, and 1-km at nadir across a 2330-km data swath from satellites in near-Earth sun-synchronous polar-orbit from a nominal altitude of 705-km (Salomonson et al., 1989; Barnes et al., 1998). The MODIS AOT product covers the total atmospheric column from the satellite to the Earth's surface and has a horizontal spatial resolution of 10-km. The AOT product is dimensionless. Observations are generated during daytime conditions only so the global refresh rate, i.e. the

maximum time between observations that cover the same location, for a single satellite sensor, is about 24-hours over most of the U.S. but increases to ~ 48-hours for points south of ~ 30N. On the other hand, ground-based pollution measurements made at TCEQ CAMS locations are generated every five minutes and reported as averages at hourly and 24-hour intervals, i.e. 12-observations are typically averaged in each hourly report. Although TCEQ may occasionally employ portable equipment, most observations are made at fixed-sites. Thus, CAMS observations represent point measurements of PM_{10} ($\mu g/m^3$), $PM_{2.5}$ ($\mu g/m^3$), and ozone [parts-per-billion (ppb)]. Information on the TCEQ CAMS sites is available at: http://www.tceq.state.tx.us/nav/eq/mon_sites.html

It is evident that there are significant differences between MODIS AOT analyses and CAMS $PM_{2.5}$ observations and these differences must be considered when attempting to relate the datasets to each other. Thus, some statistical relationship is needed to compare MODIS AOT observations with ground-based pollution measurements, both in MODIS AOT analyses and trajectory-based AOT forecasts. Most commonly this relationship is based upon the Pearson linear correlation coefficient, where values near ±1.0 indicate highly correlated in either a positive or negative direction while values toward zero are poorly correlated.

While strong AOT-$PM_{2.5}$ correlations are needed, defining the form of these relationships for a variety of pollution sources and meteorological conditions has been a challenge. CSR initially expected strong linear correlations as reported by some other authors (Chu et al., 2003; Wang and Christopher, 2003); however, weaker AOT-$PM_{2.5}$ correlations were found in datasets collected at CSR (Hutchison et al., 2005) and reported by others (Levy et al., 2004). With assistance from the NASA Aerosol Team, CSR made modifications to the aerosol retrieval algorithms improve correlations through the elimination of “hot spots” that resulted from inadequate masking of inland water surfaces (Hutchison et al., 2005). However, further analyses revealed that

unscreened thin cirrus also produced similar affects in AOT products and it was not feasible to modify the cloud mask within the MODIS AOT module, since the cloud screening logic is integrated within the aerosol retrieval algorithms (Martins et al., 2002; Remer et al., 2005), i.e. an external MODIS cloud mask such as the MOD35 product (Ackerman et al., 2002) is not used to create the AOT product. Consequently, research at CSR turned toward minimizing the effects of outliers in the AOT analyses, while assuming that some additional improvement in AOT-$PM_{2.5}$ correlations would be realized through the evolution and maturation of the MODIS aerosol retrieval algorithms as discussed in Section 2. In Section 3 techniques developed at CSR to evaluate MODIS aerosol algorithms are shown along with procedures to identify outliers in the MODIS AOT observations and minimize their impact on AOT-$PM_{2.5}$ correlations. In Section 4, these techniques are extended to compensate for variations in aerosol profiles using vertical motions in the forecast trajectories, with the aid of airborne lidar data collected during the intensive Texas Air Quality Study-I (TXAQS) data collection of 2000.

2. EVOLUTION OF THE MODIS AOT RETRIEVAL ALGORITHMS

There is a lengthy heritage in using satellite data to monitor atmospheric aerosols, such as dust and sand particles (Carlson and Prospero, 1972; Shenk and Curran, 1974). While early research was directed toward the detection of these aerosols over ocean surfaces, major improvements in global aerosol monitoring were achieved when additional spectral data became available with the first launch of the MODIS sensor on the EOS Terra satellite in December 1999. Today, EOS satellites are used to monitor aerosols on a global scale and to understand the impact of aerosols on cloud and climate feedback mechanisms (Kaufman, 2002a).

The MODIS aerosol module contains two independent algorithms that were developed before the EOS Terra spacecraft launched in 1999. The algorithm used to retrieve aerosols over land was

first described by Kaufman, et al. (1997b) while the algorithm used over the ocean was described in a separate publication by Tanré, et al. (1997). NASA states that the central approach used in these MODIS aerosol algorithms has remained relatively unchanged through versions 3.0 - 5.1; however, there have been "minor" modifications (Remer et al., 2005; Remer et al., 2006). Basically, the core algorithm exploits atmospheric reflectance ratios, corrected for Rayleigh scattering, between 0.47-μm and 2.1-μm along with 0.65-μm and 2.1-μm to retrieve the AOT product. The underlying assumption is that these relationships are applicable under global conditions, e.g. differences in bi-directional reflectance functions in these bandpasses across the Earth's surface are negligible (Kaufman et al., 1997c; Kaufman et al., 2002b). In essence, the algorithmic modifications alter the logic that determines which pixels in a 10-km region are used to generate AOT values. Historically, these algorithm updates have been implemented through a process known as a "collection" which consists of products that were generated by similar, but not necessarily the same, versions of the algorithms (Remer et al., 2006). The MODIS algorithm theoretical basis document, dated 1996, described the pre-launch aerosol algorithms while the Collection 3 (i.e. version 3.0) algorithms were used to produce the first globally validated products over ocean backgrounds (Remer et al., 2002) and over land surfaces (Chu et al., 2002). The Collection 3 MODIS AOT algorithms were acquired by CSR through the purchase of a MODIS DBGS in 2003. The next major update to the aerosol products came with the release of the MODIS Collection 4 algorithms. CSR hosted the Collection 4.2.2 algorithms at the DBGS in March 2004. More recently, the NASA Aerosol Team created two additional versions: the Collection 5.1 algorithms which CSR hosted in March 2005 and the Collection 5.2 algorithms which became the operational algorithms used at the NASA Earth Science Data Information System (ESDIS). Results presented herein are based upon retrievals made at CSR with the MODIS Collection 3, 4.2.2, and Collection 5.1 algorithms. A history of changes to the MODIS AOT algorithms can be found in the algorithm theoretical basis document (Remer et al., 2006),

various publications (Kaufman et al., 1997a; Remer et al., 2005; Chu et al., 2003) and at NASA Aerosol Team website, i.e. http://modis-atmos.gsfc.nasa.gov/MOD04_L2/history.

Table 1 summarizes some of the modifications to the MODIS aerosol retrieval algorithms that affect the quality of the aerosol products and impact attempts to correlate these products with ground-based air quality measurements. First, it is seen that there are nominally 400 pixels used to retrieve aerosol optical thickness with all versions of the algorithm. Initially cloud screening was based upon the MODIS 1-km cloud mask (Ackerman et al., 1998) as noted by Chu et al., (2003). However, dissatisfaction with the performance of the MODIS cloud mask (Brennan et al., 2005) resulted first in the use of supplemental cloud tests with version 4 algorithms (Martins et al., 2002; Remer et al., 2005) and finally with a replacement of the MODIS cloud mask in favor of internally-generated cloud mask. The current procedure employs spatial tests with the 0.47-μm bands to detect water clouds and threshold tests with the 1.38-μm band to exclude ice clouds (Gao et al., 2002) from AOT analyses (Remer et al., 2006). To further reduce the possibility of clouds being included in the pixels used to retrieve AOT, a correction is applied that is referred to as a bright pixel correction in Table 1. After removing from the 400 pixel group, all cloudy pixels along with those found to contain snow or ice, the remaining pixels are prioritized by descending reflectances in the 0.65-μm channel ($\rho_{0.65\text{-}\mu m}$). Between 40-50% of the pixels, depending upon which version of the algorithm is used, with the highest reflectance in this band are discarded to reduce cloud effects.

In addition to clouds, two other phenomena can degrade the quality of AOT retrievals with MODIS data. These include unscreened inland water features (Hutchison et al., 2005; Levy et al., 2004) and cloud shadows. Different approaches have been used to effectively detect and eliminate most problems associated with ephemeral inland water. However, at this time, there seems to be no suitable logic to identify cloud shadows and failure to detect these shadows can

result in depressed aerosol retrievals. The MODIS aerosol retrieval approach attempts to eliminate cloud shadows and inland water surfaces using, what is referred to here, as a dark pixel correction. First, pixels with a normalized difference vegetation index (NDVI) < 0.1 are assumed to contain inland water (Chu et al., 2003). In addition, between 10-20% of the pixels, depending upon which version of the algorithm is used, with the lowest reflectance in the 0.65-μm band are discarded to further reduce cloud shadow and inland water effects. Finally, the MODIS AOT algorithms have varied the range of reflectance in the 2.1-μm ($\rho_{2.1\text{-}\mu m}$) band that is allowed to be part of the AOT retrieval. All versions of the MODIS AOT algorithms reviewed at CSR require 12 "good" pixels to remain after applying the aforementioned screening procedures to the 400 pixels that make up a nominal 10-km AOT analysis area. Those pixels remaining for analysis are examined in the 2.1-μm band to consider if 12 pixels are found in the range of 0.01-0.05. If there are at least 12 valid 500-m pixels, these values are averaged and the AOT retrieval is performed, otherwise, the upper limit is increased to 0.10 and the process repeated. If 12 valid pixels are not found after the upper limit is increased to 0.15, in the earlier versions of the algorithm, no AOT retrieval was attempted. This upper limit was increased to 0.25 in the collection 4 algorithms. Thus, over bright surfaces, aerosol retrievals are made up to reflectances of 0.40 in the 2.13-μm band but the results are flagged as lower quality.

These modifications to the AOT algorithmic logic can have a direct impact on correlations with ground-based air quality measurements. As a result, CSR has maintained a multi-year database which is used to retrieve AOT values with each release of the NASA algorithms. Through the analysis of this dataset, techniques and procedures have been developed to assess the value of AOT retrievals for air quality management as the MODIS AOT algorithms have continued to evolve. Some of those techniques are now presented in detail along with AOT-$PM_{2.5}$ correlations obtained with the Collection 4 and Collection 5 algorithms hosted at CSR.

3. ASSESSING AOT-$PM_{2.5}$ CORRELATIONS FOR AIR QUALITY MANAGEMENT

Procedures have been developed at CSR to assess the changes in AOT-$PM_{2.5}$ correlations as enhancements are made to the MODIS AOT retrieval algorithms, using a database of all $PM_{2.5}$ observations collected at CAMS location across Texas during the 2004 calendar year. Tests with this database compare hourly $PM_{2.5}$ average corresponding to the satellite overpass to (1) the nearest MODIS 10-km product, (2) averaged MODIS AOT values in the 30-km^2 grid centered on the CAMS location and (3) averaged AOT values in the 50-km^2 grid surrounding the CAMS site, as illustrated in Figure 1 for several CAMS locations in the Houston-Galveston area (HGA).

In general, results show a steady improvement in AOT-$PM_{2.5}$ correlations with each MODIS aerosol algorithm collection. Initial correlation tests with coincident Collection 3 and ground observations across Texas returned Pearson coefficients ranging 0.4-0.65; however, test coefficients revealed noticeable regional differences, with higher correlations at central and northeastern sites and outlying areas without regular patterns of diurnal variability. Results with the MODIS Collection 4 algorithms indicated a dramatic reduction in the number of valid retrievals with 25-40% fewer AOT center pixels and 65-85% fewer 50-km^2 grid retrievals compared to prior observation counts. Correlation coefficients increased 0.11 on average with maximum improvement of 0.35, but worsened slightly, e.g. typically less than - 0.1, at southern coastal sites. The version 5.1 algorithms incorporated only slight modifications to Collection 4, with an 11% increase in the frequency of 50-km^2 grid retrievals, central pixel retrievals declined by 16%. Frequency of central pixel retrieval coincident with the ground monitor was 28% for MODIS Collection 5 retrievals with at least one valid pixel within a 50-km^2 grid. Results with the Collection 5 algorithms did reflect a striking seasonal redistribution of retrievals from winter months with low values (80% AOT < 0.2), to late summer months. Combined retrievals for

November-February drop in proportion from 45% to 32%, while retrievals for the August-September time frame increase from 14% to 25% of the sample.

Table 2 contains detailed results of AOT-$PM_{2.5}$ correlations for the MODIS version 5.1 land aerosol algorithms based on 2004 dataset. The tables are arranged by sector, metropolitan area, CAMS number, latitude and longitude in columns 1-5 respectively. Stochastic correlations from all valid MODIS AOT retrievals in the area (unrestricted) are shown in columns 7 and 11 for 30-km and 50-km AOT grids, denoted AOT3U and AOT5U respectively, for each CAMS location shown in columns 4 and 5. The numbers of unrestricted, 3x3 and 5x5 AOT-$PM_{2.5}$ observations are shown in columns 6 and 10.

To reduce or eliminate effects of (1) undetected clouds and/or cloud shadows in the AOT and (2) to focus on large-scale pollution events that transit Texas borders, the dataset used to generate correlations at each site was restricted to include only grids with a minimum number of observations, i.e. at least 6 valid (of the 9 possible) AOT values were required for the 30-km grid and at least 15 (of 25) for the 50-km grid. Correlations obtained with these restricted datasets are denoted AOT3R and AOT5R and shown in columns 9 and 13, respectively along with the number of observations in columns 8 and 12. The basis for generating correlations with this restricted sample is that cloud contamination, if present, would cause fewer valid AOT pixels to be retrieved, while small-scale pollution, if detected, would be averaged with the larger-scale aerosol concentrations.

A close examination of Table 2 shows several key differences in correlations between the restricted and unrestricted datasets. First, the criterion restricts the number of data points used to generate these sets of correlations by 30-60%, dependent on geographic and weather conditions that result in sparse grid retrievals. Over 100 observations were acquired for most sites when 30-

km or 50-km grids were not restricted. Some areas, particularly coastal sites, are dominated by partially-populated grids due to the screening of water-contaminated pixels. For example, AOT retrievals in 30-km and 50-km grids for CAMS #642 (Southeast – Beaumont site) declined from 146 and 158 days to 97 and 99 days respectively in restricted datasets. Secondly, correlations based upon the restricted datasets were higher than those based upon unrestricted data, by more than 0.1 in most cases. CAMS #34 (Coastal, Galveston) shows correlations of 0.39 and 0.67 for the unrestricted and restricted data respectively on the 30-km grid. On the 50-km grid, CAMS #70 (Northeast, Fort Worth-Arlington) shows correlations of 0.60 and 0.75 for unrestricted and restricted data and CAMS #80 (Coastal, Brownsville) increases from 0.21 to 0.57. In fact, correlations at two CAMS facilities exceed 0.8 in the restricted dataset on the 50-km grid for the 2004 data set and 0.70 at both grid scales for several CAMS facilities, e.g. #401, #56, and #70.

Next, comparisons are made between correlations generated from the restricted and unrestricted datasets using the MODIS collection 4.2.2 and 5.1 AOT algorithms. AOT-$PM_{2.5}$ correlations developed from the MODIS version 4.2.2 algorithms were previously reported in Table 2 of Hutchison et al., (2005) for the 10-km and 50-km grids and are not repeated here; thus, Table 3 shows differences in correlations based upon each set of retrieval algorithms, as shown in Table 2. In this case, negative values reflect smaller correlation values obtained with the Collection 5.1 algorithms. For example, Table 3 shows far fewer AOT products were retrieved with the newer algorithms in some regions of Texas. For example, the 30-km grid surrounding CAMS #1014 had 45 fewer days where at least one value AOT retrieval was available and 64 fewer days where at least 6-AOT valid values were analyzed. In the 50-km grid surrounding CAMS #34, there were 15 and 55 fewer observations available for these corrections, respectively. On the other hand, at other CAMS locations there were more valid AOT retrievals were made with the Collection 5.1 algorithms, e.g. CAMS #64 shows 25 and 12 for the unrestricted and restricted datasets on the 30-km grid and #642 shows 28 and 12 for these same conditions on the 50-km grid.

In general, differences between correlations shown in Table 3 for most entries in columns 7, 9, 11, and 13 are positive numbers which suggests that the modifications in the Collection 5.1 algorithms will improve AOT-$PM_{2.5}$ correlations for the Texas region. In addition, higher values in the correlations based upon restricted data versus unrestricted data as shown in Table 2, suggests that users of Collection 5 aerosol products can be more confident that AOT reflects actual ground-based air quality when larger numbers of AOT retrievals are present in the database. The requirement for a minimum number of valid AOT observations in grid cells:

- reduces the probability of unscreened clouds or shadows contaminating the AOT product,
- reduces the probability of ephemeral water impacting AOT product quality, and
- emphasizes larger scale (transient) pollution events over localized events.

While in most cases, AOT-$PM_{2.5}$ correlations improved with the conversion at CSR from the collection 4.2 to the collection 5.1 MODIS algorithms, some problems remain. First, some correlations were lower with the Collection 5 algorithm as seen in the panhandle and central sectors. CAMS #601 in the central sector showed a change in correlations of -0.15 and -0.13 for the unrestricted 3x3 and 5x5 grids respectively. In addition, CSR identified cases, which are not shown, where these AOT analyses have much lower than expected values compared to $PM_{2.5}$ observations. An example of these "cold spots" occurred during the September 29 - October 3, 2004 timeframe for CAMS #64, located in Beaumont-Port Arthur region. CAMS #64 reports $PM_{2.5}$ levels near 15-20 $\mu g\ m^{-3}$ while the MODIS AOT value is only about 0.2. These cold spots appear to be associated with cloud shadows. Also hot spots were noted in the AOT retrieval on September 8, 2004 where the MODIS collection 4 AOT was 1.9 while the CAMS site reports $PM_{2.5}$ of less than 5 $\mu g\ m^{-3}$. No retrieval was made at the 10-km resolution with the Collection 5 algorithm. Thus, users these AOT products would be served well by a close manual examination of the imagery, perhaps using procedures described by Hutchison and Cracknell (2005), to

inspect for cirrus clouds and cloud shadows that could generate hot or cold spots in the AOT product.

4. INCORPORATING AEROSOL PROFILE DATA INTO AOT-$PM_{2.5}$ CORRELATIONS

Correlations approaching 0.80, as seen in Table 2, are highly encouraging but further improvement is still desirable to more fully use AOT analyses in a real-time, air quality decision support system. CSR has postulated that additional improvement could be achieved through knowledge of the vertical structure of the aerosols inferred from the vertical component of a real-time trajectory-based forecast model (Hutchison et al., 2004; Hutchison et al., 2005). More recently, others have demonstrated the value of aerosol profile information, obtained with ground-based lidar systems, for improving AOT-$PM_{2.5}$ correlations (Engel-Cox et al., 2006). However, these systems are expensive to install, maintain, and operate. Therefore, aerosol profiles are now examined, with the aid of airborne lidar data, to assess the feasibility of using the vertical component of trajectory forecasts to predict the vertical structure of aerosols and further improve AOT-$PM_{2.5}$ correlations.

Airborne lidar data were collected as part of large, multi-agency study that targeted the Houston-Galveston area (HGA) of Texas as a particulate matter supersite. The study was known as the Texas Air Quality Study 2000 or TXAQS-I. Part of the study included an intensive pollution sampling in the Texas Gulf Coast area beginning in mid-August 2000 and continuing into the middle of September. Observational data from ships, airplanes, satellites, and ground-base sensors were collected to facilitate study of the formation, composition, and day-night cycles of ozone and particulate matter, and the reaction of these pollutants with other atmospheric constituents due to changes in meteorology and ground-level activity. Additional information on TXAQS-I may be found at:

http://www.tceq.state.tx.us/assets/public/comm_exec/pubs/pd/020/00-08/texas2000.pdf

In support of TXAQS-I, the Environmental Technology Laboratory or ETL (now known as Earth System Research Library or ESRL) of the National Oceanic and Atmospheric Administration (NOAA) flew a DC-3 aircraft that harbored a lidar (LIght Detecting and Ranging) instrument to continuously measure the aerosol backscatter in air columns at various points along the aircraft's flight track. These lidar measurements were recorded during the August 25 - September 12 timeframe. A different flight path was covered by the flight team on each of eleven days of active measurements within the area of interest, which included the HGA and Harris County. CSR obtained these lidar data to assess the value of aerosol profile information for improving correlations between MODIS AOT and CAMS $PM_{2.5}$ data. In particular, CSR sought to (1) determine if the vertical motions in the trajectory forecasts could be used to gain insights into the location of the maximum aerosol concentration in the profiles and (2) assess the value of information about the aerosol profile for further improving AOT-$PM_{2.5}$ correlations. To complete this study, CSR first reduced the airborne lidar data into data comparable to MODIS AOT and secondly, analyzed these data through case studies that include advection of AOT fields using trajectories similar to those generated by the IDEA software. The results of these investigations are reported in this section.

4.1 Pre-processing Airborne Lidar Data Collected During TXAQS 2000

The lidar flow by NOAA during the TXAQS 2000 study was a single-channel device that emitted energy at 359-nm or 0.359-μm. The NOAA ESRL aircraft was flown at maximum height of approximately 3500-4000 meters Mean Sea Level (MSL) and the majority of backscatter profiles were retrieved from about 2700-3200 m to the surface (Senff, 2005). TXAQS-I lidar flight durations ranged between 2.34 and 6.9 hours, with flights starting between 15:41 and 18:63 UTC

and ending in the interval between 20:97 and 24:46 UTC. Over 60 total hours of lidar observation are represented by the collected set of 17,599 records, each record corresponding to a lidar transmission which are referred to herein as columns. The lidar transmissions generally occurred at 10-second intervals with some time gaps.

For a given location indicated by latitude-longitude coordinates, NOAA ESRL generated backscatter values in units of (m-1 sr-1) within 15-meter vertical 'range gate' intervals from the aircraft toward the ground. From these data, CSR generated total column AOT through the integration of the sum of the range gate backscatter values. This conversion included (1) conversion of backscatter for the instrument optics and (2) translation of the lidar total backscatter at 359-nm to an optical thickness at 0.55-μm for comparison with the similar MODIS AOT product. This conversion involved multiplying first by 30 sr and then by 0.81 to convert measurements at a 359-nm wavelength to the MODIS 550-nm wavelength for fine particulate matter. No attempt was made to correct for absorption processes. In addition, the lidar were not rigorously calibrated, i.e. data were considered non-calibrated by NOAA (Dr. Christoph Senff NOAA ESRL, personal communication). Therefore, these data were used only qualitatively to examine the vertical structure of the aerosol layers and not to make quantitative comparisons in AOT values. A sample of a typical plot of backscatter profiles for a portion of the flight that occurred on September 6, 2000 is shown in Figure 2. Finally, CSR converted these data from aircraft-referenced measurements to surface-based (constant altitude) observations.

Next, CSR examined all the lidar observations to identify case studies of potential value for the goals stated above. Table 4 summarizes the notable statistics for days which contained significant pollution loading in the lidar profiles. Column heights of individual lidar measurements ranged between 2653-m and 3319-m in the dataset and the total number of atmospheric columns or profiles was between 1589-2296 representing 255,832 - 358,549 measurements. September 6 had

the largest number of observations that fell within ± 1-hr of MODIS overflight and August 28 also had numerous observations that were temporally and spatially collocated with MODIS Terra overflight. Data collected on August 25th and September 12th produced few data points, i.e. 24 and 8 respectively, which met the temporal requirements established for the study. Thus, the focus for further investigations was upon August 28th and September 6th of 2000.

Detailed maps of all data collected by MODIS AOT values, ground-based CAMS sites, and airborne lidar data were generated for the datasets that contained significant pollution. The maps for September 6th are shown in Figure 3 while those for August 28th are shown in Figure 4. The left panels of each figure contain a true color composite of Terra MODIS data along with the flight-path of the NOAA aircraft on the particular day. Also shown in the left panels are the locations of CAMS sites (centered on 50-km resolution red boxes). The 100-m wind trajectories are indicated by orange arrows. A smoke plume from a fire is clearly visible in the upper right corner of the MODIS true-color image in Figure 3. In the right panels are shown gray-scale images of the MODIS AOT products, with brighter values depicting higher AOT values. The outline of the smoke plume is clearly seen in the MODIS AOT product in Figure 3. Demographic features, e.g. river, lakes, and county boundaries are also displayed. Figure 4 is seen to contain a large number of clouds which results in few AOT retrievals.

4.2 Application of the Airborne Lidar Data to Air Quality Prediction

The lidar measurements were matched to ground-based $PM_{2.5}$ measurements by rounding the time of the former to the nearest hour and retrieving the closest corresponding $PM_{2.5}$ hourly average from among the three CAMS sites nearest to the LIDAR flight location. Averages of $PM_{2.5}$ at five-minute intervals, if these were made available by TCEQ, could be used to reduce the temporal gap between the compared readings.

Next, the airborne lidar observations collected during TXAQS 2000 were used to assess the value of aerosol profile information for further improving correlations between MODIS AOT and CAMS $PM_{2.5}$ data. The aerosol profiles are shown in the left panel of Table 5 for data collected on August 28th and in the right panel for data collected on September 6th. It should be noted that some of the 15-m observations in the 100-m layer nearest to the surface may be missing in these data. Missing observations are accounted for by averaging all available observations and using this value to determine the backscatter for the layer. It is clear from Table 5 that the vast majority of the backscatter values come from the lower atmospheric levels and aerosol concentration decreases rapidly aloft. Importantly, Figure 5 shows the vertical component of the trajectory, with its terminus in the flight track, at 100-m (red), 500-m (blue) and 1-km (green). The 100-m and 500-m trajectories show subsidence occurring throughout most of the period and the air rising slightly after MODIS over flew the area.

Finally, comparisons between MODIS AOT and CAMS $PM_{2.5}$ observations were generated for days when MODIS, lidar, and CAMS data were temporally and spatially coincident. Figure 6a shows correlations of 0.98 on September 6, 2000 dataset when the lidar showed the aerosols to be concentrated near the Earth's surface while Figure 6b shows correlations of 0.47 for all MODIS data and CAMS observations collected during the TXAQS-I field experiment. Thus, these observations show that satellite-based AOT retrievals and ground-based $PM_{2.5}$ observations are more highly correlated when the aerosols are concentrated near the Earth's surface and, based upon data shown, it appears that the trajectory data do provide insights into the aerosol vertical structure which should help further improve AOT-$PM_{2.5}$ correlations. Based upon these encouraging results, CSR plans to continue analyzing larger databases that include trajectory data from the IDEA software and data from NASA A-Train, including Calipso (Cloud-Aerosol Lidar and Infrared Pathfinder Satellite) lidar profiles as these data become available.

5. SUMMARY

CSR is generating near real-time forecasts of air quality based upon MODIS AOT analyses generated at our EOS DBGS. Strong correlations between MODIS AOT and ground-based $PM_{2.5}$ observations are needed for air quality managers to fully utilize these products. Some improvements in AOT-$PM_{2.5}$ correlations are realized directly through the evolution of the MODIS retrieval algorithms and stronger correlations can be achieved using methodologies that account for the spatial differences between these observations.

In this paper, it was shown that differences in spatial resolution between point measurements made at CAMS locations and the nominal 10-km resolution MODIS AOT analysis are mitigated by requiring a minimum number of AOT retrievals in grid cells centered on each CAMS location. The requirement for a minimum number of valid AOT observations in grid cells, in effect, (1) reduces the probability of unscreened clouds or shadows contaminating the AOT product, (2) reduces the probability of ephemeral water impacting AOT product quality, and (3) emphasizes larger scale (transient) pollution events over localized events which is a goal for using satellite date in air quality management. In addition, these results demonstrate the potential for using the vertical motions of trajectories to further improve correlations by accounting for variations in aerosol profiles. Since meteorological conditions that govern transport of many pollutants into and across Texas vary with the pollution source (e.g. biomass burning from Central America, continental haze from the industrial middle of the US, and volcanic ash and Saharan dust) it appears reasonable that different correlations might be established under each set of conditions to translate MODIS AOT into measures of air quality such as $PM_{2.5}$.

Clearly, more analyses are needed before the concepts proposed in this paper can be more fully trusted. CSR continues to conduct these analyses using data collected by Calipso on the

CLoudSat mission and MODIS AOT products created from the Aqua spacecraft in NASA's A-Train constellation.

6. ACKNOWLEDGEMENTS

This work was supported by NASA Grant NNL04AA70G, Advanced EOS products for Air Quality Management, and CSR gratefully acknowledges the continued support of Dr. Lorraine Remer and staff at NASA Goddard Space Flight Center and the assistance from Dr. Christoph Senff of the NOAA ESRL in analyzing the lidar data. Finally, special thanks are extended to Mr. Clemens Delatree for constructing the many maps of MODIS, lidar, and ground-based pollution measurements similar to those shown in Figures 3 and 4.

7. REFERENCES

Ackerman S.A., Strabala K.I., Menzel W.P., Frey R.A., Moeller C.C., and L.E. Gumley, 1998: Discriminating clear sky from clouds with MODIS, J. Geophys. Res., 103 (D24): 32141-32157.

Ackerman, Strabala, Menzel, Frey, Moeller, Gumley, Baum, Schaaf, & Riggs, 2002: Discriminating Clear-Sky from Cloud with MODIS - Algorithm Theoretical Basis Document, *Products: MOD35. ATBD Reference Number: ATBD-MOD-06*

Al-Saadi, J. A., Szykman, J., Pierce, R. B., Kittaka, C., Neil, D., Chu, D. A., Remer, L., Gumley, L., Prins, E., Weinstock, L. MacDonald, C., Wayland, R., Dimmick, F., and J. Fishman, 2005: Improving national air quality forecasts with satellite aerosol observations, Bulletin of the American Meteorological Society (BAMS), **86**,1249-1261.

Barnes, W.L., T.S. Pagano, and V. Salomonson, 1998: Prelaunch characteristics of the Moderate Resolution Imaging Spectroradiometer (MODIS) on EOS AM-1. IEEE Trans. Geosci. Remote Sens., **36**, 1088-1100.

Brennan, J. I., Kaufman, Y. J., Koren, I., and R. R. Li, 2005: Aerosol-cloud interaction-misclassification of MODIS clouds in heavy aerosol." IEEE Transactions on Geoscience and Remote Sensing, **43**, 911-921.

Carlson, T. M., and J. M. Prospero, 1972: The large-scale movement of Saharan air outbreaks over the northern equatorial Atlantic, Journal of Applied Meteorology, **11**, 283-297.

Chu, D. A., Kaufman, Y. J., Ichoku, Zibordi, G., Chern, J. D., Mao, J. Li, C. and B. N. Holben, Remer, and Tanre': 2003: Global monitoring of air pollution over land from the Earth Observing System-Terra Moderate Resolution Imaging Spectroradiometer (MODIS), J. Geophy. Res., **108**, doi:10:1029/2002JD003179.

Chu, D. A., Kaufman, Y. J., Ichoku, C., Remer, L. A. Tanre', D., and B. N. Holben: 2002: Validation of the MODIS aerosol optical depth retrieval over land, Geo. Res. Lett., **29**, doi: 10.1029/2001GL013205.

Engel-Cox, J. A., Hoff, R. M., Rogers, R., Dimmick, F., Rush, A. C., Szykman, J. J., Al-Saadi, J., Chu, D. A., and E. R. Zell, 2006: Integrating lidar and satellite optical depth with ambient monitoring for 3-dimensional particulate characterization, Atmospheric Environment, **40**, 8056-8067

Gao B.C., Yang P., and R.R. Li, 2002: Distinguishing tropospheric aerosols from thin cirrus clouds for improved aerosol retrievals using the ratio of 1.38-μm and 1.24-μm channels, Geophys. Res. Ltrs., **29**, 1890, doi:10.1029/2002GL015475.

Hutchison, K.D. and A.P. Cracknell, 2005: Visible Infrared Imager Radiometer Suite, A New Operational Cloud Imager, CRC Press, Taylor & Francis Group, Boca Raton, FL, pp 230.

Hutchison, K. D., Smith, S. and S. Faruqui, 2005: Correlating MODIS aerosol optical thickness data with ground-based PM2.5 observations across Texas for use in a real-time air quality prediction system, Atmospheric Environment **39**, 7190-7203.

Hutchison, K. D., Smith, S. and S. Faruqui, 2004: The use of MODIS data and aerosol products for air quality prediction, Atmospheric Environment **38**, 5057-5070.

Hutchison, K. D., 2003: "Applications of MODIS satellite data and products for monitoring air quality in the state of Texas," Atmospheric Environment, **37**, 2403-2412.

Kalluri, S., Gilruth, P., and R. Bergman, 2003: The potential of remote sensing data for decisions makers at the state, local and tribal level: experience from NASA's Synergy Program, Environmental Science and Policy, **6**, 487-500

Kaufman, Y.J., D. Tanré, H.R. Gordon, T. Nakajima, J. Lenoble, R. Frouin, H. Grassl, B.M. Herman, M.D. King and P.M. Teillet, 1997a: Passive remote sensing of tropospheric aerosol and atmospheric correction for the aerosol effect. J. Geophys. Res., **102**, 16815-16830.

Kaufman, Y. J., Tanre, D., Remer, L. A., Vermote, E. F., Chu, A. and B. N. Holben, 1997b: "Operational remote sensing of tropospheric aerosol over land from EOS moderate resolution imaging sprectroradiometer, Journal of Geophysical Research, **102** (D14), 17051-17067.

Kaufman, Y. J., Wald, A. E., Remer, L. A., Gao, B.-C., Liand, R.-R. and L. Flynn, 1997c: The MODIS 2.1 μm Channel - Correlation with visible reflectance for use in remote sensing of aerosol. IEEE Trans. Geo, **35**, 1286-1298.

Kaufman, Y. J., Tanre', D. and O. Boucher, 2002a: A satellite view of aerosols in the climate system, Nature, **419**, 215-223.

Kaufman, Y. J., Wald, A. E., Remer, L. A., Gao, B.-C., Liand, R.-R. and L. Flynn, 2002b: Relationship between surface reflectance in the visible and mid-IR used in MODIS aerosol algorithm – theory, Geophysical Research Letters, **29**, (23), 2116, doi:10.1029/2001GL014492

Levy, R. C., Remer, L. A., Martins, J. V., Kaufman, Y. J., Plana-Fattori, A., Redemann, J. and B. Wenny, 2004: Evaluation of the MODIS aerosol retrievals over ocean and land during CLAMS, Journal of Atmospheric Sciences, **62**, 974-992

Martins, J.V., D. Tanré, L.A. Remer, Y.J. Kaufman, S. Mattoo and R. Levy, 2002: MODIS Cloud screening for remote sensing of aerosol over oceans using spatial variability. Geophys. Res. Lett., **29**, 10.1029/2001GL013252.

Salomonson, V. V., Barnes, W. L., Maymon, P.W. Montgomery, H. E., and H. Ostrow, 1989: MODIS : Advanced Facility Instrument for Studies of the Earth as a System, IEEE Transactions in Geoscience and Remote Sensing, 27, 145-153

Remer, L.A., Kaufman, Y.J., Tanré, D., Mattoo, S., Chu, D.A., Martins, J.V. Li, R-R., Ichoku, C., Levy, R. C. , Kleidman, R.G., Eck, T.F., Vermote, E. and B.N. Holben: 2005**:** The MODIS Aerosol Algorithm, Products and Validation, Journal of the Atmospheric Sciences, **62**, 947-973.

Remer, L.A., Tanré, D., and Y. Kaufman, 2006**:** Algorithm for Remote Sensing of Tropospheric Aerosol from MODIS: Collection 5, MODIS Algorithm Theoretical Basis Document, pp 87 available at: http://modis-atmos.gsfc.nasa.gov/MOD04_L2/atbd.html

Remer, L.A., Tanré, D., Kaufman, Y.J., Ichoku, C., Mattoo, S., Levy, R. C., Chu, D.A., Holben, B.N., Dubovik, O., Smirnov, A., Martins, J.V., Li, R-R., and Z. Ahmad: 2002**:** Validation of

MODIS aerosol retrieval over ocean, Geophysical Research Letters, **29**, doi:10.1029/2001GL013204.

Shenk, W., and R. Curran, 1974: The detection of dust storms over land and water with satellite visible and infrared measurements, Monthly Weather Review, **102**, 830-837.

Senff, C., 2005: NOAA-ETL, Texas Air Quality Study 2000 Airborne Lidar Aerosol Data Description (accessed October 2005) at: http://www.etl.noaa.gov/et2/data/data_pages/texaqs/air_aerosol.html

Tanre', D., Kaufman, Y. J., Herman, M., and S. Mattoo, 1997: Remote sensing of aerosol properties over oceans using the MODIS/EOS spectral radiances, J. Geophys. Res., **102**, 16971-16988.

Wang and Christopher, 2003: Intercomparison between satellite-derived aerosol optical thickness and PM-$_{2.5}$ mass: Implications for air quality studies, Geophysical Research Letters, **30**, doi:10.1029/2003GLO181174.

Figure Captions

Figure 1. Sample locations of CAMS facilities that provided useful air quality measurements with 30x30-km and 50x50-km surrounding regions.

Figure 2. Graphical presentation of lidar backscatter profiles for a portion of the flight that occurred on September 6, 2000.

Figure 3. Maps of MODIS AOT, CAMS locations, and airborne LIDAR flight path and reports for 6 September 2000.

Figure 4. Maps of MODIS AOT, CAMS locations, and airborne LIDAR flight path and reports for 28 August 2000.

Figure 5. Trajectory for air parcels terminating near Victoria, TX (100-m in red, 500-m in blue and 1-km in green) on 2300 UTC September 6, 2000.

Figure 6. Correlations between MODIS AOT and $PM_{2.5}$ for (a) CAMS locations in the Houston-Beaumont area for September 6, 2000 timeframe and (b) for CAMS locations in the Houston-Beaumont area between August 20-September 15 during TXAQS 2000.

List of Tables

Figure 1

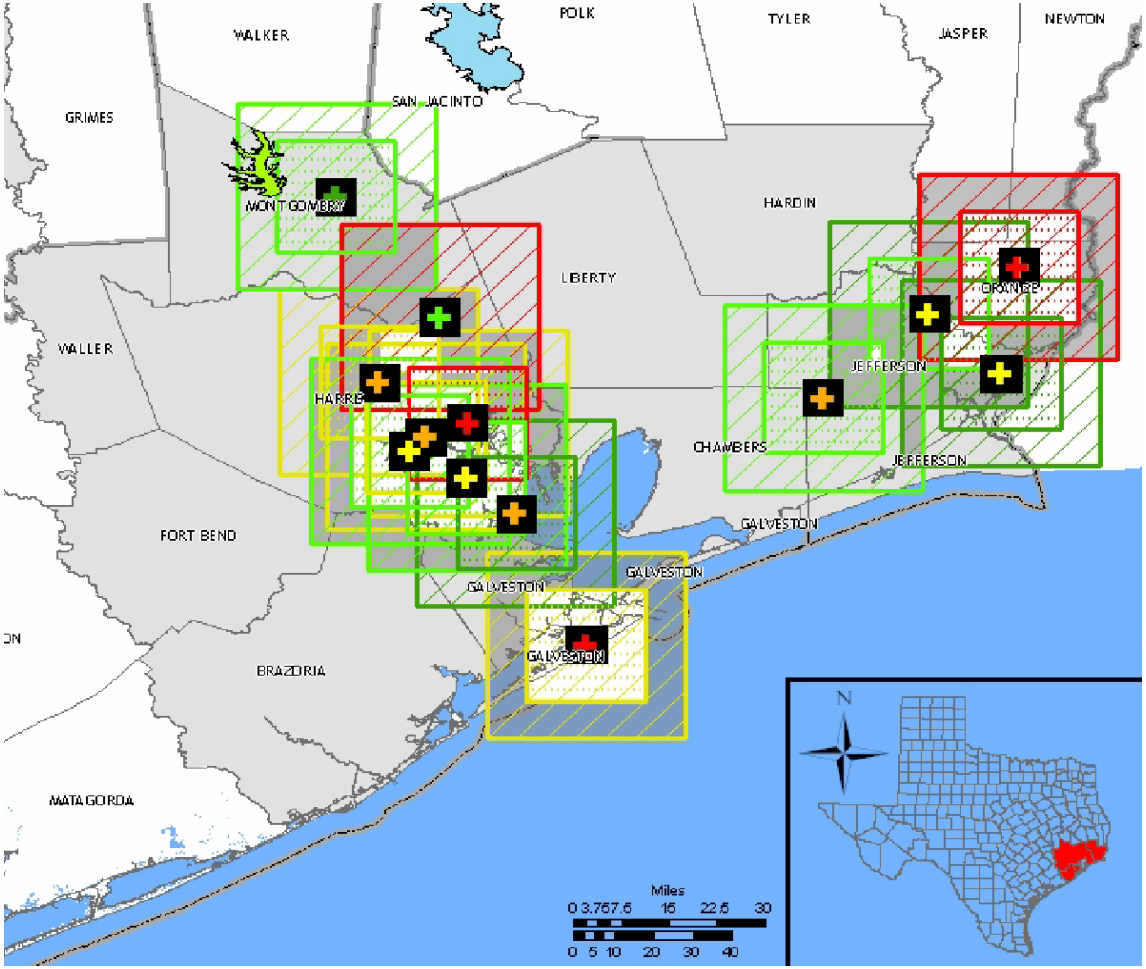
WALKER
POLK
TYLER
JASPER
NEWTON
GRIMES
SAN JACINTO
MONTGOMERY
HARDIN
LIBERTY
WALLER
HARRIS
JEFFERSON
CHAMBERS
FORT BEND
GALVESTON
BRAZORIA
MATAGORDA
N
Miles
0 3.757.5 15 22.5 30
0 5 10 20 30 40

Figure 2

Date	06 September 2000																				
LiDAR	16.75 - 17.25 UTC		Terra Satellite Overpass: 1720 UTC																		
Backscatter m^{-1} sr^{-1}	CDT Hour Time																				
Vertical Bin 100m	12:00 PM		1:00 PM																		
Time UTC -->	16.763	16.765	17.177	17.179	17.182	17.185	17.193	17.196	17.199	17.202	17.204	17.207	17.210	17.213	17.215	17.218	17.221	17.224	17.227	17.257
Latitude	29.801	29.806	29.454	29.448	29.441	29.435	29.416	29.410	29.404	29.398	29.391	29.385	29.379	29.373	29.366	29.360	29.354	29.347	29.341	29.272
2601_2700			171	183	188	193	162	172	170	159	153	172	152	156	153	158				117
2501_2600	205	211	179	188	192	202	173	177	176	163	158	174	161	161	160	167	153	159	153	121
2401_2500	214	215	184	195	204	208	180	183	182	171	167	182	171	172	170	177	161	167	158	120
2301_2400	213	219	189	202	209	212	185	192	186	176	168	185	174	176	171	181	169	168	164	127
2201_2300	221	223	195	201	217	223	188	187	194	182	175	195	177	177	179	184	167	168	165	128
2101_2200	218	225	194	211	218	232	189	192	204	184	181	197	186	185	186	193	180	179	176	141
2001_2100	236	239	218	237	235	247	212	213	221	201	194	213	200	209	206	215	196	196	190	145
1901_2000	324	298	333	329	336	310	314	316	312	297	295	320	303	310	315	311	263	260	246	149
1801_1900	696	600	451	466	469	477	430	443	430	415	398	416	380	368	361	374	369	380	362	276
1701_1800	879	860	505	522	514	547	463	467	459	428	410	451	425	407	417	411	372	365	359	318
1601_1700	905	901	561	661	681	778	575	543	547	455	425	431	402	388	390	408	455	487	465	375
1501_1600	903	923	732	835	898	1064	836	857	809	618	492	482	429	421	498	715	790	825	820	654
1401_1500	960	1002	978	1109	1149	1193	935	921	938	843	762	822	718	712	808	981	937	925	936	735
1301_1400	1065	1127	1084	1112	1153	1207	960	951	998	936	925	1102	1041	986	1041	1078	1005	962	981	711
1201_1300	1070	1099	1075	1108	1138	1170	1001	1014	1034	1014	981	1110	1065	1042	1003	1021	921	908	888	638
1101_1200	1009	1040	1025	1091	1100	1126	1021	1015	1047	976	954	1023	964	972	946	950	872	858	843	608
1001_1100	954	987	971	1026	1063	1086	941	967	980	928	911	970	916	911	922	912	832	821	798	571
901_1000	906	932	912	1023	1006	1074	890	932	953	889	865	953	938	914	928	880	795	763	793	579
801_900	880	1085	1051	1479	1168	1504	942	1018	1075	935	852	994	974	961	973	949	793	769	716	549
701_800	983	1409	1490	1918	2191	2860	2380	2500	2674	1619	1629	1824	1457	1316	1294	1041	855	871	738	468
601_700	1159	1327	1460	1654	2358	2716	2470	2365	2511	2177	2169	2255	1752	1643	1557	1318	1268	1684	1189	805
501_600	1187	1217	1391	1411	1752	1865	1802	1685	1656	1679	1660	1712	1525	1452	1415	1287	1440	1800	1497	1292
401_500	1144	1137	1170	1238	1251	1270	1321	1350	1274	1239	1216	1181	1204	1173	1172	1177	1235	1241	1239	1279
301_400	1074	1068	1076	992	1006	1006	880	854	974	985	1008	1044	1035	1036	1041	1048	980	977	996	963
201_300	927	950	797	693	785	548	502	661	791	719	740	900	782	848	962	1092	708	763	806	608
101_200	837	901	682	482	625	517	276	429	552	448	517	706	628	663	772	755	583	421	697	393
0_100	877	943	0	0	0	0	0	0	0	0	0	0	0	0	0	700	480	262	533	322

Figure 3

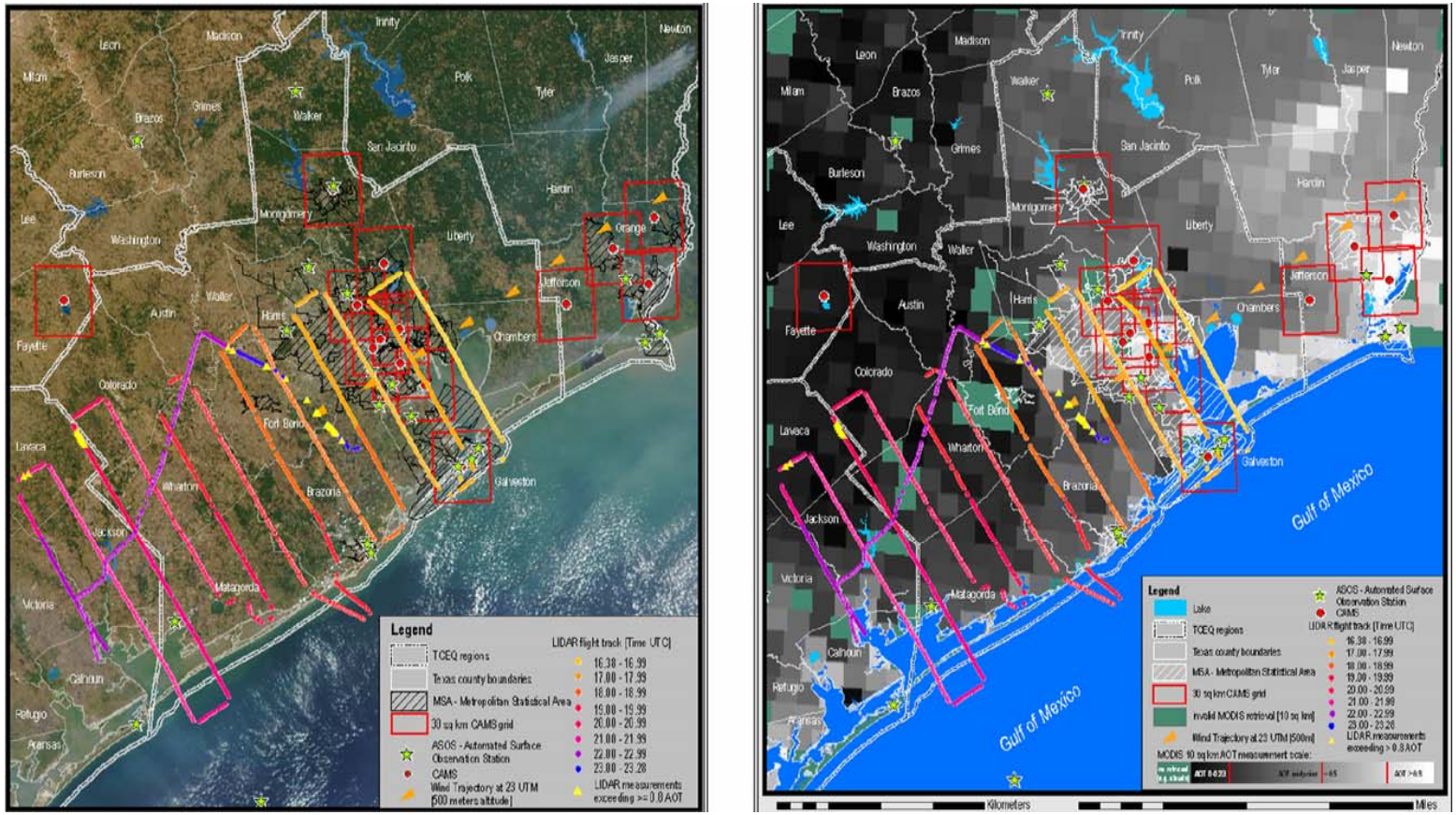
Leon
Madison
Trinity
Newton
Milam
Polk
Jasper
Brazos
Grimes
Walker
Tyler
San Jacinto
Burleson
Hardin
Lee
Montgomery
Liberty
Washington
Orange
Waller
Jefferson
Austin
Harris
Chambers
Fayette
Colorado
Fort Bend
Galveston
Lavaca
Whaton
Brazoria
Jackson
Matagorda
Victoria
Calhoun
Refugio
Aransas
Gulf of Mexico
Legend
TCEQ regions
Texas county boundaries
MSA - Metropolitan Statistical Area
30 sq km CAMS grid
ASOS - Automated Surface Observation Station
CAMS
Wind Trajectory at 23 UTM (500 meters altitude)
LIDAR flight track (Time UTC)
16.38 - 16.99
17.00 - 17.99
18.00 - 18.99
19.00 - 19.99
20.00 - 20.99
21.00 - 21.99
22.00 - 22.99
23.00 - 23.28
LIDAR measurements exceeding >= 0.8 AOT
Lake
invalid MODIS retrieval (10 sq km)
MODIS 10 sq km AOT measurement scale:
Kilometers
Miles

Figure 4

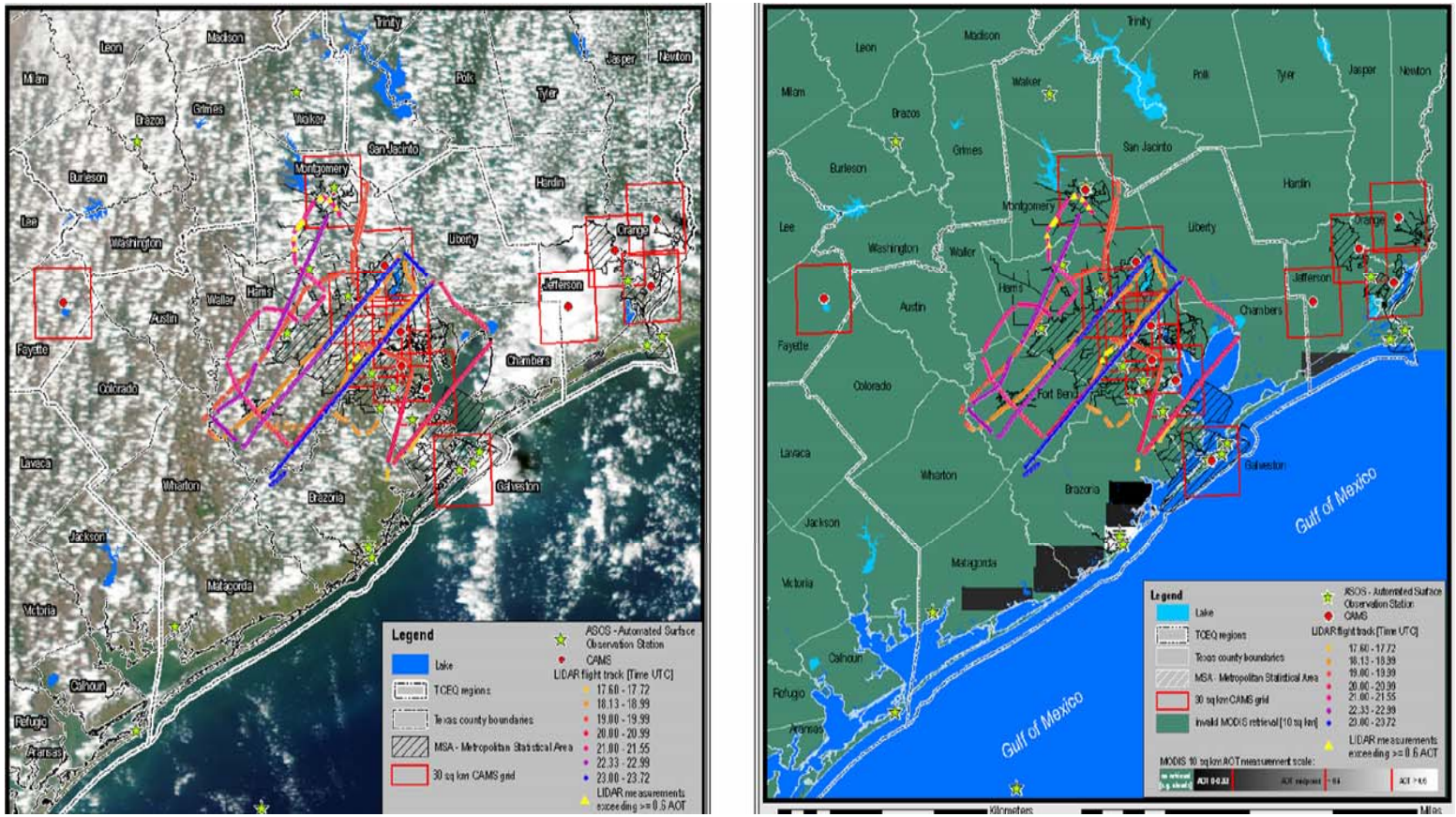
Trinity
Madison
Leon
Jasper
Newton
Milam
Polk
Tyler
Brazos
Grimes
Walker
San Jacinto
Burleson
Montgomery
Hardin
Lee
Washington
Liberty
Orange
Waller
Harris
Jefferson
Austin
Fayette
Chambers
Colorado
Lavaca
Wharton
Brazoria
Galveston
Jackson
Matagorda
Victoria
Calhoun
Refugio
Aransas
Gulf of Mexico
Legend
Lake
TCEQ regions
Texas county boundaries
MSA - Metropolitan Statistical Area
30 sq km CAMS grid
ASOS - Automated Surface Observation Station
CAMS
LIDAR flight track [Time UTC]
17.60 - 17.72
18.13 - 18.99
19.00 - 19.99
20.00 - 20.99
21.00 - 21.55
22.33 - 22.99
23.00 - 23.72
LIDAR measurements exceeding >= 0.5 AOT

Figure 5

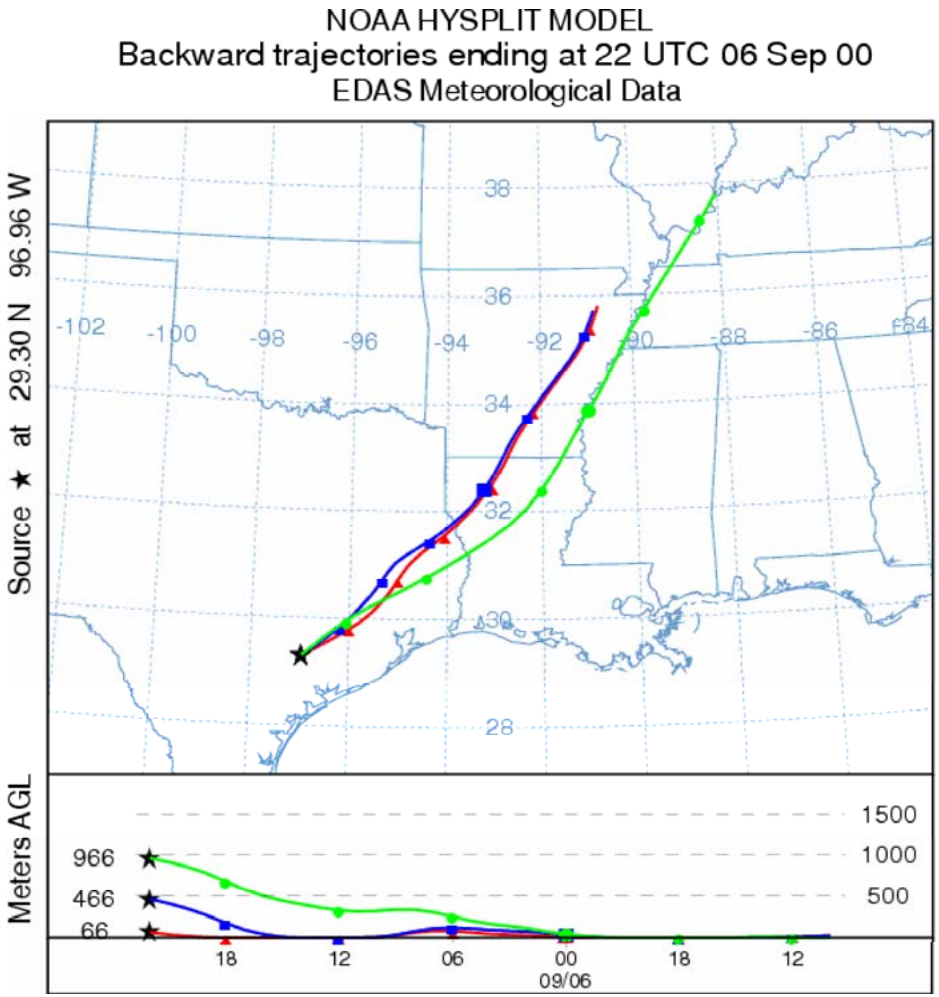
NOAA HYSPLIT MODEL
Backward trajectories ending at 22 UTC 06 Sep 00
EDAS Meteorological Data
Source ★ at 29.30 N 96.96 W
38
36
34
32
30
28
-102
-100
-98
-96
-94
-92
-90
-88
-86
-84
Meters AGL
1500
1000
500
966
466
66
18
12
06
00
18
12
09/06

Figure 6

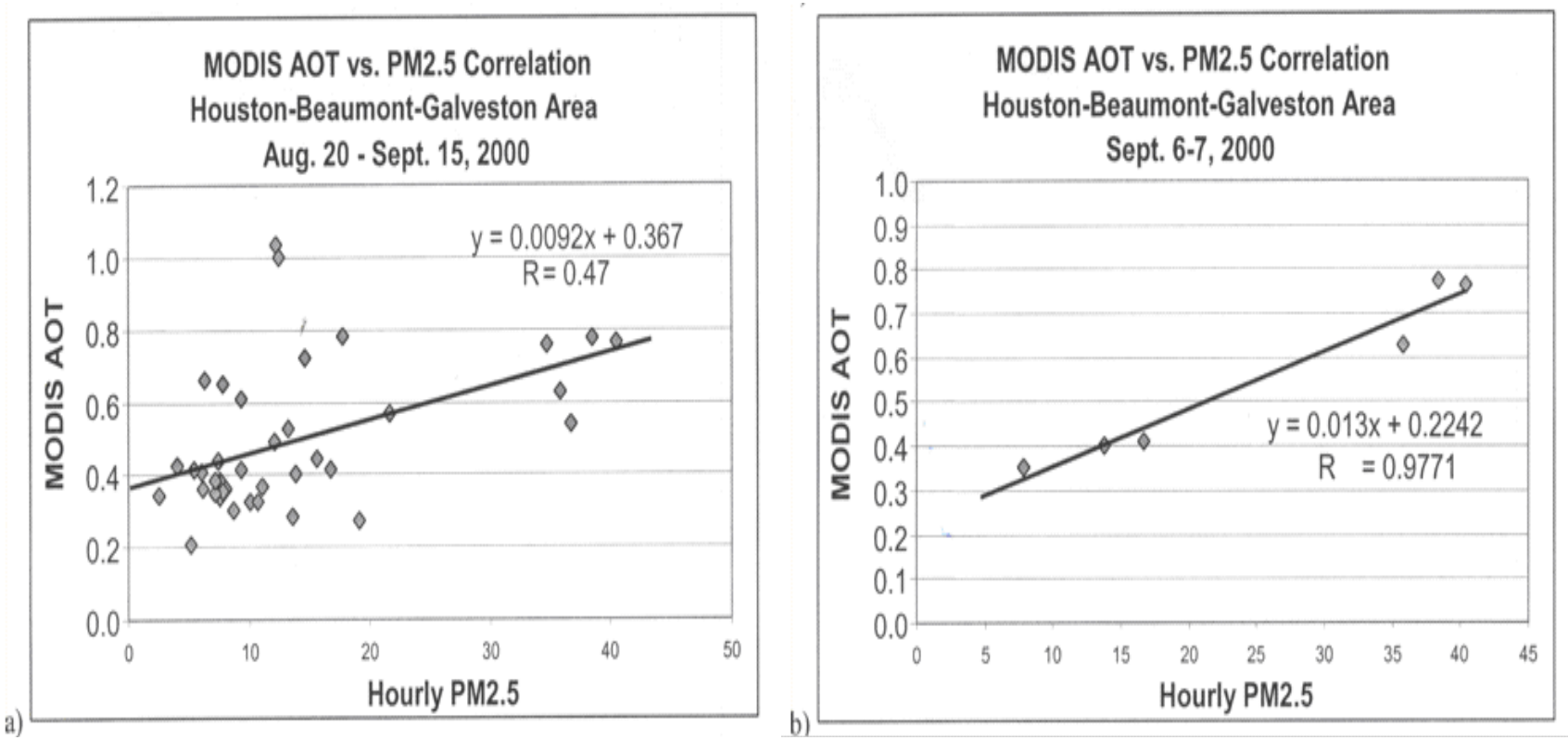
MODIS AOT vs. PM2.5 Correlation
Houston-Beaumont-Galveston Area
Aug. 20 - Sept. 15, 2000
y = 0.0092x + 0.367
R= 0.47
MODIS AOT
Hourly PM2.5
a)
MODIS AOT vs. PM2.5 Correlation
Houston-Beaumont-Galveston Area
Sept. 6-7, 2000
y = 0.013x + 0.2242
R = 0.9771
MODIS AOT
Hourly PM2.5
b)

Table 1.

Algorithm Version	Total pixels in 10-km Product	Cloud Screening Approach	Bright Pixels Correction	Dark Pixel Correction	Other comments
3.1	400 @ 500m resolution	Uses only MODIS cloud mask product	Eliminate highest 40% $\rho_{0.65\text{-}\mu m}$	Eliminate Lowest 10% $\rho_{0.65\text{-}\mu m}$	Requires 12 pixels with $\rho_{2.1\text{-}\mu m} < 0.15$
4.2.2	400 @ 500m resolution	Uses MODIS cloud mask & internal cloud tests	Eliminate highest 50% $\rho_{0.65\text{-}\mu m}$	Eliminate NDVI < 0.1 & Lowest 20% $\rho_{0.65\text{-}\mu m}$	Requires 12 pixels with $\rho_{2.1\text{-}\mu m} < 0.25$
5.1	400 @ 500m resolution	Uses only internal cloud tests	Eliminate highest 50% $\rho_{0.65\text{-}\mu m}$	Eliminate NDVI < 0.1 & Lowest 20% $\rho_{0.65\text{-}\mu m}$	Requires 12 pixels with $\rho_{2.1\text{-}\mu m} < 0.15$

Table 2.

Sector	Metro_Area	CAMS	Lat	Lon	AOT3 Unrestr Obs	AOT3 U vs PM25	AOT3 ≥ 6 Obs	AOT3 R vs PM25	AOT5 Unrestr Obs	AOT5 U vs PM25	AOT5 ≥ 15 Obs	AOT5 R vs PM25
Panhandle	Amarillo	305	35.19	-101.84	75	0.29	30	0.38	90	0.19	28	0.26
Panhandle	Odessa-Midland	1014	31.88	-102.36	46	0.35	6	0.45	68	0.32	7	0.30
Northeast	Dallas	401	32.86	-96.90	108	0.64	50	0.72	132	0.63	66	0.77
Northeast	Dallas	56	33.17	-97.25	140	0.60	95	0.71	158	0.58	96	0.74
Northeast	Dallas	74	32.76	-96.55	127	0.70	92	0.69	134	0.70	90	0.73
Northeast	Fort Worth-Arlington	61	32.67	-97.15	135	0.58	82	0.68	154	0.55	81	0.73
Northeast	Fort Worth-Arlington	308	32.78	-97.38	131	0.63	75	0.80	154	0.62	79	0.82
Northeast	Fort Worth-Arlington	70	32.97	-97.02	118	0.63	69	0.77	142	0.60	80	0.75
Northeast	Fort Worth-Arlington	310	32.78	-97.38	140	0.61	79	0.71	163	0.60	83	0.73
Northeast	Longview-Marshall	85	32.67	-94.17	148	0.56	111	0.64	160	0.53	115	0.59
Central	Austin-San Marcos	38	30.48	-97.91	102	0.63	80	0.59	118	0.61	74	0.58
Central	Austin-San Marcos	601	29.96	-96.77	87	0.52	55	0.59	97	0.49	56	0.48
Central	San Antonio	678	29.39	-98.39	98	0.54	64	0.56	118	0.55	64	0.61
Central	San Antonio	301	29.59	-98.27	98	0.60	62	0.53	120	0.63	63	0.50
Southeast	Houston	15	29.81	-95.16	119	0.47	70	0.56	148	0.45	71	0.57
Southeast	Houston	403	29.71	-95.28	95	0.49	53	0.59	118	0.50	58	0.63
Southeast	Houston	78	30.32	-95.48	132	0.48	90	0.57	153	0.46	89	0.59
Southeast	Houston	8	29.92	-95.38	104	0.56	58	0.69	134	0.52	63	0.69
Southeast	Houston	35	29.71	-95.16	113	0.60	54	0.67	146	0.53	70	0.70
Southeast	Houston	1	29.81	-95.27	107	0.56	59	0.62	133	0.55	64	0.71
Southeast	Houston	309	30.01	-95.15	105	0.49	69	0.61	130	0.51	70	0.62
Southeast	Beaumont-Port Arthur	54	30.07	-94.10	128	0.48	86	0.59	154	0.47	87	0.60
Southeast	Beaumont-Port Arthur	64	29.88	-94.34	115	0.48	83	0.62	142	0.48	81	0.62
Southeast	Beaumont-Port Arthur	642	30.15	-93.87	146	0.48	97	0.59	158	0.50	99	0.59
Coastal	Brownsville-Harlingen-San Benito	80	25.87	-97.45	87	0.22	37	0.42	108	0.21	36	0.57
Coastal	Corpus Christi	314	27.47	-97.29	130	0.53	40	0.72	143	0.51	26	0.80
Coastal	Galveston-Texas City	34	29.30	-94.84	112	0.39	24	0.67	140	0.43	15	0.72
South	McAllen-Edinburg-Mission	43	26.19	-98.33	116	0.49	69	0.54	136	0.48	70	0.53

Table 3.

Sector	Metro_Area	CAMS	Lat	Lon	AOT3 Unrestr Obs	AOT3 U vs_PM25	AOT3 ≥ 6 Obs	AOT3 R vs_PM25	AOT5 Unrestr Obs	AOT5 U vs_PM25	AOT5 ≥ 15 Obs	AOT5 R vs_PM25
Panhandle	Amarillo	305	35.19	-101.84	-14	-0.18	-39	-0.12	-16	-0.22	-33	-0.29
Panhandle	Odessa-Midland	1014	31.88	-102.36	-45	-0.09	-64	0.00	-28	-0.10	-40	-0.46
Northeast	Dallas	401	32.86	-96.90	-13	0.00	-49	0.15	1	0.00	-32	0.14
Northeast	Dallas	74	32.76	-96.55	15	0.08	5	-0.06	12	0.07	2	0.04
Northeast	Dallas	56	33.17	-97.25	7	0.00	-7	0.01	12	-0.04	-7	0.06
Northeast	Fort Worth-Arlington	61	32.67	-97.15	14	0.03	-21	0.12	19	0.02	-17	0.18
Northeast	Fort Worth-Arlington	308	32.78	-97.38	-1	0.05	-29	0.16	13	0.02	-22	0.21
Northeast	Fort Worth-Arlington	70	32.97	-97.02	-13	0.02	-34	0.13	-1	-0.01	-25	0.10
Northeast	Fort Worth-Arlington	310	32.78	-97.38	10	0.05	-27	0.16	23	0.03	-18	0.17
Northeast	Longview-Marshall	85	32.67	-94.17	34	-0.07	19	-0.07	37	-0.03	26	-0.12
Central	Austin-San Marcos	38	30.48	-97.91	-1	-0.04	-2	-0.12	0	-0.03	-4	-0.13
Central	Austin-San Marcos	601	29.96	-96.77	28	-0.15	7	-0.21	28	-0.13	10	-0.33
Central	San Antonio	678	29.39	-98.39	2	0.00	-15	0.09	14	-0.05	-10	0.08
Central	San Antonio	301	29.59	-98.27	7	0.03	-7	-0.05	14	0.11	-9	-0.16
Southeast	Houston	15	29.81	-95.16	13	0.15	-8	0.16	24	0.05	-7	0.17
Southeast	Houston	403	29.71	-95.28	-5	0.15	-19	0.20	2	0.12	-12	0.25
Southeast	Houston	78	30.32	-95.48	18	0.11	4	0.10	28	0.06	6	0.18
Southeast	Houston	8	29.92	-95.38	-2	0.04	-20	0.14	15	-0.01	-15	0.12
Southeast	Houston	35	29.71	-95.16	8	0.05	-24	0.10	25	0.05	-3	0.10
Southeast	Houston	1	29.81	-95.27	1	0.13	-17	0.08	9	0.05	-9	0.15
Southeast	Houston	309	30.01	-95.15	4	0.02	-8	0.15	14	-0.02	-4	0.16
Southeast	Beaumont-Port Arthur	54	30.07	-94.10	24	-0.01	7	0.08	27	0.11	13	0.09
Southeast	Beaumont-Port Arthur	64	29.88	-94.34	25	0.06	12	0.23	25	0.14	10	-0.01
Southeast	Beaumont-Port Arthur	642	30.15	-93.87	34	0.02	10	0.05	28	0.03	12	0.05
Coastal	Brownsville-Harlingen-San Benito	80	25.87	-97.45	10	-0.08	-21	0.04	21	-0.10	-23	0.10
Coastal	Corpus Christi	314	27.47	-97.29	13	0.08	-24	0.16	-11	0.08	-37	0.22
Coastal	Galveston-Texas City	34	29.30	-94.84	-3	-0.03	-45	0.17	-15	0.10	-55	0.20
South	McAllen-Edinburg-Mission	43	26.19	-98.33	28	0.10	4	0.18	37	0.11	6	0.02

Table 4.

Case Information	**Aug. 25**	**Aug. 28**	**Sept. 06**	**Sept. 12**
Number of atmospheric profiles	1589	1944	2296	1672
Total number of backscatter readings during flight	256,332	325,303	358,549	255,832
Mean backscatter value $*10^{-6}$ (within any column)	4.07	6.58	7.28	4.82
2σ Standard deviations (95% obs fall within -/+2 stdev spread)	12.01	88.03	27.62	40.52
Number of columns with a maximum reading exceeding $100*10^{-6}$ m-1sr-1	28	359	20	60
Number of values > $100*10^{-6}$	69	981	30	95
Number of columns with an average measurement exceeding $15*10^{-6}$ m-1sr-1	0	93	19	2
LIDAR Flight Begin Time	11:50 am	1:06 pm	11:23 pm	12:36 pm
MODIS Overpass Time	11:55 am	12:25 pm	12:20 pm	11:40 am
Columns within -/+1-hr pass with Valid MODIS Retrieval	24	83	562	8

Table 5.

Date 8/28/00	Backscatter (BSV) * 10^{-6}, units m^{-1} sr^{-1}				Date 9/06/00	Backscatter (BSV) * 10^{-6}, units m^{-1} sr^{-1}			
Time UTC	22.384	22.389	22.392	22.395	Time UTC	20.804	20.807	20.810	20.813
Latitude	30.690	30.691	30.693	30.696	Latitude	29.443	29.437	29.431	29.425
Longitude	-95.435	-95.422	-95.415	-95.408	Longitude	-96.682	-96.678	-96.674	-96.670
2601_2700	597	460	462	556	2601_2700	126	98	103	104
2501_2600	662	499	520	612	2501_2600	148	127	131	128
2401_2500	669	545	584	630	2401_2500	172	151	156	151
2301_2400	695	552	589	626	2301_2400	183	161	170	167
2201_2300	647	556	565	585	2201_2300	276	184	193	185
2101_2200	579	543	538	557	2101_2200	441	278	203	230
2001_2100	558	533	513	536	2001_2100	575	434	298	302
1901_2000	551	505	498	506	1901_2000	672	665	493	361
1801_1900	519	478	486	486	1801_1900	748	743	691	546
1701_1800	505	487	494	482	1701_1800	789	755	761	751
1601_1700	481	459	439	477	1601_1700	830	788	813	800
1501_1600	463	461	472	470	1501_1600	841	790	811	827
1401_1500	462	460	477	446	1401_1500	843	820	834	857
1301_1400	455	468	461	484	1301_1400	853	827	855	882
1201_1300	459	487	486	466	1201_1300	885	812	842	877
1101_1200	489	445	489	461	1101_1200	896	807	855	920
1001_1100	476	447	466	481	1001_1100	899	847	866	920
901_1000	416	481	516	456	901_1000	920	872	943	954
801_900	478	454	467	439	801_900	844	848	880	998
701_800	523	455	492	479	701_800	962	956	1011	976
601_700	486	427	533	462	601_700	1004	929	967	1002
501_600	466	438	511	515	501_600	967	932	982	980
401_500	511	490	489	515	401_500	1102	1083	1089	1062
301_400	527	532	538	514	301_400	1087	1117	1138	1141
201_300	554	549	655	569	201_300	1109	1118	1117	1219
101_200	10,199	11,272	5119	6541	101_200	1224	1327	1318	1258
0_100	85,280	66,858	45,795	101,358	0_100	62,057	59,464	48,826	36,699
Total Loading 108,705		90,371	63,652	120,708	Total Loading	81,454	77,932	67,346	55,294
AOT @ 550nm	2.638	2.193	1.545	2.93	AOT @ 550nm	1.977	1.891	1.634	1.342

8.2 Request to US EPA for CSR Assistance by China

Date: Mon, 24 Nov 2003 11:31:44 -0500
From: Schwengels.Paul@epamail.epa.gov
Subject: Follow-up on Remote Sensing
To: Jang.Carey@epamail.epa.gov
Cc: keithh@csr.utexas.edu, keith.hutchison@ncg.com,
Wells.Trenton@epamail.epa.gov, Evarts.Dale@epamail.epa.gov,
Wickwire.Susan@epamail.epa.gov
MIME-version: 1.0
X-MIMETrack: Serialize by Router on EPAHUB11/USEPA/US(Release 6.0.2CF1|June 9, 2003) at 11/24/2003 11:31:15 AM
Status: RO

As you know, I made some calls to the University of Texas, Center for Space Research back in late September, in response to a request for assistance on remote sensing for air pollution monitoring from Prof. Yu Tong at the Beijing Environmental Monitoring Center. Dr. Keith Hutchison of CSR was the author of the journal article which Prof. Yu had reference in his request. At that time, I spoke to Dr. Hutchison and he expressed interest in working with our Chinese colleagues to help apply methods used in Texas for the Beijing Olympics air quality management process.

Since that time I know that you have become the focal point for EPA interest in the linkage between US and China on remote sensing and analysis for air pollution management. When Dr. Hutchison recently called me to update me on the current and planned development of the UT/CSR program in this area, I suggested that he call you and communicate this information directly.

Dr. Keith Hutchison
Center for Space Research, UT
Tel: 512-471-7295

Thanks for your cooperation. Please let me know if there is anything further I can do to help in this area.

Paul Schwengels
International Capacity Building Branch
Global Programs Division (6205J)
Office of Air and Radiation, USEPA
1200 Pennsylvania Ave., NW
Washington, D.C. 20460
TEL: 1-202-343-9310
FAX: 1-202-343-2362
email: **SCHWENGELS.PAUL@EPA.GOV**

8.3 MOU Between UT Austin and Freie University, Berlin Germany

MEMORANDUM OF UNDERSTANDING

between the

The University of Texas at Austin on behalf of
Center for Space Research (CSR)
Austin, Texas USA

and the

Freie Universität Berlin
Institut für Meteorologie and
Institut für Weltraumwissenschaften (IfM/WeW)
Berlin, Germany

Objectives:

This MOU outlines general plans to collaborate in the areas of data collection and data sharing and the analyses of remotely sensed data between CSR and IfM/WeW. In particular, the MOU proposes collaborative efforts to collect, distribute, and exploit data collected by NASA's Earth Observing System (EOS) spacecraft, including data from the MODerate resolution Imaging Spectroradiometer (MODIS), Advanced Microwave Scanning Radiometer – EOS (AMSR-E), and other smaller satellites in the afternoon train (A-Train) of satellite systems such as Cloudsat and Calipso. This collaboration with also include the integration of these remotely sensed data and products derived from them into mesoscale models used in analysis and prediction of atmospheric chemistry and weather forecast fields by organizations supported by CSR and IfM/WeW at Freie Universität Berlin.
This MOU is the basis for specific projects, which will be ruled by separate contracts.

Mission of CSR

The primary mission of CSR is to conduct coordinated research in orbit determination, space geodesy, the Earth and its environment, and exploration of the solar system. Among its activities, CSR receives, processes, and provides through the public domain remotely-sensed data and data products collected by satellite and airborne sensors. CSR data products may be accessed via the internet at http://www.csr.utexas.edu – using the Texas Synergy spotlight.

In recent years, CSR has developed advanced aerosol and cloud data products from data collected by NASA's EOS satellites using direct download receiving station. This is now a credible capability to support air quality managers within the State of Texas. In particular, CSR now processes MODIS data to obtain estimates of air quality through aerosol optical thickness fields to produce predictions of future air quality with a trajectory-based software package developed at the NASA Langley Research Center. In addition, CSR has matured its significant cloud retrieval technologies to more accurately estimate 3-dimensional cloud fields from MODIS data over those products currently available from NASA via the EOS Data Gateway.

Mission of IfM/WeW

The research interests of the Institut für Weltraumwissenschaften (WeW) of the Freie Universität Berlin are focussed on the development of remote sensing techniques on the basis of radiative transfer simulations and measurements with airborne instruments. New algorithms are designed for the detection of atmospheric

properties (clouds and precipitation, aerosols and water vapour), ocean constituents and land surface properties. The basis of all retrieval algorithms is radiative transfer calculations with the MOMO program. This radiative transfer code is a development of the Institute. It belongs to the most sophisticated models and is suited especially for the simulation of clouds.
For atmospheric measurements, the WeW uses airborne radiance measurements with airborne spectrometers. These configuration capabilities are used to simulate satellite measurements of present and future satellite systems. Algorithms for the retrieval of cloud properties from multispectral radiance measurements have been developed and WeW is responsible for the operational cloud and water vapour products from the MEdium Resolution Imaging Spectrometer (MERIS) launched onboard the ENVISAT satellite in March 2002. The WeW participate in the EU-Project Parameterization of the Aerosol Indirect Climatic Effect, PACE, where a new parameterisation of the aerosol indirect effect in GCMs has been developed.

The "Tropospheric Environmental Working group" (IfM/TrUmF) is engaged in real time data processing, meteorological modeling, chemical transport modeling and trajectory calculations with special emphasis to applications. Several environmental and climatological projects are funded by Umweltbundesamt and German Ministry for Education and Sience (BMBF).

Of special interest is the modeling of tropospheric aerosols, ozone and its precursors i.e. photooxidants over Europe, Germany and selected smaller areas for administrative and political plannings, e.g. abatement strategies and traffic scenarios. This includes long term modeling of oxidant formation and ozone forecast system for real time application (summer smog warning system).

Moreover the evaluation of cloud parameters of meteorological modeling and diagnostic drivers is underway with emphasis on photooxidant processes, wet deposition and chemical processes within clouds. Long time series of cloud parameters and precipitation are determined synoptic measurements and from NOAA/Meteosat satellites for comparison to the "Lokalmodel" from German Weather Service.
Most of the model applications are planned and designed for operational use.

Goals for Collaboration

The collaboration between CSR and IfM/WEW are centered on the following four goals:

1. Participate in joint studies to explore the synergism between data products derived from MODIS with other sensor data collected by satellites in NASA's A-Train,
2. Evaluate methods to integrate remotely-sensed data products derived from NASA EOS satellite systems into multi-scale atmospheric chemistry and meteorological analysis and prediction models,
3. Assess the usefulness of data products generated through the synergies in satellite data collected by the NASA A-Train system in full-physics prediction systems, and
4. Consider opportunities for collaboration on future space missions to further improve the performance of multi-scale atmospheric chemistry and meteorological modeling systems.

Statement of Responsibilities

A. The Center for Space Research will:

- Work in collaboration with IfM/WeW to obtain funds from US agencies to support the execution of this MOU.
- Contribute to the development of technical specifications for future aircraft sensors and remotely-sensed data products for use in the US and Germany including the testing of experimental products intended to meet these standards.

- Collaborate with WeW in technical and research activities regarding data distribution, calibration and georectification techniques, digital image processing and enhancement techniques, and algorithm development, especially in the retrieval of cloud products.
- Support IfM/WeW in accomplishing objectives of mutual interest subject to the availability of personnel and funds appropriated for the purpose.
- Participate with IfM/WeW in joint initiatives, proposals, documents and reports for projects regarded as mutually beneficial to the goals of both organizations.
- Participate with IfM/WeW in appropriate training programs and workshops, meetings and seminars.
- Participate in exchange of staff and students between CSR and IfM/WeW, where appropriate and where funds and schedules support such interactions.

B. The Institute for Meteorology and Institute for Weltraumwissenschaften will:

- Work in collaboration with CSR to obtain funds from national (German) and European agencies to support the execution of this MOU.
- Cooperate on utilisation of satellite born cloud parameters (coverage, type, and 3d analysis) for chemical transport modeling and comparison to meteorological model results.
- Participate in direct adaptation of procedures into meteorological drivers for chemical transport modeling.
- Contribute to the development of technical specifications for future aircraft sensors and remotely-sensed data products for use in the US and Germany including the testing of experimental products intended to meet these standards.
- Collaborate with CSR in technical and research activities regarding data distribution, calibration and georectification techniques, digital image processing and enhancement techniques, and algorithm development, especially in the retrieval of cloud products.
- Support CSR in accomplishing objectives of mutual interest subject to the availability of personnel and funds appropriated for the purpose.
- Participate with CSR in joint initiatives, proposals, documents and reports for projects regarded as mutually beneficial to the goals of both organizations.
- Participate with CSR in appropriate training programs and workshops, meetings and seminars.
- Participate in exchange of staff and students between IfM/WeW and CSR, where appropriate and where funds and schedules support such interactions.

Limitations

Participation by CSR under this MOU is authorized pursuant to Section 65.31 of the Texas Education Code and shall be subject to and governed in compliance with

- The policies, rules and regulations of The University of Texas System Board of Regents which govern CSR, including policies governing intellectual property, and other policies and regulations of The University of Texas at Austin.
- State of Texas Constitution, laws or regulations.
- U.S. Patent and Trademark laws.
- U.S. Export Controls laws, regulations and policies.
- Neither Party incurs any liability for failing to execute the conditions set forth in this agreement due to a lack of available funds. The extent of participation depends on acquiring external funding from research sponsors.

Participation by the Freie Universität Berlin is authorized pursuant to Berliner Hochschulgesetz and shall be subject to and in compliance with

- Berliner Hochschulgesetz, Hochschulrahmengesetz and other relevant regulations of the Freie Universität Berlin laws, of state Berlin and laws of state Germany.

Period of Agreement, Renewal, and Termination

This MOU will commence upon the date of the last signature of approval specified below, and it will be in effect for a period of three years from that date. This agreement may be reviewed periodically for currency, and amended as necessary with the mutual consent of both parties. Similarly, the Memorandum may be renewed by written agreement of both parties. All modifications to this agreement will be incorporated as written amendments. The Memorandum may be terminated by either party upon 90 days' written notice to the other party and may be terminated immediately upon five (5) days written notice to the other party in the event that U.S. Export Controls laws, regulations or policies require termination of this MOU.

Points of Contact

The following individuals will be the points of contact for this agreement:

For technical matters:

Center for Space Research

Dr. Keith D. Hutchison,
Senior Research Scientist
The University of Texas at Austin
Center for Space Research
3925 W. Braker Ln, Suite 200
Austin TX 78759
Phone: (512) 471-5573
Fax: (512) 471-3570
E-mail: keithh@csr.utexas.edu

The Institut fur Weltraumwissenschaften

Dr. Jurgen Fischer
Director
Institut for Weltraumwissenschaften
Carl-Heinrich-Becker-Weg 6-10
D - 12165 Berlin

Tel. (..49) 30 838-56663
Fax : (..49) 30 838 65564
E-mail: fischer@zedat.fu-berlin.de

Approving officials

Susan W. Sedwick, PhD
Associate Vice-President for Research
The University of Texas at Austin
P. O. Box 7726
Austin TX 78713-7726
Phone: (512) 471-6424
Fax: (512) 471-6564
E-mail:: : sedwick@austin.utexas.edu

Prof. Dr. H. Keupp
Vice-President (VP IV) of
Freie Universität Berlin
Kaiserswerther Str. 16-18
D - 14195 Berlin
Phone : (..49) 30 838 73140
Fax : (..49) 30 838 73147
E–mail: vp4@fu-berlin.de

The University of Texas at Austin

Susan W. Sedwick, PhD
Associate Vice-President for Research

NOV 0 3 2006

Freie Universität Berlin

4.10.2006

Prof. Dr. Helmut Keupp
Vice-President